

---

Investigation of visual pathways in honeybees (*Apis mellifera*) and desert locusts (*Schistocerca gregaria*):  
anatomical, ultrastructural, and physiological  
approaches

Untersuchung visueller Signalwege in Honigbienen (*Apis mellifera*)  
und Wüstenheuschrecken (*Schistocerca gregaria*): anatomische,  
ultrastrukturelle und physiologische Betrachtungen

---



DISSERTATION  
zur  
Erlangung des Doktorgrades  
der Naturwissenschaften  
(Dr. rer. nat.)

dem Fachbereich Biologie  
der Philipps-Universität Marburg  
vorgelegt von  
**Martina Held**  
aus Meisenheim am Glan  
Marburg an der Lahn, 2020

---



Vom Fachbereich Biologie der Philipps-Universität Marburg als Dissertation  
angenommen am:

Erstgutachter:

Prof. Dr. Keram Pfeiffer

Zweitgutachter:

Prof. Dr. Uwe Homberg

Tag der mündlichen Prüfung:

---





# CONTENTS

<b>Erklärung: Eigene Beiträge und veröffentlichte Teile der Arbeit</b>	1
<b>Abstract</b>	5
<b>Zusammenfassung</b>	6
Kapitel 1: Transmedulla neurons in the sky-compass network of the honeybees ( <i>Apis mellifera</i> ) are a possible site of circadian input	7
Kapitel 2: Microglomerular synaptic complexes in the sky-compass network of the honeybee connect parallel pathways from the anterior optic tubercle to the central complex	9
Kapitel 3: Calcium imaging in tethered behaving honeybees	10
Kapitel 4: Anatomical and ultrastructural analysis of the posterior optic tubercle in the locust <i>Schistocerca gregaria</i>	12
<b>Introduction</b>	15
Spatial orientation	15
Sky-compass signals	18
Western honeybee ( <i>Apis mellifera</i> )	20
Desert locust ( <i>Schistocerca gregaria</i> )	23
The sky-compass pathway in the desert locust	24
Circadian rhythm and time compensation	27
Scope of this work	29
References	31
<b>Chapter I: Transmedulla neurons in the sky-compass network of the honeybee (<i>Apis mellifera</i>) are a possible site of circadian input</b>	35
Abstract	37
Introduction	38
Methods	39
Results	44
Discussion	51
Conclusion	56
Supporting information	56
References	57
<b>Chapter II: Microglomerular synaptic complexes in the sky-compass network of the honeybee connect parallel pathways from the anterior optic tubercle to the central complex</b>	63
Introduction	66
Materials and methods	66
Results	69
Discussion	72

References	77
<b>Chapter III: Calcium imaging in tethered behaving honeybees</b>	79
Introduction	81
Material and methods	88
Calcium Green-1 dextran and JF <sub>549</sub> -BAPTA-MPM ester	88
Preparation	89
Preliminary ester tests	91
Injection JF <sub>549</sub> -BAPTA-MPM ester	92
Injection Calcium Green-1 dextran	96
Imaging and behavioral recordings with custom-built two-photon microscope	96
Imaging and behavioral recordings with the Leica Multiphoton Microscope TCS SP8 MP	98
Analysis	100
Results	102
Behavioral data	102
Preliminary Testing of ester coupled dyes	111
Calcium imaging data with JF <sub>549</sub> -BAPTA-MPM ester	114
Calcium imaging data with Calcium Green-1 dextran	120
Alignment of calcium imaging data with the behavior	127
Discussion and outlook	131
References	139
<b>Chapter IV: Anatomical and ultrastructural analysis of the posterior optic tubercle in the locust <i>Schistocerca gregaria</i></b>	143
Introduction	145
Materials and methods	147
Results	153
Discussion	154
References	157
<b>Appendix</b>	159
Protocol calcium imaging	159
Table notes for calcium imaging in Leica setup	201
Wholemout preparation	205
<b>Curriculum Vitae</b>	Fehler! Textmarke nicht definiert.
<b>Danksagung</b>	207
<b>Erklärung</b>	213

## ERKLÄRUNG

### Eigene Beiträge und veröffentlichte Teile der Arbeit

Entsprechend §9 (1) der Promotionsordnung der Philipps-Universität Marburg (Fassung vom 15.07.2009) werden im Folgenden die eigenen Anteile an den einzelnen Kapiteln detailliert erläutert.

#### **Kapitel I: Transmedulla neurons in the sky-compass network of the honeybees (*Apis mellifera*) are a possible site of circadian input**

- Durchführung der Anti-Synapsin/Phalloidin Färbung (Abb. 1A & B und Abb. 3A), Farbstoffinjektion und Anti-GABA Färbung (Abb. 7 und Abb. 8C) und Evaluation dieser Daten
- Schemaerstellung Abb. 9
- Korrektur des Manuskripts
- Dieses Kapitel wurde in der hier vorliegenden Form (von geringfügigen editorischen Änderungen abgesehen) bei *PLoS ONE* veröffentlicht:

Zeller, M., Held, M., Bender, J., Berz, A., Heinloth, T., Hellfritz, T., Pfeiffer, K. 2015. Transmedulla neurons in the sky compass network of the honeybee (*Apis mellifera*) are a possible site of circadian input. *PLoS ONE* 10: e0143244. DOI: 10.1371/journal.pone.0143244

#### **Kapitel II: Microglomerular synaptic complexes in the sky-compass network of the honeybee connect parallel pathways from the anterior optic tubercle to the central complex**

- Konzeption in Zusammenarbeit mit Prof. Dr. Keram Pfeiffer, Prof. Dr. Uwe Homberg und Prof. Dr. Wolfgang Rössler
- Schemaerstellung, Rekonstruktion der Neuronentypen (Abb. 1)
- Durchführung der Anti-Synapsin/Phalloidin Färbung (Abb. 2C), aller Farbstoffinjektionen und Anti-GABA Färbungen (Abb. 5), sowie aller Elektronenmikroskopischen Aufnahmen und Rekonstruktionen (Abb. 6 und 7)
- Evaluation der Daten
- Anfertigung von 71% der Abbildungen (Abb. 1, 2, 5, 6, 7)
- Überarbeitung der Abbildungen 3 und 4

- Anfertigung des Manuskripts in Zusammenarbeit (Korrektur) mit Prof. Dr. Keram Pfeiffer
- Dieses Kapitel wurde in der hier vorliegenden Form (von geringfügigen editorischen Änderungen abgesehen) bei *Frontiers in Behavioral Neuroscience* veröffentlicht:  
Held, M., Berz, A., Hensgen, R., Muenz, T.S., Scholl, C., Rössler, W., Homberg, U., Pfeiffer, K. 2016. Microglomerular synaptic complexes in the sky-compass network of the honeybee connect parallel pathways from the anterior optic tubercle to the central complex. *Frontiers in Behavioral Neuroscience*. 10:186.  
DOI: 10.3389/fnbeh.2016.00186

### **Kapitel III: Calcium imaging in tethered behaving honeybees**

- Konzeption aller Experimente und Setup Aufbau in Zusammenarbeit mit Prof. Dr. Keram Pfeiffer und Dr. Vivek Jayaraman
- Anpassung und Etablierung des Protokolls
- Durchführung aller Experimente
- Konzeption der Auswertung in Zusammenarbeit mit Dr. Hannah Haberkern
- Durchführung der gesamten Auswertung
- Evaluation der Daten in Zusammenarbeit mit Prof. Dr. Keram Pfeiffer
- Anfertigung aller Abbildungen
- Anfertigung des Kapitels in Zusammenarbeit (Korrektur) mit Prof. Dr. Keram Pfeiffer
- Dieses Kapitel wurde bis Promotionsabgabe nicht veröffentlicht

### **Kapitel IV: Anatomical and ultrastructural analysis of the posterior optic tubercle in the locust *Schistocerca gregaria***

- Konzeption aller Experimente in Zusammenarbeit mit Prof. Dr. Uwe Homberg
- Einarbeitung von Kim Le
- Betreuung der zugrundeliegenden Bachelorarbeit von Kim Le in Zusammenarbeit mit Prof. Dr. Uwe Homberg
- Evaluation der Daten
- Anfertigung aller Abbildungen

- Verfassen des Manuskripts in Zusammenarbeit mit Prof. Dr. Uwe Homberg (Korrektur) und Prof. Dr. Keram Pfeiffer (Korrektur)
- Dieses Kapitel wurde in der hier vorliegenden Form (von geringfügigen editorischen Änderungen abgesehen) bei *Arthropod Structure & Development* veröffentlicht:  
Held, M., Le, K., Pegel, U., Dersch, F., Beetz, J.M., Pfeiffer, K., Homberg, U. 2020. Anatomical and ultrastructural analysis of the posterior optic tubercle in the locust *Schistocerca gregaria*. *Arthropod Structure & Development*. 58, 100971. DOI: 10.1016/j.asd.2020.100971



## **ABSTRACT**

Many insect species demonstrate sophisticated abilities regarding spatial orientation and navigation, despite their small brain size. The behaviors that are based on spatial orientation differ dramatically between individual insect species according to their lifestyle and habitat. Central place foragers like bees and ants, for example, orient themselves in their surrounding and navigate back to the nest after foraging for food or water. Insects like some locust and butterfly species, on the other hand, use spatial orientation during migratory phases to keep a stable heading into a certain direction over a long period of time. In both scenarios, homing and long-distance migration, vision is the primary source for orientation cues even though additional features like wind direction, the earth's magnetic field, and olfactory cues can be taken into account as well. Visual cues that are used for orientational purposes range from landmarks and the panorama to celestial cues. The latter consists in diurnal insects of the position of the sun itself, the sun-based polarization pattern and intensity and spectral gradient, and is summarized as sky-compass system. For a reliable sky-compass orientation, the animal needs, in addition to the perception of celestial cues, to compensate for the daily movement of the sun across the sky. It is likely that a connection from the circadian pacemaker system to the sky-compass network could provide the necessary circuitry for this time compensation.

The present thesis focuses on the sky-compass system of honeybees and locusts. There is a large body of work on the navigational abilities of honeybees from a behavioral perspective but the underlying neuronal anatomy and physiology has received less attention so far. Therefore, the first two chapters of this thesis reveals a large part of the anatomy of the anterior sky-compass pathway in the bee brain. To this end, dye injections, immunohistochemical stainings, and ultrastructural examinations were conducted. The third chapter describes a novel methodical protocol for physiological investigations of neurons involved in the sky-compass system using calcium imaging in behaving animals. The fourth chapter of this thesis deals with the anatomical basis of time compensation in the sky-compass system of locusts. Therefore, the ultrastructure of synaptic connections in a brain region of the desert locust where the contact of both systems could be feasible has been investigated.

## ZUSAMMENFASSUNG

Viele Insektenarten zeigen trotz ihrer geringen Gehirngröße komplexe Fähigkeiten zur räumlichen Orientierung und Navigation. Die Verhaltensweisen, die auf räumlicher Orientierung basieren, unterscheiden sich jedoch je nach Lebensweise und -raum erheblich zwischen den verschiedenen Arten. Nestgebundene Sammler, wie beispielsweise Ameisen und Bienen, orientieren sich nach ihrer Futter- und Wassersuche anhand ihrer Umgebung und navigieren zurück zu ihrem Nest. Manche Heuschrecken- und Schmetterlingsarten nutzen räumliche Orientierung hingegen, um während ihrer Migrationsphasen einen stabilen Kurs über eine längere Zeit in eine bestimmte Richtung zu halten. In beiden Szenarien, Rückkehr zum Nest und Langstreckenmigration, werden primär visuelle Informationen zur Orientierung verwendet. Zusätzliche Eindrücke beispielsweise von Windrichtungen, dem Erdmagnetfeld und olfaktorischen Informationen können jedoch mit einbezogen werden. Visuelle Orientierungshilfen reichen von Landmarken und dem Panorama bis hin zu Himmelsinformationen. Letztere bestehen bei tagaktiven Insekten aus der Position der Sonne, dem sonnenbasierten Polarisationsmuster und Gradienten in Intensität und Wellenlänge am Himmel, welche unter dem Begriff des Himmelskompasssystems zusammengefasst werden. Für eine zuverlässige Himmelskompass-orientierung muss das Tier jedoch nicht nur die Himmelssignale wahrnehmen, sondern auch die tägliche Sonnenbewegung mit einbeziehen. Es ist daher wahrscheinlich, dass eine Verbindung vom zirkadianen System zum Himmelskompasssystem das nötige Netzwerk für diese Zeitkompensation bieten könnte.

Die vorliegende Arbeit behandelt das Himmelskompasssystem von Honigbienen und Heuschrecken. Es gibt bereits umfassende Verhaltensstudien über die Navigationsfähigkeiten von Bienen, wohingegen die zugrundeliegende Neuroanatomie und -physiologie bisher kaum untersucht wurden. Daher werden in den ersten zwei Kapiteln dieser Arbeit Studien vorgestellt, die große Teile der Anatomie des anterioren Himmelskompasssignalwegs im Bienenhirn beschreiben. Dazu wurden Farbstoffinjektionen, immunhistochemische Färbungen und ultrastrukturelle Untersuchungen durchgeführt. Das dritte Kapitel beschreibt ein neues Methodenprotokoll, in dem Calcium Imaging in sich verhaltenden Tieren etabliert wurde. Dabei waren Neurone, die am Himmelskompasssystem beteiligt sind, Ziel der physiologischen Untersuchungen. Das vierte Kapitel dieser Arbeit befasst sich mit der



anatomischen Grundlage der Zeitkompensation im Himmelskompasssystem. Hierbei wurde eine mögliche synaptische Verbindung der beiden Systeme auf ultrastruktureller Ebene in Wüstenheuschrecken untersucht.

---

## KAPITEL 1: TRANSMEDULLA NEURONS IN THE SKY-COMPASS NETWORK OF THE HONEYBEES (*APIS MELLIFERA*) ARE A POSSIBLE SITE OF CIRCADIAN INPUT

Honigbienen benutzen während ihrer Sammelflüge unter anderem ein Himmelskompasssystem, um zu ihrem Nest zurück zu finden. Auch sind sie dabei fähig, den täglichen Sonnenverlauf in ihre Orientierung mit einzubeziehen. Dies wurde bereits in vielen Verhaltensstudien nachgewiesen, wobei der Signalweg dahinter bisher unbekannt ist. Auch ist unklar, welche neuromodulatorischen Prozesse daran beteiligt sind. Das Ziel der Studie in diesem Kapitel war daher, die Eingangsneurone und die ersten Stationen des Himmelskompasssignalweges im Bienenhirn aufzudecken. Dazu wurden Farbstoffkristalle in verschiedene Regionen injiziert und die gefärbten Neurone anatomisch untersucht und kategorisiert. Darüber hinaus wurden in manchen Präparaten, zusätzlich zu den Injektionen, immunhistochemische Färbungen gegen verschiedene Neurotransmitter durchgeführt. Dies hatte zum Ziel, mögliche Verbindungen zum System der inneren Uhr zu finden und weitere neuromodulatorische Einflüsse auf das Kompasssystem zu charakterisieren.

Die Injektionen legten verschiedene Neuronentypen im Signalweg von der Retina bis ins Zentralgehirn offen, die anatomisch große Ähnlichkeiten zu bereits untersuchten Neuronen im Heuschreckengehirn aufweisen. Der Eingang des anterioren Himmelskompasssignalweges erfolgt in der Heuschrecke über die dorsale Randregion der Retina (DRA). Dies wurde hier in der Biene durch Injektionen in die DRA bestätigt, die eine direkte Verbindung von der DRA zur dorsalen Randregion der Medulla, ein Neuropil im optischen Lobus, offenbarten. Durch zusätzliche Injektionsfärbungen konnte der weitere Verlauf über Transmedulla Neurone in den Komplex der unteren Einheit (LUC) des anterioren optischen Tuberkels (AOTU) gezeigt werden. Die Transmedulla Neurone ziehen hierbei von dorsal nach ventral etwa bis zur Hälfte der Medulla, machen dann einen Knick und ziehen im anterioren optischen Trakt in den LUC des AOTU. Dort verzweigen sie in allen Untereinheiten, wobei sich das Verzweigungsmuster je nach Typ der Transmedulla Neurone unterscheidet. Von dort ziehen sowohl Intertuberkelneurone in den LUC auf der kontralateralen Seite, als auch

ein weiterer Neuronentyp in Richtung Zentralgehirn, wo sie in den Bulbi des Lateralkomplexes mit erstaunlich großen synaptischen Endigungen verzweigen. Auch diese Neuronentypen weisen in Bienen große Ähnlichkeiten zur Heuschrecke auf, wobei die Neurone anatomisch und zum Teil physiologisch bereits beschrieben wurden. Zusätzlich zu den Injektionsfärbungen wurden Phalloidinfärbungen und Antikörperfärbungen gegen Synapsin angefertigt, um die involvierten Neuropilstrukturen genauer visualisieren zu können.

Um neuromodulatorische Einflüsse auf das Kompasssystem zu untersuchen, wurde zusätzlich zu den Injektionen auch immunhistochemische Färbungen durchgeführt. Hierzu wurden Antikörper gegen das Neuropeptid pigment dispersing factor (PDF), das biogene Amin Serotonin (5HT) und das biogene Amin  $\gamma$ -Aminobuttersäure (GABA) verwendet. Das Neuropeptid PDF ist ein Ausgangssignal der inneren Uhr von Insekten. 5HT und PDF zeigten in Studien in Fliegen und Grillen zirkadiane Modulationseinflüsse im visuellen System. Da Doppelfärbungen oder räumliche Überlappungen auf einen modulatorischen Eingang ins Kompasssystem hindeuten könnten, wurden Injektionsfärbungen mit Antikörperfärbungen gegen diese Transmitter kombiniert. Tatsächlich wurden in der Medulla PDF- und 5HT-immunoreaktive Fasern gefunden, die Verzweigungen in der gleichen Schicht aufwiesen, wie die Transmedulla Neurone. Es wurden keine Doppelfärbungen gefunden, jedoch eine räumliche Nähe der Neuronentypen, die auf eine mögliche Verschaltung der PDF- und 5HT-Neurone auf die Transmedulla Neurone entlang deren Neurite hindeutet. Die dorsale Randregion der Medulla und der LUC des AOTU waren dahingegen in beiden Antikörperfärbungen nicht markiert. Neben PDF und 5HT wurde auch eine Färbung gegen GABA vorgenommen. Dieser Transmitter ist bekannt für eine inhibitorische Wirkung auf Neurone im Insektengehirn und könnte eine weitere Modulation im Kompasssystem bewirken. Tatsächlich wurde auch in diesen Färbungen eine enge räumliche Nähe zu den Transmedulla Neuronen festgestellt. Im Gegensatz zu PDF und 5HT wurde GABA jedoch auch in der Randregion der Medulla gefunden. Wie auch bei den anderen beiden Antikörperfärbungen zeigte der LUC des AOTU keine Markierung. Zusammengefasst wurden in dieser Studie somit die Neurone des ersten Teils des Himmelskompasssystems von der DRA bis hin zum Zentralgehirn anatomisch beschrieben, sowie die involvierten Neuropile genauer charakterisiert. Die Transmedulla Neurone erwiesen sich hierbei als möglicher Ort, wo sowohl zeitkompensatorische als auch andere modulatorische Einflüsse in das Kompasssystem

gelangen könnten, was jedoch durch weitere Studien noch genauer untersucht werden sollte.

---

## KAPITEL 2: MICROGLOMERULAR SYNAPTIC COMPLEXES IN THE SKY-COMPASS NETWORK OF THE HONEYBEE CONNECT PARALLEL PATHWAYS FROM THE ANTERIOR OPTIC TUBERCLE TO THE CENTRAL COMPLEX

Im vorangegangenen Kapitel und der dort vorgestellten Studie wurde die Anatomie des anterioren Himmelskompasssignalweges von der dorsalen Randregion des Komplexauges (DRA) bis hin zu den Bulbi im Zentralgehirn der Honigbiene beschrieben. Die anatomische Charakterisierung der involvierten Neurone wurde in diesem Kapitel weitergeführt. Dabei wurden die TuLAL1 Neurone, die heute TuBu Neurone genannt werden, von dem Komplex der unteren Einheit (LUC) des anterioren optischen Tuberkels (AOTU) zu den Bulbi des Lateralkomplexes durch Farbstoffinjektionen visualisiert. Eine Subpopulation der TuLAL1 Neurone verzweigt im medialen Bulbus, während eine andere Population im lateralen Bulbus endet. TuLAL1 Neurone besitzen in beiden Bulbi einzigartig große synaptische Endigungen, die bereits in der Heuschrecke und Hummel beschrieben wurden. Aus diesen Studien ist ebenfalls bekannt, dass die synaptischen Partner der TuLAL1 Neurone GABA-erge Tangentialneurone (TL Neurone) sind. TL Neurone haben eine Verzweigung in den Bulbi und ziehen dann in die untere Einheit des Zentralkörpers, wo sie weitere Endigungen aufweisen. Der Zentralkörper ist Teil des Zentralkomplexes, eine Gruppe von Neuropilen im Zentralgehirn vieler Insekten, die als Integrationszentrum von Kompasssignalen beschrieben wurde. In der vorliegenden Studie wurde daher, zusätzlich zu den Injektionen, Antikörperfärbungen gegen GABA angefertigt. Dabei konnte die Erkenntnis aus der Heuschrecke, dass TuLAL1 Neurone in großen synaptischen Komplexen Endigungen von TL Neuronen umfassen, auch für Bienen gezeigt werden. Außerdem war es möglich die Anzahl dieser synaptischen Komplexe durch Phalloidininfärbungen kombiniert mit Antikörpermarkierungen gegen Synapsin in den beiden Bulbi beider Hirnhemisphären zu bestimmen. Um ein aussagekräftiges Bild der synaptischen Verschaltung innerhalb der Komplexe treffen zu können, wurden transmissions-elektronenmikroskopische Untersuchungen durchgeführt. Hierbei konnte ein Ergebnis aus der Heuschrecke bezüglich der synaptischen Polarität in Bienen ebenfalls beobachtet werden. In Bienen und Heuschrecken sind TuLAL1 Neurone in

den synaptischen Komplexen präsynaptisch, während die TL Neurone als postsynaptische Partner dienen. Zudem offenbarten die elektronenmikroskopischen Daten, dass einzelne Komplexe von Gliazellen umhüllt sind, was eine Art Isolation zur Umgebung darstellen könnte. Außerdem wurden verschiedene Synapsentypen divergenter Natur gefunden. Das bedeutet, dass eine präsynaptische aktive Zone auf mehrere postsynaptische Profile verschaltet. Diese synaptische Verschaltung deutet zusammen mit der isolierenden Glia-schicht auf eine schnelle und robuste Signalweiterleitung hin. Zusammengefasst zeigen die Ergebnisse in der Honigbiene eine hohe Ähnlichkeit zu denen in der Heuschrecke, obwohl die beiden Insektenarten in keiner nahen Verwandtschaft zu einander stehen.

---

### KAPITEL 3: CALCIUM IMAGING IN TETHERED BEHAVING HONEYBEES

Im dritten Kapitel steht die Entwicklung und Etablierung eines neuen Protokolls im Fokus, welches es ermöglicht Calcium Imaging Experimente durchzuführen, während die Honigbiene Laufverhalten zeigt. Die außergewöhnlichen Navigationsfähigkeiten von Bienen, die sich sowohl im Sammelflug, als auch im Schwänzeltanz widerspiegeln, wurden in ethologischen Studien bereits vor über 70 Jahren aufgedeckt. Während ihrer Sammelflüge sind Bienen und andere nestgebundene Insekten in der Lage durch Wegintegration und einem ausgeprägten visuellen Gedächtnis nach einem langen, kurvigen Suchflug auf direktem Weg zu ihrem Nest zurück zu finden. Dabei wird durch den Himmelskompass und zum Teil durch Landmarken die Richtung, in der das Nest liegt bestimmt, während ein Entfernungsmesser die Distanz speichert. In Bienen basiert der Entfernungsmesser auf dem optischen Fluss, den das Tier während des Flugs wahrnimmt, also die translationale Bewegung von Bildern über die Retina. Im Schwänzeltanz gibt die Biene die direkte Weginformation zu einer lohnenswerten Futterquelle an andere Sammlerinnen im Stock weiter, um diese dorthin zu rekrutieren. Dabei führt die tanzende Biene eine bestimmte Abfolge von Kreisen und Vibrationen in Form einer Acht durch, welche die Entfernung vom Stock und den Winkel der Futterquelle zur Sonne kodieren.

Obwohl dieses erstaunliche und mit der Tanzkommunikation einzigartige Verhalten der Bienen bereits seit langem bekannt und erforscht ist, ist der neuronale Hintergrund bisher weitgehend unerforscht. In den ersten beiden Kapiteln wurden Teile der involvierten Anatomie untersucht, während in diesem Kapitel eine Möglichkeit zur

physiologischen Untersuchung der beteiligten Neurone etabliert werden sollte. Dabei wurden verschiedene Aspekte berücksichtigt: die physiologische Methode sollte auf Grund des unbekannten Systems eine visuelle Untersuchung der Neurone zulassen. Da der anteriore Himmelskompasssehweg im Fokus stand sollte des Weiteren eine visuelle Stimulation während der Datenaufnahme möglich sein. Als dritter Punkt war die Bewegungsfähigkeit des Tieres von großem Interesse, da die meisten bisherigen physiologischen Untersuchungen des Sehsystems und des Himmelskompasses in Bienen und anderen Insekten an komplett fixierten Tieren durchgeführt wurde. Dies hat den Nachteil, dass etwaige zustandsabhängige Antworten von Neuronen nicht hervorgerufen und somit nicht aufgenommen werden können. Besonders im visuellen System wurde jedoch bereits gezeigt, dass sich die Zellantwort deutlich unterscheiden kann, wenn das Tier seinen Zustand, zum Beispiel von Stehen zu Laufen, ändert. All diese Anforderungen an die neue Methode führten zu einem innovativen Protokoll, bei dem Calcium Imaging in sich verhaltenden Tieren ermöglicht wurde. Hierzu wurden die Bienen mit dem Kopf an eine spezielle Halterung geklebt, wobei Augen, Beine und das Abdomen frei blieben. Im Verlauf des Projekts wurden zwei verschiedene Kalziumindikatoren getestet und in die Zielneurone des Bienengehirns eingebracht. Diese zeigen durch Fluoreszenzänderungen Unterschiede in der Kalziumkonzentration innerhalb der Zelle an, die durch neuronale Aktivität ansteigt. Nach erfolgreicher Farbstoffaufnahme durch die Zellen, wurden die Tiere dann auf einen Styroporball gesetzt, der auf einem Luftstrom schwebte und dadurch von der Biene in alle Richtungen gedreht werden konnte. Die Biene auf dem Ball wurde dann in die Mitte einer blauen LED Arena positioniert. Diese befand sich wiederum unter einem Zwei-Photonen Mikroskop, an dem Imaging Experimente durchgeführt wurden. Die Ballbewegung, die durch das Tier ausgelöst wurde, wurde mit einem Kamerasystem aufgenommen, um das Laufverhalten später auswerten zu können. Am Ende der Etablierungsphase war es möglich dem Tier verschiedene visuelle Reize zu zeigen und gleichzeitig sowohl die neuronale Antwort der injizierten Zellen, als auch das Laufverhalten aufzunehmen. Anschließend wurden die einzelnen Komponenten zeitlich synchronisiert und dann ausgewertet. Das etablierte Protokoll bietet somit einen neuen methodischen Ansatz, um neuronale Grundlagen im visuellen System der Honigbienen mit gleichzeitigen Verhaltensantworten zu erforschen.

## KAPITEL 4: ANATOMICAL AND ULTRASTRUCTURAL ANALYSIS OF THE POSTERIOR OPTIC TUBERCLE IN THE LOCUST *SCHISTOCERCA GREGARIA*

Viele Erkenntnisse über den neuronalen Signalweg des Himmelskompasses stammen aus zahlreichen Studien an Wüstenheuschrecken. Vor allem die Perzeption und Weitergabe von polarisiertem Licht wurden hierbei in verschiedenen Neuronentypen physiologisch untersucht und die Zellen anatomisch beschrieben. Weitgehend unbekannt ist jedoch auch in diesem recht gut untersuchten Insekt, wie nötige Informationen zur Zeitkompensation in das System integriert werden. Vorangegangene Studien stellten die Hypothese auf, dass es eine Verbindung vom Zentrum des zirkadianen Zeitgebersystems, der sogenannten akzessorischen Medulla, zur Protozerebralbrücke, ein Neuropil des Zentralkomplexes, besteht. Der Zentralkomplex ist eine Gruppe von Neuropilen im Zentralgehirn, die als wichtige Integrationsstelle des Himmelskompasssystems gilt. Der mutmaßliche Kontakt zwischen Protozerebralbrücke und akzessorischen Medulla erfolgt nach der bestehenden Hypothese in einem kleinen Neuropil namens posteriorer optischer Tuberkel (POTU). Einzelzelleableitungen und -färbungen, sowie Antikörperfärbungen gegen das Neuropeptid pigment dispersing hormone (PDH) zeigten, dass Neurone der Protozerebralbrücke im POTU wahrscheinlich ihre Eingangsregion haben, während PDH-immunreaktive Neurone möglicherweise Informationen von der akzessorischen Medulla in den POTU bringen und dort ihren Ausgang haben. In dem vorliegenden Kapitel wurde nun eine Studie angefertigt, in der die Anatomie des POTU genauer beleuchtet wurde. Dazu wurde aus immunhistochemischen Färbungen die durchschnittliche dreidimensionale Form des POTUs rekonstruiert. Außerdem wurden Semidünnschnitte angefertigt, um die Neurite, die den POTU mit anderen Hirnarealen verbindet, genauer darstellen zu können. Anschließend wurde die Ultrastruktur des Neuropils in transmissionselektronenmikroskopische Präparaten untersucht. Hierbei wurden synaptische Profile charakterisiert und die synaptische Polarität zwischen ihnen bestimmt. Anschließend wurde eine Immunogoldmarkierung gegen PDH durchgeführt, um synaptische Profile, die von Zellen der akzessorischen Medulla stammen identifizieren zu können. Darüber hinaus konnten Zellen, die den POTU mit der Protozerebralbrücke verbinden, durch Einzelzellefärbungen im Elektronenmikroskop sichtbar gemacht werden. All diese anatomischen Daten zum ultrastrukturellen Aufbau des POTUs bestätigten die Annahme, dass die Neurone der Medulla dort

präsynaptisch sind, also ihren Ausgang haben. Die untersuchten Zellen der Protozerebralbrücke hingegen erhalten im POTU ihren Eingang und leiten dann die Information in die Protozerebralbrücke, und somit in den Zentralkomplex, weiter. Somit konnten vorangegangene Annahmen bestätigt werden, was einen wichtigen Schritt zum Verständnis des zeitkompensatorischen Einflusses auf das Himmelskompasssystem liefert.





## INTRODUCTION

Goal-directed behavior of insects and other animals is guided by a combination of external cues and internal physiological states. External stimuli range from environmental factors like light, temperature, available water and food to species-specific determinants such as present mating partners, conspecifics, resource competitors, and predators. Internal physiological states that are motivators for directed behavior are for example hunger and thirst, reproduction phase, discomfort or pain, and the circadian rhythm. Those factors can elicit goal-directed behaviors of various complexity. One very basic behavior is escape behavior, either quickly from an approaching predator, or on varying time scales from unpleasant to even harmful conditions. Escape behavior can range from simple appearing short movements to very sophisticated long-term behavior. A quick escape jump due to a looming stimuli, as observed in flies or locusts, appears very simplistic and robust. In fact, this movement already comprises stimuli-dependent posture and leg movement adjustments and therefore allows for some flexibility regarding the escape direction (reviewed in Card, 2012). If the escape motion contains for example a constant straight-line movement, the underlying processes are much more intricate. For that motion, the animal needs to update its current position over a longer period of time to keep a straight line away from the point of origin. The most impressive forms of goal-directed behavior in insects are long-distance migration and homing. Long-distance migration enables some insects to leave a place with unfavorable conditions, like harmful temperatures or food shortages, towards a better environment. Another sophisticated goal-directed behavior including demanding memory performances is homing behavior of central place foragers like bees and ants. Failing the task of finding home after foraging is often deadly for the individuals but also harmful for the colony in social insects. All those goal-directed behaviors, escape behavior, straight-line motion, long-distance migration, and foraging and homing, demand for a reliable spatial orientation system.

---

## SPATIAL ORIENTATION

Spatial orientation requires a sense for the own body orientation in the environment in combination with the perception, processing, and integration of external sensory information to assess the own position during self-motion. Sensory information originates from different cues and insects as well as other animals are usually able to perceive multiple cues to make the system more robust. Utilizing more

than one cue might be physiologically more costly but it ensures a reliable orientation even when one cue is not available while it also increases the accuracy of the reference system. Sensory cues that can be used for spatial orientation are manifold, depending on the animal's habitat and goal. Moths that are searching for a mating partner use for example olfactory cues in pheromone plums (Hansson, 1995). Dung beetles are able to use olfaction, visual cues but also mechanosensory information from steady winds for straight-line rolling of a dung ball (Tribe and Burger, 2011; Dacke et al., 2003; Dacke et al., 2012; Dacke et al., 2019). However, the most reliable sensory source for spatial orientation in most insects is vision, offering multiple reference types. They can range from local visual cues, like landmarks (Wehner et al., 1996), and distant visual cues, like the panoramic skyline (Collett, 2008), to global cues of the sky, like the sun, polarization pattern, the moon, stars, the Milky Way and spectral and intensity gradients (Wehner, 1984; Wehner and Müller, 2006; Dacke et al., 2004; Dacke et al., 2013; el Jundi et al., 2014; el Jundi et al., 2015). The usage of different cues from the sky are cumulated under the term “sky-compass orientation” which is used by many species, for example bees, locusts, ants, butterflies, and dung beetles. The complexity of the behaviors in which the same reference frame is used varies significantly between species. Dung beetles use primarily the sky compass to roll the dung ball in a straight line away from the dung pile and therefore away from competitors (Fig. 1A; Dacke et al., 2003; Dacke et al., 2012; Khaldy et al., 2018). Another form of spatial orientation is exhibited by bees and ants. As central place foragers, they have one nest they return to after foraging for food. The outbound route is often several hundred meters to many kilometers long and tortuous while the homebound path is in a shorter and straighter beeline (Fig. 1B). To achieve this path integration, central place foragers integrate visual cues with an odometer to build up a homing vector (Hoinville and Wehner, 2018). Homing ants and bees use celestial cues to gather directional information but take landmarks into account as well to fine-tune their steering (Wehner, 2008; Grob et al., 2019). Recent studies showed furthermore, that ants calibrate their orientation system in learning walks by using the gradient information of the earth's magnetic field (Fleischmann et al., 2018). Bees calculate the covered distance using the optic flow, meaning the motion of images over the retina to estimate the traveled distance (reviewed by Srinivasan, 2014). Ants estimate the walked distance primarily by utilizing a stride integrator but in some cases also by using optic flow information (Wittlinger, 2006; Pfeffer and Wittlinger, 2016). Spatial orientation is also the basis of long-distance migration in butterflies that use the

sky cues for orientation. Monarch butterflies migrate by millions every fall thousands of kilometers from Canada and the northern US to central Mexico to escape the cold winter. In spring, the next generations return back north, mainly relying on the sky compass for orientation (Fig. 1C; Mouritsen and Frost, 2002; Heinze and Reppert, 2011).

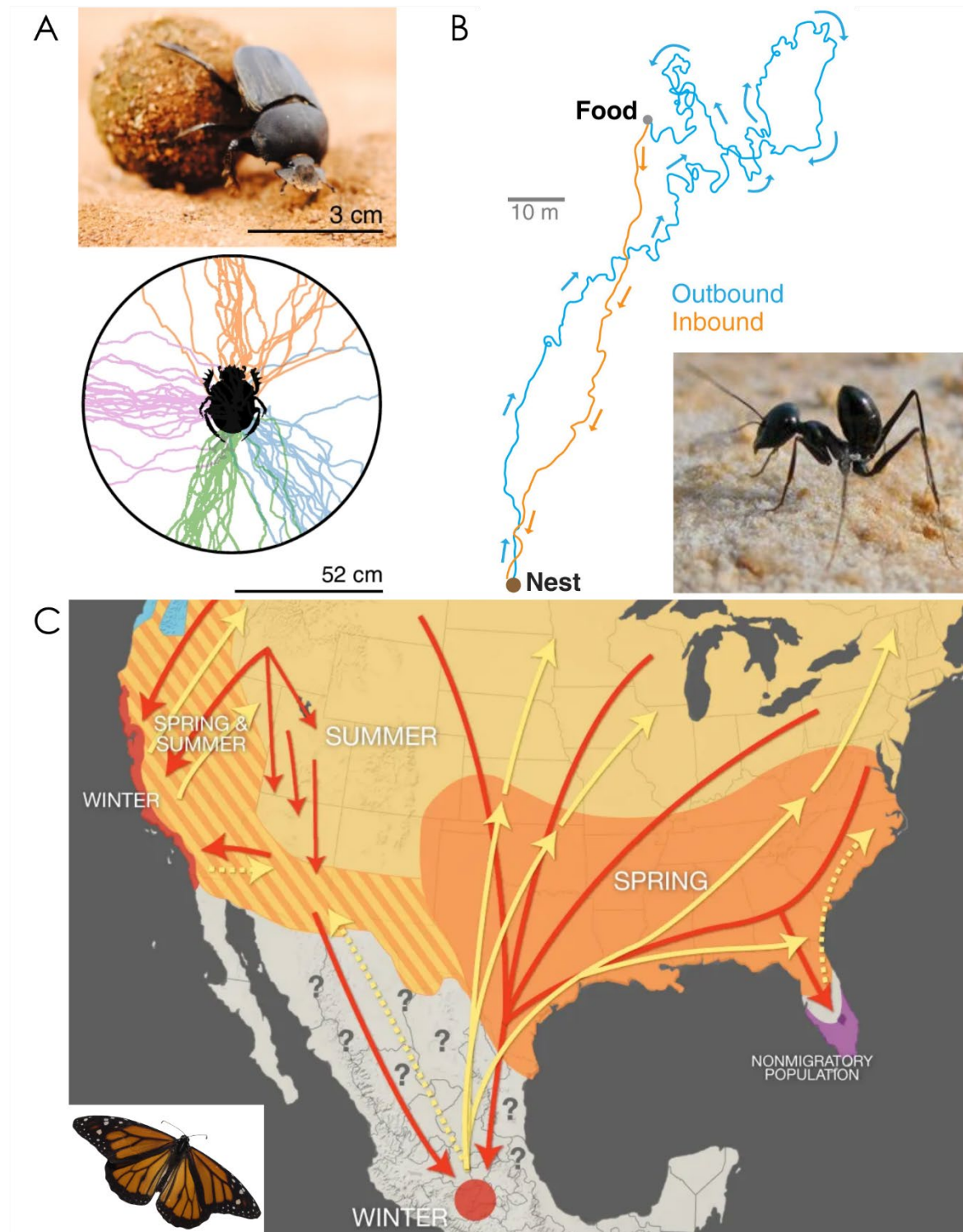


**Fig. 1: Three examples of goal-directed behavior based on spatial orientation.** A: straight-line orientation exhibited by the dung beetle *Scarabaeus lamarcki* under a natural sky. Colored lines indicate trajectories of four individual beetles with their balls with twenty rolling trajectories each. Adapted from Khaldy et al., 2018. B: Desert ants *Cataglyphis fortis* use path integration to walk back to the nest in a straight line after a tortuous outbound search for food. Adapted from Heinze et al., 2018, picture *C. fortis* ©M. Wittlinger. C: The monarch butterfly *Danaus plexippus* performs seasonal long-distance migrations, with one generation leaving North America towards Mexico during winter and the next generations migrating back in spring. ©Xerces Society, picture *D. plexippus* ©M. Franzke

Taken together, all those species demonstrate different behaviors but all are based on spatial orientation and at least partly on utilizing information from a sky compass. This thesis focuses on the sky-compass system of honeybees and locusts and therefore a more detailed introduction into the relevant sky-compass cues, as well as the ethology and neuroanatomy of those species is provided in the following sections.

---

## SKY-COMPASS SIGNALS

The most prominent and by diurnal insects primarily used cue in the sky is the sun itself. If the sun is visible, insects use its position as a reference point for spatial orientation for the individual behaviors. The same is true at night for the moon or patterns at the night sky, like the Milky Way. These night sky cues have been shown to serve as a basing point for orientation in nocturnal insects, for example in some dung beetle species (Dacke et al. 2013). If the sun is obscured during the day, for example by clouds, many insects are able to resort to other cues. One important feature of the blue sky is the polarized light that forms a specific pattern. Physically, unpolarized sunlight can be described as transverse waves with the electric field components of the light oscillating in every possible direction perpendicular to the direction of propagation. If sunlight enters the earth's atmosphere those oscillating waves get scattered by atmospheric molecules and particles in a way that polarizes the light, meaning one oscillation plane is predominant. This scattering phenomenon is called "Rayleigh scattering", and leads to a polarization pattern in concentric circles perpendicular to the sun. With 75% oscillation in one plane, the highest degree of polarization is reached 90° away from the sun (Strutt, 1871; Brines and Gould, 1982). If polarization-sensitive insects see a blue patch of the sky, they are able to deduce the position of the sun from the specific orientation of the polarization pattern (Fig. 2A;

Wehner, 1989; Wehner, 2001; Homberg, 2004). Another physical property of the blue sky is the spectral or intensity gradient. Due to the light scattering in the atmosphere, short-wavelength light (300-460 nm) is relatively homogeneously distributed across the sky while the intensity of long-wavelength light (460-700 nm) is higher on the solar hemisphere than on the opposite sky hemisphere (Fig. 2B & C).

## A Polarization pattern

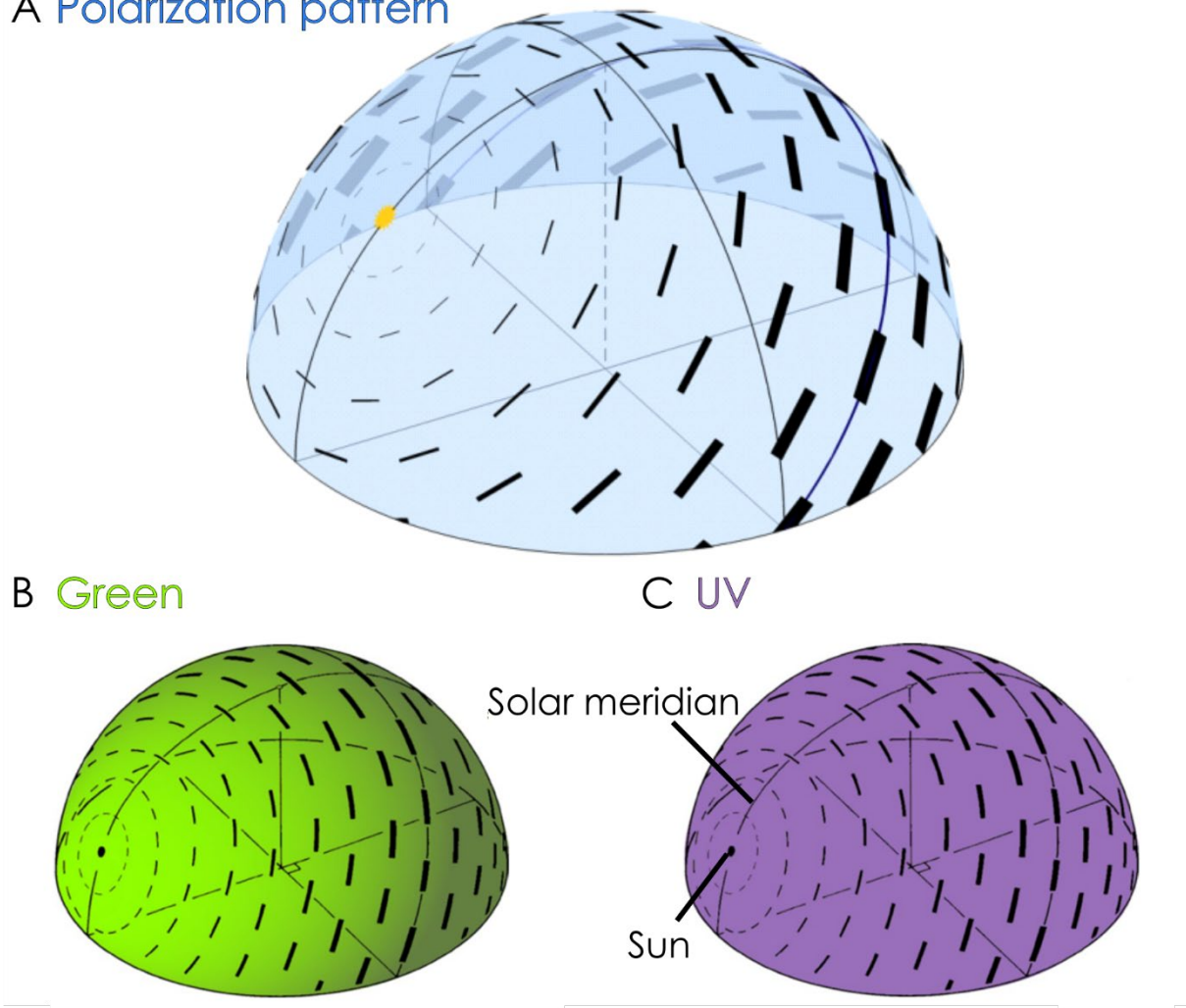


**Fig. 2: Illustrations of the celestial dome and physical properties of the blue sky.** A: Rayleigh scattering of unpolarized sunlight in the earth's atmosphere leads to a distinct pattern of the electric field vectors of partly polarized light. The pattern is arranged in concentric circles around the sun, with the highest degree of polarization  $90^\circ$  away from the sun (indicated in the thickness of the bars). ©K. Pfeiffer. B: Light scattering causes long-wavelength light, indicated by green color, to have a higher intensity in the solar hemisphere than in the anti-solar side. Short-wavelength UV light is distributed uniformly causing a spectral gradient across the sky with a higher chromatic contrast close to the sun. Adapted from el Jundi et al., 2014.

This leads to a spectral gradient with a higher ratio of long- and short-wavelength light in the solar hemisphere than in the antisolar hemisphere that some insects can utilize for orientation purposes (Coemans et al., 1994; el Jundi et al., 2014).

---

## WESTERN HONEYBEE (*APIS MELLIFERA*)

The Western honeybee is the main model organism used in this thesis. Honeybees are eusocial insects, living in a hive with up to 80,000 individuals. Their social network has a defined structure, with one queen as the only fertile female, a few hundred male drones in early summer during mating season, and sterile female worker bees (Fig. 3).



**Fig. 3: Morphology of the three castes in a honeybee colony.** A: The queen bee is larger than the worker bees, especially due to the elongated abdomen. B: Female worker bee. C: Male drones are identifiable by their large eyes that are double the size of worker bee or queen eyes. The body size is between queen and worker bees. © A. Wild

The worker bees fulfill different age-dependent tasks in the bee colony. After hatching, they operate first as nursing bees, cleaning and feeding the brood. Getting older, they shift to building honeycombs and covering the brood with wax. 20 days after hatching, worker bees transition from the inside of the hive to the outside world. First, they stay as guards at the nest entrance and then they start to forage, collecting water, pollen, and nectar. They forage until they reach their natural life expectancy of five to six weeks (reviewed by Kilani, 1999). Like other central place foragers, honeybees need a reliable orientation system to find their way home after a long tortuous outbound flight. Over 70 years ago, it has been shown in behavioral studies that bees utilize the position of the sun but are also able to resort to the polarization pattern of the blue sky and landmarks for orientation (von Frisch, 1949; Brines and Gould, 1979; Wehner et al., 1996). In addition to their foraging behavior, honeybees exhibit a remarkable and unique behavior that is based on spatial orientation as well: the waggle dance. Foraging bees that are returning from a worthwhile food source give important information to other forager bees in the hive through the waggle

dance, recruiting them to collect there as well. By walking and turning on the combs in a very distinct way, while vibrating with the abdomen, the dancing bee encodes multiple parameters that are tailored to that specific foraging path. The angle between the food source and the current position of the sun is encoded as well as the distance from the hive (von Frisch, 1949). The recruited bees learn all those information for spatial guidance in darkness in the hive, mainly over tactile input via vibrations of the dancing bee. That means the returning forager has to encode visual information from the outside world into vibrations and walking movements on vertical combs in the hive, while the recruits have to decode those the information and align them with visual input when they forage themselves. Even though the waggle dance has been described decades ago on a behavioral level and ethologists decoded the contained information, it is still vastly unknown how honeybees manage to precisely transition between those considerably different modalities. The underlying neural network is not discovered yet and therefore it is uncharted how and where the complex integration of visual and tactile processing, learning, and memory is taking place in the brain. Nevertheless, it is clear that those behaviors, foraging and the waggle dance, are based on spatial orientation (Menzel et al., 2005). Due to those behaviors, the honeybee is an unique model organism that has been in the focus of ethological investigations for some time but the underlying neural system is brought to the fore just recently. The general anatomy of the honeybee brain has been investigated in a couple of studies, leading to a coarse three-dimensional average shape atlas (Fig. 4; Brandt et al., 2005). In this thesis the neuroanatomy (chapter I and II) and physiology (chapter III) of neurons involved in the sky-compass system has been investigated on several levels and partly compared to other model organisms.



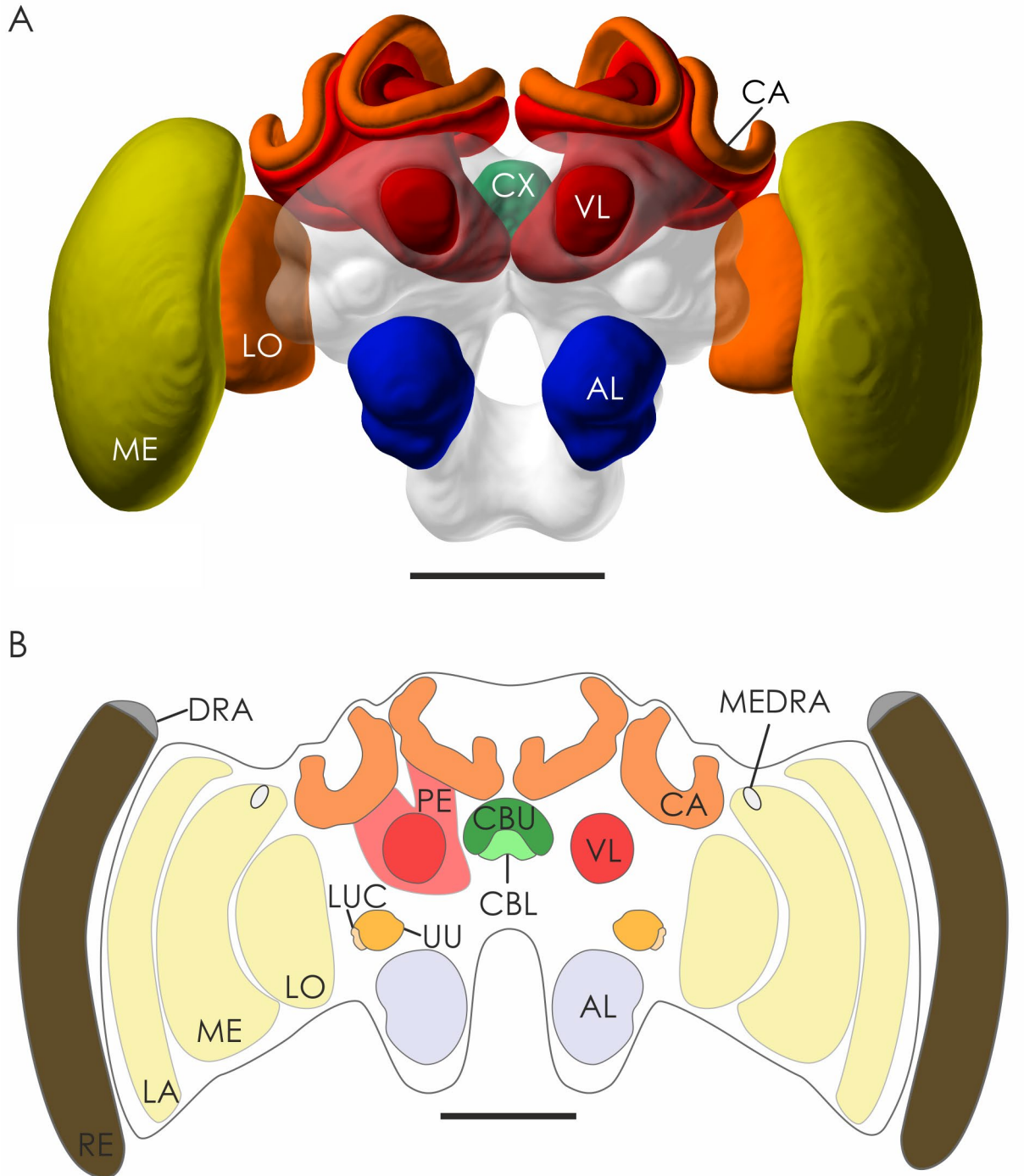


**Fig. 4: Illustrations of the brain of the western honeybee *Apis mellifera*.** A: Three-dimensional average shape atlas of major neuropils in the honeybee brain. Adapted from Brandt et al. (2005) and the insect brain database ([insectbraindb.org](http://insectbraindb.org)) B: Frontal schematic drawing of the honeybee brain and prominent neuropils. AL: antennal lobe, CA: calyx, CBU: upper division of the central body, CBL: lower division of the central body, CX: central complex, DRA: dorsal rim area, LA: lamina, LO: lobula, LUC: lower unit complex of the anterior optic tubercle, ME: medulla, MEDRA: dorsal rim area of the medulla, PE: peduncle, RE: retina, VL: vertical lobe of the mushroom body. Scale bars = 500  $\mu$ m.



## DESERT LOCUST (*SCHISTOCERCA GREGARIA*)

Desert locusts occur in two states: solitary and gregarious, with completely different behaviors and significant morphological distinctions (Fig. 5A & B). Solitary animals are for example nocturnal, while gregarious locusts are active and migrate during the day. Desert locusts are known to form swarms of millions of animals in their gregarious phase, migrating long distances across the desert of Africa and the Middle East. That migration appears seasonal to find new feeding grounds and mating partners (Fig. 5C; reviewed in Symmons and Cressman, 2001).

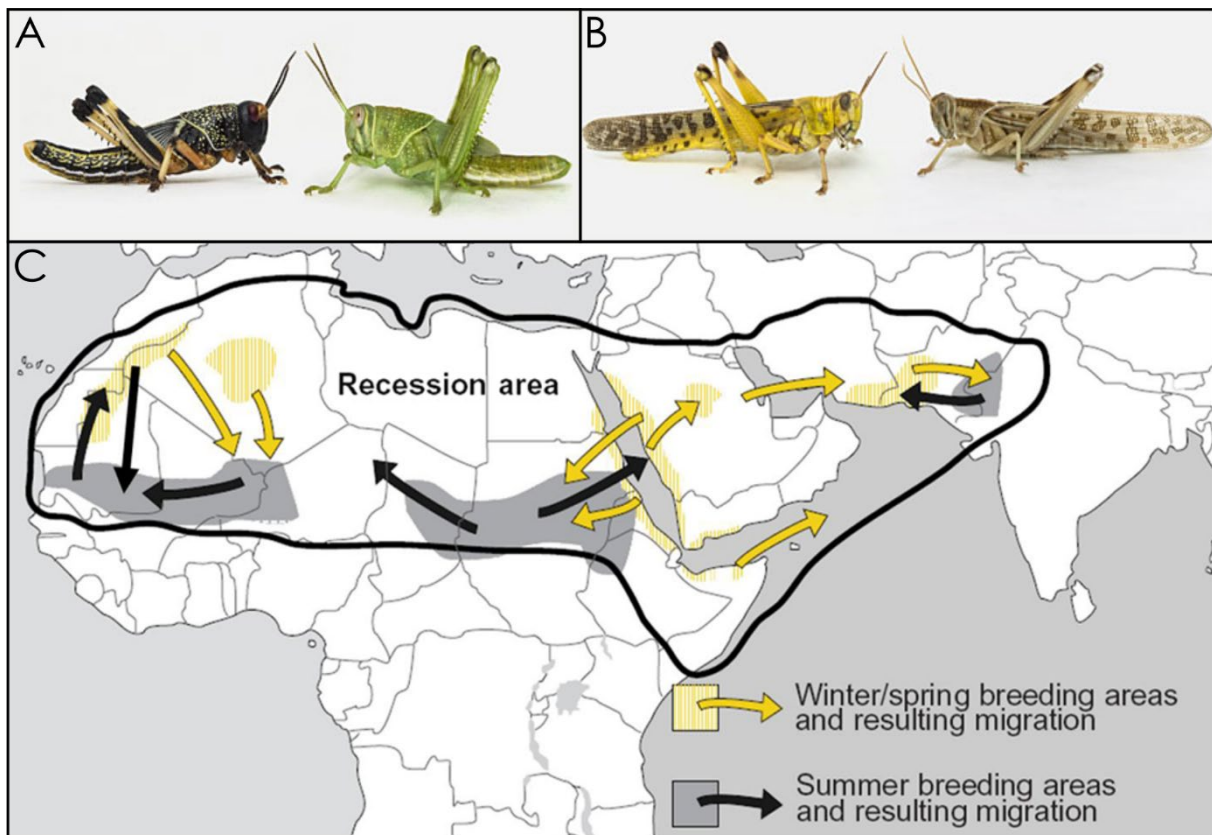


**Fig. 5: Morphology of solitary and gregarious desert locusts (*Schistocerca gregaria*) and migration map.** A: Morphological comparison of nymphs in the gregarious (left side) versus the solitary stage (right side). Gregarious nymphs show an aposematic coloration, while solitary ones have a more concealing appearance. B: Morphological comparison between a male adult locust in the gregarious stage (left side), versus one in solitary stage (right side), with the gregarious one exhibiting a bright mustard yellow coloring, while the solitary locusts appear brown. A&B adapted from Burrows et al., 2011. C: Map of the seasonal migrations areas of desert locust swarms in northern Africa and the Middle East. Adapted from Symmons and Cressman, 2001.

How locusts keep a certain heading over a long distance has been investigated for over 70 years, with first behavioral observations suggesting, that the swarms are just flying downwind (Rainey, 1951). A behavioral study of flying tethered locusts showed later that the animals respond with a 180°-periodic turning movement to a dorsally rotating polarizer (Mappes and Homberg, 2004). This experiment demonstrated that locusts are not only able to perceive linear polarized light but also have a behavioral response to it. This suggests that locusts are capable of using information of the celestial polarization pattern for orientation purposes. Based on that hypothesis, numerous anatomical and physiological studies in the brain of locusts have been conducted, revealing distinct neuronal pathways for polarized light information as well as multitudinous involved neuron types and neuropils (Homberg, 2004; reviewed in Homberg, 2015). In many of those studies, the physiological response of polarized light sensitive neurons to short-wavelength UV and long-wavelength green unpolarized light has been investigated. On top of that, a detailed three-dimensional average shape atlas has been established for the locust brain (Fig. 6A; Kurylas et al., 2008; von Hadeln et al., 2018). That opened the possibility to register neurons into the atlas to create a network model of the sky-compass pathway (for example el Jundi et al., 2010; von Hadeln et al., 2019). Taken all those studies together, earlier beliefs that locusts are migrating by just flying downwind are unlikely. The whole body of knowledge that has been acquired over the past years makes the desert locust the longest and most extensively investigated model organism for celestial compass orientation. However, many aspects of the sky-compass system are still unknown, especially the connection patterns on an ultrastructural level that are the basis for integration networks. Hence, a part of this thesis investigated the anatomy and ultrastructure of a neuropil of the sky-compass system called the posterior optic tubercle that has so far received less attention but might be important for the integration of time information into the network (chapter IV).

---

## THE SKY-COMPASS PATHWAY IN THE DESERT LOCUST

In the desert locust, there are two sky-compass pathways described anatomically and to some extend physiologically through immunohistochemical labelings, dye injections, and single cell recordings. One is called the anterior sky-compass pathway while the second one is the posterior sky-compass pathway (Fig. 6B; el Jundi et al., 2010). Most neurons involved in both of them have been shown to

be sensitive to polarized light and other stimuli that imitate skylight information like an unpolarized green light spot mimicking the sun (Kinoshita et al., 2007; Pfeiffer and Homberg, 2007; el Jundi and Homberg, 2010; Pegel et al., 2018). The input of polarized light to this pathway is captured by a distinct region of the retina of the compound eyes called the dorsal rim area (DRA). Due to the aligned arrangement of the rhabdomeres of the receptor cells and other specializations of the ommatidia, the DRA is specialized in the perception of polarized light. From the receptor cells the information is brought to the dorsal rim area of the lamina (LADRA) via short visual fibers, while long visual fibers run through the lamina into the medulla where they branch in the dorsal rim area of the medulla (MEDRA; Schmeling et al., 2015). Transmedulla neurons transmit the input from the MEDRA further towards the central brain into the lower unit (LU) of a neuropil called anterior optic tubercle (AOTU; el Jundi et al., 2011). From there intertubercle neurons connect one AOTU to the tubercle of the contralateral brain hemisphere. In addition, tubercle-bulbs neurons (TuBu neurons, formerly called TuLAL neurons) run through the anterior optic tract (AOT) towards the lateral complex (LX), where they branch in two distinct subcompartments called the medial and lateral bulbs (MBU and LBU; Kinoshita et al., 2007; Pfeiffer and Homberg, 2007; Träger et al., 2008). Regarding their size, the synaptic endings are remarkable with a diameter of up to 9 – 11  $\mu\text{m}$ . They build large microglomerular synaptic complexes with tangential neurons of the central body (TL neurons) as postsynaptic partners. TL neurons bring the information into the lower division of the central body (CBL), a subcompartment of a neuropil group in the central brain called the central complex (CX; Müller et al., 1996; Träger et al., 2008; Heinze et al., 2009). This group consists of an upper (CBU) and a lower division of the central body (CBL), paired noduli (NO), and the protocerebral bridge (PB); but TL neurons only branch in the CBL. Different types of columnar, pontine, and tangential neurons interconnect all neuropils of the CX and the adjacent bilateral LX (Heinze and Homberg, 2008).

The CX has been in the focus of numerous studies across different insect species for the last decade leading to astonishing findings about the role and the mechanisms of this neuropil group. Those studies showed that the CX plays for example a role in the integration of visual cues, especially spatial information from sky-compass cues like polarized light. In addition, a spatial representation of visual cues like landmarks has been demonstrated as well as spatial visual memory features.

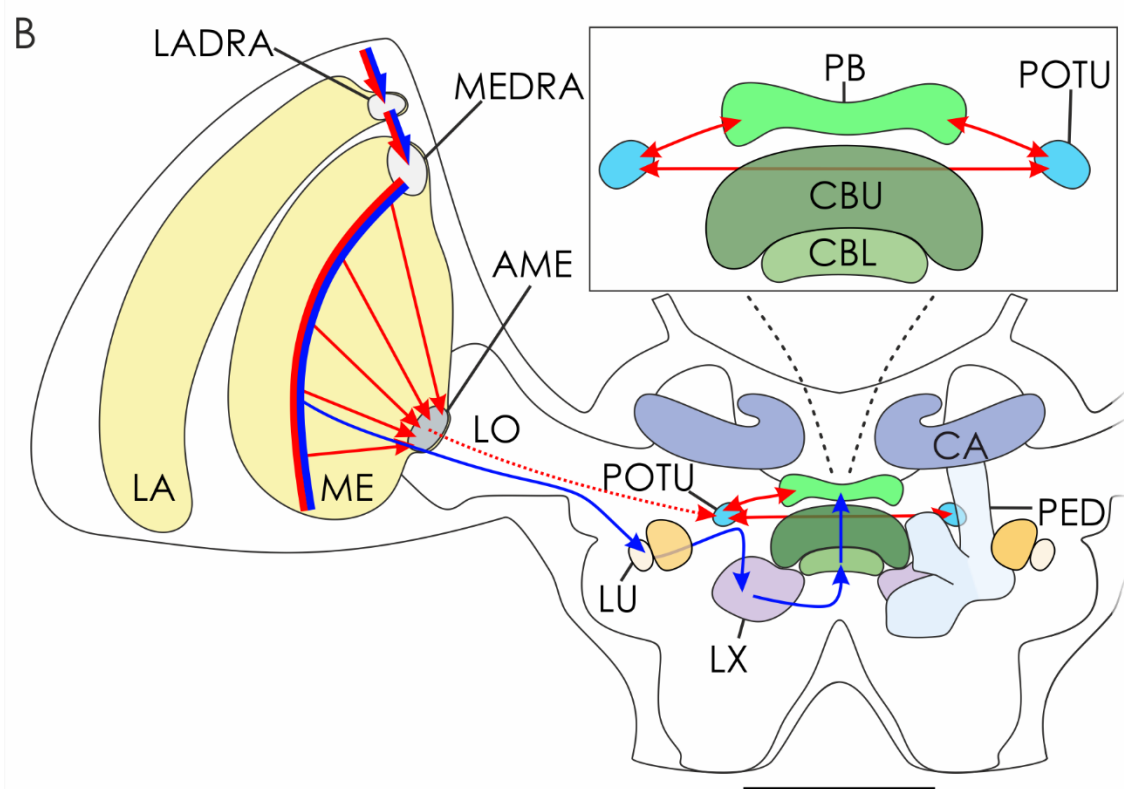
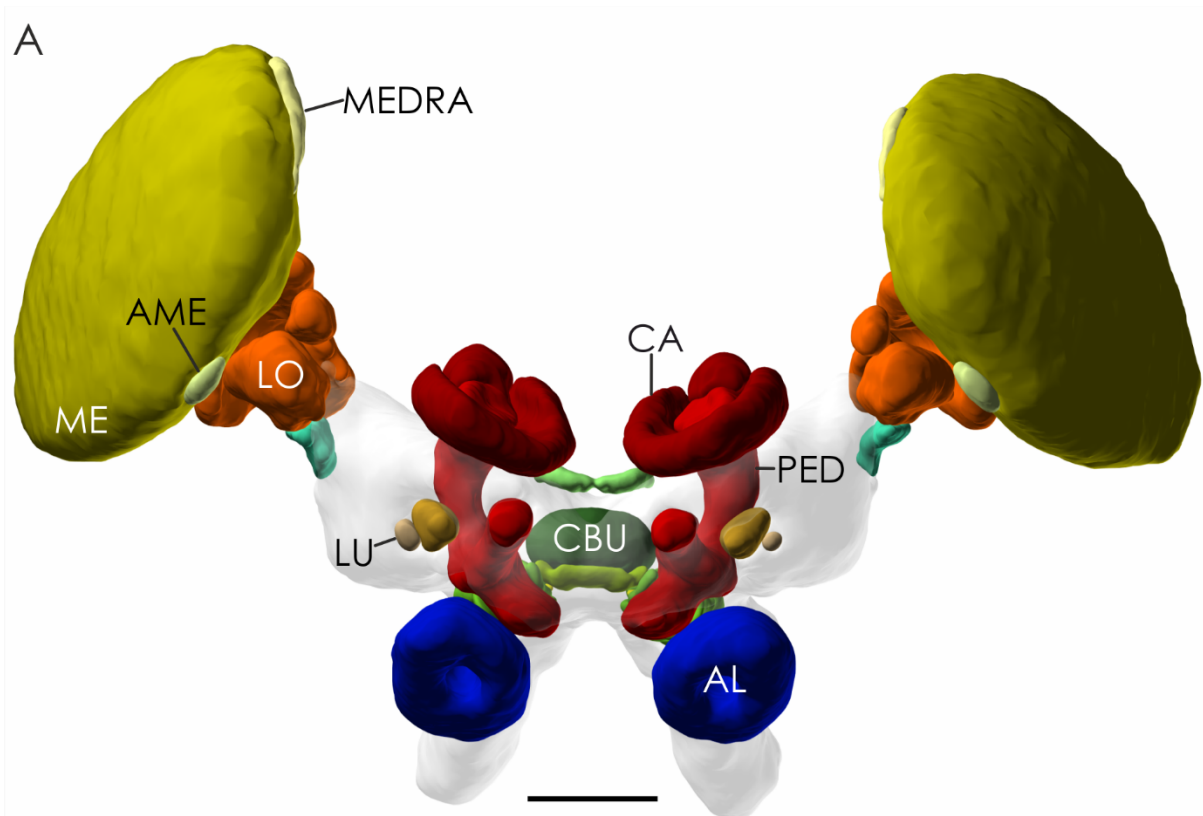


**Fig. 6: Illustrations of the brain of the desert locust *Schistocerca gregaria* and the two sky-compass pathways.** A: Three-dimensional average shape atlas of important neuropils within the locust brain. Adapted from Kurylas et al. (2008) and the insect brain database (insectbraindb.org). B: Frontal schematic diagram of the locust brain, showing the anterior sky-compass pathway (blue) and the posterior sky-compass pathway (red) from the optic lobe to the central complex. The expanded diagram shows the connections in the posterior sky-compass pathway of the posterior optic tubercles with each other and the protocerebral bridge. AME: accessory medulla, CA: calyx, CBL: lower division of the central body, CBU: upper division of the central body, LA: lamina, LADRA: dorsal rim area of the lamina, LO: lobula, LU: lower unit of the anterior optic tubercle, LX: lateral complex, ME: medulla, MEDRA: dorsal rim area of the medulla, PB: protocerebral bridge, PED: peduncle, POTU: posterior optic tubercle. Scale bars = 500  $\mu$ m.

The integration of visual input and the transformation into a spatial memory system leads to an output of directional control of walking or flight behavior of the CX (reviewed in Pfeiffer and Homberg, 2014; Turner-Evans and Jayaraman, 2016).

The posterior sky-compass pathway runs to the MEDRA in parallel to the anterior one. From there, medulla tangential neurons connect the MEDRA with the accessory medulla (AME). Further downstream in the central brain, neurons from the AME project to the posterior optic tubercle (POTU), a small neuropil located laterally to the PB of the CX. Beyond that, the POTU is connected with the PB via tangential neurons of the protocerebral bridge (TB neurons), and via posterior intertubercle neurons (pTuTu) reciprocally with the contralateral counterpart. Except for the connections from the AME to the POTU, that have not been studied physiologically yet, all involved types of neuron are sensitive to the oscillation plane of polarized light (el Jundi and Homberg, 2010; Beetz et al., 2015). How all those different parts of the sky-compass system are integrated with each other is not fully understood yet, therefore further anatomical and physiological studies of the cell-to-cell connection patterns are vital to uncover this complex network.

---

## CIRCADIAN RHYTHM AND TIME COMPENSATION

A circadian rhythm describes an approximately 24-hour long, periodic, endogenous, self-sustaining rhythm of organisms, synchronized to the length of the day. There are, in some instances, huge changes in the physiological functions, endocrine systems, and behaviors like activity in the organism between periods, for example day versus night (reviewed in Numata et al., 2015). Periodically changing

environmental properties like light or temperature can act as "Zeitgeber", shifting a period partly or entirely (Aschoff and Pohl, 1978). A circadian rhythm has been described across kingdoms, in animals, plants, fungi and even some bacteria (Saini et al., 2019). There are rhythmic processes that are not bound by a 24-hours length, for example infradian rhythms that are in some cases connected to the seasons, like in hibernation or the migration of certain animals (Lloyd and Stupfel, 1991).

The circadian rhythm is controlled and maintained by a circadian clock. Studies in cockroaches, fruit flies, and other insects showed that the center of the circadian clock is the AME and that its associated neurons function as pacemakers, influencing behaviors that are controlled by the circadian rhythm (reviewed by Helfrich-Förster et al., 1998; Homberg et al., 2003). Important neuropeptides, secreted in the circadian clock system, are pigment dispersing factors (PDF) which are encoded by the eponymous gene and closely related to the crustacean pigment dispersing hormone (PDH) family (Helfrich-Förster et al., 2000). The circadian clock in insects is not only important to synchronize the activity level with the preferred activity time of the day but also in some species to stabilize orientation behaviors. It has been shown that central place foragers like ants and honeybees who orient themselves with the help of sky-compass cues compensate for angular changes between the solar azimuth and the targeted direction in course of the day (reviewed by Lindauer, 1960; Wehner, 1992). That holds true for the individual foragers but also for honeybees that communicate the position of food in relation to the sun to recruits via the waggle dance. Here, it has been shown that honeybees can dance inside the hive without seeing the sun in an updated and therefore correct direction over a period of several hours (Lindauer, 1954). Besides central place foragers, all insects that use the position of the sun over a longer period of time need to update their own position. Therefore, they need that time component in their orientation system to compensate for solar azimuth changes. Monarch butterflies, that use sky-compass cues to keep a certain heading, have to adjust their direction as well, otherwise they would not be able to migrate into a specific direction or to a specific place. Behavioral studies in monarch butterflies confirmed the ability to compensate for the azimuthal changes in the sun's position (Mouritsen and Frost, 2002) and single cell recordings in locusts pointed towards time compensated neuronal responses (Pfeiffer and Homberg, 2007). However, how and where exactly the time compensating information is factored into the sky-compass system in the brain is still poorly understood. Therefore, chapter IV of this thesis focused on the ultrastructure of connections in the POTU and investigated

the linkage of the AME with the CX by using, inter alia, immunogold labeling techniques against PDH.

---

## SCOPE OF THIS WORK

For many years, honeybees and locusts have been model organisms to study orientation behavior. In both species, behavioral responses to sky-compass cues have been recorded and therefore their ability to use them for their respective orientation movements has been demonstrated. While in locusts the different layers of the neural basis for sky-compass orientation have been investigated in numerous studies the picture changes in honeybees. Even though the waggle dance and in connection to that, the orientation capacities have been decoded decades ago, the neural system has so far received less attention. To this end, in the first study of this thesis the sky-compass pathway in honeybees has been investigated at the anatomical level with dye injections and immunohistochemical methods from the DRA to the lower unit complex (LUC) of the AOTU (chapter I). The involved types of neuron are comparable to those in locusts and show high anatomical similarities between species. Furthermore, in one type of neuron, so called transmedulla neurons, an interesting anatomical feature has been identified. Those neurons run through a very specific layer of the medulla towards the AOTU. In the same layer PDF-immunoreactive fibers have been traced and show a strong overlapping staining pattern with the transmedulla neurons. This finding suggests that in that layer of the medulla the PDF-ir neurons could provide input from the circadian clock into the sky-compass system. The second study traced the pathway in honeybees further from the LUC of the AOTU towards the central body of the CX (chapter II). Here, bulk injections into the LUC, combined with an immunostaining against gamma-aminobutyric acid, revealed connections between TuLAL neurons, now called TuBu neurons, and TL neurons. The connection between the two neuronal types is outstanding in the sky-compass pathway due to the uncommon large size of the synaptic complexes in the bulbs of the LX. In addition to the investigation at the light microscopic level, a three-dimensional model of the complexes has been generated. To investigate a possible cell-to-cell connection between the two neuronal types, the synaptic complexes were characterized on a cellular level by investigations with a transmission electron microscope. The third project of this thesis evolved around a new method to perform physiological studies on the sky-compass pathway in honeybees (chapter III). The aim was to establish calcium imaging in neurons of the sky-compass network while

tethered animals show walking behavior on a treadmill. For that, an innovative preparation protocol was developed as well as a novel setup in a multiphoton microscope. The successful establishment of this unprecedented approach in honeybees has been demonstrated by promising preliminary data. The last project was performed in desert locusts, more precisely in the posterior sky-compass pathway in the locust brain (chapter IV). This pathway has been described anatomically and for the most parts physiologically in previous studies. Due to anatomical data of overlapping branching patterns, it has been hypothesized that this pathway brings circadian clock information from the AME via the POTU into the CX. Here, it has been shown at the cellular level, that neurons from the AME containing PDH provide input into the POTU. Furthermore, the study showed that TB neurons are postsynaptic in this neuropil, meaning they receive input in the POTU. Together with a newly established three-dimensional average shape atlas of the POTU that has now been included in the locust standard brain, the last study of this thesis provides, as well as the other three studies, important details of the sky-compass pathways in honeybees and locusts. Furthermore, the established new method of calcium imaging in behaving honeybees provides a fruitful basis for further studies of that complex topic.



## REFERENCES

- Aschoff, J., Pohl, H. 1978. Phase relations between a circadian rhythm and its Zeitgeber within the range of entrainment. *Naturwissenschaften*. 65, 80-84. DOI: 10.1007/BF00440545
- Beetz, J.M., el Jundi, B., Heinze, S., Homberg, U. 2015. Topographic organization and possible function of the posterior optic tubercles in the brain of the desert locust *Schistocerca gregaria*. *J. Comp. Neurol.* 523:1589-1607. DOI: 10.1002/cne.23736
- Brandt, R., Rohlfig, T., Rybak, J., Kroficz, S., Maye, A., Westerhoff, M., Hege, H.C., Menzel, R. 2005. Three-dimensional average-shape atlas of the honeybee brain and its applications. *J. Comp. Neurol.* 492:1-19. DOI: 10.1002/cne.20644
- Brines, M.L., Gould, J.L. 1979. Bees have rules. *Science*. 206:571-3. DOI: 10.1126/science.206.4418.571
- Brines, M.L., Gould, J.L. 1982. Skylight polarization patterns and animal orientation. *J. Exp. Biol.* 96, 69-91.
- Burrows, M., Rogers, S.M., Ott, S.R. 2011. Epigenetic remodeling of brain, body and behaviour during phase change in locusts. *Neural Syst. Circuits*. 1:11. DOI: 10.1186/2042-1001-1-11
- Card, G.M. 2012. Escape behaviors in insects. *Curr. Opin. Neurobiol.* 22:180-186. DOI: 10.1016/j.conb.2011.12.009
- Coemans, M.A.J.M, Vos Hzn, J.J., Nuboer, J.F.W. 1994. The relations between celestial colour gradients and the position of the sun, with regard to the sun compass. *Vision Res.* 34, 1461-1470. DOI: 10.1016/0042-6989(94)90148-1
- Collett, T.S. 2008. Insect navigation: Visual panoramas and the sky compass. *Curr. Biol.* 22, 1058-1061. DOI: 10.1016/j.cub.2008.10.006
- Dacke, M., Nilsson, D.E., Scholtz, C.H., Byrne, M.J., Warrant, E.J. 2003. Insect orientation to polarized moonlight. *Nature*. 424:33. DOI: 10.1038/424033a
- Dacke, M., Byrne, M.J., Scholtz, C.H., Warrant, E.J. Lunar orientation in a beetle. *Proc. Biol. Sci.* 271:361-365. DOI: 10.1098/rspb.2003.2594.
- Dacke, M., Byrne, M.J., Smolka, J., Warrant, E., Baird, E.J. 2012. Dung beetles ignore landmarks for straight-line orientation. *J. Comp. Physiol. A.* 199, 17-23. DOI: 10.1007/s00359-012-0764-8
- Dacke, M., Baird, E., Byrne, M., Scholtz, C.H., Warrant, E.J. 2013. Dung beetles use the Milky Way for orientation. *Curr. Biol.* 23, 298-300. DOI: 10.1016/j.cub.2012.12.034
- Dacke, M., Bell, A.T.A., Foster, J.J., Baird, E.J., Strube-Bloss, M.F., Byrne, M.J., el Jundi, B. 2019. Multimodal cue integration in the dung beetle compass. *PNAS*. 116, 14248-14253. DOI: 10.1073/pnas.1904308116
- el Jundi, B., Homberg, U. 2010. Evidence for the possible existence of a second polarization-vision pathway in the locust brain. *J. Insect Physiol.* 56, 971-979. DOI: 10.1016/j.jinsphys.2010.05.011
- el Jundi, B., Heinze, S., Lenschow, C., Kurylas, A., Rohlfig, T., Homberg, U. 2010. The locust standard brain: a 3D standard of the central complex as a platform for neural network analysis. *Front. Syst. Neurosci.* 3:21. DOI: 10.3389/neuro.06.021.2009

- el Jundi, B., Pfeiffer, K., Homberg, U. A distinct layer of the medulla integrates sky compass signals in the brain of an insect. *PLoS ONE*. 6:e27855. DOI: 10.1371/journal.pone.0027855
- el Jundi, B., Pfeiffer, K., Heinze, S., Homberg, U. 2014. Integration of polarization and chromatic cues in the insect sky compass. *J. Comp. Physiol. A*. 200:575-89. DOI:10.1007/s00359-014-0890-6
- el Jundi, B., Foster, J.J., Byrne, M.J., Baird, E., Dacke, M. 2015. Spectral information as orientation cue in dung beetles. *Biology Letters*. 11:20150656. DOI: 10.1098/rsbl.2015.0656.
- Fleischmann, P.N., Grob, R., Müller, V.L., Wehner, R., Rössler, W. 2018. The geomagnetic field is a compass cue in *Cataglyphis* ant navigation. *Curr. Biol.* 28, 1140-1444. DOI: 10.1016/j.cub.2018.03.043
- Grob, R., Fleischmann, P.N., Rössler, W. 2019. Learning to navigate – how desert ants calibrate their compass system. *Neuroforum*. 25:109-120. DOI: 10.1515/nf-2018-0011
- Hansson, B.S. 1995. Olfaction in Lepidoptera. *Experientia*. 51, 1003-1027. DOI: 10.1007/BF01946910
- Heinze, S., Homberg, U. 2008. Neuroarchitecture of the central complex of the desert locust: intrinsic and columnar neurons. *J. Comp. Neurol.* 511:454-478. DOI: 10.1002/cne.21842
- Heinze, S., Gotthardt, Homberg, U. 2009. Transformation of polarized light information in the central complex of the locust. *J. Neurosci.* 29:11783-11793. DOI: 10.1523/JNEUROSCI.1870-09.2009
- Heinze, S., Reppert, S.M. 2011. Sun compass integration of skylight cues in migratory monarch butterflies. *Neuron*. 69, 345-358. DOI: 10.1016/j.neuron.2010.12.025
- Heinze, S., Narendra, A., Cheung, A. 2018. Principles of insect path integration. *Curr. Biol.* 28, R1043-1058. DOI: 10.1016/j.cub.2018.04.058
- Helfrich-Förster, C., Stengl, M., Homberg, U. 1998. Organization of the circadian system in insects. *Chronobiol. Int.* 15, 567-594. DOI: 10.3109/07420529808993195
- Helfrich-Förster, C., Täuber, M., Park, J.H., Mühlig-Versen, M., Schneuwly, S., Hofbauer, A. 2000. Ectopic expression of the neuropeptide pigment-dispersing factor alters behavioral rhythms in *Drosophila melanogaster*. *J. Neurosci.* 20:3339-3353. DOI: 10.1523/JNEUROSCI.20-09-03339.2000
- Hoinville, T., Wehner, R. 2018. Optimal multiguidance integration in insect navigation. *PNAS*. 115:2824-2829. DOI: 10.1073/pnas.1721668115
- Homberg, U., Reischig, T., Stengl, M. 2003. Neural organization of the circadian system of the cockroach *Leucophaea maderae*. *Chronobiol. Int.* 20:577-91. DOI: 10.1081/CBI-120022412
- Homberg, U. 2004. In search of the sky compass in the insect brain. *Naturwissenschaften*. 91:199-208. DOI: 10.1007/s00114-004-0525-9
- Homberg, U. 2015. Sky compass orientation in desert locusts – evidence from field and laboratory studies. *Front. Behav. Neurosci.* 9:346. DOI: 10.3389/fnbeh.2015.00346
- Khalidy, L., Tocco, C., Byrne, M., Baird, E., Dacke, M. 2018. Straight-line orientation in the woodland-living beetle *Sisyphus fasciculatus*. *J. Comp. Physiol. A*. DOI: 10.1007/s00359-019-01331-7
- Kilani, M. 1999. Biology of the honeybee. *CIHEAM*. Pp: 9-24.

- Kinoshita, M., Pfeiffer, K., Homberg, U. 2007. Spectral properties of identified polarized-light sensitive interneurons in the brain of the desert locust *Schistocerca gregaria*. *J. Exp. Biol.* 210, 1350-1361. DOI: 10.1242/jeb.02744
- Kurylas, A.E., Rohlfig, T., Kroficz, S., Jenett, A., Homberg, U. 2008. Standardized atlas of the brain of the desert locust, *Schistocerca gregaria*. *Cell Tissue Res.* 333:125-145. DOI: 10.1007/s00441-008-0620-x
- Lindauer, M. 1954. Dauertänze im Bienenstock und ihre Beziehung zur Sonnenbahn. *Naturwissenschaften.* 41:506-507.
- Lloyd, D., Stupfel, M. 1991. The occurrence and functions of ultradian rhythms. *Biol. Rev. Comp. Physiol. Soc.* 66:275-299. DOI: 10.1111/j.1469-185x.1991.tb01143.x
- Mappes, M., Homberg, U. 2004. Behavioral analysis of polarization vision in tethered flying locusts. *J. Comp. Physiol. A.* 190:61-68. DOI: 10.1007/s00359-003-0473-4
- Menzel, R., de Marco, R.J., Greggers, U. 2005. Spatial memory, navigation and dance behavior in *Apis mellifera*. *J. Comp. Physiol. A.* DOI: 10.1007/s00359-006-0136-3
- Mouritsen, H., Frost, B.J. 2002. Virtual migration in tethered flying monarch butterflies reveals their orientation mechanisms. *PNAS.* 99, 10162-10166. DOI: 10.1073/pnas.152137299
- Müller, M., Homberg, U., Kühn, A. 1996. Neuroarchitecture of the lower division of the central body in the brain of the locust (*Schistocerca gregaria*). *Cell Tissue Res.* 288:159-176. DOI: 10.1007/s004410050803
- Numata, H., Miyazaki, Y., Ikeno, T. 2015. Common features in diverse insect clocks. *Zool. J. lett.* 1:10. DOI: 10.1186/s40851-014-0003-y
- Pegel, U., Pfeiffer, K., Homberg, U. Integration of celestial compass cues in the central complex of the locust brain. *J. Exp. Biol.* 221: jeb171207. DOI: 10.1242/jeb.171207
- Pfeffer, S.E., Wittlinger, M. 2016. Optic flow odometry operates independently of stride integration in carried ants. *Science.* 353:1155-1157. DOI: 10.1126/science.aaf9754
- Pfeiffer, K., Homberg, U. 2007. Coding of azimuthal directions via time-compensated combination of celestial compass cues. *Curr. Biol.* 17, 960-965. DOI: 10.1016/j.cub.2007.04.059
- Pfeiffer, K., Homberg, U. 2014. Organization and functional roles of the central complex in the insect brain. *Annu. Rev. Entomol.* 59:165-84. DOI: 10.1146/annurev-ento-011613-162031
- Rainey, R.C. 1951. Weather and the movement of locust swarms: a new hypothesis. *Nature.* 168, 1057-1060. DOI: 10.1038/1681057a0
- Saini, R., Jaskolski, M., Davis, S.J. 2019. Circadian oscillator proteins across the kingdoms of life: structural aspects. *BCM Biol.* 17:13. DOI: 10.1186/s12915-018-0623-3
- Srinivasan, M.V. 2014. Going with the flow: a brief history of the study of the honeybee's navigational "odometer". *J. Comp. Physiol. A.* 200:563-573. DOI: 10.1007/s00359-014-0902-6
- Strutt, J.W. 1871. On the light from the sky, its polarization and colour. *Philos. Mag.* 41:107-120. DOI: 10.1080/14786447108640452
- Symmons, P. M., Cressman, K. 2001. Desert Locust Guidelines: Biology and Behavior. Rome: Food and Agriculture Organization of the United Nations.

- Träger, U., Wagner, R., Bausenwein, B., Homberg, U. 2008. A novel type of microglomerular synaptic complex in the polarization vision pathway of the locust brain. *J. Comp. Neurol.* 506:288-300. DOI: 10.1002/cne.21512
- Tribe, G.D., Burger, B.V. 2011. Olfactory ecology. In *Ecology and Evolution of Dung Beetles*. Pp. 87-106. Wiley-Blackwell. DOI: 10.1002/9781444342000.ch5
- Turner-Evans, D.B., Jayaraman, V. 2016. The insect central complex. *Curr. Biol.* 26, R453-R457. DOI: 10.1016/j.cub.2016.04.006.
- Vitzthum, H., Müller, M., Homberg, U. 2002. Neurons of the central complex of the locust *Schistocerca gregaria* are sensitive to polarized light. *J. Neurosci.* 22:1114-1125. DOI: 10.1523/JNEUROSCI.22-03-01114.2002
- von Frisch, K. 1949. Die Polarisation des Himmelslichtes als orientierender Faktor bei den Tänzen der Bienen. *Experientia* 5, 142–148. DOI: 10.1007/bf02174424
- von Hadeln, J., Althaus, V., Häger, L., Homberg, U. Anatomical organization of the cerebrum of the desert locust *Schistocerca gregaria*. *Cell Tissue Res.* 374:39-62. DOI: 10.1007/s00441-018-2844-8
- von Hadeln, J., Hensgen, R., Bockhorst, T., Rosner, R., Heidasch, R., Pegel, U., Pérez, M.Q., Homberg, U. 2019. Neuroarchitecture of the central complex of the desert locust: tangential neurons. *J. Comp. Neurol.* 528:6. DOI: 10.1002/cne.24796
- Wehner, R. 1984. Astronavigation in insects. *Annu. Rev. Entomol.* 29:277-298. DOI: 10.1146/annurev.en.29.010184.001425
- Wehner, R. 1989. Neurobiology of polarization vision. *Trends Neurosci.* 12:353-9. DOI: 10.1016/0166-2236(89)90043-x
- Wehner, R., Michel, B., Antonsen, P. 1996. Visual navigation in insects: coupling of egocentric and geocentric information. *J. Exp. Biol.* 199, 129-140.
- Wehner, R. 2001. Polarization vision – a uniform sensory capacity? *J. Exp. Biol.* 204, 2589-2596.
- Wehner, R., Müller, M. 2006. The significance of direct sunlight and polarized skylight in the ant's celestial system of navigation. *Proc. Natl. Acad. Sci.* 103:12575-12579. DOI: 10.1073/pnas.0604430103.
- Wehner, R. 2008. The desert ant's navigational toolkit: Procedural rather than positional knowledge. *Navigation.* 55, 101-114. DOI: 10.1002/j.2161-4296.2008.tb00421.x.
- Wittlinger, M., Wehner, R., Wolf, H. 2006. The ant odometer: stepping on stilts and stumps. *Science.* 312:1965-1967. DOI: 10.1126/science.1126912

---

## **CHAPTER I:**

# **TRANSMEDULLA NEURONS IN THE SKY-COMPASS NETWORK OF THE HONEYBEE (*APIS MELLIFERA*) ARE A POSSIBLE SITE OF CIRCADIAN INPUT**

---



RESEARCH ARTICLE

# Transmedulla Neurons in the Sky Compass Network of the Honeybee (*Apis mellifera*) Are a Possible Site of Circadian Input

Maximilian Zeller, Martina Held, Julia Bender, Annuska Berz, Tanja Heinloth, Timm Hellfritz, Keram Pfeiffer\*

Department of Biology - Animal Physiology, Philipps-University Marburg, Marburg, Germany

\* keram.pfeiffer@staff.uni-marburg.de



## OPEN ACCESS

Citation: Zeller M, Held M, Bender J, Berz A, Heinloth T, Hellfritz T, et al. (2015) Transmedulla Neurons in the Sky Compass Network of the Honeybee (*Apis mellifera*) Are a Possible Site of Circadian Input. PLoS ONE 10(12): e0143244. doi:10.1371/journal.pone.0143244  
Editor: Eric James Warrant, Lund University, SWEDEN

Received: August 21, 2015

Accepted: November 2, 2015

Published: December 2, 2015

Copyright: © 2015 Zeller et al. This is an open access article distributed under the terms of the [Creative Commons Attribution License](https://creativecommons.org/licenses/by/4.0/), which permits unrestricted use, distribution, and reproduction in any medium, provided the original author and source are credited.

Data Availability Statement: All relevant data are within the paper and its Supporting Information files.

Funding: The authors have no support or funding to report.

Competing Interests: The authors have declared that no competing interests exist.

## ABSTRACT

Honeybees are known for their ability to use the sun's azimuth and the sky's polarization pattern for spatial orientation. Sky compass orientation in bees has been extensively studied at the behavioral level but our knowledge about the underlying neuronal systems and mechanisms is very limited. Electrophysiological studies in other insect species suggest that neurons of the sky compass system integrate information about the polarization pattern of the sky, its chromatic gradient, and the azimuth of the sun. In order to obtain a stable directional signal throughout the day, circadian changes between the sky polarization pattern and the solar azimuth must be compensated. Likewise, the system must be modulated in a context specific way to compensate for changes in intensity, polarization and chromatic properties of light caused by clouds, vegetation and landscape. The goal of this study was to identify neurons of the sky compass pathway in the honeybee brain and to find potential sites of circadian and neuromodulatory input into this pathway. To this end we first traced the sky compass pathway from the polarization-sensitive dorsal rim area of the compound eye via the medulla and the anterior optic tubercle to the lateral complex using dye injections. Neurons forming this pathway strongly resembled neurons of the sky compass pathway in other insect species. Next we combined tracer injections with immunocytochemistry against the circadian neuropeptide pigment dispersing factor and the neuromodulators serotonin, and  $\gamma$ -aminobutyric acid. We identified neurons, connecting the dorsal rim area of the medulla to the anterior optic tubercle, as a possible site of neuromodulation and interaction with the circadian system. These neurons have conspicuous spines in close proximity to pigment dispersing factor-, serotonin-, and GABA-immunoreactive neurons. Our data therefore show for the first time a potential interaction site between the sky compass pathway and the circadian clock.

## INTRODUCTION

Honeybees possess a time-compensated sun-compass, which enables them to use the solar azimuth, i.e. the horizontal component of the sun's position, as a reference direction for navigation [1]. In his seminal studies, Karl von Frisch was able to show that bees can infer the solar azimuth from a patch of blue sky [2]. Using a polarizer von Frisch manipulated the bee's orientation during waggle dances on a horizontal comb, showing for the first time polarization-sensitivity and its use for orientation in any animal [3]. Employing polarized light as a navigational cue in lieu of the sun is possible, because the scattering of sunlight in the atmosphere leads to a regular pattern of electric field vectors (*E*-vectors) that are oriented tangentially to concentric circles around the sun [4]. In addition, scattering leads to a chromatic and an intensity gradient across the sky [5, 6], both of which can be the source of directional information for orienting insects [7, 8]. Recent evidence from desert ants of the genus *Cataglyphis* shows that these animals can learn homing directions using only the sun as an orientational cue and later use this information to navigate solely by the polarization pattern and vice versa [9]. This suggests that the neuronal correlates of the sun-compass and polarization compass can either exchange information or that they are identical. The latter hypothesis is supported by the finding that the same neurons in the anterior optic tubercle of the locust that code for *E*-vector orientation of polarized light also code for the azimuthal position and wavelength of unpolarized light stimuli [10, 11]. Similarly, polarization-sensitive neurons in monarch butterflies and dung beetles also code for the azimuth of an unpolarized light stimulus, albeit wavelength sensitivity in these species is either lacking (monarch) or has not been tested (dung beetle) [12, 13]. Most insects, including honeybees, perceive the *E*-vector of polarized light with a specialized dorsal rim area (DRA) of their compound eye [14]. As polarization-vision systems are normally homochromatic, perception of the color gradient and the direct sun light is performed with the remainder of the compound eye [10, 14]. It is currently not clear at which stage of the sky compass pathway these pieces of information are integrated, but electrophysiological data from locusts suggest that a central layer of the medulla might be important for this task [15].

In order for an animal to use the sun as a spatial reference cue throughout the entire day, it has to continuously update its orientation with respect to the changing solar azimuth. An intuitive demonstration of this time-compensation capability was provided by Martin Lindauer [16] who observed that bees that performed waggle dances for extended periods of time continuously updated their dancing directions to match the changing solar azimuth. In addition to compensating for changes in solar azimuth, a system that integrates polarized and unpolarized celestial cues also needs to compensate for potential cue conflicts that arise from changes in solar elevation. Such a compensation mechanism has been shown to be present in neurons of the anterior optic tubercle, but the underlying mechanisms are unknown [11]. A fundamental requirement for both types of time-compensation is that neurons representing solar azimuth receive time information from neurons of the circadian clock.

In the cockroach (*Rhyparobia maderae*) and the fruit fly (*Drosophila melanogaster*), some neurons of the accessory medulla that contain the neuropeptide pigment dispersing factor (PDF), have been shown to be the pacemakers of the circadian clock. [17–19]. PDF is an output signal of the insect circadian clock [20–22]. In honeybees the expression level of pdf mRNA shows a circadian rhythm both under light-dark and constant darkness conditions [23]. Both PDF and the biogenic amine serotonin (5-hydroxytryptamine, 5HT) have been shown to mediate circadian effects in the visual system of insects, including size changes of lamina monopolar neurons in the housefly [24], as well as sensitivity changes in visual interneurons of crickets [25–27] and ERGs of blowflies [28]. In honeybees, 5HT has been shown to modulate the sensitivity of visual interneurons in the lobula [29].

There is now a large body of work regarding the navigational capabilities of honeybees with respect to



celestial cues, but beyond the level of the polarization sensitive photoreceptors of the DRA [30], neither the neural substrates nor mechanisms that underlie this sophisticated behavior are known. In other insect species the morphology and physiology of polarization-sensitive neurons in the brain have been studied in some detail, but a locus for time-compensation has not yet been identified. The goals of this study were to morphologically characterize the honey- bee sky compass pathway and to identify potential sites of interaction with the circadian clock within this pathway.

## METHODS

### Animals

Honeybees (*Apis mellifera*) were obtained from hives maintained at the University of Marburg, Germany. Between April and October, bees were kept outdoors. In October, hives were moved to a greenhouse under natural light/dark conditions, temperatures between 20 and 25°C, and relative humidities between 60% and 80%. Bees could freely forage for ground pollen, honey water (20–30% v/v), and water within a volume of 2 m x 2 m x 2 m. All experiments were performed on foraging worker honey bees collected outside the hive. According to the German animal welfare act, no approval is required for experiments on insects.

### Preparation 1

Animals were cold anesthetized on ice or in the refrigerator. To immobilize the animals they were attached to a custom made holder using dental wax. The head capsule was opened frontally and trachea, air sacs and glands were removed to expose the brain.

### Mass dye injections

To trace the sky compass pathway, we used mass injection of dextrans that were either coupled to fluorescent dyes (dextran Texas Red, 3000 MW, lysine fixable; dextran Alexa Fluor 488, 10000 MW, anionic, fixable) or to biotin (3000 MW, lysine fixable, Molecular Probes; all dextrans: Molecular Probes, Eugene, USA). To stain photoreceptors of the dorsal rim area, the cornea and crystalline cone layer of the DRA were removed using a microscalpel. A tracer crystal was placed into the opening, which was then sealed with petroleum jelly to avoid desiccation. For injection into the anterior optic tubercle and the dorsal rim area of the medulla, intracellular recording pipettes were pulled from borosilicate glass (inner diameter 0.75 mm, outer diameter 1.5 mm, Hilgenberg, Malsfeld, Germany) using a p-97 horizontal puller (Sutter Instrument, Novato, CA, USA) and broken to a tip diameter of approximately 5–30 µm. The tip of the pipette was dipped into petroleum jelly which allowed us to pick up a small tracer crystal. After removing the neural sheath above the target area, the handheld pipette was inserted into the brain to deposit the dye. Superficial excess dye was removed by extensive rinsing with honey bee Ringer solution (in mM: NaCl 130, KCl 5, MgCl<sub>2</sub> 4, HEPES 15, Glucose 25, Sucrose 160). After the injection, the previously removed piece of cuticle from the head capsule was replaced and covered with a tissue soaked in bee Ringer. The animals were placed overnight in a moist chamber at 4°C to allow for tracer uptake and diffusion.

### Extracellular iontophoretical dye injections

To stain small numbers of neurons (1–20) with processes in the anterior optic tubercle (AOTU), we used extracellular iontophoretical dye injections. Intracellular recording pipettes with resistances between 100 and 300 MO in the tissue were fabricated as described above.

Electrode tips were filled with 4% Neurobiotin (Vector Laboratories Burlingame, USA) in 1 M KCl and backed with 1–2.5 M KCl. After removing the neural sheath, electrodes were frontally inserted into the AOTU using a micromanipulator (Leica Microsystems, Wetzlar, Germany). To eject the tracer, and to create an electroporating electrical field [31], we applied rectangular current pulses of 10 nA amplitude with a frequency of 1 Hz and a duty cycle of 50% for 15 to 45 minutes, using a custom built amplifier.

## Preparation 2

Brains were dissected from the head capsule during continuous submersion in fixative solution. Brains were then fixated overnight at 4°C. In some preparations, the entire head capsule was fixated overnight and the brain was removed the next day. Fixative solutions depended on the type of subsequent antibody staining and are listed in Table 1. Specimen that were not immunostained, were fixated in 4% paraformaldehyde, 0.2% glutaraldehyde, and 0.2% saturated picric acid in 0.1 M phosphate buffered saline (PBS, pH 7.4).

## Biotin/streptavidin labeling

In preparations where either Neurobiotin or biotinylated streptavidin was injected, neurons were visualized through incubation of the tissue with streptavidin conjugated to Cy3 (1:1000, Jackson ImmunoResearch, West-Grove, PA, USA, RRID: AB\_2337244). Streptavidin was applied for 3 to 5 days in 0.1 M PBS, 0.3% TrX, and 0.02% sodium azide. In brains that underwent subsequent immunostaining, streptavidin was added to either the primary and secondary, or only the secondary antibody solution.

## Antibody characterization

For immunolabeling, we used polyclonal antibodies against *Apis mellifera* pigment dispersing factor (NSELINSLLGLPKNMNNA-NH<sub>2</sub>, PDF), *Uca pugilator*  $\beta$ -pigment dispersing hormone (NSELINSILGLPKVMNDA-NH<sub>2</sub>, PDH),  $\gamma$ -aminobutyric acid (GABA), and serotonin (5-hydroxytryptamine, 5HT) and a monoclonal antibody against the synaptic vesicle protein synapsin (Table 1).

The polyclonal PDF antiserum (kindly provided by Dr. M. Shimohigashi, Fukuoka University, Japan) was raised in rabbits against synthetic Cys-attached *Apis mellifera* PDF, which was conjugated to keyhole limpet hemocyanin (KLH). Specificity of the antibody was tested using ELISA. No cross reaction was found to the PDFs of *Bombyx mori* or *Gryllus bimaculatus*, but about 20% cross reactivity was observed for the PDF of *Musca domestica*. In-situ hybridization, using an antisense cRNA probe that hybridized specifically to all types of pdf mRNA, labeled the same number of cell bodies (n = 14) in the same region as the polyclonal antibody did [23].

The polyclonal PDH antiserum (kindly provided by Dr. Heinrich Dirksen, Stockholm University, Sweden, RRID:AB\_2315088) was raised in rabbits against a glutaraldehyde conjugate of synthetic *Uca pugilator* pigment dispersing hormone and thyroglobulin [32]. This antiserum has been well characterized through ELISAs and immunoassays [32, 33]. It has been previously used to stain PDH-ir neurons in a large number of different insect species including the honeybee [17, 34–36, 36–39]. Staining patterns in the honeybee brain using either the PDF antiserum or the PDH antiserum are highly similar, with a slightly larger number of cell bodies stained by the PDH antibody [23, 37].

The polyclonal antiserum against 5HT was purchased from ImmunoStar (Hudson, NY, USA, Cat# 20080, RRID:AB\_572263). It was raised in rabbit against 5HT conjugated to bovine serum albumin. According to the manufacturer's datasheet this antiserum exhibited no cross reactivity to 5-hydroxytryptophan, 5-hydroxyindole-3-acetic acid, or dopamine in Bn-SA/HRP

**Table 1. Primary antibodies, dilutions and fixatives.**

Antibody	Raised against	Raised in	Fixative	Working dilution	Source	reference
Anti-synapsin	<i>Drosophila</i> SYNORF1-GSA fusion protein	mouse	4% PFA, 0.2% saturated PA, 0.25% GA	1:50	Dr. E. Buchner, Würzburg, Germany	Klagges et al. 1996, RRID: AB_2315425
Anti- <i>Apis</i> pigment dispersing factor	<i>Apis</i> PDF coupled to KLH with MBS	rabbit	4% PFA	1:2000	Dr. M. Shimohigashi, Fukuoka, Japan	Sumiyoshi et al. 2011
Anti <i>Uca pugilator</i> pigment dispersing hormone	conjugate of synthetic <i>Uca pugilator</i> $\beta$ -PDH and bovine thyroglobulin	rabbit	4% PFA, 7.5% saturated PA	1:1000	Dr. H. Dirksen, Stockholm, Sweden	Dirksen et al. 1987, RRID: AB_2315088
Anti-5HT	5HT coupled to BSA with PFA	rabbit	4% PFA, 7.5% saturated PA	1:1000	ImmunoStar, Cat	ImmunoStar; histochemical 5HT antisera specification sheet, RRID:AB_572263
Anti-GABA No. 9/24;	GABA coupled to KLH with GA	rabbit	4% PFA, 0.5% GA	1:500	Dr. T. Kingan	Hoskins et al. 1986, RRID: AB_2314457

GA, glutaraldehyde; GSA, glutathione-S-transferase; KLH, keyhole limpet hemocyanin; MBS, m-maleimidobenzoyl-N-hydroxysuccinimide ester; PA, picric acid; PFA, paraformaldehyde.

doi:10.1371/journal.pone.0143244.t001

labeling assays. Preadsorption of the antiserum with 5HT-BSA conjugate abolished, or strongly reduced immunoreactivity in bumblebee brains [40], while preadsorption with BSA had no effect on the staining [41]. The staining pattern in the optic lobe using this antiserum was virtually identical to that described by Ehmer and Gronenberg [42], who used a different antiserum (DiaSorin, Stillwater, MN).

The antiserum against GABA (kindly provided by Dr. T. G. Kingan, No. 9/24, RRID: AB\_2314457) was raised in rabbit against GABA conjugated to KLH and has been affinity purified against KLH [43]. Preadsorption experiments on brain sections of *Manduca sexta*, and *Schistocerca gregaria* have previously demonstrated the specificity of the antiserum [43, 44].

The monoclonal antibody against the synaptic vesicle protein synapsin (kindly provided by Dr. E. Buchner Würzburg, Germany, SYNORF1, RRID: AB\_2315425) was raised against fusion proteins of glutathione-S-transferase and *Drosophila* SYN1 protein [45] and has been used in many insect species, including honeybees, to label synaptic neuropils [45–49]. The specificity of the antibody has been characterized by Klagges et al. [45]. *Drosophila* synapsin null mutants (syn79) completely lack immunoreactivity [50].

### *Apis* PDF immunohistochemistry on whole mount brains

Brains were washed in PBS with 0.3% Triton X-100 (TrX, Sigma, Deisenhofen, Germany) and incubated overnight at 4°C in blocking solution containing 5% normal goat serum (NGS, Dianova, Hamburg, Germany), 0.3% TrX, and 0.02% sodium azide in PBS. After rinsing in PBS, brains were incubated for five days at 4°C with the primary antibody solution containing anti- PDF antiserum at a dilution of 1:1000, 1% NGS, 0.5% TrX and 0.02% sodium azide in PBS. After washing in PBS, brains were incubated for three days at 4°C with the secondary antibody solution. It contained goat anti-rabbit IgG conjugated to Cy2 (1:300, Dianova, Hamburg, Germany), 1% NGS and 0.5% TrX and 0.02% sodium azide in PBS. After several rinses in PBS, brains were dehydrated in an ascending ethanol series (25%, 50%, 70%, 90%, 95%, 100%, 15 min each) and transferred to a 1:1 mixture of 100% ethanol and methylsalicylate for 30 min. Eventually they were cleared in methylsalicylate for at least 45 min and mounted between two coverslips using Permount (Fisher Scientific, Pittsburgh,

PA, USA). To avoid deformation of the brain, eight stacked hole reinforcements (Zweckform, Oberlaindern, Germany) were used as a spacer.

### PDH immunostaining on gelatin sections from rehydrated brains

Brains were washed, dehydrated, cleared and mounted as described in the previous section. Tracer injection was evaluated using a fluorescence microscope (Zeiss Axioskop, Zeiss, Jena Germany) and brains with successful injections into the AOTU were selected for further processing. To recover the embedded brains, Permount was removed by incubation in xylene for 1–3 hours at room temperature. Following a descending ethanol series (100%, 95%, 90%, 70%, 50%, 25%) brains were washed in PBS, embedded in albumin/gelatin (12% ovalbumin, 4.8% gelatin in demineralized water) and fixated overnight at 4°C with 8% formaldehyde in PBS. Brains were sectioned at 130 µm in the frontal plane using a vibrating blade microtome (VT1200 S, Leica Microsystems, Wetzlar, Germany). After several washes in 0.01 M PBS with 0.3% TrX, sections were pre-incubated with 5% NGS, 0.02% sodium azide and 0.01 M PBS with 0.3% TrX overnight at 4°C. The primary antibody solution was then applied for 5 days at 4°C. It contained PDH antiserum (1:1000), 1% NGS, 0.3% TrX, 0.02% sodium azide and 0.01 M PBS. After extensive rinses in 0.01 M PBS with 0.3% TrX, the secondary antibody solution was applied for 3 days at 4°C. It consisted of goat anti rabbit IgG conjugated to Cy2 (1:200, Dianova, Hamburg, Germany), 1% NGS, 0.3% TrX, 0.02% sodium azide and 0.01 M PBS. After washing, dehydrating, and clearing, as described for the whole mount preparations, sections were mounted on microscopic slides using Permount and spacers.

### GABA and 5HT immunohistochemistry on gelatin sections

Brains were embedded in albumin/gelatin and fixated overnight at 4°C with 8% formaldehyde in PBS and sliced in the frontal plane at a thickness of 40 µm using a vibrating-blade microtome (VT1200 S, Leica Microsystems, Wetzlar, Germany).

For GABA immunohistochemistry, slices were washed with saline substituted Tris-buffer (SST; pH 7.4) containing 0.1% TrX. To reduce background fluorescence caused by Schiff's bases as a result from glutaraldehyde fixation, free floating sections were treated for 10 minutes with 10 mg/ml NaBH<sub>4</sub> and 0.1% TrX in 0.01 M phosphate buffer [51]. After rinsing with 0.1% TrX in SST, sections were pre-incubated for one hour at room temperature with 10% normal donkey serum (NDS; Dianova, Hamburg, Germany), 0.5% TrX and SST. The primary antiserum against GABA was diluted 1:500 in a solution of 1% NDS, 0.02% sodium azide and 0.5% TrX in SST. Slices were incubated overnight at 30°C in an incubator. After washing in SST containing 0.1% TrX, the secondary antibody solution, which was composed of donkey anti-rabbit IgG Cy2 (1:200; Dianova, Hamburg, Germany) 1% NDS and 0.5% TrX in SST, was applied for one hour at room temperature. After washing with 0.1% TrX in SST sections were mounted on chrome-alum/gelatin-coated microscope slides, dehydrated in an ascending ethanol series and coverslipped using Entellan (Merck, Darmstadt, Germany).

To label 5HT immunoreactive neurons, slices were washed in PBS. Unspecific binding sites were blocked for one hour at room temperature using 5% NGS in PBS containing 0.5% TrX. The primary antibody solution was applied for two days at 4°C and consisted of rabbit-anti-5HT antiserum (1:2000, ImmunoStar, Cat No. 20080) 5% NGS, and 0.5% TrX in PBS. After several rinses in PBS containing 0.5% TrX, sections were incubated overnight at 4°C with goat anti-rabbit IgG conjugated to Alexa Fluor 488 (1:200; Molecular Probes, Eugene, OR), 5% NGS and 0.5% TrX in PBS. After rinsing in PBS, sections were mounted on chromalum/gelatin-coated microscope slides, dehydrated

in an ascending ethanol series and coverslipped using Entellan (Merck, Darmstadt, Germany).

### Synapsin/phalloidin staining

For general observation of brain structures we combined f-actin labeling using phalloidin with anti-synapsin immunostaining, as described previously by others [52, 53]. Brains were fixed in 4% paraformaldehyde in PBS at 4°C overnight. After washing in PBS, brains were embedded in 5% low-melting point agarose (Typ I-A, low EEO, Sigma-Aldrich Chemie GmbH, Steinheim, Germany) and sectioned in the frontal plane at 100 µm using a vibrating blade microtome (VT1200 S, Leica Microsystems, Wetzlar, Germany). To increase antibody permeability, sections were treated with subsequent rinses in 2% TrX (10 min) and 0.2% TrX (2x10 min) at room temperature. After pre-incubation with 2% NGS, 0.2% TrX in PBS for 1 h at room temperature, sections were incubated for 3 days at 4°C with the primary antibody solution containing anti-synapsin (1:50, SYNORF 1, RRID: AB\_2315425), 2% NGS, and 0.2% TrX in PBS. After at least 5 rinses in PBS, the sections were incubated overnight at 4°C with a solution containing goat-anti-mouse antiserum conjugated to Cy3 (1:300, Dianova, Hamburg, Germany), 1% NGS and 0.2 units phalloidin conjugated to AlexaFluor 488 (Life technologies, Thermo Fischer scientific Inc., Rockford IL, USA) in PBS (500 µl per brain). After five rinses in PBS, sections were transferred to 60% glycerol in PBS for at least 30 min, before they were mounted and coverslipped in 80% glycerol.

### Image acquisition and processing

Fluorescence was detected using a confocal laser scanning microscope (Leica TCS SP5, Leica Microsystems, Wetzlar, Germany). Depending on the required resolution we used either a 10x or 20x oil immersion objective (HC PL APO 10x/0.40 IMM CS, HCX PL APO 20x/0.70 Imm Corr Lbd. bl.) or a 63x glycerin immersion objective (HCX PL APO 63X/1.3 GLY CORR CS 21; all Objectives: Leica). The fluorophores were excited using the following lasers and wavelengths: Cy2/Alexa Fluor 488, argon laser, 488 nm; Texas Red, helium neon laser, 594 nm; Cy5, helium neon laser, 633 nm. Image stacks were acquired at a z-step size of 3 µm (10x objective), 1.5 µm (20x objective) or 0.5 µm (63x objective) and a resolution of 1024x1024 pixels per image. All scans were acquired at 200 Hz scanning frequency and a pinhole size of 1 Airy unit. Specimens containing more than one fluorophore were always scanned sequentially.

All primary image processing on the data stacks was carried out using Amira 5.3.3 (FEI Visualization Sciences Group, Mérignac Cedex, France; RRID:nif-0000-00262). For 3D reconstruction of neuropils, data stacks were resampled to a voxel size of 3x3x3 µm<sup>3</sup>. Images were manually segmented based on background staining (medulla, lobula) or tracer injection (MEDRA) in selected slices of all three cardinal planes using the segmentation editor. The outline of the entire neuropil was then interpolated using the wrapping function with each one single subsequent run of the shrinking and the smoothing function.

The morphology of tracer injected neurons was visualized by intensity-based direct volume rendering using the voltex function. To remove background fluorescence, neuronal staining was segmented in each slice using a combination of threshold based and manual selection in the segmentation editor. The resulting labelfield was used to remove any background using the arithmetic function.

In one preparation from an injection experiment (TuLAL1 neurons) image brightness and contrast were locally adjusted using Photoshop (Adobe Systems, San Jose, CA, USA) to visualize weakly stained projections in the lateral bulb. If not explicitly stated otherwise, confocal images of double labeling experiments show a single confocal section.



## Axes and naming conventions

All positional information is given with respect to the body axis, not the neuraxis. We followed the naming conventions for neuropils suggested by Ito et al. [54] wherever possible. This includes the designation “upper unit” rather than “major unit” (as suggested by Mota et al. [55]) for the large subcompartment of the anterior optic tubercle. To facilitate comparison with other species we coined the new term “lower unit complex” (abbreviated AOTU-LUC) embracing all small neuropils of the anterior optic tubercle (lateral unit and ventrolateral unit in honeybees, 55), as they seem to be functionally connected. For further details see [Discussion](#). The names of neuron types were adapted from publications describing homologous neurons in other insect species (bumblebee: [56]; locust: [57, 58]; monarch butterfly: [59]).

## RESULTS

### Dorsal rim area of the medulla

Using an antibody against the synaptic vesicle protein synapsin (syn-ir) and phalloidin, which binds to filamentous actin, we identified the dorsal rim area of the medulla (MEDRA) as a small neuropil area, at the dorsal edge of the medulla ([Fig 1](#)). It was not spatially separated from the medulla proper, but rather integrated into the outer medulla ([Fig 1A](#)). Syn-ir strongly labeled two distinct structures within the MEDRA. Most conspicuously, numerous processes entered the neuropil from dorsal (asterisks in [Fig 1B](#)) and terminated in large irregular swellings which were most likely the terminals of long visual fibers. At the ventral face of the MEDRA syn-ir labeled a band of granular appearance (arrowheads in [Fig 1B](#)). In the phalloidin staining the MEDRA was delineated by a darker outline (arrowheads in [Fig 1B'](#)). Tracer application to the dorsal rim area of the compound eye (DRA) showed that long visual fibers terminate exclusively in the MEDRA ([Fig 1C](#)). Additional injection of a different tracer into the lower unit complex of the anterior optic tubercle (AOTU-LUC) revealed overlapping branching areas of DRA photoreceptors and transmedulla neurons throughout the MEDRA ([Fig 1C](#)). Based on the ramifications of these transmedulla neurons we created a 3D reconstruction of the MEDRA. In addition, the medulla proper was reconstructed based on background staining. The 3D reconstruction shows the MEDRA as an elongated structure which was located posteriorly in the dorsal medulla ([Fig 1D–1F](#)). Transmedulla neurons branching in the MEDRA extended ventrally approximately half way to two thirds in the dorsoventral axis ([Fig 1E](#), see also [Fig 2A, 2B and 2D](#)), but were present almost throughout the entire anterior-posterior axis ([Fig 1F](#)). Double labeling of syn-ir and transmedulla neurons stained through tracer injection into the AOTU-LUC, revealed that a narrow layer, highlighted by syn-ir, corresponded to the layer in which the transmedulla neurons ran ([Figs 1A and 2B–2B'](#) arrows). Closer inspection showed that the syn-ir was in close proximity to the transmedulla neurons, but did not colocalize with them suggesting synaptic output of yet unknown neurons onto the transmedulla neurons ([Fig 2C–2C'](#)). The cell bodies of the transmedulla neurons were located between the outer face of the medulla and the inner face of the lamina ([Fig 2A](#), asterisk). The primary neurite entered the medulla and gave off two branches approximately in the middle of the neuropil. A presumably axonal branch projected through the 2<sup>nd</sup> optic chiasm and the lobula to the AOTU-LUC. The other, presumably dendritic, neurite ran along the innermost layer of the outer medulla to the MEDRA, where it gave rise to an extensive field of arborizations. For a closer morphological investigation of this type of neuron, we used extracellular iontophoretic dye injections into the AOTU-LUC, which allowed us to stain small numbers of transmedulla neurons ([Fig 2D–2F](#)). The extensive ramifications within the MEDRA of only two individual neurons suggest input from numerous photoreceptors of the DRA

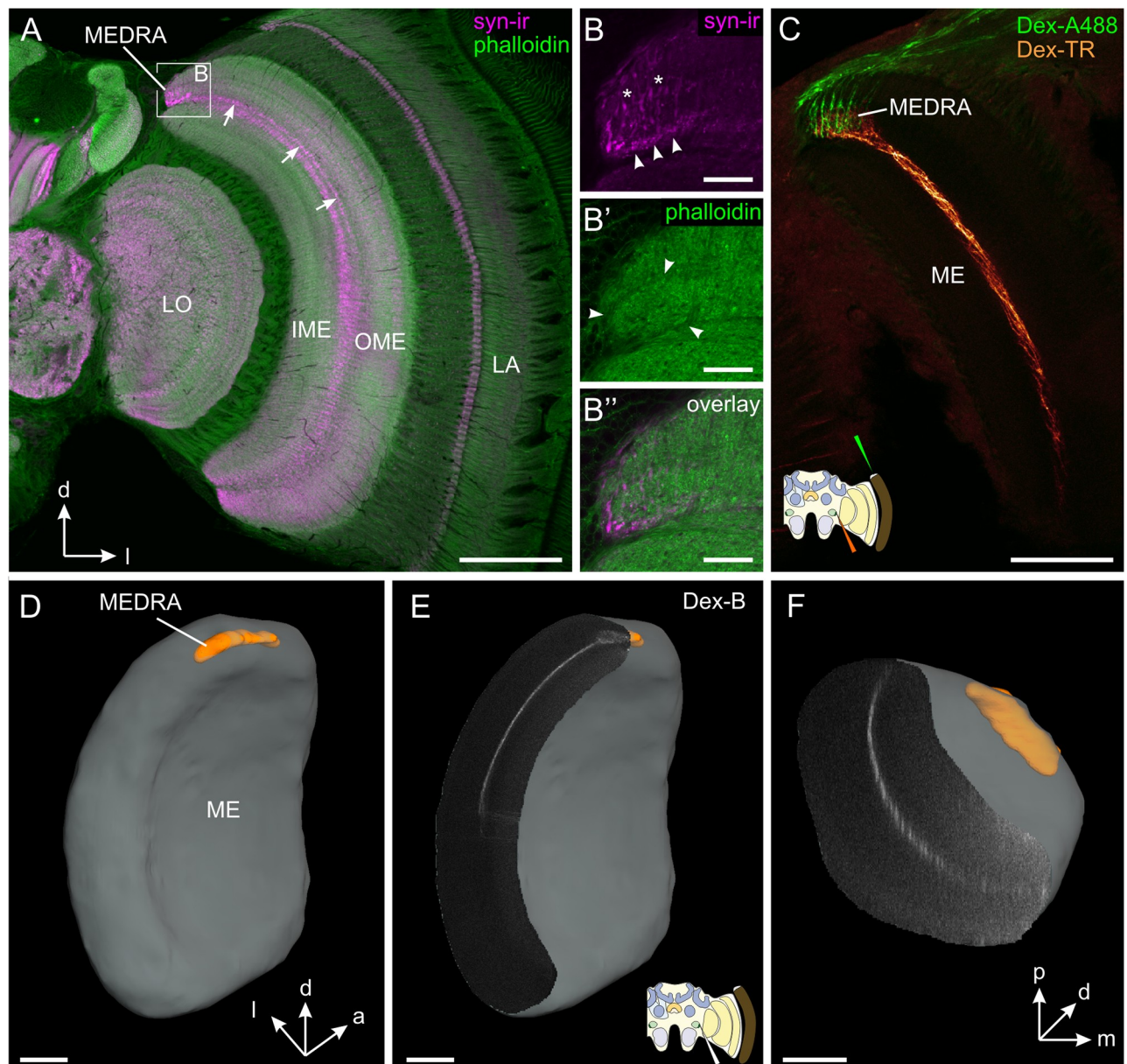


**Fig 1. Input layer of the honeybee sky compass system: dorsal rim area of the medulla (MEDRA).** (A) Confocal image of anti synapsin (syn-ir, magenta) and phalloidin (green) labeled frontal section of the honeybee optic lobe. Arrows mark a distinct layer within the dorsal half of the outer medulla (OME). (B) Maximum intensity projection (20 slices, z-pitch: 0.5 µm) of the MEDRA shows strongly synapsin-ir labeled terminals, probably of long visual fibers, entering the MEDRA at its dorsal edge (asterisks). Additionally a granular band of unknown origin shows strong synapsin immunoreactivity (arrowheads). (B') Phalloidin labeling in the dorsal medulla shows a clear delineation of the MEDRA by a darker border (arrowheads). (B'') Overlay of B and B'. (C) Double injection of dextran-Alexa488 (Dex-A488, green) into the dorsal rim area of the compound eye and dextran Texas Red (Dex-TR, orange) into the AOTU-LUC shows common projection area of DRA-photoreceptor terminals and transmedulla neurons of the anterior optic tubercle in the MEDRA. (D-E) 3D-reconstruction of the medulla (gray) and the MEDRA (orange) based on whole mount background staining and dextran Texas Red injection into the AOTU-LUC. (D) Posterior-median view. The MEDRA is an elongated structure at the dorsal posterior edge of the medulla. (E) Frontal section through medulla shows a thin layer that is defined by transmedulla neurons branching out in the MEDRA. Neurons were stained by injection of biotinylated dextran (Dex-B, gray) and labeling with streptavidin-cy3. (F) Ventral view of the same preparation as in D shows that the layer of transmedulla neurons extends almost from the anterior to the posterior end of the medulla. IME, inner medulla; LA, lamina; LO, lobula. Cartoons illustrate injection site. Scale bars: 200 µm in A; 30 µm in B; 100 µm in C-F.

doi:10.1371/journal.pone.0143244.g001



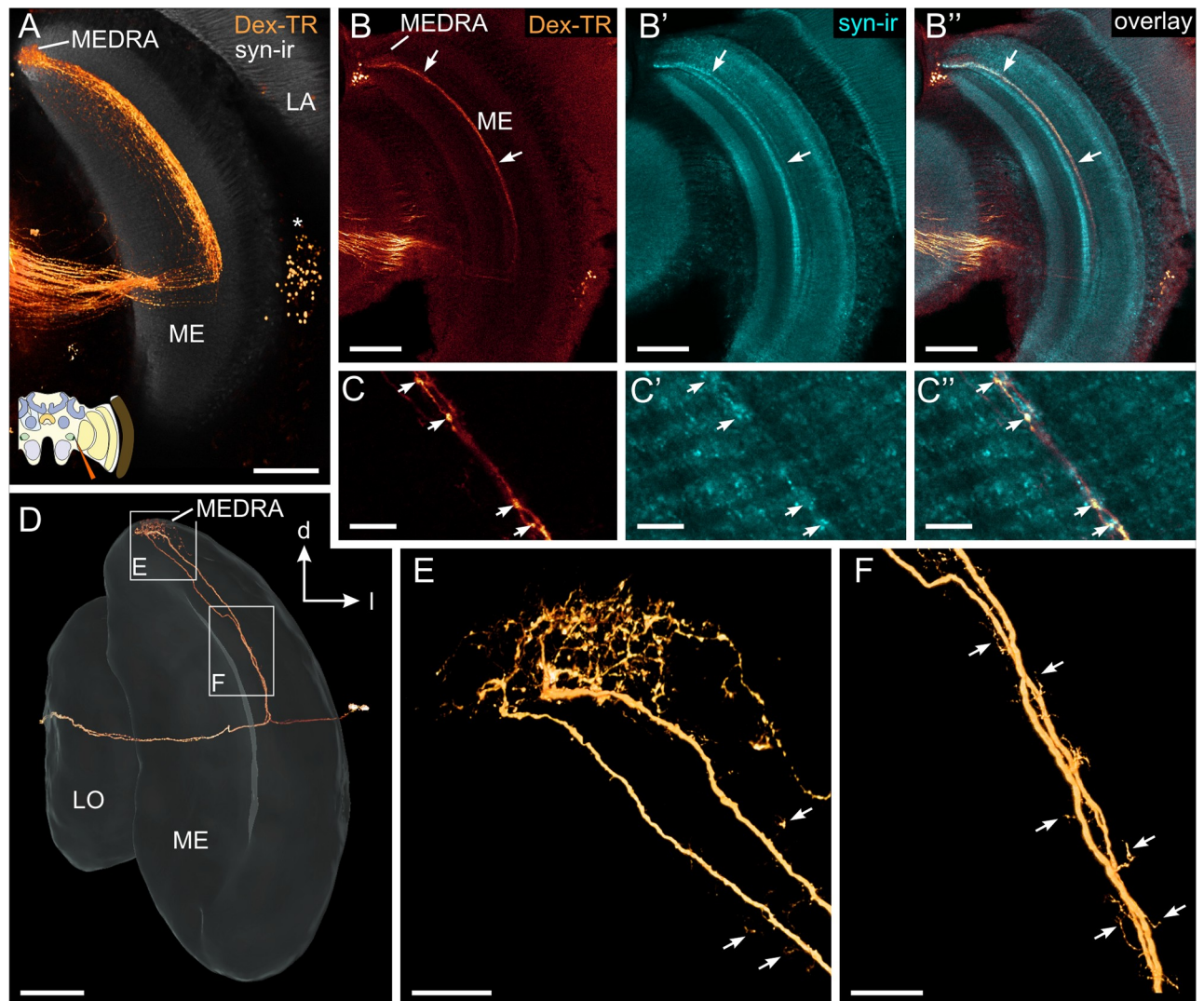


**Fig 2. Transmedulla neurons: Ramifications within the medulla.** Tracer injection into the lower unit of the anterior optic tubercle labels transmedulla neurons within a thin layer of the dorsal half of the medulla (ME) which extend into the dorsal rim area of the medulla (MEDRA). (A) Direct volume rendering of dextran Texas Red labeling superimposed on synapsin-ir slice. The neurons have their cell bodies at the distal face of the medulla (asterisk), branch in the MEDRA, run through a thin layer within the medulla and enter the 2nd optic chiasm. (B) Transmedulla neurons, labeled through Dex-TR injection into the AOTU-LUC, lie in the same layer (arrows) as a narrow band of synapsin-ir (cyan). (C) Higher magnification/resolution shows that synapsin-ir punctae are next to, but not identical to swellings of the transmedulla neurons, suggesting synaptic input onto the latter. (D-F) Direct volume rendering of two neurobiotin- injected sibling transmedulla neurons. (D) Extracellular iontophoretic injection of Neurobiotin into the AOTU-LUC labeled with streptavidin-Cy3 shows two sibling transmedulla. From an extensive meshwork of branches within the MEDRA, a single, unbranched neurite runs in dorsoventral direction through the medulla. (E, F) Higher magnification/resolution images of MEDRA (E) and a more ventral part of the neurite running dorsoventrally through the medulla (F). Arrows indicate small processes both medially and laterally of the neurite. LA, lamina; LO, Lobula. All views in frontal plane. Scale bars: 100  $\mu$ m in A, B, and D; 20  $\mu$ m in C, E, and F.

doi:10.1371/journal.pone.0143244.g002

(Fig 2E) onto each neuron within the population. Higher resolution imaging of the neurites showed studding with spine-like appendages that extended both laterally and medially suggesting input not only in the MEDRA but along the entire dorsoventral extent of the neurite (arrows Fig 2E and 2F).



## Anterior optic tubercle

To identify the target neuropil of the transmedulla neurons, we injected dextran Texas Red into the MEDRA. Central projections were exclusively found in the AOTU. We therefore investigated the AOTU using syn-ir/phalloidin labeling to get a better understanding of its anatomical fine structure. As shown previously by Mota et al. [55] the AOTU-LUC is not a continuous neuropil, but is further segmented into a lateral unit and a ventrolateral unit (Fig 3A).

Beyond these two main compartments, syn-ir/phalloidin labeling revealed further segmentation into a complicated aggregation of numerous small subregions with irregular shape (Fig 3A–3A’). Tracer injection into the MEDRA further confirmed this observation: each subcompartment was innervated by a different fascicle given off by the anterior optic tract (Fig 3B–3D). In each individual preparation, we found staining in a different set of subcompartments that were usually in close spatial proximity to each other, suggesting a spatial mapping between the medulla and the subcompartments of the AOTU-LUC. A large, highly stained area around the injection site, however, precluded the systematic investigation of such a spatial mapping.

Compartmentalization of the AOTU-LUC was also observed when injecting dye directly into this neuropil and observing the projections within the complementary neuropil on the contralateral side. We were able to identify three morphological types of heterolateral interneuron interconnecting the AOTU-LUC of both sides through the intertubercle tract (Fig 4A–4C). Following the naming conventions in other insects this type of neuron was termed tubercle-tubercle neuron 1 (TuTu1) [57–59]. The first subtype (TuTu1a, Fig 4A and 4A’) entered the AOTU with its main neurite between the dorsal and ventral lobe of the upper unit and then branched almost exclusively in the dorsalmost compartment of the AOTU-LUC (termed lateral unit by Mota et al. [55]). The second and the third subtype (TuTu1b, Fig 4B and 4B’ TuTu1c, Fig 4C and 4C’) also entered the AOTU from median, but their neurites first bent dorsally and subsequently deflected downwards where they gave rise to several large sidebranches that then innervated several subcompartments within the ventral two thirds of the AOTU-LUC (collectively termed ventrolateral unit by Mota et al. [55]). While the ramifications of these two subtypes generally overlapped, the dorsal field of ramifications was dense in TuTu1b neurons (Fig 4B, green arrows) and sparse in TuTu1c neurons (Fig 4C, white arrow), whereas the opposite was true for the ventral ramification area. Both types seemed to spare the neuropil area that was innervated by TuTu1a neurons. In all three types of neuron the distribution of processes within the AOTU-LUC appeared similar in the ipsilateral and contralateral brain hemisphere (S1 Fig).

## Central projections

Most successful dye injections into the AOTU-LUC stained neurons that projected through the AOTU-LAL tract around the vertical lobe of the mushroom body. As the tract deflected downwards the fibers segregated into a medial and a lateral fascicle projecting to two focal areas in the vicinity of the central complex termed the lateral and medial bulb (Fig 4D and 4E). According to the naming conventions in desert locusts these neurons were termed TuLAL1a if they projected to the lateral bulb and TuLAL1b, if they projected to the medial bulb [57, 60]. The presynaptic terminals of TuLAL1 neurons were conspicuously large having a diameter of up to 8 µm. To check whether the projections within the medial and the lateral bulb were associated with specific compartments of the AOTU-LUC, we analyzed the subtypes of TuTu1 and TuLAL1 neurons that were stained in the same brains. Most injections that predominantly labeled projections in the lateral bulb also stained TuTu1a neurons in the contralateral

AOTU-LUC, suggesting that the dorsalmost compartment of the AOTU-LUC (lateral unit) is connected to the lateral bulb. Likewise injections labeling projections in the medial bulb usually

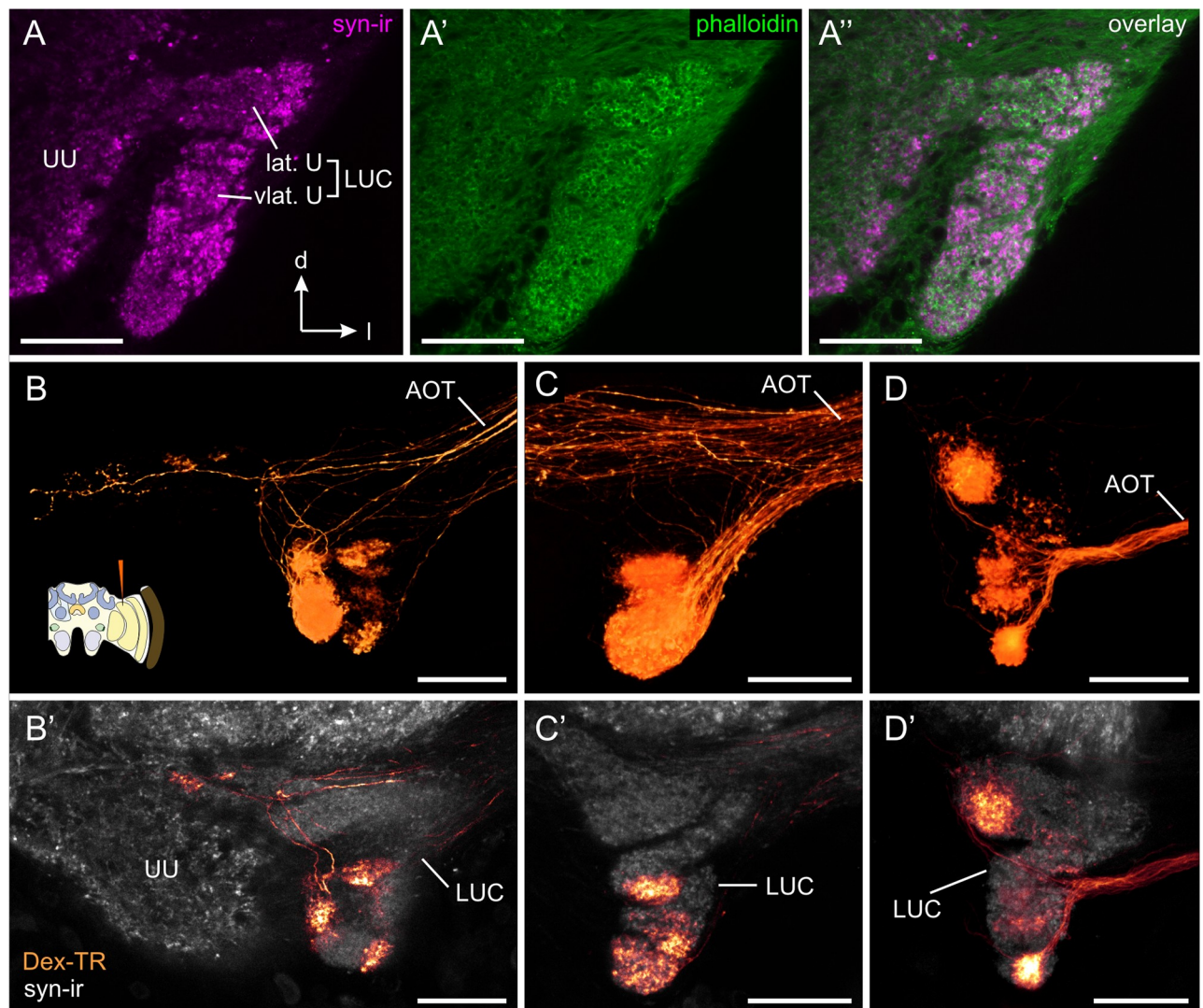


**Fig 3. Transmedulla neurons: Ramifications within the lower unit complex of the anterior optic tubercle (AOTU-LUC).** (A) Confocal image of synapsin-ir (syn-ir, magenta) and f-actin labeling (phalloidin, green) of the anterior optic tubercle. The AOTU-LUC has been previously divided into the lateral unit (lat. U) and the ventrolateral unit (vlat. U) [55]. Synapsin/phalloidin labeling reveals that these two units are further structured into a complicated assembly of multiple small subcompartments. B-D) Direct volume rendering of AOTU-LUC projections from transmedulla neurons labeled through dextran Texas Red (Dex-TR) injection into the MEDRA. In each sample a different combination of focal projection areas is stained. Cartoon in (B) illustrates injection site. B'-D') Single confocal sections (B', C') and maximum intensity projection of 10 adjacent slices (D') of the neurons shown in B-D, combined with anti-synapsin labeling (grey). Projections from MEDRA neurons are exclusively found in the AOTU-LUC. AOT, anterior optic tract; UU, upper unit of the anterior optic tubercle. All views in frontal plane. All scale bars: 30  $\mu$ m.

doi:10.1371/journal.pone.0143244.g003

also stained TuTu1b and/or TuTu1c neurons, suggesting a link between the ventral compartments of the AOTU-LUC (ventrolateral unit) and the medial bulb.

### Transmedulla neurons are in close proximity to PDF-ir, 5HT-ir and GABA-ir fibers

The neuropeptide pigment dispersing factor (PDF) has been shown to be an output signal of the insect circadian clock [20–22]. To locate possible sites of interaction between the circadian clock and the sky compass network, and thus potential neural substrates for time-compensation, we used an

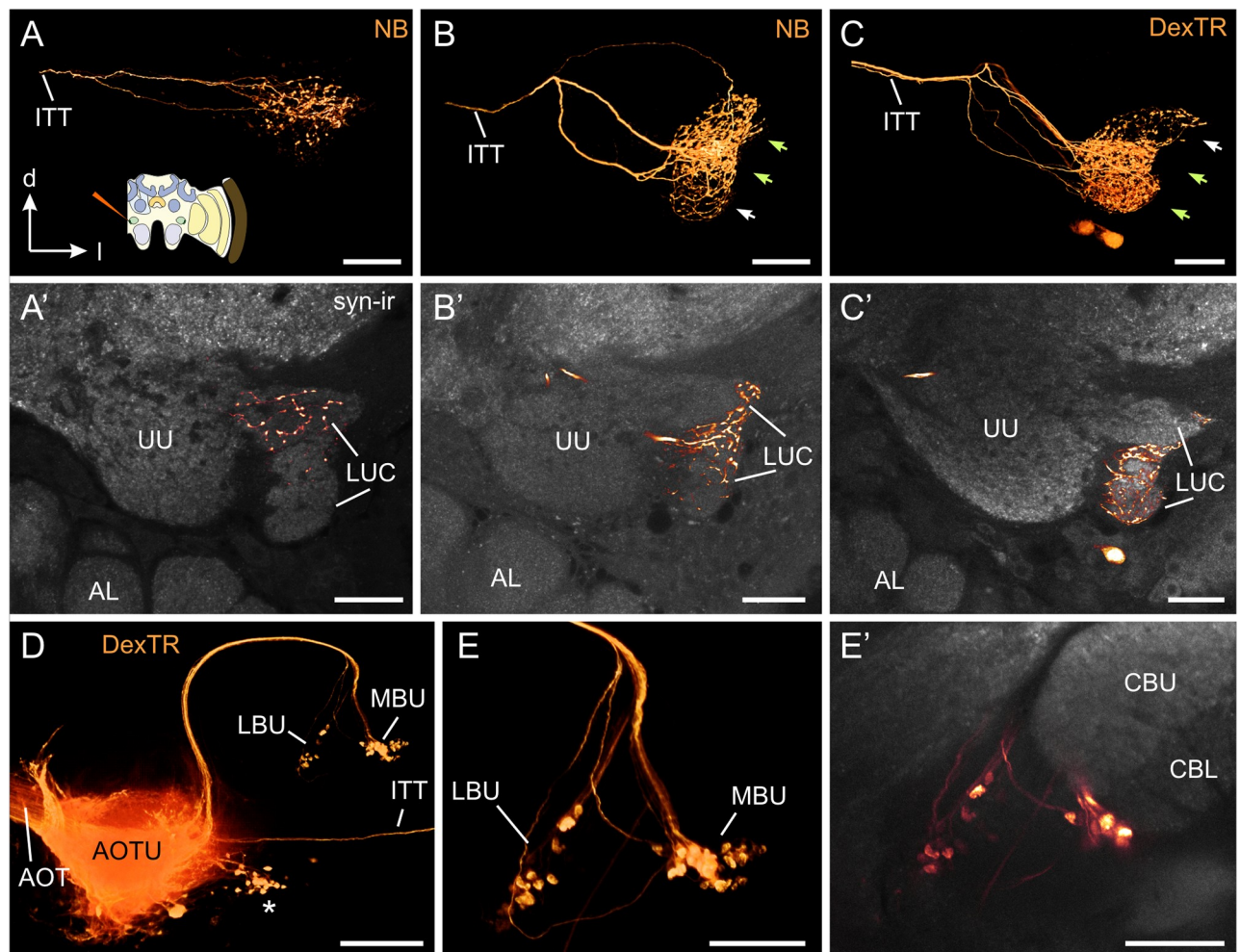


**Fig 4. Central projections of neurons in the lower unit complex of the anterior optic tubercle (AOTU-LUC).** (A-E) Neurobiotin (NB) injection into the AOTU-LUC reveals central projection areas. Cartoon in A illustrates injection site. (A-C) Direct volume rendering from projections in the contralateral AOTU-LUC shows three morphologically different types of TuTu1 neuron (TuTu1a, TuTu1b, TuTu1c). (A'-C') Maximum intensity projections of six (A') or three (B', C') adjacent slices from preparations shown in A-C, combined with anti-synapsin labeling (syn-ir, grey). (A') TuTu1a neurons connecting only the dorsal areas of the AOTU-LUC. (B', C') Two similar types of TuTu1 neuron with ramifications in the ventral and median areas of the AOTU-LUC. These neurons had dense (green arrows) and sparse (white arrows) ramification areas. While TuTu1b neurons ramified densely within their dorsal, and sparsely within their ventral branching areas (B'), the opposite was true for TuTu1c neurons (C'). (D, E) Projections of TuLAL1 neurons from the AOTU-LUC to the medial and lateral bulb. (D) Overview (direct volume rendering) shows course of the axons which run within the AOTU-LAL tract. The tract separates into two fascicles that innervate the lateral or the medial bulb (LBU, MBU), respectively. The cell bodies of TuLAL1 neurons were located medially of the AOTU (asterisk). Also stained are axons of TuTu1 neurons that run in the intertubercle tract (ITT). (E) Direct volume rendering of large synaptic terminals of TuLAL1 neurons within the median and the lateral bulbs. (E') Maximum intensity projection of three adjacent slices of preparation shown in E combined with anti-synapsin labeling (grey) illustrates the projection areas of TuLAL1 neurons with respect to the central complex. AL, antennal lobe; CBU, central body upper division; CBL, central body lower division; UU, upper unit of AOTU. All views in frontal plane. Scale bars: 30  $\mu$ m in A-C; 100  $\mu$ m in D; 50  $\mu$ m in E.

doi:10.1371/journal.pone.0143244.g004

antiserum directed against the PDF of honeybees. Spatial overlap between PDF-immunoreactivity (PDF-ir) and ramifications of sky compass neurons was exclusively found in the medulla (Fig 5). PDF-ir fibers sparsely innervated a narrow layer in the medulla from the dorsal to the ventral edge of the neuropil. The PDF-ir neurons in the medulla strongly overlapped with the layer defined by the transmedulla neurons of the sky compass system (Fig 5A). Imaging at high magnification/resolution showed that the two fiber systems did not colocalize. Rather we observed small PDF-ir punctae in close proximity to transmedulla neurons of the sky compass system,



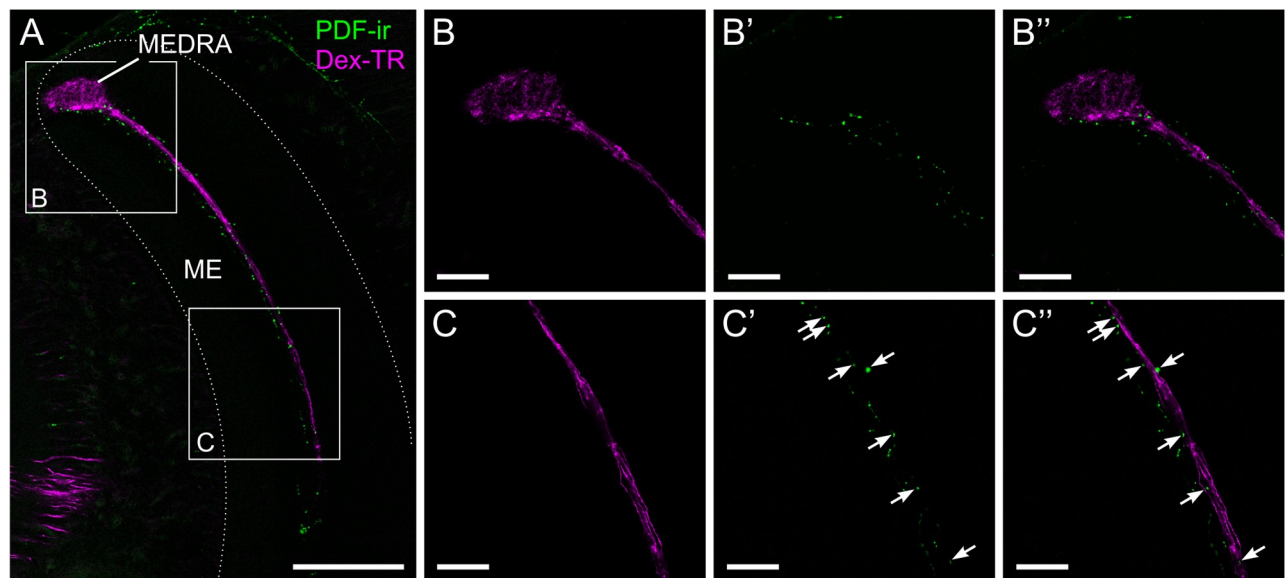


**Fig 5. Spatial relationship between transmedulla neurons and PDF-ir fibers.** (A) Confocal image of PDF-immunoreactive neurons (PDF-ir, green) and transmedulla neurons stained by dextran Texas Red injection into the AOTU-LUC (DEX-TR, magenta). Both types of neuron run in the same layer of the medulla (ME). (B, C). Higher magnification/resolution images of the areas indicated in A shows close proximity, but no colocalization of the two stainings. (B) PDF-ir is not found within the dorsal rim area of the medulla (MEDRA), only at its ventral edge. (C) PDF-ir sparsely labels small punctae which are in close proximity to the transmedulla neurons. All views in frontal plane. Scale bars: 100  $\mu$ m in A; 30  $\mu$ m in B, C.

doi:10.1371/journal.pone.0143244.g005

allowing for the possibility of PDF release onto these neurons. Overlap was not found within the MEDRA (Fig 5B) but only along the vertical passage of the transmedulla neuron's fibers through the medulla (Fig 5C). Experiments where an antiserum against crustacean  $\beta$ -pigment dispersing hormone (PDH) was used instead of the *Apis* PDF antiserum gave virtually identical staining patterns in the medulla (S2 Fig).

It has previously been shown that 5HT immunoreactivity (5HT-ir) is only found in the dorsal half of one of the median layers of the medulla [42]. 5HT has also been shown to mediate several circadian effects within the insect visual system. To test whether 5HT-ir neurons also overlap with neurons of the sky compass system in the honeybee's medulla, we combined 5HT-immunostaining with tracer injection into the AOTU-LUC (Fig 6). We found a clear overlap between the immunostaining and transmedulla neurons of the sky compass network projecting to the AOTU-LUC (Fig 6A). The antiserum against 5HT stained a broader layer of dense punctae overlapping the layer of transmedulla neurons on its lateral side. A striking feature of the 5HT-ir in relation to the transmedulla neurons was, that both sets of neuron only occupied approximately the dorsal half to two thirds of the neuropil. As with the PDF-ir we observed no overlap within the MEDRA (Fig 6B) but only along the vertical passage through the medulla (Fig 6C). Again, no colocalization was detected, i.e. injection and immunostaining labelled two distinct neuron populations, allowing for the possibility of 5HT release onto neurons of the sky compass system.

In search of further candidate substances that could provide modulatory input to the sky compass system we combined immunostaining using an antiserum against  $\gamma$ -aminobutyric acid (GABA) with tracer injection into the AOTU-LUC (Fig 7). Dense GABA immunoreactivity (GABA-ir) was found throughout the medulla as previously described by Schäfer and Bicker [61], including the layer defined by the transmedulla neurons of the sky compass system (Fig 7A). At high resolution/magnification, we identified GABA-ir of beaded appearance in close proximity to the transmedulla neurons. Different from PDF-ir and 5HT-ir, GABA-ir was found along the entire length of the transmedulla neurons, including the MEDRA. No colocalization was found between the two

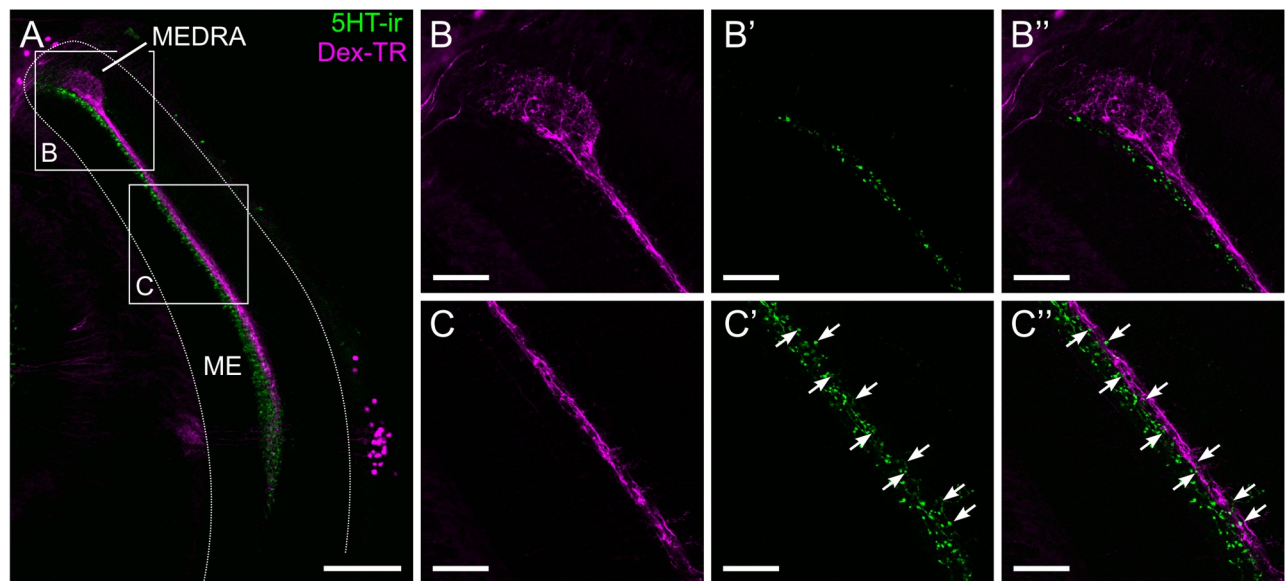


**Fig 6. Spatial relationship between transmedulla neurons and 5HT-ir fibers.** (A) Confocal image of 5HT-immunoreactive (5HT-ir) neurons (green) and transmedulla neurons labelled by dextran biotin/streptavidin Texas Red (magenta). Both stainings are restricted to the dorsal and medial parts of the medulla. (B, C) Higher magnification/resolution images of the areas indicated in A show close proximity, but no colocalization of the two stainings. (B) The dorsal rim area of the medulla (MEDRA) is devoid of 5HT-ir. (C) Transmedulla neurons overlap with the band of 5HT-ir, but the latter is wider and extends more medially. ME, medulla. All views in frontal plane. Scale bars: 100 µm in A; 30 µm in B, C.

doi:10.1371/journal.pone.0143244.g006

stainings, suggesting that they represent different neuron populations.

### The AOTU-LUC is devoid of PDF-ir, 5HT-ir and GABA-ir

To assess whether there are other potential modulation sites within the honeybee sky compass pathway, we studied immunoreactivity against PDH, 5HT and GABA within the AOTU. While the upper unit of the AOTU, which is not part of the sky compass pathway, was labelled by antisera against 5HT and GABA, the AOTU-LUC was devoid of immunoreactivity to all three antisera (Fig 8A–8C).

## DISCUSSION

In this study we combined anatomical tracing techniques with immunocytochemistry against PDF, 5HT and GABA, to unravel the sky compass pathway of the honeybee and to find potential sites of circadian and neuromodulatory input to this system. We show a neuronal pathway that originates in the dorsal rim area of the medulla, connects to the AOTU-LUC and projects to the bulbs near the central complex (Fig 9). One major finding was that transmedulla neurons connecting the MEDRA to the AOTU-LUC have numerous short spines along their passage through the medulla. This suggests that they receive additional input, like unpolarized light information and/or neuromodulatory input there. PDF-ir, 5HT-ir and GABA-ir neurons all branch in the vicinity of these neurons in the medulla pointing towards modulatory input, some of it potentially of circadian nature.

### Comparison to the sky compass pathway of other insect species

The sky compass pathway has previously been described in locusts [57, 62], bumblebees [56] and desert ants [63]. The DRA visual fibers and some elements from the AOTU have also been



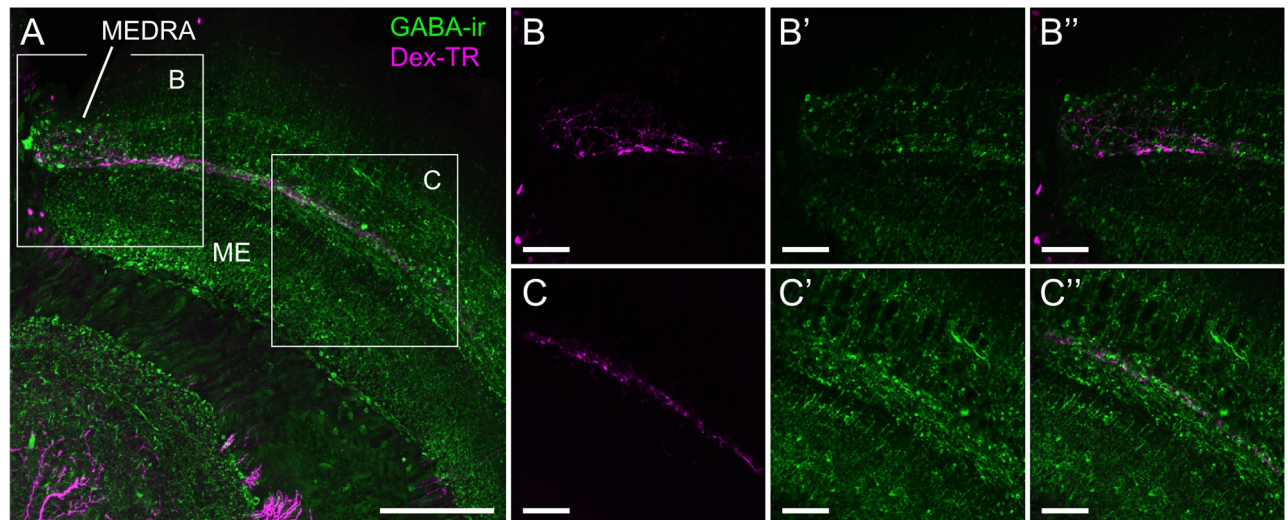


**Fig 7. Spatial relationship between transmedulla neurons and GABA-ir fibers.** (A) Confocal image of GABA-ir neurons (green) and transmedulla neurons stained by dextran Texas Red injection into the AOTU-LUC (magenta). GABA-ir is found throughout the medulla, but is more concentrated in some layers than in others. (B, C) Higher magnification/resolution images of the areas indicated in A show close proximity, but no colocalization of the two stainings. (B) GABA-ir is also present within the dorsal rim area of the medulla (MEDRA). (C) Varicose GABA-ir is in close proximity to the transmedulla neurons. ME, medulla. All views in frontal plane. Scale bars: 100  $\mu$ m in A; 30  $\mu$ m in B, C.

doi:10.1371/journal.pone.0143244.g007

reported from the honeybee [55, 64] and the monarch butterfly [12, 59, 65]. With the exception of LoTu1 neurons, which bilaterally connect the lobulae and AOTUs of both brain hemispheres in locusts [66], we found counterparts for all previously described types of sky compass pathway neurons in the honeybee. As expected from the close relationship of honeybees and bumblebees the systems in the two species were extremely similar. The similarities between the locust and the honeybee sky compass pathway were also striking, particularly considering the evolutionary distance between holometabolous and hemimetabolous insects.

One conspicuous difference, however, was the dorsoventral extent of the transmedulla neurons. While in honeybees, as described before in bumblebees [56], these neurons extended from the MEDRA only about halfway ventrally, they span the entire dorsoventral extent of the

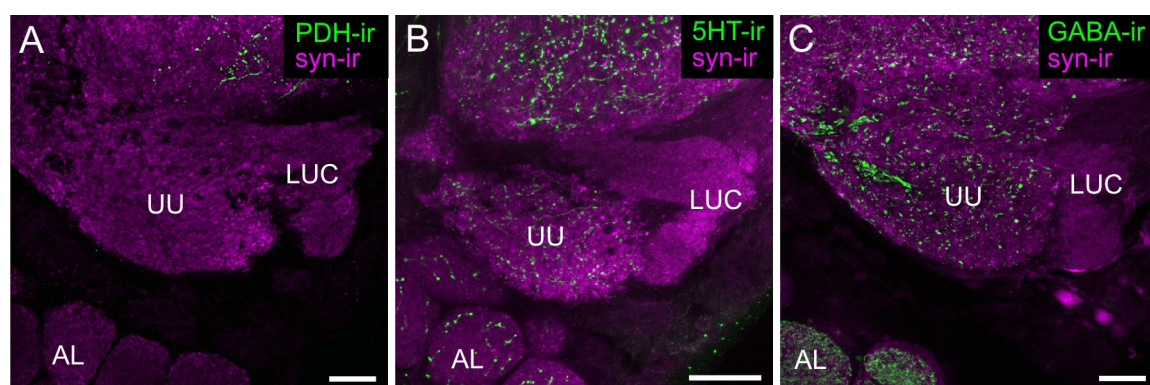


**Fig 8. Absence of PDF-, 5HT, and GABA-ir in the lower unit complex of the anterior optic tubercle (AOTU-LUC).** Synapsin-immunoreactivity (syn-ir, magenta) and immunoreactivity to antisera against PDH (PDH-ir), 5HT (5HT-ir) and GABA (GABA-ir), shown in green, in the anterior optic tubercle. (A) The entire AOTU is devoid of PDH-ir. (B) 5HT-ir was found in the upper unit of the anterior optic tubercle (UU), but not in the AOTU-LUC. (C) GABA-ir, green was found in the AOTU-UU, but not in the AOTU-LUC. AL, antennal lobe. All views in frontal plane. All scale bars: 30  $\mu$ m.

doi:10.1371/journal.pone.0143244.g008

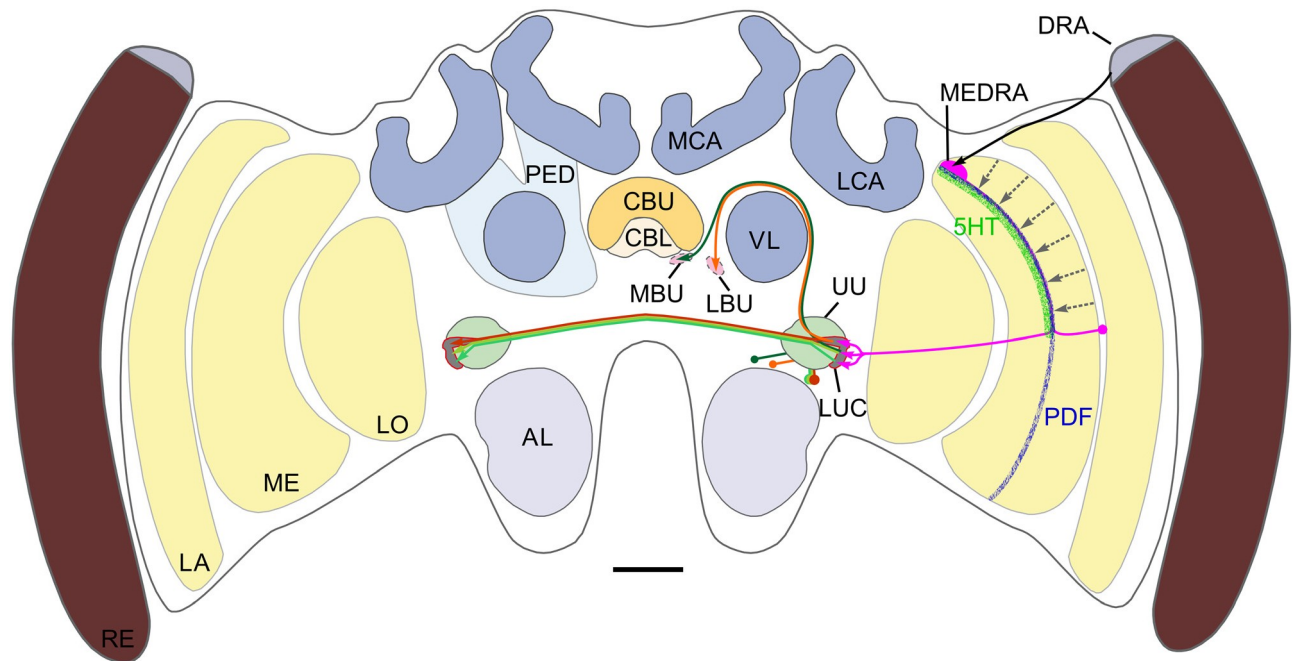


**Fig 9. Summary of the main findings.** Frontal schematic diagram of the honeybee brain illustrates the main neuropils and the sky compass pathway. The dorsal rim area of the eye (DRA) is connected to the dorsal rim area of the medulla (MEDRA) through long visual fibers. Transmedulla neurons project from the MEDRA to the lower unit complex of the anterior optic tubercle (LUC). TuLAL1 neurons project from the LUC around the vertical lobe of the mushroom body (VL) to the median and lateral bulb (MBU, LBU). Three Types of TuTu1 neurons project to the contralateral LUC. Stippled grey lines in medulla (ME) indicate hypothetical unpolarized light input pathways. Also shown is immunoreactivity in the medulla to antisera against pigment dispersing factor (PDF) and 5HT (5HT). AL, antennal lobe; CBL, lower division of the central body; CBU, upper division of the central body; LA, lamina; LCA and MCA, lateral and medial calyx of the mushroom body; LO, lobula; PED, pedunculus. Scale bar: 200  $\mu$ m.

doi:10.1371/journal.pone.0143244.g009

medulla in locusts [15, 57]. This probably creates a receptive field covering only the area above the horizon in bees, while in locusts it is to be expected that the receptive field extends ventrally. The functional implications of this finding are not clear at present.

### The anterior optic tubercle

The anterior optic tubercle of insects is composed of one large and up to three small subunits. (locust: [57]; blowfly: [67]; sphinx moth: [68]; honeybee: [55]; butterflies: [69, 70]; bumblebee: [56]). In most insects the large compartment is called the upper unit (it has previously been called the major unit in honeybees [55]) and is probably homologous across species. It has been implicated in the processing of color and motion in honeybees [55, 71, 72] and in figure-ground discrimination and phototaxis in *Drosophila* [73, 74]. The smaller units have been assigned varying names and are not easily homologized across species. However, in all species that have been investigated so far, the upper unit is not part of the sky compass pathway, whereas all the small compartments are (locust: [58]; monarch butterfly: [12, 59]; bumblebee: [56]; honeybee: this study). Heinze et al. [59] demonstrated a spatial mapping between the small compartments of the AOTU and the projection areas of TuLAL1 neurons in the bulb (of which monarch butterflies only have one per hemisphere). We found a similar mapping in the honeybee, where TuLAL1 neurons from different subcompartments of the AOTU-LUC either projected to the lateral or the medial bulb, suggesting two separate input pathways into the central complex. Although in locusts there is only one small subunit, called the lower unit, there are also two sets of TuLAL1 neurons projecting to the lateral and the medial bulb in the lateral

complex [58, 60]. Taken together the findings from different species suggest that the small units in holometabolous insects have been derived from a single small unit as represented by the AOTU-LU in the locust brain. To facilitate comparison between species, we suggest using the term lower unit (AOTU-LU) in species that possess only a single small AOTU subunit, and the term lower unit complex (AOTU-LUC) in species with multiple small subunits, to collectively signify all of them.

### Integration of polarized and unpolarized sky compass cues

It is well known that polarization-sensitive neurons in the sky compass system of insects also code for the azimuth of unpolarized light spots (locust: [10, 11]; monarch butterfly: [12]; dung beetle: [13]), but the integration site of these different stimuli is unknown. While integration could theoretically take place in the AOTU itself, the morphology of the transmedulla neurons studied here and their position within the pathway strongly suggest that these are the neuronal elements performing the integration. The overlap of their prominent ramifications in the MEDRA with terminals of DRA photoreceptors suggests polarized light information input in this neuropil. Recent data from the locust show that the MEDRA is organized in a retinotopical way [75]. Therefore, their extensive dendritic fields in the MEDRA indicate that these neurons sample polarization information from a large area of the sky. This agrees with electrophysiological data from a different type of polarization-sensitive Neuron (POL1) in the medulla of crickets which receives input from the entire DRA [76]. Large-field integration is an important property of neuronal systems processing celestial polarized light, because it makes the system robust against local irregularities of the polarization pattern [76–78]. In contrast, accurate detection of the solar azimuth requires the opposite: narrow receptive fields.

The transmedulla neurons studied here are likely to fulfill this condition as well. The spines along their dorsoventral passage through the medulla suggest additional input to this segment of the neurons. The insect visual system is organized retinotopically, i.e. neighboring points of the environment are represented by neighboring neuronal elements [79]. According to the anatomy of the transmedulla neurons one can therefore assume a receptive field in the shape of a narrow vertical bar directed at a certain azimuth. Thus, each neuron in the population could be tuned to respond maximally when the sun is located at a certain azimuth with respect to the animal and due to their long extent in dorsoventral direction, this response should be independent of solar elevation.

While the DRA photoreceptors seem to project directly onto the transmedulla neurons, the unpolarized light information is probably neither provided directly by long visual fibers nor by lamina monopolar cells, because these elements terminate in the outer layers (layers 1 and 2) of the medulla [80]. Instead it has to be expected that a connection is made by local interneurons within the medulla, as indicated in Fig 9 (grey stippled arrows).

### Circadian input into the sky-compass system

While multimodal integration can help to make systems more robust by adding redundancy, it bears the risk that different input channels provide conflicting information. In the case of the sky compass system, this problem can occur through changes in the spatial relationship between non-zenithal *E*-vectors and the solar azimuth, arising from changes in solar elevation [11]. In neurons of the locust AOTU, two physiological properties help to avoid cue conflicts. First, an area of about 50° around the sun, where these changes are particularly prominent, provides no polarization information to the system due to its subthreshold degree of polarization [81]. Second, these neurons continuously adjust their tuning throughout the day so that changes in the angle between *E*-vectors in the sky and the solar azimuth are compensated for [11]. Similar properties have been shown for neurons in the monarch



butterfly [82]. Clearly, such a compensation mechanism has to be implemented upstream of, or directly at, the integration site of polarization-information and solar azimuth information. Furthermore it is necessary that either only the polarization channel or only the unpolarized light channel is modulated (or at least that they are modulated differentially). Both conditions could be met through the interaction of transmedulla neurons and the circadian system in the honeybee. PDF-ir fibers were found in close proximity to transmedulla neurons as they pass through the medulla, while the MEDRA was devoid of PDF-ir. PDF is an output signal of the insect circadian clock and has been shown to cause dose- and daytime-dependent changes (increases and decreases) in the sensitivity of visual interneurons in the medulla of crickets [26].

Similarly to PDF-ir, 5HT-ir spared the MEDRA, but otherwise overlapped prominently with the transmedulla neurons of the sky compass pathway. In the optic lobe of crickets, 5HT levels undergo circadian fluctuations [25]. Furthermore 5HT has been shown to downregulate the sensitivity of visual interneurons in the medulla of crickets and the lobula of honeybees [26, 29]. It is therefore conceivable that selective local release of PDF and 5HT onto the transmedulla neurons of the sky compass pathway aids to shape the solar azimuth tuning of neurons further downstream in a circadian manner.

Our findings fit well with a previous study in monarch butterflies that also located a potential connection between the sky-compass system and the circadian clock in a central layer of the medulla [65]. These authors used an antiserum against CRYPTOCHROME-1 (CRY1), which is part of the molecular clock network, as a proxy for neurons of the circadian system. Similar to PDF-ir fibers in the honeybee, CRY1-ir fibers in the monarch had fine varicose branchings restricted to a central layer of the medulla. Terminals of DRA photoreceptors, traced by injection of fluorescent dyes terminated in the dorsal part of this medulla layer. This was interpreted as an indication of circadian input into the sky compass system.

In locusts, PDH-ir fibers only branch in the outermost layers of the medulla and hence do not overlap with the transmedulla neurons in this species [35]. This is a profound species specific difference between bees and locusts and particularly interesting regarding the fact that compensation for changes in the angle between the solar azimuth and celestial *E*-vectors has been shown in the AOTU of locusts, i.e. downstream of the transmedulla neurons [11]. It raises the question how time information is integrated in the medulla of these animals. El Jundi et al. showed that several types of polarization- and azimuth sensitive large-field tangential neurons branching throughout the same layer as the transmedulla neurons have additional branches in the accessory medulla [15]. These neurons could act as the interface between the circadian clock and the peripheral sky-compass network in locusts.

In two studies on locusts and monarch butterflies the distribution of preferred *E*-vector angles from all recorded neurons shows a substantially larger scatter than the corresponding distribution of preferred azimuth tuning angles from the same cells [11, 12]. This was interpreted as an indication that *E*-vector tuning rather than azimuth tuning is adjusted in the course of the day to compensate for diurnal changes arising from changes in solar azimuth. Such a mechanism would call for modulatory input into the DRA rather than the unpolarized input sites of the transmedulla neurons as reported here. Since there is no physiological description of the bee's sky-compass system to date, it is not clear if a compensation for changes in solar elevation in bees is carried out in these insects as it is in locusts and monarch butterflies.

Circadian input into the sky compass system could also have other functions as well. Bees indeed compensate for changes in solar azimuth and this specifically requires adjustment of the azimuth sensitivity somewhere in the network. It is also conceivable that a peripheral circadian modulation of the sky compass network simply globally modulates sensitivity to account for different light levels.

Physiological studies are needed in the future to distinguish between these possibilities.

### GABA-ir in the medulla

GABA-ir is abundant in the optic lobe of a variety of insect species (honeybee: [61]; hawkmoth: [83]; locust: [84]; swallowtail butterfly: [85]). GABA usually has inhibitory effects on the post-synaptic neurons, but its specific functions in the optic lobe of honeybees are unknown. In flies, GABA plays a crucial role in shaping the tuning of visual interneurons in the lobula plate. In direction sensitive movement detectors, called H1, selective blocking of GABA<sub>A</sub> receptors using picrotoxin reverses directional selectivity [86]. Similarly, the preference for small object over large field motion in FD1 neurons is inverted by picrotoxin [87]. In the sky compass pathway of honeybees GABA might also play a role in shaping the tuning of the neurons. Unlike PDF-ir and 5HT-ir, GABA-ir was present throughout the MEDRA, as reported previously for locusts [62], and could therefore interact with the processing of both polarized and unpolarized-light information. GABA can act both neuromodulatory or as a regular transmitter. The GABA-ir fibers in proximity to the transmedulla neurons could therefore provide photic inputs into these fibers rather than modulating them. In the MEDRA, however one can assume that the principal input comes from the photoreceptors of the DRA and that the GABA-ir fibers serve a different function.

### CONCLUSION

Our results show that the sky compass pathway is highly conserved between different insect species. Immunocytochemistry combined with tracer injection suggests interaction between PDF-ir, 5HT-ir and GABA-ir fibers with transmedulla neurons. Our data are a first hint of circadian and neuromodulatory input to the sky compass pathway in the medulla of honeybees. Future experiments, including electron microscopy and especially neurophysiological experiments combined with pharmacology, will help to better understand the function of the sky compass system and its modulation.

### SUPPORTING INFORMATION

**S1 Fig. Comparison of ipsi- and contralateral ramifications of three TuTu1 neuron types.** (A, B) Ipsi- (A, ipsi) and contralateral (B, contra) ramifications of a single TuTu1a neuron stained by extracellular iontophoretic dye injection of Neurobiotin (NB, orange). Neuropil stained through synapsin immunoreactivity (syn-ir, gray). Maximum intensity projections showing entire AOTU (A, 117 slices, z-pitch: 0.5  $\mu$ m) and ramifications in the lower unit complex of the anterior optic tubercle only (LUC; A', ipsilateral, 16 slices; B, contralateral, 6 slices, z-pitch: 0.5  $\mu$ m). Ramifications are restricted to the dorsalmost compartments of the (LUC) on both sides of the brain. On the ipsilateral side, TuLAL1a neurons and some unidentified neuron types are stained as well. B is identical to Fig 4A'. (C, D) Ipsi- (C) and contralateral (D) ramifications of a single TuTu1b neuron stained by extracellular iontophoretic dye injection of NB. Maximum intensity projections showing entire AOTU (C, 42 slices, z-pitch: 3  $\mu$ m) and ramifications in the LUC only (C', ipsilateral, 15 slices; D, contralateral, 30 slices, z-pitch:

0.5  $\mu$ m). On both sides of the brain, TuTu1b neurons have characteristic ramification areas with only sparse innervation of the ventralmost compartments of the LUC (arrows in C', D) close to the cellular cortex (asterisk) and a dorsally tapered denser ramification area in the medial LUC compartments. Also stained on the ipsilateral side are TuLAL1 neurons and some unidentified neuron types. (E, F) Contra- (E) and ipsilateral ramification areas (F) of TuTu1c neurons stained through dextran Texas-Red injection (Dex-TR) in two different preparations. Maximum intensity

projections showing entire AOTU (E, 145 slices, z-pitch: 0.5  $\mu$ m) and ramifications in the LUC (E', contralateral, 21 slices; D, ipsilateral, 3 slices, z-pitch: 0.5  $\mu$ m). This type of neuron has branches

predominantly in the ventral LUC, including the ventralmost area that is only sparsely innervated in TuTulb neurons. Also stained is an axon of a heterolateral lobula neuron running in the anterior optic tract (arrowhead). F is identical to Fig 4C'. AL, antennal lobe; ITT, intertubercle tract; UU upper unit of anterior optic tubercle; d dorsal; l, lateral; m, medial; Scale bars: 30  $\mu$ m. (TIF)

**S2 Fig. Spatial relationship between transmedulla neurons and PDH-ir fibers.** (A) Confocal image of PDH-immunoreactive neurons (PDH-ir, green) and transmedulla neurons stained by dextran Texas Red injection into the AOTU-LUC (DEX-TR, magenta) combined with immunostaining against synapsin (gray). Both types of neuron run in the same layer of the medulla (ME). (B, C). Higher magnification/resolution images of approximate areas indicated in A shows close proximity, but no colocalization of the two stainings. (B) PDH-ir is not found within the dorsal rim area of the medulla (MEDRA), only at its ventral edge. (C) PDH-ir sparsely labels small punctae which are in close proximity to the transmedulla neurons. All views in frontal plane. Scale bars: 100  $\mu$ m in A; 30  $\mu$ m in B, C. (TIF)

## Acknowledgments

We are grateful to Drs. Miki Shimohigashi (Fukuoka, Japan), Heinrich Dircksen (Stockholm, Sweden), Erich Buchner (Würzburg, Germany), and Tim. G. Kingan for generous donations of antisera. We thank Dr. Uwe Homberg for his support, and access to antibodies, Joss von Hadeln and Dr. Basil el Jundi for help with Amira, Drs. Andrew French and Basil el Jundi for critically reading an earlier version of the manuscript, Drs. Achim Werckenthin and Nico Funk for helpful discussions on circadian clocks, Drs. Michiyo Kinoshita and Yoshitaka Hama-naka for sharing the 5HT staining protocol, Jutta Seyfarth for expert bee keeping, and Martina Kern and Jutta Seyfarth for technical assistance.

## Author Contributions

Conceived and designed the experiments: KP. Performed the experiments: MZ MH JB AB T. Heinloth T. Hellfritz KP. Analyzed the data: MZ MH JB AB T. Heinloth T. Hellfritz KP. Contributed reagents/materials/analysis tools: KP. Wrote the paper: KP.

## REFERENCES

1. von Frisch K. Die Sonne als Kompass im Leben der Bienen. *Experientia* 1950; 6:210–21.
2. von Frisch K. Gelöste und ungelöste Rätsel der Bienensprache. *Naturwissenschaften* 1948; 35:12–23.
3. von Frisch K. Die Polarisation des Himmelslichtes als orientierender Faktor bei den Tänzen der Bienen. *Experientia* 1949; 5:142–8. PMID: 18126348
4. Strutt JW. On the light from the sky, its polarization and color. *Phil Mag* 1871; 41:274–9.
5. Coulson KL. Polarization and intensity of light in the atmosphere. Hampton: A. Deepak Publishing; 1988.
6. Coemans MA, Vos Hzn JJ, Nuboer JF. The relation between celestial colour gradients and the position of the sun, with regard to the sun compass. *Vision Res* 1994; 34:1461–70. PMID: 8023458
7. Lehrer M, editor. Orientation and Communication in Arthropods. Basel: Birkhäuser; 1997.
8. el Jundi B, Smolka J, Baird E, Byrne MJ, Dacke M. Diurnal dung beetles use the intensity gradient and the polarization pattern of the sky for orientation. *J Exp Biol* 2014; 217: 2422–9. doi: 10.1242/jeb. 101154 PMID: 24737763

9. Leebhardt F, Ronacher B. Transfer of directional information between the polarization compass and the sun compass in desert ants. *J Comp Physiol A* 2014; 201:599–608. doi: 10.1007/s00359-014-0928-9
10. Kinoshita M, Pfeiffer K, Homberg U. Spectral properties of identified polarized-light sensitive interneurons in the brain of the desert locust *Schistocerca gregaria*. *J Exp Biol* 2007; 210:1350–61. doi: 10.1242/jeb.02744 PMID: 17401118
11. Pfeiffer K, Homberg U. Coding of azimuthal directions via time-compensated combination of celestial compass cues. *Curr Biol* 2007; 17:960–5. doi: 10.1016/j.cub.2007.04.059 PMID: 17524646
12. Heinze S, Reppert SM. Sun compass integration of skylight cues in migratory monarch butterflies. *Neuron* 2011; 69:345–58. doi: 10.1016/j.neuron.2010.12.025 PMID: 21262471
13. el Jundi B, Warrant EJ, Byrne MJ, Khaldy L, Baird E, Smolka J, et al. Neural coding underlying the cue preference for celestial orientation. *Proc Nat Acad Sci* 2015; 112:11395–400. doi: 10.1073/pnas.1501272112 PMID: 26305929
14. Labhart T, Meyer EP. Detectors for polarized skylight in insects: a survey of ommatidial specializations in the dorsal rim area of the compound eye. *Microsc Res Tech* 1999; 47:368–79. doi: 10.1002/(SICI) 1097-0029(19991215)47:6<368::AID-JEMT2>3.0.CO;2-Q PMID: 10607378
15. el Jundi B, Pfeiffer K, Homberg U. A distinct layer of the medulla integrates sky compass signals in the brain of an insect. *PLoS One* 2011; 6:e27855. doi: 10.1371/journal.pone.0027855 PMID: 22114712
16. Lindauer M. Dauertänze im Bienenstock und ihre Beziehung zur Sonnenbahn. *Naturwissenschaften* 1954; 41:506–7.
17. Helfrich-Förster C, Homberg U. Pigment-dispersing hormone-immunoreactive neurons in the nervous system of wild-type *Drosophila melanogaster* and of several mutants with altered circadian rhythmicity. *J Comp Neurol* 1993; 337:177–90. doi: 10.1002/cne.903370202 PMID: 8276996
18. Helfrich-Förster C, Stengl M, Homberg U. Organization of the circadian system in insects. *Chronobiol Int* 1998; 15:567–94. PMID: 9844747
19. Stengl M, Homberg U. Pigment-dispersing hormone-immunoreactive neurons in the cockroach *Leuco-phaea maderae* share properties with circadian pacemaker neurons. *J Comp Physiol A* 1994; 175:203–13. PMID: 8071895
20. Park JH, Helfrich-Förster C, Lee G, Liu L, Rosbash M, Hall JC. Differential regulation of circadian pace-maker output by separate clock genes in *Drosophila*. *Proc Nat Acad Sci* 2000; 97:3608–13. doi: 10.1073/pnas.070036197 PMID: 10725392
21. Hassaneen E, El-Din Sallam A, Abo-Ghaila A, Moriyama Y, Karpova SG, Abdelsalam S, et al. Pigment-dispersing factor affects nocturnal activity rhythms, photic entrainment, and the free-running period of the circadian clock in the cricket *Gryllus bimaculatus*. *J Biol Rhythms* 2011; 26:3–13. doi: 10.1177/ 0748730410388746 PMID: 21252361
22. Shafer OT, Zepeng Y. Pigment-dispersing factor signaling and circadian rhythms in insect locomotor activity. *Curr Opin Insect Sci* 2014; 1:73–80. doi: 10.1016/j.cois.2014.05.002 PMID: 25386391
23. Sumiyoshi M, Sato S, Takeda Y, Sumida K, Koga K, Itoh T, et al. A circadian neuropeptide PDF in the honeybee, *Apis mellifera*: cDNA cloning and expression of mRNA. *Zoolog Sci* 2011; 28:897–909. doi: 10.2108/zsj.28.897 PMID: 22132787
24. Pyza E, Meinertzhagen IA. Neurotransmitters regulate rhythmic size changes amongst cells in the fly's optic lobe. *J Comp Physiol A* 1996; 178:33–45. PMID: 8568723
25. Tomioka K, Ikeda M. Involvement of serotonin in the circadian rhythm of an insect visual system. *Naturwissenschaften* 1993; 80:137–9.
26. Saifullah ASM, Tomioka K. Serotonin sets the day state in the neurons that control coupling between the optic lobe circadian pacemakers in the cricket *Gryllus bimaculatus*. *J Exp Biol* 2002; 205:1305–14. PMID: 11948207
27. Saifullah ASM, Tomioka K. Pigment-dispersing factor sets the night state of the medulla bilateral neurons in the optic lobe of the cricket, *Gryllus bimaculatus*. *J Insect Physiol* 2003; 49:231–9. PMID: 12769998
28. Chen B, Meinertzhagen IA, Shaw SR. Circadian rhythms in light-evoked responses of the fly's compound eye, and the effects of neuromodulators 5-HT and the peptide PDF. *J Comp Physiol A* 1999; 185:393–404. PMID: 10573867
29. Kloppenburg P, Erber J. The modulatory effects of serotonin and octopamine in the visual system of the honey bee (*Apis mellifera* L.). II. Electrophysiological analysis of motion-sensitive neurons in the lobula. *J Comp Physiol A* 1995; 176:119–29.
30. Labhart T. Specialized photoreceptors at the dorsal rim of the honeybee's compound eye: polarizational and angular sensitivity. *J Comp Physiol A* 1980; 141:19–30.
31. Neumann E, Kakorin S, Toensing K. Fundamentals of electroporative delivery of drugs and genes. *Bioelectrochemistry and bioenergetics* (Lausanne, Switzerland) 1999; 48:3–16. doi: 10.1016/S0302-4598(99)00008-2
32. Dirksen H, Zahnow C, Gaus G, Keller R, Rao K, Riehm J. The ultrastructure of nerve endings containing pigment-dispersing hormone (PDH) in crustacean sinus glands: Identification by an antiserum against a synthetic PDH. *Cell Tissue Res* 1987; 250:377–87.
33. Bonomelli SL, Rao KR, Riehm JP. Development and application of an ELISA for crustacean beta-PDH. *Am Zool* 1988; 28:A117–117.

34. Homberg U, Davis NT, Hildebrand JG. Peptide-immunocytochemistry of neurosecretory cells in the brain and retrocerebral complex of the sphinx moth *Manduca sexta*. *J Comp Neurol* 1991; 303:35–52. doi: 10.1002/cne.903030105 PMID: 1706364
35. Homberg U, Würden S, Dirksen H, Rao KR. Comparative anatomy of pigment-dispersing hormone-immunoreactive neurons in the brain of orthopteroid insects. *Cell Tissue Res* 1991; 266:343–57. doi: 10.1007/BF00318190
36. Frisch B, Fleissner G, Brandes C, Hall JC. Staining in the brain of *Pachymorpha sexguttata* mediated by an antibody against a *Drosophila* clock-gene product: labeling of cells with possible importance for the beetle's circadian rhythms. *Cell Tissue Res* 1996; 286:411–29. PMID: 8929344
37. Bloch G, Solomon SM, Robinson GE, Fahrbach SE. Patterns of PERIOD and pigment-dispersing hormone immunoreactivity in the brain of the European honeybee (*Apis mellifera*): age- and time-related plasticity. *J Comp Neurol* 2003; 464:269–84. PMID: 12900924
38. Sehadová H, Sauman I, Sehna F. Immunocytochemical distribution of pigment-dispersing hormone in the cephalic ganglia of polyneopteran insects. *Cell and Tissue Research* 2003; 312:113–25. PMID: 12712321
39. Weiss R, Dov A, Fahrbach SE, Bloch G. Body size-related variation in pigment dispersing factor-immunoreactivity in the brain of the bumblebee *Bombus terrestris* (Hymenoptera, Apidae). *J Insect Physiol* 2009; 55:479–87. doi: 10.1016/j.jinsphys.2009.01.016 PMID: 19232530
40. Paulk AC, Dacks AM, Gronenberg W. Color processing in the medulla of the bumblebee (Apidae: *Bombus impatiens*). *J Comp Neurol* 2009; 513:441–56. doi: 10.1002/cne.21993 PMID: 19226517
41. Dacks AM, Christensen TA, Hildebrand JG. Phylogeny of a serotonin-immunoreactive neuron in the primary olfactory center of the insect brain. *J Comp Neurol* 2006; 498:727–46. doi: 10.1002/cne.21076 PMID: 16927264
42. Ehmer B, Gronenberg W. Segregation of visual input to the mushroom bodies in the honeybee (*Apis mellifera*). *J Comp Neurol* 2002; 451:362–73. PMID: 12210130
43. Hoskins SG, Homberg U, Kingan TG, Christensen TA, Hildebrand JG. Immunocytochemistry of GABA in the antennal lobes of the sphinx moth *Manduca sexta*. *Cell Tissue Res* 1986; 244:243–52. doi: 10.1007/BF00219199 PMID: 3521878
44. Homberg U, Vitzthum H, Müller M, Binkle U. Immunocytochemistry of GABA in the central complex of the locust *Schistocerca gregaria*: identification of immunoreactive neurons and colocalization with neuropeptides. *J Comp Neurol* 1999; 409:495–507. doi: 10.1002/(SICI)1096-9861(19990705)409:3<495::AID-CNE12>3.0.CO;2-F PMID: 10379833
45. Klagges BR, Heimbeck G, Godenschwege TA, Hofbauer A, Pflugfelder GO, Reifegerste R, et al. Invertebrate synapsins: a single gene codes for several isoforms in *Drosophila*. *J Neurosci* 1996; 16:3154–65. PMID: 8627354
46. Brandt R, Rohlfing T, Rybak J, Kroficzek S, Maye A, Westerhoff M, et al. Three-dimensional average-shape atlas of the honeybee brain and its applications. *J Comp Neurol* 2005; 492:1–19. doi: 10.1002/cne.20644 PMID: 16175557
47. Wei H, el Jundi B, Homberg U, Stengl M. Implementation of pigment-dispersing factor-immunoreactive neurons in a standardized atlas of the brain of the cockroach *Leucophaea maderae*. *J Comp Neurol* 2010; 518:4113–33. doi: 10.1002/cne.22471 PMID: 20878779
48. Leitinger G, Pabst MA, Rind FC, Simmons PJ. Differential expression of synapsin in visual neurons of the locust *Schistocerca gregaria*. *J Comp Neurol* 2004; 480:89–100. doi: 10.1002/cne.20333 PMID: 15514920
49. Kurylas AE, Rohlfing T, Kroficzek S, Jenett A, Homberg U. Standardized atlas of the brain of the desert locust, *Schistocerca gregaria*. *Cell Tissue Res* 2008; 333:125–45. doi: 10.1007/s00441-008-0620-x PMID: 18504618
50. Godenschwege TA, Reisch D, Diegelmann S, Eberle K, Funk N, Heisenberg M, et al. Flies lacking all synapsins are unexpectedly healthy but are impaired in complex behaviour. *Eur J Neurosci* 2004; 20:611–22. doi: 10.1111/j.1460-9568.2004.03527.x PMID: 15255973
51. Baschong W, Duerrenberger M, Mandinova A, Suetterlin R. Three-dimensional visualization of cytoskeleton by confocal laser scanning microscopy. *Methods Enzymol* 1999; 307:173–89. PMID: 10506974
52. Groh C, Tautz J, Rössler W. Synaptic organization in the adult honey bee brain is influenced by brood-temperature control during pupal development. *Proc Nat Acad Sci* 2004; 101:4268–73. PMID: 15024125
53. Groh C, Rössler W. Comparison of microglomerular structures in the mushroom body calyx of neopteran insects. *Evolution of the Arthropod Nervous System: Part 2* 2011; 40:358–67. doi: 10.1016/j.asd.2010.12.002
54. Ito K, Shinomiya K, Ito M, Armstrong JD, Boyan G, Hartenstein V, et al. A Systematic Nomenclature for the Insect Brain. *Neuron* 2014; 81:755–65. doi: 10.1016/j.neuron.2013.12.017 PMID: 24559671
55. Mota T, Yamagata N, Giurfa M, Gronenberg W, Sandoz J. Neural organization and visual processing in the anterior optic tubercle of the honeybee brain. *J Neurosci* 2011; 31:11443–56. doi: 10.1523/JNEUROSCI.0995-11.2011 PMID: 21832175
56. Pfeiffer K, Kinoshita M. Segregation of visual inputs from different regions of the compound eye in two parallel pathways through the anterior optic tubercle of the bumblebee (*Bombus ignitus*). *J Comp Neurol* 2012; 520:212–29. doi: 10.1002/cne.22776 PMID: 21953619



57. Homberg U, Hofer S, Pfeiffer K, Gebhardt S. Organization and neural connections of the anterior optic tubercle in the brain of the locust, *Schistocerca gregaria*. J Comp Neurol 2003; 462:415–30. PMID: 12811810
58. Pfeiffer K, Kinoshita M, Homberg U. Polarization-sensitive and light-sensitive neurons in two parallel pathways passing through the anterior optic tubercle in the locust brain. J Neurophysiol 2005; 94:3903–15. doi: 10.1152/jn.00276.2005 PMID: 16049147
59. Heinze S, Florman J, Asokaraj S, el Jundi B, Reppert SM. Anatomical basis of sun compass navigation II: The neuronal composition of the central complex of the monarch butterfly. J Comp Neurol 2013; 521:267–98. doi: 10.1002/cne.23214 PMID: 22886450
60. Träger U, Wagner R, Bausenwein B, Homberg U. A novel type of microglomerular synaptic complex in the polarization vision pathway of the locust brain. J Comp Neurol 2008; 506:288–300. doi: 10.1002/cne.21512 PMID: 18022957
61. Schäfer S, Bicker G. Distribution of GABA-like immunoreactivity in the brain of the honeybee. J Comp Neurol 1986; 246:287–300. doi: 10.1002/cne.902460302 PMID: 3700720
62. Homberg U, Paech A. Ultrastructure and orientation of ommatidia in the dorsal rim area of the locust compound eye. Arthropod Struct Dev 2002; 30:271–80. doi: 10.1016/S1467-8039(02)00010-5 PMID: 18088961
63. Schmitt F, Stieb SM, Wehner R, Rössler W. Experience-related reorganization of giant synapses in the lateral complex: Potential role in plasticity of the sky-compass pathway in the desert ant *Cataglyphis fortis*. Dev Neurobiol 2015. doi: 10.1002/dneu.22322
64. Brockmann A, Robinson GE. Central projections of sensory systems involved in honey bee dance language communication. Brain Behav Evol 2007; 70:125–36. PMID: 17519525
65. Sauman I, Briscoe AD, Zhu H, Shi D, Froy O, Stalleicken J, et al. Connecting the navigational clock to sun compass input in monarch butterfly brain. Neuron 2005; 46:457–67. PMID: 15882645
66. Vitzthum H, Müller M, Homberg U. Neurons of the central complex of the locust *Schistocerca gregaria* are sensitive to polarized light. J Neurosci 2002; 22:1114–25. PMID: 11826140
67. Strausfeld NJ, Okamura J. Visual system of calliphorid flies: organization of optic glomeruli and their lobula complex efferents. J Comp Neurol 2007; 500:166–88. doi: 10.1002/cne.21196 PMID: 17099891
68. el Jundi B, Hütteroth W, Kurylas AE, Schachtner J. Anisometric brain dimorphism revisited: Implementation of a volumetric 3D standard brain in *Manduca sexta*. J Comp Neurol 2009; 517:210–25. doi: 10.1002/cne.22150 PMID: 19731336
69. Heinze S, Reppert SM. Anatomical basis of sun compass navigation I: The general layout of the monarch butterfly brain. J Comp Neurol 2012; 520:1599–628. doi: 10.1002/cne.23054 PMID: 22473804
70. Montgomery SH, Ott SR. Brain composition in *Godyris zavaleta* a diurnal butterfly, Reflects an increased reliance on olfactory information. J Comp Neurol 2015; 523:869–91. doi: 10.1002/cne.23711 PMID: 25400217
71. Mota T, Gronenberg W, Giurfa M, Sandoz J. Chromatic processing in the anterior optic tubercle of the honey bee brain. J Neurosci 2013; 33:4–16. doi: 10.1523/JNEUROSCI.1412-12.2013
72. Hertel H, Maronde U. The physiology and morphology of centrally projecting visual interneurons in the honeybee brain. J Exp Biol 1987; 133:301–15.
73. Aptekar JW, Kele MF, Lu PM, Zolotova NM, Frye MA. Neurons forming optic glomeruli compute figure-ground discriminations in *Drosophila*. J Neurosci 2015; 35:7587–99. doi: 10.1523/JNEUROSCI.0652-15.2015 PMID: 25972183
74. Otsuna H, Shinomiya K, Ito K. Parallel neural pathways in higher visual centers of the *Drosophila* brain that mediate wavelength-specific behavior. Front Neural Circuits 2014; 8:8. doi: 10.3389/fncir.2014.00008 PMID: 24574974
75. Schmeling F, Tegtmeyer J, Kinoshita M, Homberg U. Photoreceptor projections and receptive fields in the dorsal rim area and main retina of the locust eye. J Comp Physiol A 2015. doi: 10.1007/s00359-015-0990-y
76. Labhart T, Petzold J, Helbling H. Spatial integration in polarization-sensitive interneurons of crickets: a survey of evidence, mechanisms and benefits. J Exp Biol 2001; 204:2423–30. PMID: 11511657
77. Labhart T. How polarization-sensitive interneurons of crickets see the polarization pattern of the sky: a field study with an opto-electronic model neurone. J Exp Biol 1999; 202:757–70. PMID: 10069965
78. Bech M, Homberg U, Pfeiffer K. Receptive fields of locust brain neurons are matched to polarization patterns of the sky. Curr Biol 2014; 24:2124–9. doi: 10.1016/j.cub.2014.07.045 PMID: 25201687
79. Strausfeld N. Atlas of an insect brain. New York: Springer; 1976.
80. Ribi WA, Scheel M. The second and third optic ganglia of the worker bee: Golgi studies of the neuronal elements in the medulla and lobula. Cell Tissue Res 1981; 221:17–43. PMID: 7032703
81. Pfeiffer K, Negrello M, Homberg U. Conditional perception under stimulus ambiguity: polarization- and azimuth-sensitive neurons in the locust brain are inhibited by low degrees of polarization. J Neurophysiol 2011; 105:28–35. doi: 10.1152/jn.00480.2010 PMID: 20962068
82. Merlin C, Heinze S, Reppert SM. Unraveling navigational strategies in migratory insects. Curr Opin Neurobiol 2012; 22:353–61. doi: 10.1016/j.conb.2011.11.009 PMID: 22154565
83. Homberg U, Kingan TG, Hildebrand JG. Immunocytochemistry of GABA in the brain and suboesophageal ganglion of *Manduca sexta*. Cell Tissue Res 1987; 248:1–24. PMID: 3552234

84. Homberg U. Neurotransmitters and neuropeptides in the brain of the locust. *Microsc Res Tech* 2002; 56:189–209. doi: 10.1002/jemt.10024 PMID: 11810722
85. Hamanaka Y, Kinoshita M, Homberg U, Arikawa K. Immunocytochemical localization of amines and GABA in the optic lobe of the butterfly, *Papilio xuthus*. *PLoS One* 2012; 7:e41109. doi: 10.1371/journal.pone.0041109 PMID: 22844431
86. Bülthoff H, Bülthoff I. GABA-antagonist inverts movement and object detection in flies. *Brain research* 1987; 407:152–8. doi: 10.1016/0006-8993(87)91230-3 PMID: 3107753
87. Warzecha AK, Egelhaaf M, Borst A. Neural circuit tuning fly visual interneurons to motion of small objects. I. Dissection of the circuit by pharmacological and photoinactivation techniques. *J Neurophysiol* 1993; 69:329–39. PMID: 8459270





---

**CHAPTER II:**

**MICROGLOMERULAR SYNAPTIC COMPLEXES IN THE SKY-  
COMPASS NETWORK OF THE HONEYBEE CONNECT PARALLEL  
PATHWAYS FROM THE ANTERIOR OPTIC TUBERCLE TO THE CENTRAL  
COMPLEX**

---





# Microglomerular Synaptic Complexes in the Sky-Compass Network of the Honeybee Connect Parallel Pathways from the Anterior Optic Tubercle to the Central Complex

Martina Held <sup>1</sup>, Annuska Berz <sup>1</sup>, Ronja Hensgen <sup>1</sup>, Thomas S. Muenz <sup>2</sup>, Christina Scholl <sup>2</sup>, Wolfgang Rössler <sup>2</sup>, Uwe Homberg <sup>1</sup> and Keram Pfeiffer <sup>1\*</sup>

<sup>1</sup>Department of Biology, Animal Physiology, Philipps-University Marburg, Marburg, Germany, <sup>2</sup>Biozentrum, Behavioral Physiology and Sociobiology (Zoology II), University of Würzburg, Würzburg, Germany

## OPEN ACCESS

### Edited by:

Nuno Sousa, University of Minho, Portugal

### Reviewed by:

Wolf Huetteroth, University of Konstanz, Germany

Wulfila Gronenberg, University of Arizona, USA

### \*Correspondence:

Keram Pfeiffer  
keram.pfeiffer@staff.uni-marburg.de

Received: 01 June 2016

Accepted: 21 September 2016

Published: 07 October 2016

### Citation:

Held M, Berz A, Hensgen R, Muenz TS, Scholl C, Rössler W, Homberg U and Pfeiffer K (2016) Microglomerular Synaptic Complexes in the Sky-Compass Network of the Honeybee Connect Parallel Pathways from the Anterior Optic Tubercle to the Central Complex. *Front. Behav. Neurosci.* 10:186.  
doi: 10.3389/fnbeh.2016.00186

While the ability of honeybees to navigate relying on sky-compass information has been investigated in a large number of behavioral studies, the underlying neuronal system has so far received less attention. The sky-compass pathway has recently been described from its input region, the dorsal rim area (DRA) of the compound eye, to the anterior optic tubercle (AOTU). The aim of this study is to reveal the connection from the AOTU to the central complex (CX). For this purpose, we investigated the anatomy of large microglomerular synaptic complexes in the medial and lateral bulbs (MBUs/LBUs) of the lateral complex (LX). The synaptic complexes are formed by tubercle-lateral accessory lobe neuron 1 (TuLAL1) neurons of the AOTU and GABAergic tangential neurons of the central body's (CB) lower division (TL neurons). Both TuLAL1 and TL neurons strongly resemble neurons forming these complexes in other insect species. We further investigated the ultrastructure of these synaptic complexes using transmission electron microscopy. We found that single large presynaptic terminals of TuLAL1 neurons enclose many small profiles (SPs) of TL neurons. The synaptic connections between these neurons are established by two types of synapses: divergent dyads and divergent tetrads. Our data support the assumption that these complexes are a highly conserved feature in the insect brain and play an important role in reliable signal transmission within the sky-compass pathway.

**Keywords: sky-compass orientation, insect brain, central complex, polarization vision, honeybee, synaptic connections, anterior optic tubercle**

**Abbreviations:** AL, antennal lobe; AOT, anterior optic tract; AOTU, anterior optic tubercle; CB, central body; CBL, lower division of the central body; CBU, upper division of the central body; CNS, central nervous system; cV, clear vesicle; CX, central complex; dcV, dense core vesicle; DRA, dorsal rim area; GABA,  $\gamma$ -aminobutyric acid; GS, glia sheath; IT, isthmus tract; KLH, keyhole-limpet hemocyanin; LA, lamina; LBU, lateral bulb; LCA, lateral calyx; LO, lobula; LP, large profile; LUC, lower unit complex of the anterior optic tubercle; LX, lateral complex; M, mitochondrion; MBU, medial bulb; ME, medulla; MEDRA, dorsal rim area of the medulla; N, nucleus; NO, nodulus; NOL, lower division of the nodulus; NOU, upper division of the nodulus; PED, pedunculus; RE, retina; SP, small profile; TL, tangential neuron; TuLAL, tubercle-lateral accessory lobe neuron; UU, upper unit of the anterior optic tubercle; VL, vertical lobe.

## INTRODUCTION

Many insects have well developed abilities for orientation and navigation. En route, they rely on different strategies, like landmark navigation or vector integration (reviewed by Wehner, 2003; Menzel et al., 2006; Collett et al., 2013; Srinivasan, 2015). For spatial orientation many insects use sky-compass cues, like the position of the sun, the chromatic gradient and the polarization pattern of the sky (reviewed in Homberg et al., 2011). The ability to navigate in relation to the polarization pattern of the sky was first shown in behavioral studies on honeybees by von Frisch (1949). The neuronal basis and mechanisms underlying sky-compass orientation have been investigated anatomically and physiologically in a most detailed manner in locusts and crickets (reviewed by Homberg et al., 2011), whereas in honeybees, research into this topic is still at the beginning. Recently the sky-compass pathway in the honeybee brain has been described anatomically from the compound eye up to the lateral complex (LX; Zeller et al., 2015). The goal of this study is to investigate the anatomy of this pathway further from the LX into the central complex (CX), a neuropil which, amongst other functions, holds a neuronal representation of space around the animal (reviewed by Pfeiffer and Homberg, 2014).

The sky-compass pathway receives input via a specialized area of the compound eye, the dorsal rim area (DRA). DRA photoreceptors project through the lamina (LA) and terminate in the DRA of the medulla (MEDRA). Transmedulla neurons ramify in the MEDRA. Their fibers run dorsoventrally through the medulla (ME) and enter the lower unit complex (LUC) of the anterior optic tubercle (AOTU) via the anterior optic tract (AOT). From there two types of neuron, tubercle-lateral accessory lobe neuron 1a (TuLAL1a) and TuLAL1b project toward the LX and end in conspicuously large synaptic terminals in the lateral and the medial bulbs (LBUs, MBUs; Mota et al., 2011; Zeller et al., 2015). In the desert locust tangential TL2 and TL3 neurons of the lower division of the central body (CBL) have dendritic branches in the bulbs, forming large synaptic complexes with the terminals of TuLAL1 neurons (Vitzthum et al., 2002; Träger et al., 2008). The boundaries of the bulbs are defined by the presence of these microglomerular synaptic complexes. Locust TL2 and TL3 neurons are immunoreactive with antisera against  $\gamma$ -aminobutyric acid (GABA) and therefore, can be labeled using immunocytochemistry (Homberg et al., 1999). Large synaptic structures in the bulbs, either from TuLAL1 or TL neurons, have been found in other insect species as well, such as the fruit fly *Drosophila melanogaster* (Hanesch et al., 1989; Seelig and Jayaraman, 2013), the moth *Manduca sexta* (Homberg et al., 1990), the cricket *Gryllus bimaculatus* (Sakura et al., 2008), the monarch butterfly *Danaus plexippus* (Heinze and Reppert, 2011), the bumblebee *Bombus ignitus* (Pfeiffer and Kinoshita, 2012), and the desert ant *Cataglyphis fortis* (Schmitt et al., 2016). While in most of these species these neurons are involved in sky-compass vision, in *Drosophila melanogaster* a different function has been found. The dendrites of the

equivalent to TL neurons, called ring neurons, represent visual features of the environment with a strong preference for a vertical stripe. The associated microglomeruli in the bulbs are arranged retinotopically and therefore form a spatial map of the visual field of the fly (Seelig and Jayaraman, 2013). Additionally, these neurons have been found to be activated by an optic flow pattern around the yaw axis (Weir and Dickinson, 2015). Thus far the sky-compass pathway of the honeybee has been traced with anatomical methods from the DRA to the bulbs of the LX (Mota et al., 2011; Zeller et al., 2015). The neurons in this pathway share many anatomical features with those of locusts, where electrophysiological studies revealed their sensitivity to polarized and chromatic light stimuli (el Jundi et al., 2014). In this study we investigate the sky-compass pathway in the honeybee from the LUC of the AOTU to the central body (CB). To reveal whether neurons from the LUC are connected to GABA-immunoreactive tangential neurons of the CB as shown in locusts, we analyzed the anatomy and ultrastructure of synaptic complexes in the MBUs and LBUs.

## MATERIALS AND METHODS

### Animals

Worker honeybees (*Apis mellifera*) were caught at the entrance of the hive, which was maintained at the Department of Biology at the Philipps-University Marburg. Injections and immunostainings were performed in spring and summer, when the colony was outside. The preparations for transmission electron microscopy were made in winter. At this time the hive was kept inside a greenhouse at 25°C, and bees were fed with honey water (20–30% honey) and pollen. Experiments for synapsin/f-actin double labeling for 3D reconstructions were made during the winter season using adult worker bees (“winterbees”) from inside a colony maintained at the departmental bee station at the University of Würzburg.

### Preparation

Bees were cooled at 4°C until immobilized. For better handling during preparation, the animals were waxed to a holder with dental wax. The cuticle of the frons between the compound eyes, ocelli and labrum was removed. For getting access to the brain, the hypopharyngeal glands and air-sacks as well as the neural sheath were removed.

### Extracellular Iontophoretic Dye Injection

Extracellular iontophoretic dye injections were performed to achieve staining of small numbers of neurons (1–20) connecting the AOTU to the bulbs of the LX or the bulbs to the CX. Sharp glass microelectrodes were fabricated by pulling borosilicate capillary tubes (outer diameter 1.5 mm, inner diameter 0.75 mm, Hilgenberg, Malsfeld, Germany) with a Flaming/Brown puller (P97, Sutter instrument, Novato, CA, USA). Electrode tips were filled with 4% Neurobiotin tracer (Vector Laboratories, Burlingame, CA, USA) in 1 M KCl and backed up with 2.5 M KCl. These electrodes had a resistance of 100–200 M $\Omega$  in the tissue. Using a micromanipulator an electrode was positioned in the area of the LUC of the AOTU or the CBL. By applying a

the tracer was ejected from the electrode and entered the neurons

pulsed current of 10 nA (1 Hz, 50% duty cycle) for 20–45 min

in the vicinity of the tip presumably through pores created by an electroporating effect of the electric field. After removing the electrode, brains were dissected from the head capsule and immersed in a fixative containing 4% paraformaldehyde (Sigma-Aldrich, Steinheim, Germany), 0.25% glutaraldehyde (Carl Roth, Karlsruhe, Germany) and 0.25% saturated picric acid in 0.1 M phosphate buffered saline (PBS, pH 7.4) overnight at 4°C. They were then washed with PBS. To detect neurons labeled with Neurobiotin, brains were immersed in a solution containing Cy3-conjugated streptavidin (1:1000, Jackson ImmunoResearch Laboratories, West Grove, PA, USA), 0.3% Triton X-100 (TrX; Sigma, Deisenhofen, Germany) and PBS. After incubation at 4°C for 3 days, brains were washed with PBS and 0.3% TrX (PBT) and afterwards with PBS. The brains were then dehydrated in an ascending ethanol series. To increase image quality brains were cleared with methyl salicylate (Merck, Darmstadt, Germany). Finally, the brains were embedded between two cover slips in Permount (Fisher Scientific, Pittsburgh, PA, USA). Eight reinforcement rings (Zweckform, Oberlaindern, Germany) served as spacers to prevent squishing the tissue.

## Mass Staining Procedure

For tracing of TuLAL1 neurons, dextran Texas Red crystals (lysine-fixable, 3000 MW, Molecular Probes, Eugene, OR, USA) were inserted into the LUC. To do this, the tip of a sharp glass microcapillary, that was created as described above, was broken to a diameter of about 5–30 µm. The tip was dipped into petroleum jelly and then into the dextran Texas Red to pick up a few tracer crystals. After removing all liquid around the brain with a piece of paper tissue, the microcapillary was manually advanced into the target area. Excess dye was washed off with Ringer solution (130 mM NaCl, 5 mM KCl, 4 mM MgCl<sub>2</sub>, 15 mM HEPES, 25 mM glucose, 160 mM saccharose, 5 mM CaCl<sub>2</sub>). To allow for complete uptake and distribution of the tracer in the neurons, the head capsule was covered with tissue paper and the bee was kept overnight at 4°C in a moist chamber. To prevent bleaching of the fluorescent dye all further steps were performed in darkness if possible. After removing the brain from the head capsule it was fixed overnight at 4°C in 4% paraformaldehyde and 0.5% glutaraldehyde in 0.1 M sodium phosphate buffer (NaPi; pH 7.4). The brain was then washed with 0.01 M PBS. After embedding in albumin-gelatin (12% ovalbumin and 4.8% gelatin in demineralized water) and fixation overnight at 4°C with 8% formaldehyde in NaPi, the brain was sectioned at 40 µm in the frontal plane using a vibrating-blade microtome (VT 1000S or VT 1200S; Leica, Wetzlar, Germany).

## GABA Immunostaining

To label GABA-immunoreactive neurons, we used two different antisera that were raised against GABA conjugated to keyhole-limpet hemocyanin (KLH) via glutaraldehyde. The first antiserum was raised in guinea pig (ab17413; Lot GR51659; Abcam, Cambridge, UK). According to the

manufacturer the specificity of the antiserum was tested on Schwerte, Germany) in PBS overnight at 4°C. After washing

brain slices of rats by preadsorption with 100 nM GABA conjugated to glutaraldehyde, which abolished all staining. Preadsorption with 500 nM of similar conjugates of glutamic acid, glutamate and taurine failed to block staining (product datasheet anti-GABA antibody ab17413). The second antibody was raised in rabbit (# 9/24; kindly provided by Dr. T.G. Kingan). It had been affinity purified against KLH. The specificity of this antiserum was tested on brain sections of the sphinx moth *Manduca sexta*, the honeybee and the desert locust *Schistocerca gregaria*. In *Manduca sexta* liquid-phase preadsorption of the diluted antiserum with GABA-glutaraldehyde-KLH and similar conjugates of L-glutamic acid, β-alanine, L-glutamine and taurine was performed (Hoskins et al., 1986). GABA-glutaraldehyde-KLH blocked immunostaining at a concentration of 24 nM, whereas similar concentrations of the other amino acid conjugates were without effect (Hoskins et al., 1986). Likewise, on brain sections of the honeybee, preadsorption with 1 mM GABA-glutaraldehyde completely blocked labeling (Schäfer and Bicker, 1986), and in the desert locust, preadsorption with 15 nM GABA-glutaraldehyde-bovine serum albumin (BSA) conjugate abolished all staining on brain sections (Homberg et al., 1999).

For double staining of tracer-injected brains with GABA antiserum, gelatin slices were washed with 0.1% TrX in saline substituted Tris-buffer (SST; pH 7.4). Sodium borohydride was used to reduce background autofluorescence caused by Schiff bases that occur during glutaraldehyde fixation (Baschong et al., 1999). Sections were covered for 10 min with 10 mg/ml NaBH<sub>4</sub> and 0.1% TrX in NaPi. Deposit was washed out with 0.1% TrX in SST. To block unspecific binding sites the slices were pre-incubated for 1 h at room temperature on a shaker with 10% normal donkey serum (NDS; Dianova, Hamburg, Germany), 0.5% TrX and SST. The primary antibody against GABA was diluted 1:500 in a solution of 1% NDS, 0.02% sodium azide and 0.5% TrX in SST. Slices were incubated overnight at 30°C in an incubator on a shaker. After washing in SST containing 0.1% TrX, sections were treated with the secondary antibody solution. It consisted of Cy2-conjugated donkey anti-guinea pig IgG against the antiserum from Abcam (1:300; Dianova, Hamburg, Germany) and donkey anti-rabbit IgG against the antiserum from Kingan (1:200; Dianova, Hamburg, Germany), 1% NDS and 0.5% TrX in SST. The secondary antiserum was applied for 1 h on a shaker at room temperature. After further washing with 0.1% TrX in SST the sections were mounted on chromalum/gelatin-coated microscope slides, dehydrated in an ascending ethanol series, and embedded in Entellan (Merck, Darmstadt, Germany) under cover slips.

## F-actin Staining and Immunolabeling for Synapsin

To obtain an overview of all synaptic complexes in the bulbs of the LX, we performed double labeling for the vesicle-associated protein synapsin and filamentous actin (see Groh et al., 2004; Schmitt et al., 2016). Brains were dissected from the head capsule and immediately fixed with ice-cold 4% paraformaldehyde (methanol free, 28908, Fischer Scientific,

with PBS, brains were embedded in 5% low-melting point agarose (Agarose II, no. 210–815, Amresco, Solon, OH, USA),



adjusted to a frontal plane and sectioned at 100  $\mu\text{m}$  thickness using a vibrating-blade microtome (VT 1000S; Leica, Wetzlar, Germany). Preincubation was performed using 0.2% TrX in PBS containing 2% normal goat serum (NGS, 005-000-121, Jackson ImmunoResearch Laboratories, West Grove, PA, USA) for 1 h at room temperature. To visualize f-actin, sections were incubated with 0.2 units Alexa Fluor 488 conjugated phalloidin (A12379, Molecular Probes, Eugene, OR, USA) in 0.2% TrX and 2% NGS in PBS for 3 days at 4°C. For the additional labeling of synapsin, a monoclonal antibody raised against the *Drosophila* synaptic-vesicle-associated protein synapsin I (SYNORF1, kindly provided by E. Buchner, University of Würzburg, Germany) was added (1:50). SYNORF1 in honeybee tissue has been characterized by Pasch et al. (2011). Sections were washed several times in PBS, before incubated in Alexa Fluor 568 conjugated goat anti-mouse (1:250, A11004, Molecular Probes, Eugene, OR, USA) in PBS with 1% NGS for 2 h at room temperature. After washing with PBS, sections were transferred into 60% glycerol in PBS for 30 min. They were then mounted in 80% glycerol in PBS on glass slides covered with cover slips.

## Wholemount Preparation for Neuropil Reconstruction

Brains were dissected from the head capsule as described above and fixed with ice-cold 2% paraformaldehyde and 2% glutaraldehyde in PBS for 4 days at 4°C. After several washing steps with PBS the brain tissue was dehydrated in an ascending ethanol series (50%, 70%, 90%, 95% and 3 $\times$ 100% for 10 min each) before being cleared in methyl salicylate for 4 days at 4°C. Brains were then mounted in methyl salicylate in custom metal slides covered with cover slips (method adapted from Kuebler et al., 2010).

## Transmission Electron Microscopy

To investigate the ultrastructure of synaptic complexes brains were fixed using the high-pressure freezing technique (McDonald, 2007; Müller-Reichert et al., 2007; Rachel et al., 2010; Peschke et al., 2013). Dissected brains were prefixed overnight at 4°C with 4% paraformaldehyde and 2.5% glutaraldehyde in 0.1 M sodium cacodylate buffer (NaCB; pH 7.2). After washing in 0.1 M NaCB, brains were embedded in 7% low-melting point agarose (LM3, AppliChem GmbH, Darmstadt, Germany), and a 200  $\mu\text{m}$  thick slice, containing the area of interest, was cut with a vibratome. These sections were then high-pressure frozen with a Wohlwend HPF Compact 02 (M. Wohlwend, Engineering Office, Sennwald, Switzerland). They were then transferred to an automatic ASF2 freeze substitution unit (Leica Microsystems, Wetzlar, Germany) to replace the water and enhance contrast. For cryo-substitution fixation (CSF) a solution of 0.2% OsO<sub>4</sub>, 0.25% uranyl acetate and 5% (vol/vol) H<sub>2</sub>O in acetone (A.O.U.H; Walther and Ziegler, 2002; Junglas et al., 2008; Rachel et al., 2010) was

added. Freeze-substitution was carried out at 90°C for 46.5 h, 60°C for 8 h, 30°C for 8 h and held at 0°C for 3 h. The heating time between the steps was 1 h. Afterwards, the sections were washed twice with ice-cold acetone (100%) and were then gradually infiltrated with Epon at room temperature, followed by polymerization for 72 h at 60°C. Ultrathin sections (60–80 nm) were cut with an ultramicrotome (Ultracut; Reichert-Labtech, Wolfartshausen, Germany), collected on uncoated copper 400 mesh grids (Plano, Wetzlar, Germany) and contrast enhanced by positive staining with 2% uranyl acetate and lead citrate (Reynolds, 1963).

## Image Acquisition and Processing

Images of fluorescent samples were acquired with a confocal laser scanning microscope (CLSM; TCS SP5 and TCS SP2, Leica Microsystems, Wetzlar, Germany). Optical serial sections of an overview of all synaptic complexes in the tracer-injected brains immunostained for GABA were scanned using a 40 $\times$  objective (HCX PL APO 40 $\times$  /1.25 0.75 Oil Lbd. bl.; Leica, Bensheim, Germany) at a resolution of 1024  $\times$  1024 pixels and a z-stepsize of 1.5  $\mu\text{m}$ . For detailed scans at the same resolution with a z-stepsize of 1  $\mu\text{m}$  a 63 $\times$  objective (HCX PL APO 63 $\times$  /1.3 GLY CORR CS 21, Leica, Bensheim, Germany) was used. For double labeled synapsin/f-actin preparations, physical sections containing the whole two clusters of synaptic complexes in the bulbs were selected and scanned at a resolution of 1024  $\times$  1024 pixels using a 20 $\times$  objective (HC PL APO 20 $\times$  /0.70 Imm, Leica, Bensheim, Germany) and 63 $\times$  objective (HCX PL APO 63 $\times$  /1.4 0.6 Oil, Leica, Bensheim, Germany) to obtain image stacks at a z-stepsize of 1  $\mu\text{m}$ . Exploiting the increased autofluorescence attributes of the paraformaldehyde/glutaraldehyde-fixed wholemount preparations, these brains were scanned with a 10 $\times$  objective (HC PL APO 10 $\times$  /0.4 Imm, Leica, Bensheim, Germany) at a z-stepsize of 4  $\mu\text{m}$  in three tiles to create a panoramic overview image stack of the whole brain.

All image stacks were processed with Amira (versions 3.1.1 and 5.3.3; FEI Visualization Sciences Group, Mérignac Cedex, France). Amira was further used for the 3D reconstruction of individual synaptic complexes in the bulbs based on f-actin positive profiles in synapsin/f-actin double labeled preparations and to create a whole brain reconstruction of all major neuropils based on autofluorescence wholemount preparations. To evaluate the spatial distribution and localization of synaptic complexes in the context of the whole brain the synaptic reconstructions were transformed into the whole brain reconstruction using the CX as a landmark for orientation. Volumes of the reconstructed postsynaptic portion of the microglomeruli were calculated using Amira 5.6. The data for the lateral and medial cluster were statistically compared using the Mann-Whitney test (VassarStats<sup>1</sup>).

Transmission electron micrographs were taken using a JEOL JEM-2100 transmission electron microscope (JEOL, Tokio, Japan) at an acceleration voltage of 120 kV.

<sup>1</sup><http://vassarstats.net/>

Images were taken with a 2k $\times$ 2k pixel CCD-camera F214 and the software EM-Menu 4 (TVIPS, Gauting, Germany). Contrast

and brightness were optimized with Adobe Photoshop CC (Adobe Systems, San Jose, CA, USA) software if necessary, and all figures were created with Adobe Illustrator CC.

## RESULTS

We investigated the anatomy and ultrastructure of microglomerular synaptic complexes in the bulbs of the LX that connect the AOTU to the CB in the brain of the honeybee *Apis mellifera* (**Figure 1**). We first describe the different neuron types that are involved in these conspicuous connections. Then the general distribution and appearance of the synaptic complexes is shown. Last, we present data on the subcellular organization and show two types of synapses forming cell-cell connections. Positional information within the brain is given with respect to the body axis. For neuropils we followed the terminology suggested by Ito et al. (2014) wherever possible. Additionally, we refer to the entirety of small subunits of the AOTU as “LUC” as suggested by Zeller et al. (2015). The nomenclature of all neurons corresponds to the terminology used in locusts, monarch butterflies and bumblebees (Müller et al., 1997; Homberg et al., 2003; Pfeiffer et al., 2005; Heinze and Reppert, 2011; Pfeiffer and Kinoshita, 2012).

### Neurons Innervating the Bulbs

Using extracellular iontophoretic dye injections, we were able to identify and distinguish two subtypes of TuLAL1 neuron connecting the LUC of the AOTU to the bulbs. The bulbs are neuropils located laterally on both sides of the CX. In each hemisphere there are two bulbs: the MBU and LBU. Together with the lateral accessory lobe they form the LX which is closely associated with the CX (Ito et al., 2014). Both subtypes of TuLAL1 neuron had their cell bodies medially to the AOTU and their axons extended around the vertical lobe (VL) of the mushroom body toward the CX. The axons of both subtypes ended in conspicuous large, hat-like terminals. The majority of the injected neurons had only one of those synaptic endings, but in a few cases the axon ended in more than one terminal. In these cases, the terminals were always in close proximity to each other and in the same bulb. The terminals of TuLAL1a neurons were located in the LBU, ventrolaterally to the CB (**Figure 1B**). The second subtype, TuLAL1b neurons, projected to the MBU which lies directly adjacent to the groove formed between the lateral boundary of the lower and upper divisions of the CB (**Figure 1C**). The transmission of information from the bulbs into the CB is assumed to take place in tangential neurons of the type TL2 and TL3, the presumptive equivalent to ring neurons in the fruit fly (*Schistocerca gregaria*: Vitzthum et al., 2002; Träger et al., 2008; *Drosophila melanogaster*: Seelig and Jayaraman, 2013; Wolff et al., 2015). We were able to identify these neuronal cell types in the honeybee brain. They had their cell bodies medially to the AOTU and posteriorly from the somata of TuLAL1 neurons. Their primary neurites ran toward the isthmus tract (IT), where they gave off single large side branches that extended into one of the bulbs and had dense accumulations of protrusions at their tips (**Figures 1D,E** arrowheads). These dendritic side branches were about 20  $\mu\text{m}$  to 50  $\mu\text{m}$  long in TL2 neurons (**Figure 1D**) and invaded the LBU. In contrast, in TL3

neurons they had a stub-like appearance of only a few  $\mu\text{m}$  and innervated the MBU (**Figure 1E**). The axons of both types of neuron extended into the CBL, where they branched in all slices of defined layers.

Owing to the close morphological similarity of these four neuron types with equivalent neurons in locusts, monarch butterflies and bumblebees (Müller et al., 1997; Homberg et al., 2003; Pfeiffer et al., 2005; Heinze and Reppert, 2011; Pfeiffer and Kinoshita, 2012), we suppose that these neurons form the large synaptic complexes found in the bulbs. More precisely, TuLAL1a neurons develop synaptic connections with TL2 and TuLAL1b with TL3 neurons (**Figure 1A**).

### Appearance of the Microglomerular Synaptic Complexes

To obtain an overview of the synaptic complexes within the bulbs, we performed double labeling experiments using anti-synapsin and f-actin phalloidin staining. Synaptic complexes were clearly visible using this method and arranged in two distinct clusters, one group of synaptic complexes very close to the CBL in the MBU, and another group located more laterally in the LBU (**Figure 2A**). Higher magnification revealed that synapsin-immunoreactivity (IR) was localized within a cup-shaped profile, and dense f-actin phalloidin staining was concentrated inside the halo of synapsin-IR (**Figure 2B**). The anterior-posterior expansion of both clusters becomes obvious in horizontal sections (**Figure 2C**). **Figures 3A,B** show a complete 3D reconstruction of the lateral (red) and medial (blue) clusters of one brain hemisphere of synaptic complexes merged into a tissue section of phalloidin- labeled fiber bundles. The total number of synaptic complexes within each of the two clusters was assessed by individual 3D reconstructions of phalloidin-labeled profiles revealing  $68 \pm 1.9$  SD ( $n = 4$ ) complexes in the lateral cluster and  $197.5 \pm 37.5$  SD ( $n = 4$ ) in the medial cluster (**Figures 3C–E**). Because synapsin-positive presynaptic profiles often appeared fused, we used the more distinct phalloidin-labeled profiles to quantify individual synaptic complexes. It cannot be excluded, however, that in some cases, particularly in the medial cluster, more than one phalloidin-labeled profile was associated with one (fused) synapsin-positive complex at this level of resolution. In addition to the total numbers of synaptic complexes defined by phalloidin- labeled clusters, the 3D reconstructions illustrate the position and extension of the two clusters in relation to other brain structures, in particular the CB. Based on the 3D reconstruction of the f-actin positive (postsynaptic) portion of the microglomeruli, we measured their volumes (**Figure 4**). Owing to the rather small size of these structures, compared to the z-resolution of the image stacks, these values should be treated with caution and should not be taken as absolute measurements. However, they illustrate the size difference between the elements of the lateral and the medial cluster as well as the distribution of volumes within the clusters.

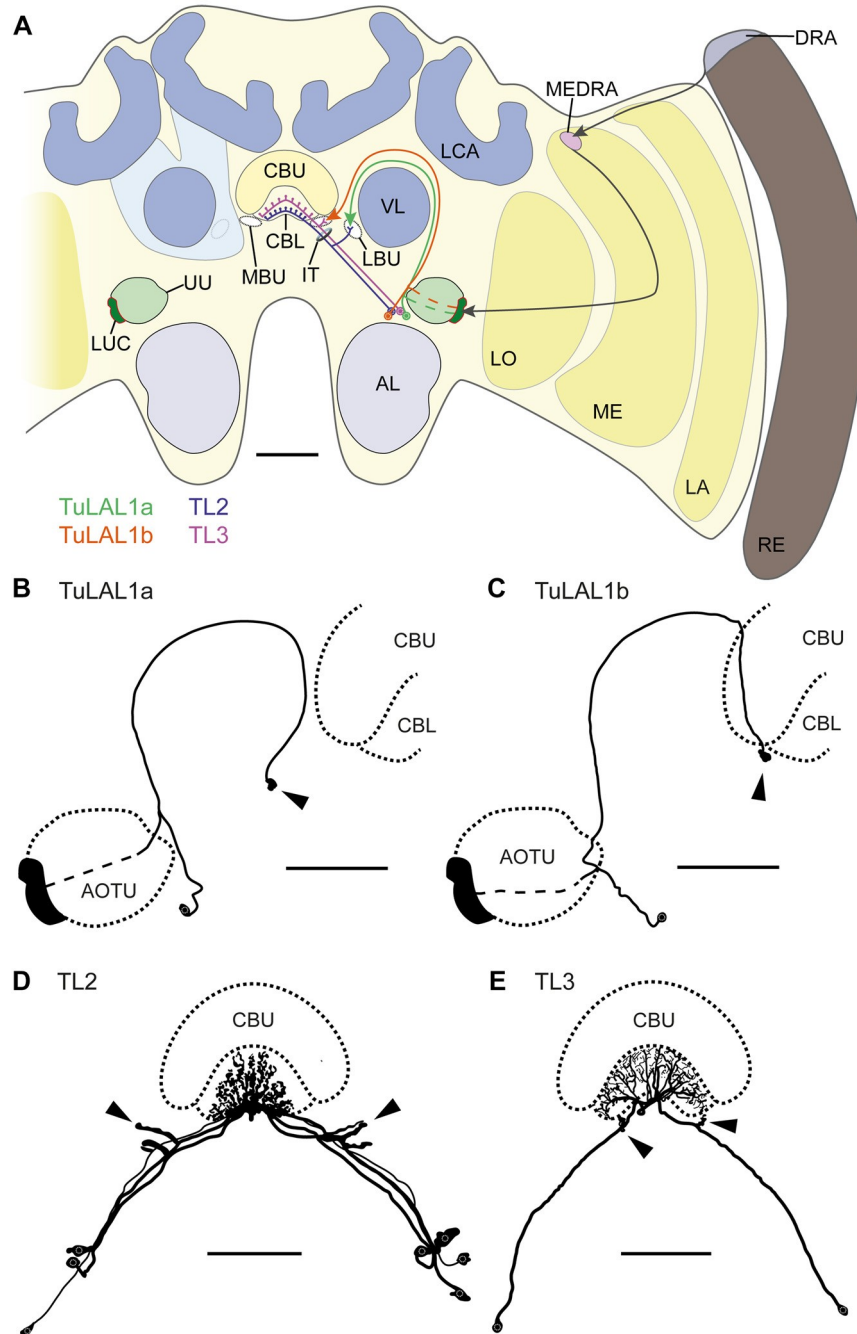


**FIGURE 1** | (A) Schematic drawing of the position of the neuron types forming microglomerular synaptic complexes in the medial and lateral bulbs of the honeybee *Apis mellifera*. The connection from the anterior optic tubercle to the central complex (CX) is formed by tubercle-lateral accessory lobe neurons 1a (TuLAL1a; green) and TuLAL1b neurons (orange). Two types of tangential neuron (TL2, blue; TL3, purple) provide input into the lower division of the central body (CBL). (B–E) Reconstructed morphologies of neurons labeled by extracellular dye injections. TuLAL1a (B) and TuLAL1b (C) neurons have their cell bodies medially from the AOTU. The axons of both types run toward the central body (CB), where they end in large terminals (arrowheads). In TuLAL1a neurons these terminals are located in the LBU (B, arrowhead), whereas TuLAL1b neurons terminate in the MBU (C, arrowhead), close to the CBL. TL neurons have their cell bodies medially to the AOTU and posteriorly to the somata of TuLAL1 neurons. Their primary neurites run toward the isthmus tract (IT), where they give off sidebranches. The sidebranches of TL2 neurons extend into the LBU, and those of TL3 to the MBU (D,E, arrowheads). The axons extend from the bulbs further into the CBL, where they branch in all slices but not in all layers. TL2 neurons branch in the dorsal part of the CBL, TL3 neurons in the ventral part. AL, antennal lobe; CBU, upper division of the CB; DRA, dorsal rim area; LA, lamina; LBU, lateral bulb; LCA, lateral calyx; LO, lobula; LUC, lower unit complex of the AOTU; MBU, medial bulb; ME, medulla; MEDRA, dorsal rim area of the medulla; RE, retina; UU, upper unit of the AOTU; VL, vertical lobe. Scale bars: A = 200  $\mu$ m, B–E = 100  $\mu$ m.



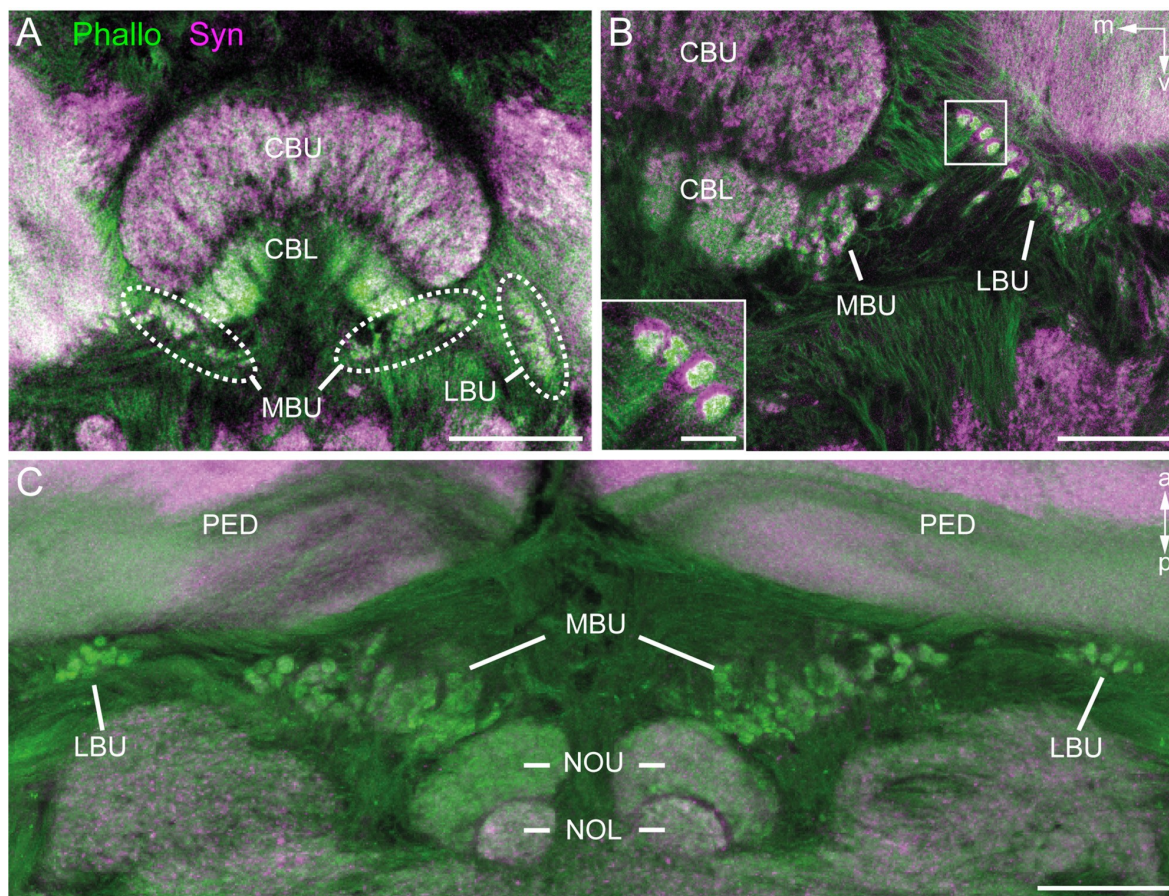


**FIGURE 2 | Anti-synapsin (Syn, magenta) and f-actin phalloidin (Phallo, green) staining of the microglomerular synaptic complexes.** (A) Frontal sections show that the synaptic complexes are arranged in two clusters: one in the MBU close to the connection of the CBL and the upper division (CBU). The second cluster is located in the LBU. (B) At higher magnification of both clusters the distribution of the anti-synapsin and f-actin phalloidin staining reveals a synapsin-positive cup-shaped structure with an f-actin containing profile in the center. (C) In horizontal sections the distribution in the anterior-posterior axis becomes apparent. The synaptic complexes in both bulbs appear posterior to the pedunculi (PED). Those of the MBU extend posterior to the upper division of the noduli (NOU). a, anterior; m, medial; NOL, lower division of the noduli; p, posterior; v, ventral. Scale bars: A = 100  $\mu\text{m}$ , B,C = 50  $\mu\text{m}$ , inset in B = 10  $\mu\text{m}$ .

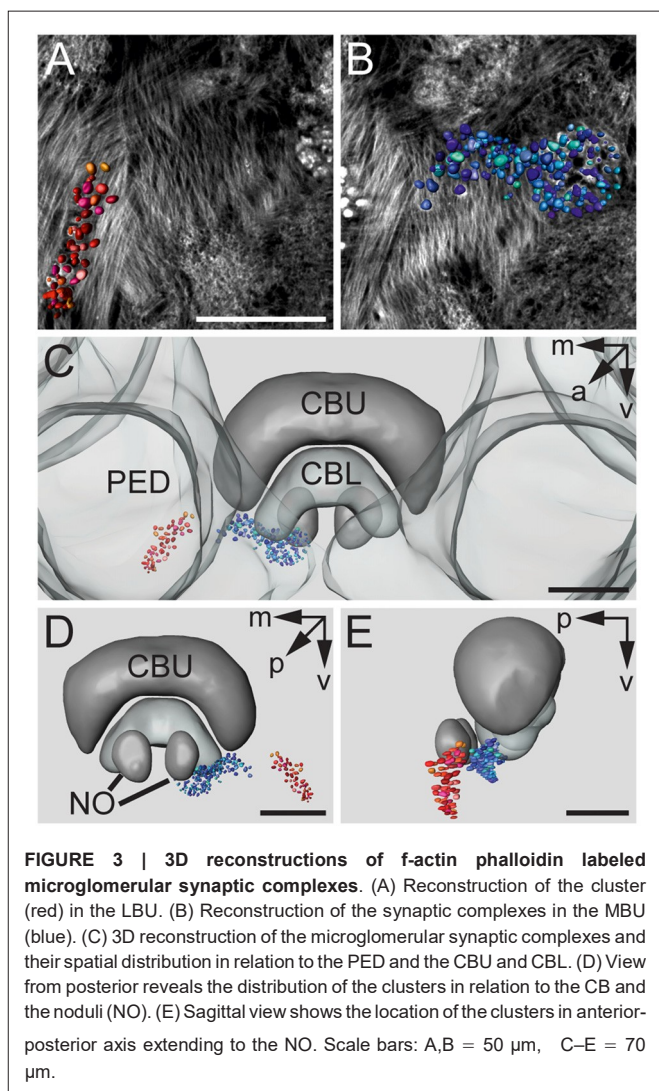
The median volume of the postsynaptic elements from four brains in the medial cluster was 33  $\mu\text{m}^3$ , whereas it was 79  $\mu\text{m}^3$  in the lateral cluster. This difference was statistically significant (Mann-Whitney test,  $P < 0.0001$ ,  $U = 157060.5$ ,  $z = 13.39$ ,  $N_{\text{medial}} = 772$ ,  $N_{\text{lateral}} = 262$ ). The total volume of all postsynaptic elements was 8485  $\mu\text{m}^3$  in the medial cluster and 6244  $\mu\text{m}^3$  in the lateral cluster (median values,  $n = 4$ ).

To investigate whether the synaptic complexes are formed by TuLAL1a/b and TL2/3 neurons we performed double label experiments. In *Schistocerca gregaria*, TL2 and TL3 tangential neurons of the CB are GABA-immunoreactive (Homberg et al., 1999; Träger et al., 2008). In honeybees immunostaining for GABA also labels putative tangential neurons in the CBL (Schäfer and Bicker, 1986). Immunofluorescent labeling for GABA confirmed the data of Schäfer and Bicker (1986) and revealed a subdivision of terminals of the labeled TL neurons lateral to the CB into two larger medial groups and two smaller lateral groups (Figure 5A). It also confirmed that branching of these neurons in the CB is restricted to the CBL. The few fibers stained in the upper division of the central body (CBU) likely belong to TU1 and TU2 neurons as described in *Schistocerca*

*gregaria* (Homberg et al., 1999). To analyze whether the TL neurons are candidates for postsynaptic partners of TuLAL1 neurons, we stained TuLAL1 neurons through tracer injection into the LUC of the AOTU, followed by marking of TL neurons through GABA immunofluorescence labeling. Terminals of TuLAL1 neurons were large hat-like structures with an uneven surface (Figures 5B,C). Close inspection of single complexes in double labeled samples revealed a distinct pattern: hat-like terminals from TuLAL1 neurons partly enclosed the terminals of side branches of TL neurons (Figures 5B,C).

### Ultrastructure and Synaptic Connections

To investigate the synaptic connectivity between TuLAL1 and TL neurons, we studied the microglomeruli at the ultrastructural level. Transmission electron micrographs showed that the synaptic complexes have a diameter of up to 8  $\mu\text{m}$  and are partly enwrapped by layers of glia (Figures 6A,B). Therefore, individual synaptic complexes were clearly distinguishable from one another. Each microglomerular complex consisted of a single large cup-shaped profile,



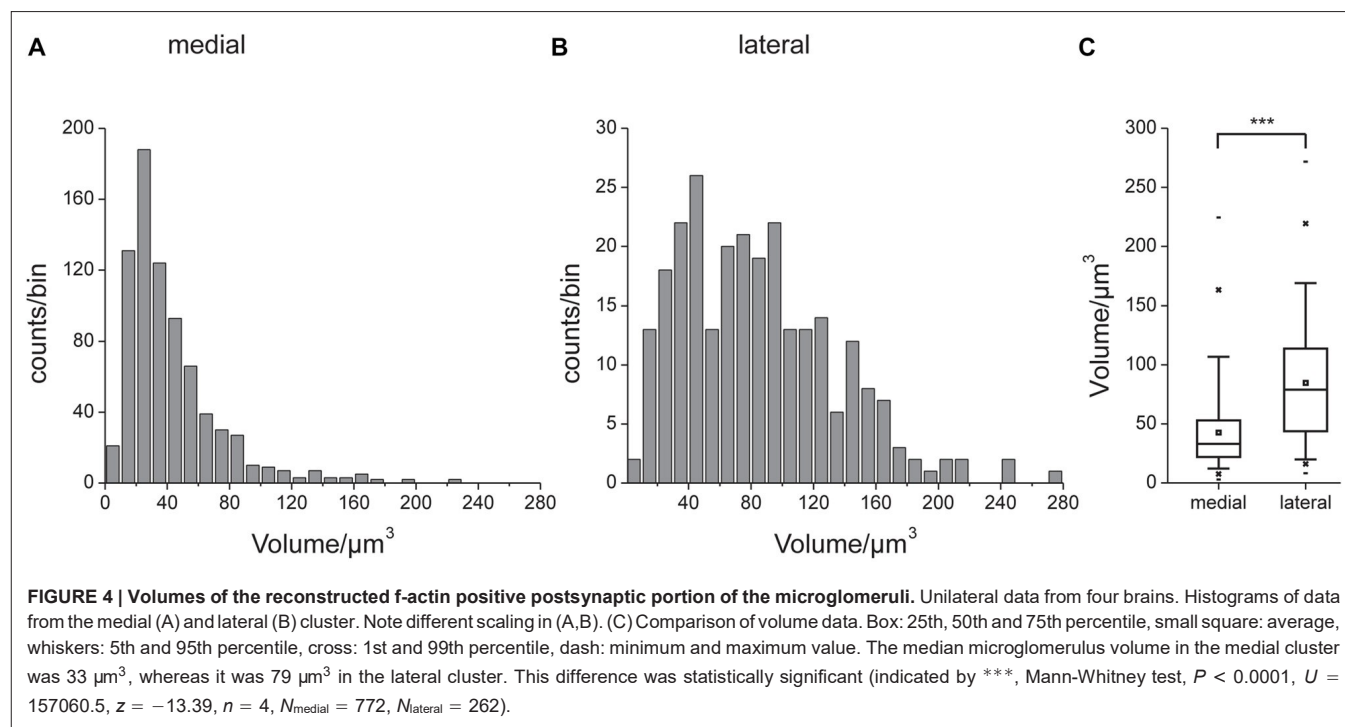
apparently from a TuLAL1 neuron, enclosing numerous small profiles (SPs), apparently originating from TL neurons. The large profiles (LPs) of TuLAL1 neurons were less electron dense than the small central profiles. They contained many mitochondria and two types of vesicle, numerous clear vesicles (cVs) with a diameter of 20–60 nm and a small number of dense core vesicles (dcVs) with a diameter of 50–80 nm (Figure 6). The bulk of vesicles was concentrated close to the internal membrane of the cup-shaped LP. The synaptic endings of the TL neurons formed many SP surrounded by the single LP. Apparently, one or a few processes from TL neurons enter the microglomerulus and give rise to a dense bush of ramifications in the center (Figure 6). These profiles also contained some mitochondria but additional organelles were difficult to distinguish. All synaptic connections were made at the inside of the complexes; we never found active zones at the exterior membrane of the LP. Synaptic release sites were identified based on their electron dense ultrastructural specializations as described previously in other studies (Gray, 1959; Uchizono,

1965; Aghajanian and Bloom, 1967; Colonnier, 1968; Mayhew, 1996; Watson and Schürmann, 2002). The synapses we found were only formed between LPs and SPs, no synaptic connections were found between SPs. The electron dense synaptic release sites enabled us to identify the LPs of TuLAL1 neurons as presynaptic terminals. They included transmitter-containing vesicles and a number of mitochondria as described above. Additionally, an electron-dense membrane structure was present as transmitter release site. The associated membranes of the small postsynaptic profiles of TL neurons showed an electron-dense thickening, implying postsynaptic densities. Another feature of synaptic sites was a cleft of diverse thickness between the pre- and postsynaptic membranes. We were able to distinguish two types of synapses. The more frequent type was a divergent dyad where one presynaptic profile (Figure 7A, LP) was connected to two postsynaptic partners (Figure 7A, arrowheads). Due to the triangular arrangement and the preserved membranes the synaptic cleft was well defined. The presynaptic membranes showed aggregations of cVs in the vicinity of the electron-dense region. All involved postsynaptic profiles showed characteristic electron-dense membrane regions. The inside of the postsynaptic profiles was devoid of synaptic vesicles but contained mitochondria. The second type of synapse was a divergent tetrad, where the presynaptic profile (Figure 7B, LP) formed one synapse with four postsynaptic profiles (Figure 7B, arrowheads). The structure was nearly the same as in dyads: the presynaptic membrane showed an electron-dense fusion region with adjacent cVs, and a visible thickening of the postsynaptic membranes.

## DISCUSSION

We characterized the anatomy and ultrastructure of microglomerular synaptic complexes in the bulbs of the honeybee brain. These complexes have been investigated previously in the sky-compass pathway of the locust *Schistocerca gregaria* (Träger et al., 2008) and in the brain of the desert ant *Cataglyphis fortis* (Schmitt et al., 2016), and therefore, seem to be a highly conserved feature of the insect brain. The sky-compass pathway in locusts originates in specialized photoreceptors of the DRA of the compound eye and runs through the ME toward the LUC of the AOTU and from there to the LX and into the CB (reviewed by Pfeiffer and Homberg, 2014). This pathway has been characterized anatomically in the honeybee from the DRA to the LX, and the involved neurons strongly resemble those described in the locust (Zeller et al., 2015). In this study, we focused on the synaptic contacts in the bulbs of the LX, connecting the LUC of the AOTU to the CBL. In the locust (Träger et al., 2008) and desert ant (Schmitt et al., 2016) these microglomeruli have a remarkable size and structure. Therefore, they are likely to play an important role in the processing of visual information,





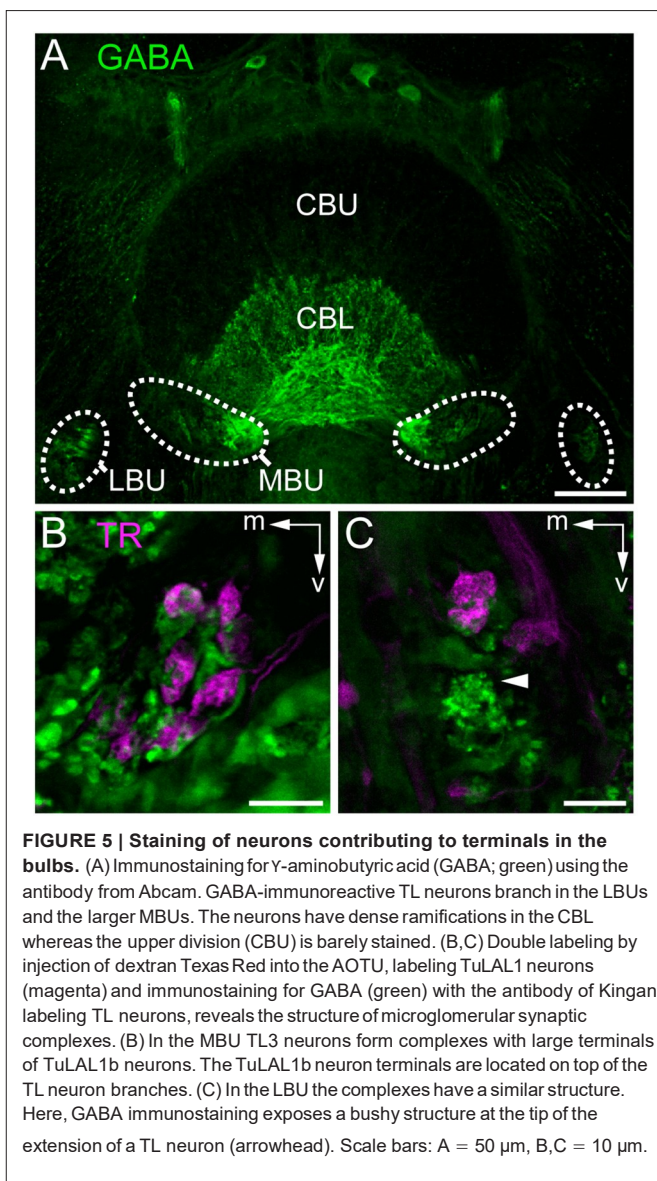
like sky-compass cues or visual detection, by providing proper visual input into the CX.

## Structure of the Microglomeruli of the LX Compared to Other Species

The large microglomerular synaptic complexes in *Apis mellifera* are located in the MBU and LBU of the LX. Each synaptic complex consists of one large presynaptic terminal formed by a TuLAL1a or TuLAL1b projection neuron from the LUC of the AOTU (Zeller et al., 2015). These terminals have been mentioned in a previous study (Mota et al., 2011) but have not been investigated in bees any further. The TuLAL1 neurons are connected to GABA-immunoreactive TL2 and TL3 tangential neurons of the CBL. Those TL neurons have conspicuous dendritic endings with single bushy structures at the tip of a stalk. At the ultrastructural level these endings appear as SP that are enclosed by a single LP of a TuLAL1 neuron. The large presynaptic terminals contain two types of vesicles: cVs and dcVs, but no information exists on their transmitter content. Single complexes are enclosed by glia cells. This glia can be referred to as astrocyte-like, as described in the fruit fly (Awasaki et al., 2008). It is the only known type of glia located within neuropils and associated with synaptic connections. Its function is likely the support of neurons, which in our case is very crucial considering the size and the amount of mitochondria in pre- and postsynaptic profiles. Additionally, this type of glia probably takes part in the modulation of neural connections (Awasaki et al., 2008; Edwards and Meinertzhagen, 2010). Homologs of the involved neuron types were characterized anatomically and physiologically in many other insect species and, therefore, seem to be highly conserved.

In the fruit fly *Drosophila melanogaster* GABAergic ring neurons of the ellipsoid body are homologous to TL neurons in honeybees. They form microglomeruli in the bulbs and connect them to the ellipsoid body, the equivalent of the CBL in the honeybee (Hanesch et al., 1989). Calcium-imaging experiments in tethered fruit flies showed that these microglomeruli are sensitive to visual features with an orientation tuning to vertical stripes (Seelig and Jayaraman, 2013; Weir and Dickinson, 2015). In the cricket *Gryllus bimaculatus* compass-neuron like cells (homologs of TL2 neurons in other species) that connect the LX with the CBL are sensitive to polarized light (Sakura et al., 2008). In the monarch butterfly (*Danaus plexippus*) there is only one cluster, the LBU, but different subtypes of TuLAL1 neuron ramify in spatially segregated areas. That is suggestive for a similar connectivity specificity as in honeybees. Colabeling of TL3- and TuLAL1 neurons revealed spatial proximity of large terminals of TuLAL1 neurons and profiles of TL3 neurons (Heinze and Reppert, 2011, 2012; Heinze et al., 2013). In the bumblebee *Bombus ignitus* TuLAL1a/b neurons share a very similar anatomy to the two cell types shown here (Pfeiffer and Kinoshita, 2012).

Although in all of these species one or both types of TuLAL1- and TL neuron have been described morphologically and partly investigated physiologically, the synaptic complexes they form have been explored only in desert ants and desert locusts. In the desert ant *Cataglyphis fortis* the microglomerular synaptic complexes are clustered in a single bulb (LBU; Schmitt et al., 2016) whereas in honeybees we found two clusters, one in the LBU and the other one in the MBU. Although the general anatomy appears very similar in honeybees and ants, a closer look reveals some distinct differences.



In honeybees the complexes have a diameter of up to 8  $\mu$ m compared to only 5  $\mu$ m in ants (Schmitt et al., 2016). Likewise, the presynaptic terminals appear larger and swollen whereas in ants they have the shape of a thin cup. Another difference between the two species lies in the vesicle pool within the presynaptic terminals. In ants the LP is densely packed with cVs and only a few dcVs and mitochondria are visible (Schmitt et al., 2016). In the honeybee a higher number of mitochondria and dcVs, but fewer cVs were found. The reason for the differences in the vesicle stock is currently unknown, fixation artifacts seem unlikely due to the high-quality conservation of the tissue.

Microglomerular synaptic complexes of the bulbs in the desert locust *Schistocerca gregaria* share a similar

distribution, anatomy and ultrastructure to those in honeybees (Träger et al., 2008). However, one difference arises again in the vesicle stock. In locusts the presynaptic terminal is filled with cVs throughout the profile like in ants, whereas in honeybees vesicles are concentrated near synaptic release sites. Electrophysiological and anatomical studies in locusts showed that these synaptic complexes are part of the sky-compass pathway (Vitzthum et al., 2002; Pfeiffer et al., 2005; Träger et al., 2008). Taken together, the pathway described by Zeller et al. (2015) and the anatomical similarity to locusts shown here strongly suggest that the complexes are part of the sky-compass pathway in honeybees as well.

### Synaptic Complexes in Other Species

In insects, neuromuscular junctions are monads, and most chemical synaptic connections in the central nervous system (CNS) are dyads (Wernitznig et al., 2015). In the visual system, more complex multi-contact synapses have been described in the optic lobes, more precisely in the LA, of muscomorph flies (Shaw and Meinertzhagen, 1986; Meinertzhagen and O'Neil, 1991) and locusts (Wernitznig et al., 2015). In both taxa, photoreceptor neurons provide input to LA monopolar cells via triads and tetrads. At a later stage of visual processing, multi-contact synapses have been mentioned in the calyces of honeybees and in the microglomerular synaptic complexes in the bulbs of the desert locust *Schistocerca gregaria* and in the desert ant *Cataglyphis fortis*. In ants the synaptic connection is formed by triads, tetrads and only a few dyads (Schmitt et al., 2016). Our data revealed a slightly different synaptic formation in the honeybee, with connections being formed by dyads and tetrads. By contrast in locusts the synaptic connections within the microglomerular complexes consists solely of regular ribbons of dyads (Träger et al., 2008). Neither in ants nor in honeybees synapses in the microglomerular complexes are arranged in such a distinguishable and regular manner.

Microglomeruli containing multi-contact synapses also occur in the calyces of the mushroom bodies of insects that are regarded as high-order sensory integration centers. The organization of microglomerular complexes in the calyces is reversed compared to those in the bulbs. In the mushroom body, a microglomerulus consists of one central presynaptic bouton that is surrounded by many postsynaptic profiles belonging to several Kenyon cells (Trujillo-Cenóz and Melamed, 1962; Schürmann, 1974; Ganeshina and Menzel, 2001; Groh and Rössler, 2011). In the complexes in the bulbs of the honeybee it is so far not known if the postsynaptic profiles are related to one or various neurons in one microglomerulus. The calycal microglomerular complexes are smaller than those in the bulbs. In the bulbs of the bee, complexes have a diameter of approximately 8  $\mu$ m, whereas the size of the microglomeruli in the calyx of honeybees reaches only 2–3  $\mu$ m (Ganeshina and Menzel, 2001). The synaptic connections in the calyx of honeybees are formed by dyads, triads and tetrads (Groh et al., 2012). In the calycal microglomeruli of fruit flies the number of postsynaptic profiles within one synapse can differ between 1 and 14 (Butcher et al., 2012).



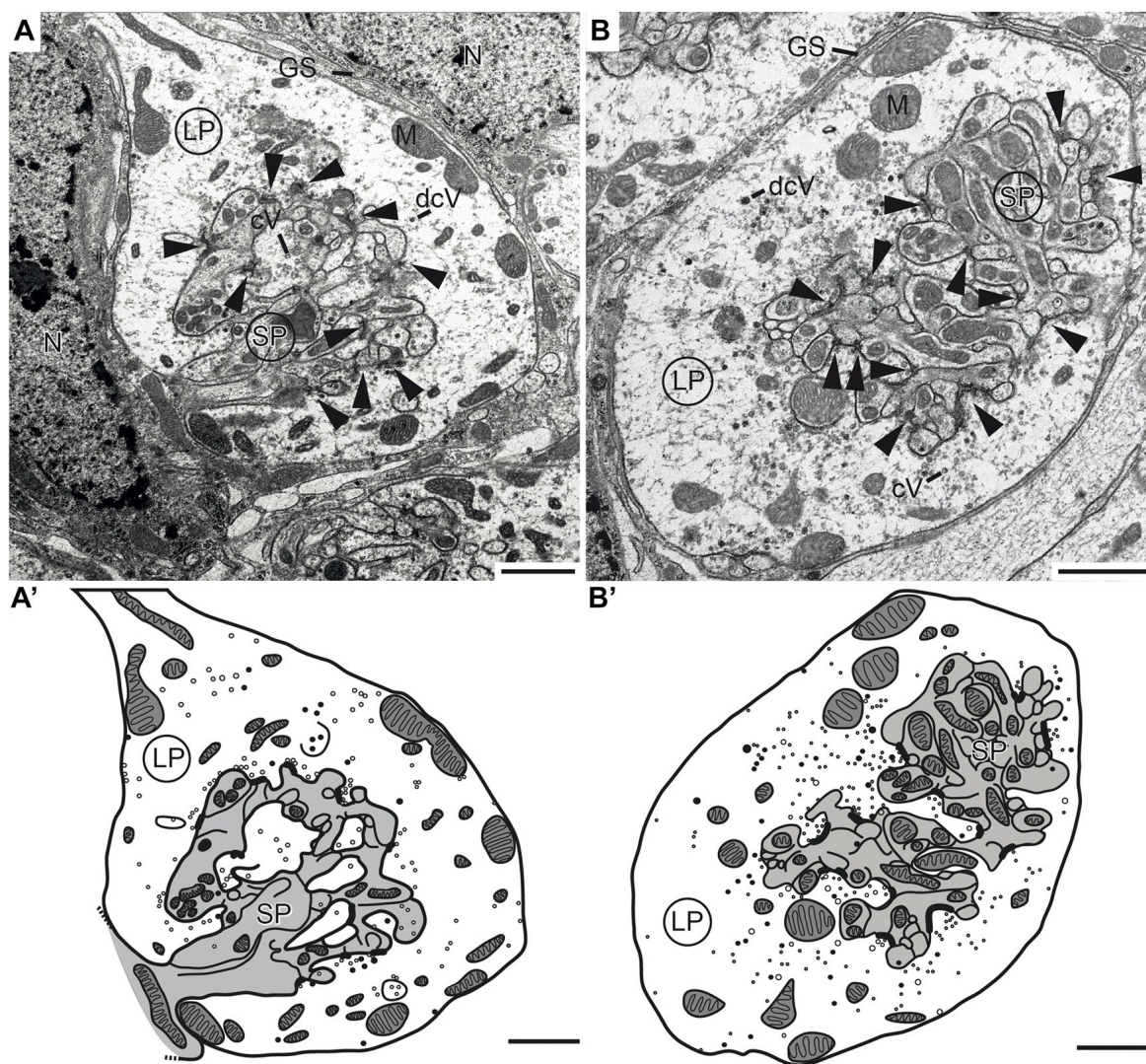


**FIGURE 6 | Transmission electron micrographs showing the ultrastructure of microglomerular synaptic complexes in the LBU (A,A') and the MBU (B,B') of the lateral complex (LX).** (A) The complex consists of one large profile (LP) enclosing many small profiles (SPs). The LP contains clear vesicles (cVs), some large dense core vesicles (dcVs) and many mitochondria (M) and forms numerous synaptic connections with the SP (arrowheads). A glial sheath (GS) is wrapped around the complex. It is located in proximity to two nuclei of other cells (N). (A') Drawing of the complex in (A) shows the borders of the profiles, organelles and synaptic connections. All parts of the LP are shown in white and the SP in gray. (B,B') The structure of the complex in the LBU is similar to the one in the MBU: one LP encloses many SP. Scale bars = 1  $\mu$ m.

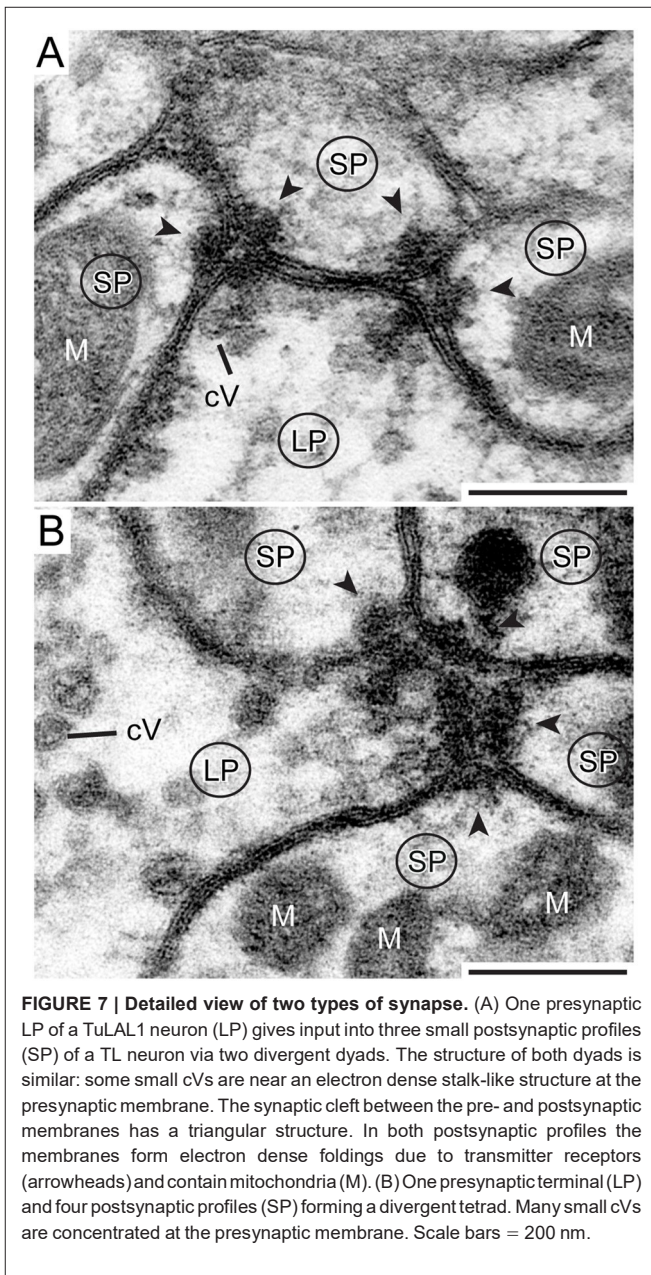
Similar to the synaptic complexes in the bulbs, the postsynaptic elements of mushroom body microglomeruli contain high concentrations of motile f-actin (Groh and Rössler, 2011).

Microglomerular synaptic complexes do not only occur in insects. Two well studied types of giant axosomatic synapses in the mammalian CNS, more precisely in the auditory pathway, are the endbulb and the calyx of Held. The presynaptic calyx of Held, probably the largest synaptic terminal in the mammalian CNS, envelops the soma of a principal cell (Walmsley et al., 1998; review von Gersdorff and Borst, 2002; Schneggenburger and Forsythe, 2006; Rodríguez-Contreras et al., 2008). EM studies in rats showed that one calyx contains about 550

active zones (Sätzler et al., 2002). In comparison, a small glomerulus in the LX of locusts had around 150 active zones (Träger et al., 2008).

### Functional Implications of Microglomerular Synaptic Complexes

Indications for the functional implication of these complexes exist so far only for ring neurons, the *Drosophila melanogaster* equivalent to honeybee TL neurons. There, activity patterns of the dendrites in the bulbs, triggered by a vertical stripe, suggest a retinotopic arrangement and therefore a representative map of the visual surrounding (Seelig and Jayaraman, 2013).



While the anatomical data presented in this study provide no direct insight into the physiology of the synaptic complexes of the LX, their structural characteristics allows for some speculations concerning functionality. First, their striking size is remarkable and to our knowledge unique within the insect brain. We assume that the organization and ultrastructure of the complexes leads to a fast and reliable signal transmission. The composition of one large presynaptic terminal enclosing the postsynaptic profiles with all active zones in the center might indicate a low-noise signal transmission. Additionally, the astrocyte-like glial layers around the synaptic complexes likely support reliable transmission. In *Drosophila* astrocyte-like glia is important to clear the synaptic cleft from neurotransmitters

and their enzymatic breakdown products (reviewed in Freeman, 2015). In honeybees acetylcholinesterase has been detected in the microglomerular synaptic complexes in the bulbs (Kreissl and Bicker, 1989), suggesting that acetylcholine is likely to act as a transmitter there. NADPH diaphorase labeling in locusts, suggesting nitric oxide synthase activity, revealed staining in TL2 neurons and the LBUs, suggesting the presence of nitric oxide (Kurylas et al., 2005). Nitric oxide is known to function as a retrograde messenger in sensory processing in the nervous system. Since it is gaseous it can pass membranes and diffuse into the surrounding tissue without synaptic release (Dawson and Snyder, 1994; Müller, 1997; Bicker, 2001). Therefore, the glia sheaths (GS) around the single complexes might work as diffusion barrier for NO as well as transmitters between adjacent complexes like the ensheathing glia around individual neuropils.

Electrophysiological data of the calyx of Held showed that one single action potential in the presynaptic profile leads to rapid depolarization of the postsynaptic profiles. This on the other hand ensures not only a rapid transmission but also the retention of the timing of signals (Schneggenburger and Forsythe, 2006). Given that the organization of the calyces of Held is comparable to the synaptic complexes in the LX of honeybees, the same principle for fast transmission could be valid here as well. The divergent multi-contact synapses support this assumption, as the transmitter release from one presynaptic membrane simultaneously addresses two or four postsynaptic partners. This could lead to a depolarization of the postsynaptic neuron above threshold by only one presynaptic action potential. So far we could not determine the ratio between the involved pre- and postsynaptic neurons. Whether this ratio is 1:1 as in the calyx of Held, divergent as in locusts, or convergent might be addressed in further studies.

Why do honeybees need such large complexes promoting reliable signal transmission? A closer look at the localization might give some indications. These microglomerular complexes are part of the visual pathway. The preservation of timing is a crucial feature in most sensory pathways to maintain all information of a stimulus. The calyces of Held are part of a pathway for sound-source localization based on time delays, where signal timing is absolutely essential. Another example for the importance of timing for an efficient signal processing is the dual olfactory pathway of the honeybee, where the responses within and between the two tracts reveal an odor-dependent latency (Brill et al., 2013, 2015). Studies on experience-related plasticity of the synaptic complexes in the LX of the desert ant (Schmitt et al., 2016) revealed that the number of synaptic complexes increases upon first exposure to light. The relatively high variation in the total number of synaptic complexes we found in the honeybee may arise from different levels of visual experience in the samples of winter bees used for the present study.

Taken together, the anatomical formation, compared to well-known features of other synaptic complexes, strongly suggests that the microglomerular synaptic complexes in the LX of



honeybees and other insects are essential for reliable signal transmission in the sky-compass pathway. It seems plausible that transmission speed and input timing is crucial in a sophisticated visual task like navigation and orientation during flight. However, future neurophysiological experiments on the neurons described here and their synaptic complexes are needed to better understand the properties of signal transmission at this specific point of the visual neuronal system.

## AUTHOR CONTRIBUTIONS

KP, UH and WR designed the study. MH, AB, CS and RH acquired the data. MH and TSM analyzed and interpreted the data and drafted the manuscript. All authors revised the manuscript critically for important intellectual content, approved the final version to be published and are accountable for all aspects of the work.

## REFERENCES

- Aghajanian, G. K., and Bloom, F. E. (1967). The formation of synaptic junctions in developing rat brain: a quantitative electron microscopic study. *Brain Res.* 6, 716–727. doi: 10.1016/0006-8993(67)90128-x
- Awasaki, T., Lai, S. L., Ito, K., and Lee, T. (2008). Organization and postembryonic development of glia cells in the adult central brain of *Drosophila*. *J. Neurosci.* 28, 13742–13753. doi: 10.1523/jneurosci.4844-08.2008
- Baschong, W., Duerrenberger, M., Mandinova, A., and Suetterlin, R. (1999). Three dimensional visualization of the cytoskeleton by confocal laser scanning microscopy. *Methods Enzymol.* 307, 173–189. doi: 10.1016/S0076-6879(99)07013-5
- Bicker, G. (2001). Sources and targets of nitric oxide signaling in insect nervous systems. *Cell Tissue Res.* 303, 137–146. doi: 10.1007/s0044100 00321
- Brill, M. F., Meyer, A., and Rössler, W. (2015). It takes two—coincidence coding within the dual olfactory pathway of the honeybee. *Front. Physiol.* 6:208. doi: 10.3389/fphys.2015.00208
- Brill, M. F., Rosenbaum, T., Reus, I., Kleineidam, C. J., Nawrot, M. P., and Rössler, W. (2013). Parallel processing via a dual olfactory pathway in the honeybee. *J. Neurosci.* 33, 2443–2456. doi: 10.1523/jneurosci.4268-12.2013
- Butcher, N. J., Friedrich, A. B., Lu, Z., Tanimoto, H., and Meinertzhagen, I. A. (2012). Different classes of input and output neurons reveal new features in microglomeruli of the adult *Drosophila* mushroom body calyx. *J. Comp. Neurol.* 520, 2185–2201. doi: 10.1002/cne.23037
- Collett, M., Chittka, L., and Collett, T. S. (2013). Spatial memory in insect navigation. *Curr. Biol.* 23, R789–R800. doi: 10.1016/j.cub.2013.07.020
- Colonnier, M. (1968). Synaptic patterns on different cell types in the different laminae of the cat visual cortex. An electron microscope study. *Brain Res.* 9, 268–287. doi: 10.1016/0006-8993(68)90234-5
- Dawson, T. M., and Synder, S. H. (1994). Gases as biological messengers: nitric oxide and carbon monoxide in the brain. *J. Neurosci.* 14, 5147–5159.
- Edwards, T., and Meinertzhagen, I. A. (2010). The functional organization of glia in the adult brain of *Drosophila* and other insects. *Prog. Neurobiol.* 90, 471–497. doi: 10.1016/j.pneurobio.2010.01.001
- el Jundi, B., Pfeiffer, K., Heinze, S., and Homberg, U. (2014). Integration of polarization and chromatic cues in the insect sky compass. *J. Comp. Physiol. A Neuroethol. Sens. Neural Behav. Physiol.* 200, 575–589. doi: 10.1007/s00359-014-0890-6
- Freeman, M. R. (2015). *Drosophila* central nervous system glia. *Cold Spring Harb. Perspect. Biol.* 7:a020552. doi: 10.1101/cshperspect.a 020552
- Ganeshina, O., and Menzel, R. (2001). GABA-immunoreactive neurons in the mushroom bodies of the honeybee: an electron microscopic study. *J. Comp. Neurol.* 437, 335–349. doi: 10.1002/cne.1287
- Gray, E. G. (1959). Axosomatic and axodendritic synapses in the cerebral cortex: an electron microscopy study. *J. Anat.* 93, 420–433.
- Groh, C., Lu, Z., Meinertzhagen, I. A., and Rössler, W. (2012). Age-related plasticity in the synaptic ultrastructure of neurons in the mushroom body calyx of the honeybee *Apis mellifera*. *J. Comp. Neurol.* 520, 3509–3527. doi: 10.1002/cne.23102
- Groh, C., and Rössler, W. (2011). Comparison of microglomerular structures in the mushroom body calyx of neopteran insects. *Arthropod Struct. Dev.* 40, 358–367. doi: 10.1016/j.asd.2010.12.002
- Groh, C., Tautz, J., and Rössler, W. (2004). Synaptic organization in the adult honey bee brain is influenced by brood-temperature control during pupal development. *Proc. Natl. Acad. Sci. USA* 101, 4268–4273. doi: 10.1073/pnas.0400773101
- Hanesch, U., Fischbach, K.-F., and Heisenberg, M. (1989). Neuronal architecture of the central complex in *Drosophila melanogaster*. *Cell Tissue Res.* 257, 343–366. doi: 10.1007/bf00261838
- Heinze, S., and Reppert, S. M. (2011). Sun compass integration of skylight cues in migratory monarch butterflies. *Neuron* 69, 345–358. doi: 10.1016/j.neuron.2010.12.025
- Heinze, S., and Reppert, S. M. (2012). Anatomical basis of sun compass navigation I: the general layout of the monarch butterfly brain. *J. Comp. Neurol.* 520, 1599–1628. doi: 10.1002/cne.23054
- Heinze, S., Florman, J., Asokaraj, S., el Jundi, B., and Reppert, S. M. (2013). Anatomical basis of sun compass navigation II: the neuronal composition of the central complex of the monarch butterfly. *J. Comp. Neurol.* 521, 267–298. doi: 10.1002/cne.23259
- Homberg, U., Heinze, S., Pfeiffer, K., Kinoshita, M., and el Jundi, B. (2011). Central neural coding of sky polarization in insects. *Philos. Trans. R. Soc. Lond. B Biol. Sci.* 366, 680–687. doi: 10.1098/rstb.2010.0199
- Homberg, U., Hofer, S., Pfeiffer, K., and Gebhardt, S. (2003). Organization and neural connections of the anterior optic tubercle in the brain of the locust, *Schistocerca gregaria*. *J. Comp. Neurol.* 462, 415–430. doi: 10.1002/cne.10771
- Homberg, U., Kingan, T. G., and Hildebrand, J. G. (1990). Distribution of FMRamide-like immunoreactivity in the brain and suboesophageal ganglion of the sphinx moth *Manduca sexta* and colocalization with SCP $\beta$ , BPP and GABA-like immunoreactivity. *Cell Tissue Res.* 259, 401–19. doi: 10.1007/bf01740767
- Homberg, U., Vitzthum, H., Müller, M., and Binkle, U. (1999). Immunocytochemistry of GABA in the central complex of the locust *Schistocerca gregaria*: identification of immunoreactive neurons and colocalization with neuropeptides. *J. Comp. Neurol.* 409, 495–507. doi: 10.1002/(SICI)1096-9861(19990705)409:3<495::AID-CNE12>3.0.CO;2-F
- Hoskins, S. G., Homberg, U., Kingan, T. G., Christensen, T. A., and Hildebrand, J. G. (1986). Immunocytochemistry of GABA in the antennal lobes of the sphinx moth *Manduca sexta*. *Cell Tissue Res.* 244, 243–252. doi: 10.1007/bf00219199
- Ito, K., Shinomiya, K., Ito, M., Armstrong, J. D., Boyan, G., Hartenstein, V., et al. (2014). A systematic nomenclature for the insect brain. *Neuron* 81, 755–765. doi: 10.1016/j.neuron.2013.12.017
- Junglas, B., Briegel, A., Burghardt, T., Walther, P., Wirth, R., Huber, H., et al. (2008). *Ignicoccus hospitalis* and *Nanoarchaeum equitans*: ultrastructure, cell-cell interaction and 3D reconstruction from serial sections of freeze-substituted cells and by electron cryotomography. *Arch. Microbiol.* 190, 395–408. doi: 10.1007/s00203-008-0402-6
- Kreissl, S., and Bicker, G. (1989). Histochemistry of acetylcholinesterase and immunocytochemistry of an acetylcholine receptor-like antigen in the brain of the honeybee. *J. Comp. Neurol.* 286, 71–84. doi: 10.1002/cne.9028 60105
- Kuebler, L. S., Kelber, C., and Kleineidam, C. J. (2010). Distinct antennal lobe phenotypes in the leaf-cutting ant (*Atta vollenweideri*). *J. Comp. Neurol.* 518, 352–365. doi: 10.1002/cne.22217

- Kurylas, A. E., Ott, S. R., Schachtner, J., Elphick, M. R., Williams, L., and Homberg, U. (2005). Localization of nitric oxide synthase in the central complex and surrounding midbrain neuropils of the locust *Schistocerca gregaria*. *J. Comp. Neurol.* 484, 206–223. doi: 10.1002/cne.20467
- Mayhew, T. M. (1996). How to count synapses unbiasedly and efficiently at the ultrastructural level: proposal for a standard sampling and counting protocol. *J. Neurocytol.* 25, 793–804. doi: 10.1007/bf02284842
- McDonald, K. (2007). Cryopreparation methods for electron microscopy of selected systems. *Methods Cell Biol.* 79, 23–56. doi: 10.1016/s0091-679x(06)79002-1
- Meinertzhagen, I. A., and O'Neil, S. D. (1991). Synaptic organization of columnar elements in the lamina of the wild type in *Drosophila melanogaster*. *J. Comp. Neurol.* 305, 232–263. doi: 10.1002/cne.903050206
- Menzel, R., De Marco, R. J., and Greggers, U. (2006). Spatial memory, navigation and dance behavior in *Apis mellifera*. *J. Comp. Physiol. A Neuroethol. Sens. Neural Behav. Physiol.* 192, 889–903. doi: 10.1007/s00359-006-0136-3
- Mota, T., Yamagata, N., Giurfa, M., Gronenberg, W., and Sandoz, J. C. (2011). Neural organization and visual processing in the anterior optic tubercle of the honeybee brain. *J. Neurosci.* 31, 11443–11456. doi: 10.1523/jneurosci.0995-11.2011
- Müller, U. (1997). The nitric oxide system in insects. *Prog. Neurobiol.* 51, 363–381. doi: 10.1016/s0301-0082(96)00067-6
- Müller, M., Homberg, U., and Kühn, A. (1997). Neuroarchitecture of the lower division of the central body in the brain of the locust (*Schistocerca gregaria*). *Cell Tissue Res.* 288, 159–176. doi: 10.1007/s004410050803
- Müller-Reichert, T., Srayko, M., Hyman, A., O'Toole, E. T., and McDonald, K. (2007). Correlative light and electron microscopy of early *Caenorhabditis elegans* embryos in mitosis. *Methods Cell Biol.* 79, 101–119. doi: 10.1016/s0091-679x(06)79004-5
- Pasch, E., Muenz, T. S., and Rössler, W. (2011). CaMKII is differentially localized in synaptic regions of Kenyon cells within the mushroom bodies of the honeybee brain. *J. Comp. Neurol.* 519, 3700–3712. doi: 10.1002/cne.22683
- Peschke, M., Moog, D., Klingl, A., Maier, U. G., and Hempel, F. (2013). Evidence for glycoprotein transport into complex plastids. *Proc. Natl. Acad. Sci. USA* 110, 10860–10865. doi: 10.1073/pnas.1301945110
- Pfeiffer, K., and Homberg, U. (2014). Organization and functional roles of the central complex in the insect brain. *Annu. Rev. Entomol.* 59, 165–184. doi: 10.1146/annurev-ento-011613-162031
- Pfeiffer, K., and Kinoshita, M. (2012). Segregation of visual inputs from different regions of the compound eye in two parallel pathways through the anterior optic tubercle of the bumblebee (*Bombus ignitus*). *J. Comp. Neurol.* 520, 212–229. doi: 10.1002/cne.23016
- Pfeiffer, K., Kinoshita, M., and Homberg, U. (2005). Polarization-sensitive and light-sensitive neurons in two parallel pathways passing through the anterior optic tubercle in the locust brain. *J. Neurophysiol.* 94, 3903–3915. doi: 10.1152/jn.00276.2005
- Rachal, R., Meyer, C., Klingl, A., Gürster, S., Heimerl, T., Wasserburger, N., et al. (2010). Analysis of the ultrastructure of archaebacteria by electron microscopy. *Methods Cell Biol.* 96, 47–69. doi: 10.1016/s0091-679x(10)96003-2
- Reynolds, E. S. (1963). The use of lead citrate at high pH as an electron- opaque stain in electron microscopy. *J. Cell Biol.* 17, 208–213. doi: 10.1083/jcb.17.1.208
- Sakura, M., Lambrinos, D., and Labhart, T. (2008). Polarized skylight navigation in insects: model and electrophysiology of e-vector coding by neurons in the central complex. *J. Neurophysiol.* 99, 667–682. doi: 10.1152/jn.00784.2007
- Sätzler, K., Söhl, L. F., Bollmann, J. H., Borst, J. G. G., Frotscher, M., Sakmann, B., et al. (2002). Three-dimensional reconstruction of a calyx of Held and its postsynaptic principal neuron in the medial nucleus of the trapezoid body. *J. Neurosci.* 22, 10567–10579.
- Schäfer, S., and Bicker, G. (1986). Distribution of GABA-like immunoreactivity in the brain of the honeybee. *J. Comp. Neurol.* 246, 287–300. doi: 10.1002/cne.902460302
- Schmitt, F., Stieb, S. M., Wehner, R., and Rössler, W. (2016). Experience-related reorganization of giant synapses in the lateral complex: potential role in plasticity of the sky-compass pathway in the desert ant *Cataglyphis fortis*. *Dev. Neurobiol.* 76, 390–404. doi: 10.1002/dneu.22322
- Schneggenburger, R., and Forsythe, I. D. (2006). The calyx of Held. *Cell Tissue Res.* 326, 311–337. doi: 10.1007/s00441-006-0272-7
- Schürmann, F. W. (1974). Bemerkungen zur Funktion der Corpora Pedunculata im Gehirn der Insekten aus morphologischer Sicht. *Exp. Brain Res.* 19, 406–432. doi: 10.1007/bf00234464
- Seelig, J. D., and Jayaraman, V. (2013). Feature detection and orientation tuning in the *Drosophila* central complex. *Nature* 503, 262–266. doi: 10.1038/nature12601
- Shaw, S. R., and Meinertzhagen, I. A. (1986). Evolutionary progression at synaptic connections made by identified homologous neurons. *Proc. Natl. Acad. Sci. USA* 83, 7961–7965. doi: 10.1073/pnas.83.20.7961
- Srinivasan, M. V. (2015). Where paths meet and cross: navigation by path integration in the desert ant and the honeybee. *J. Comp. Physiol. A Neuroethol. Sens. Neural Behav. Physiol.* 201, 533–546. doi: 10.1007/s00359-015-1000-0
- Träger, U., Wagner, R., Bausenwein, B., and Homberg, U. (2008). A novel type of microglomerular synaptic complex in the polarization vision pathway of the locust brain. *J. Comp. Neurol.* 506, 288–300. doi: 10.1002/cne.21512
- Trujillo-Cenóz, O., and Melamed, J. (1962). Electron microscope observations on the calyces of the insect brain. *J. Ultrastruct. Res.* 7, 389–398. doi: 10.1016/s0022-5320(62)90035-7
- Uchizono, K. (1965). Characteristics of excitatory and inhibitory synapses of the central nervous system. *Nature* 207, 642–643. doi: 10.1038/207642a0
- Vitzthum, H., Müller, M., and Homberg, U. (2002). Neurons of the central complex of the locust *Schistocerca gregaria* are sensitive to polarized light. *J. Neurosci.* 22, 1114–1125.
- von Frisch, K. (1949). Die Polarisation des Himmelslichtes als orientierender Faktor bei den Tänzen der Bienen. *Experientia* 5, 142–148. doi: 10.1007/bf02174424
- von Gersdorff, H., and Borst, J. G. G. (2002). Short-term plasticity at the calyx of Held. *Nat. Rev. Neurosci.* 3, 53–64. doi: 10.1038/nrn705
- Walmsley, B., Alvarez, F. J., and Fyfe, R. E. W. (1998). Diversity of structure and function at mammalian central synapses. *Trends Neurosci.* 21, 81–88. doi: 10.1016/s0166-2236(97)01170-3
- Walther, P., and Ziegler, A. (2002). Freeze substitution of high-pressure frozen samples: the visibility of biological membranes is improved when the substitution medium contains water. *J. Microsc.* 208, 3–10. doi: 10.1046/j.1365-2818.2002.01064.x
- Watson, A. H. D., and Schürmann, F. W. (2002). Synaptic structure, distribution and circuitry in the central nervous system of the locust and related insects. *Microsc. Res. Tech.* 56, 210–226. doi: 10.1002/jemt.10031
- Wehner, R. (2003). Desert ant navigation: how miniature brains solve complex tasks. *J. Comp. Physiol. A Neuroethol. Sens. Neural Behav. Physiol.* 189, 579–588. doi: 10.1007/s00359-003-0431-1
- Weir, P. T., and Dickinson, M. H. (2015). Functional divisions for visual processing in the central brain of flying *Drosophila*. *Proc. Natl. Acad. Sci. USA* 112, E5523–E5532. doi: 10.1073/pnas.1514415112
- Wernitznig, S., Rind, F. C., Pöhl, P., Zankel, A., Pritz, E., Kolb, D., et al. (2015). Synaptic connections of first-stage visual neurons in the locust *Schistocerca gregaria* extend evolution of tetrad synapses back 200 million years. *J. Comp. Neurol.* 523, 298–312. doi: 10.1002/cne.23682
- Wolff, T., Iyer, N. A., and Rubin, G. M. (2015). Neuroarchitecture and neuroanatomy of the *Drosophila* central complex: a GAL4-based dissection of protocerebral bridge neurons and circuits. *J. Comp. Neurol.* 523, 997–1037. doi: 10.1002/cne.23705
- Zeller, M., Held, M., Bender, J., Berz, A., Heinloth, T., Hellfritz, T., et al. (2015). Transmedulla neurons in the sky compass network of the honeybee (*Apis mellifera*) are a possible site of circadian input. *PLoS One* 10:e0143244. doi: 10.1371/journal.pone.0143244

**Conflict of Interest Statement:** The authors declare that the research was conducted in the absence of any commercial or financial relationships that could be construed as a potential conflict of interest.

Copyright © 2016 Held, Berz, Hensgen, Muenz, Scholl, Rössler, Homberg and Pfeiffer. This is an open-access article distributed under the terms of the Creative Commons Attribution License (CC BY). The use, distribution and reproduction in other forums is permitted, provided the original author(s) or licensor are credited and that the original publication in this journal is cited, in accordance with accepted academic practice. No use, distribution or reproduction is permitted which does not comply with these terms.



---

**CHAPTER III:**  
**CALCIUM IMAGING IN TETHERED BEHAVING HONEYBEES**

---



## INTRODUCTION

Honeybees have been in the focus of insect ethologists for decades, offering many-faceted behaviors with some being unique in the insect world. The social structure of a hive of these eusocial insects comprise one fertile queen, male drones occurring only in early summer, and thousands of infertile female worker bees. The age-dependent division of labor of worker bees came to the fore in recent neuroethological investigations, especially regarding experienced-based neural plasticity due to the transition from inside workers to foragers (e.g. Fahrbach et al., 1998; Groh et al., 2012; Cabirol et al., 2018). Another important behavioral aspect of honeybees that has been investigated by ethologists over 70 years ago and is now studied from a neurobiological and neuroethological angle is the orientational and navigational capability of these central place foragers. Their outbound flight to forage for water or to collect pollen and nectar often has a sinuous path stretching over several kilometers whereas the flight path back to the hive is in a rather straight beeline (Wehner and Srinivasan, 2003; Srinivasan, 2015). For the direct inbound flight, bees use a navigational tool known as path integration, a combination of directional information and an odometer which stores the traveled distance. In bees, the odometer system calculates the covered distance using optic flow, which is translational motion of images across the retina (Esch et al., 2001; reviewed by Srinivasan, 2014). Furthermore, behavioral studies showed that they rely heavily on visual information to stay on course back to the hive. They use primarily celestial cues like the sun and the polarization pattern of the blue sky in a sun-based compass system but also refine their steering by using landmarks during their inbound flight (von Frisch, 1949; Zeil et al., 1996; Kraft et al., 2011; Menzel et al., 2019). The navigational abilities of honeybees also emerge in the waggle dance, a communication behavior that is unique in the insect world. The waggle dance is performed by foragers that are returning from a rewarding collecting site on the vertical comb. The goal of the dance is to transmit the information of the target site to recruit other worker bees to forage at the same location. The incoming foragers are performing in a figure-eight shape a specific sequence of turns and vibrations on the straight stretch with the latter encoding the distance to the food source. The direction of the destination is indicated by the angle to the right or the left between the vertical line on the comb and the straight stretch of the dance. The vertical line is based on the force of gravity and

indicates the azimuth of the sun. The angle between the straight stretch of the figure-eight shaped dance and the vertical line signals recruited bees the angle they have to take from the hive with respect to the sun's position (Fig. 1; von Frisch, 1949).

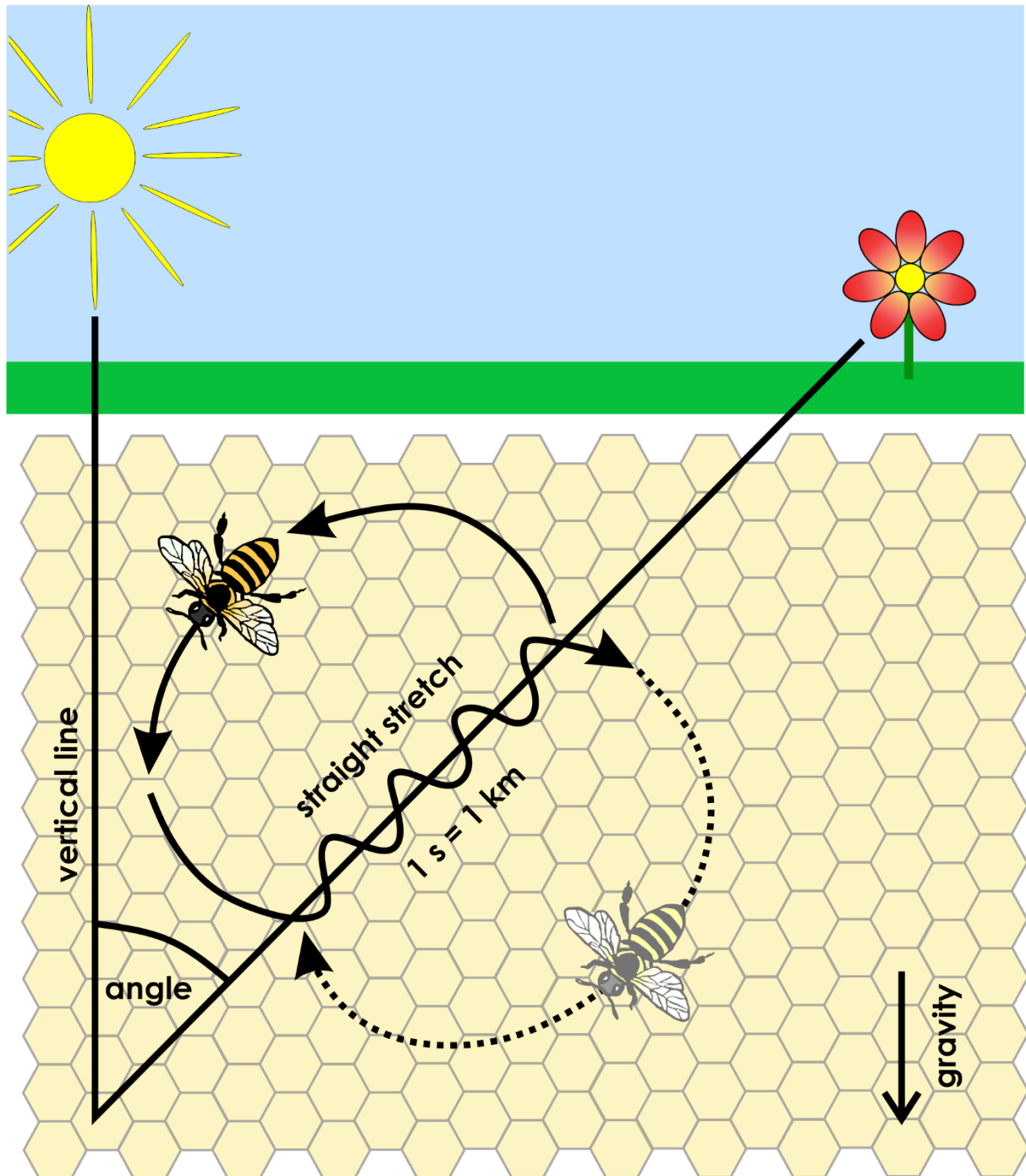


**Fig. 1: Structure of the waggle dance of honeybees.** A bee coming back from a foraging trip is dancing on the vertical comb in the hive in a figure-eight shape. The gravitational force is used as reference system, with the upward vertical line indicating the position of the sun. The bee dances in an angle to the vertical line that represents the angle between the position of the sun's azimuth and the food source. On the straight stretch of the figure-eight shape, the recruiting bee vibrates with her abdomen, with the duration of the vibration indicating the distance to the foraging site.

It is worth mentioning that the waggle dance is not only astonishing solely because of the recruiting system. Bees are furthermore capable to precisely translate the visual information gathered during the food search into vibrations and turns using the gravity on the vertical comb in the dark hive as a reference system. The recruited bees on the other hand receive the information mainly over tactile input. Therefore, they have to decode this input and compare it with the visual cues they receive during their own foraging flight, which requires a complex integration of different modalities. Even though the astonishing navigational and communication skills of bees have been described by ethological studies in detail, the underlying neuronal system has only partly been described anatomically. The location and mechanisms of the integration processes of the different modalities are however still largely unknown.

As a first step to close this gap, this project focused on the investigation of physiological responses of neurons within the sky-compass pathway to visual stimulation. Since visual interneurons exhibit state dependent responses (Seelig and Jayaraman, 2013; Weir and Dickinson, 2015; Rosner et al., 2019; Ache et al., 2019) and a long-term goal is to investigate visual guided behavior, the aim of this project was to record physiological responses from the compass system of behaving animals. This undertaking, which would be a novelty in the field of physiological investigations in honeybees, raised some serious methodical challenges. The physiological recordings had to be stable enough without completely restraining the animal. It was also crucial to be able to visualize the recorded cells since the physiology of neurons involved in the sky-compass system is still largely uncharted in the bee brain. For the same reason it was also favorable to be able to record from a population of neurons opposed to a single cell recording. Taken all those requirements together, calcium imaging appeared to be the method of choice for the presented project. There have been

two studies conducted in the upper unit of the anterior optic tubercle in honeybees brain using calcium imaging (Mota et al., 2011; Mota et al., 2013). This part of the tubercle receives visual input, especially color information, but is not part of the sky-compass pathway. In addition, some calcium imaging experiments have been performed in the antennal lobes of bees, the main olfaction input center (e.g. Rigosi et al., 2015; Jernigan et al., 2019). All these studies were carried out in completely restrained bees though, which prevented any investigation of the interaction between sensory stimulation and behavior. Especially state dependent physiological changes in neurons are not taken into account if the animals are not able to perform some sort of self-motion or behavioral responses. This disadvantage is particularly crucial because recent studies in locusts and fruit flies showed, that, depending on the behavioral state, some neurons of the sky-compass pathway show drastic changes in their responses to visual stimulation (Seelig and Jayaraman, 2013; Weir and Dickinson, 2015; Rosner et al., 2019). Therefore, current research is focusing more and more on performing physiological recordings in animals that are as little restrained as possible. For this reason, this project focused on the development and establishment of a new protocol that would allow for the first time ever calcium imaging in a walking honeybee. Calcium imaging is so far not as broadly established in honeybees as it is for example in fruit flies, especially regarding the indicators and the indicator delivery system. In fruit flies, genetically encoded calcium indicators are broadly used, while in bees and other insects those genetically tools are not available. Therefore, chemical dyes have to be injected into the neurons. For this reason, the first step included an extensive search for a suitable calcium indicator. In the end, the conventionally used Calcium Green-1 dextran was utilized, as well as a custom-made JF<sub>549</sub>-BAPTA dye coupled to ester groups. The lower unit complex of the anterior optic tubercle (LUC) was chosen as target area. The reasons for this choice is its part in the sky-compass pathway at the junction of the optic lobes to the central brain and its superficial location (Zeller et al., 2015; Fig. 2). The latter is crucial for this project since the LUC still lays within the depth limit of multiphoton microscopes to image in living tissue.

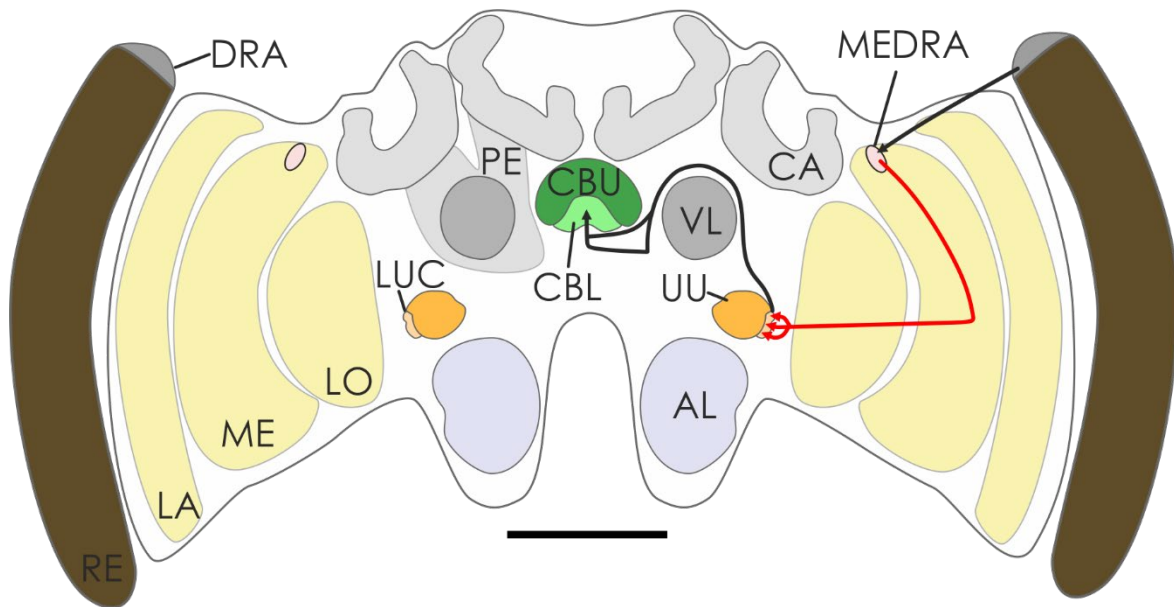


**Fig. 2: Schematic drawing of the honeybee brain and the input part of the anterior sky-compass pathway.** The targeted transmedulla neurons (red line) are part of the sky-compass pathway that receives input from the dorsal rim area of the compound eye. Neurons project through the lamina and branch in the dorsal rim area of the medulla. From there the transmedulla neurons project through the medulla and lobula to the lower unit complex of the anterior optic tubercle, where they branch in all sub-compartments. From the lower unit complex the pathway projects further around the vertical lobes of the mushroom bodies into the central brain, where they end up in the central body. Further branchings in the central complex, to the contralateral side as well as the projections further downstream are not shown. AL: antennal lobe, CA: calyx, CBL: lower division of the central body, CBU: upper division of the central body, DRA: dorsal rim area, LA: lamina, LO: lobula, LUC: lower unit complex of the anterior optic tubercle, ME: medulla, MEDRA: dorsal rim area of the medulla, PE: peduncle, RE: retina, VL: vertical lobe. Scale bar = 500  $\mu\text{m}$ .

Anatomical studies revealed furthermore a distinct subcompartmentalization of the structure into five subunits (Heinloth unpublished, 2013; Zeller et al., 2015; Fig. 3A). One question of this project was therefore if the compartments have a mechanistic purpose, for example if there is a retinotopic allocation of the input neurons. To this end, the input neurons, called transmedulla neurons, were labeled in the medulla and their dendrites in the LUC were imaged (Fig. 3B - D).

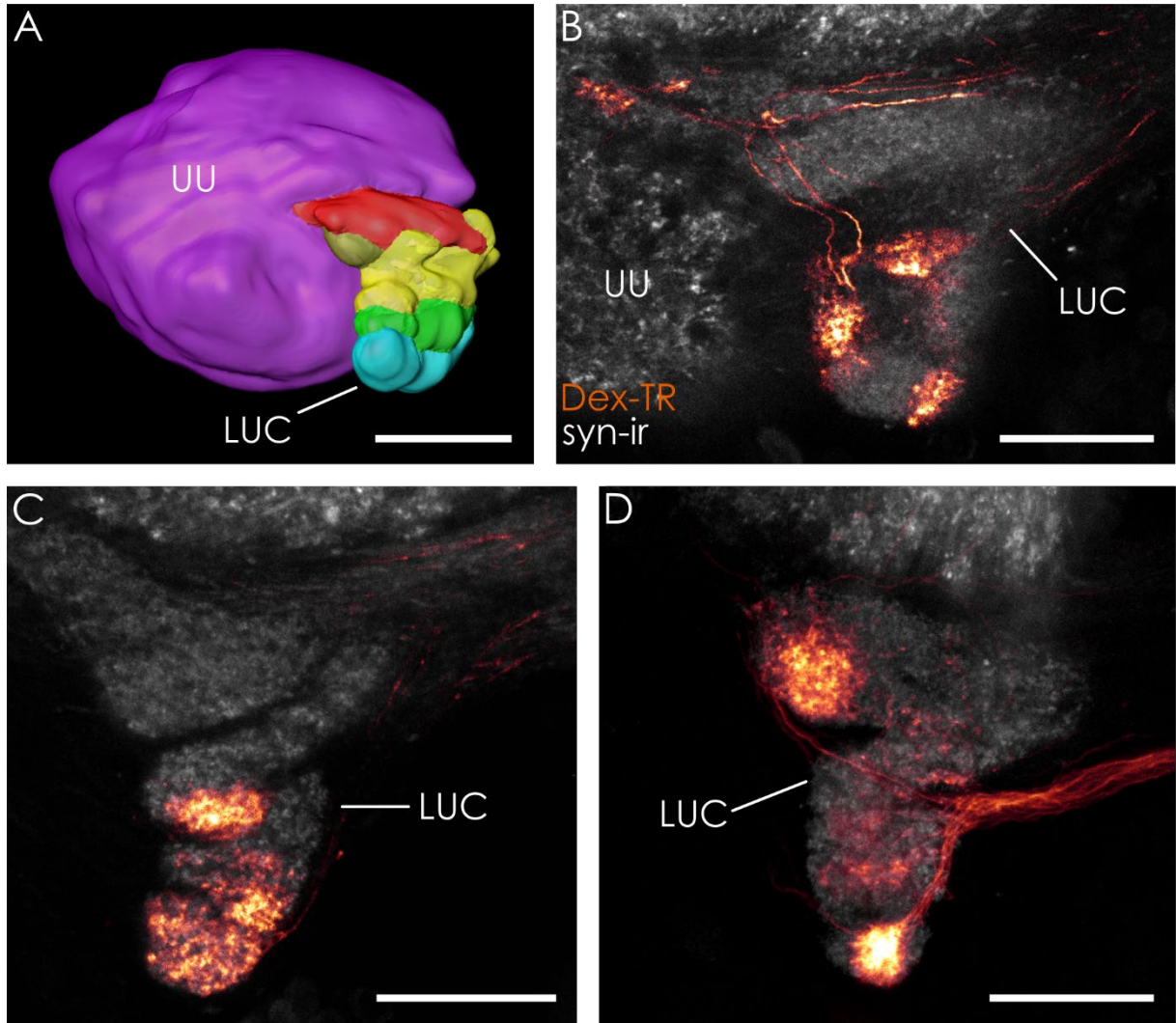


**Fig. 3: Three-dimensional average shape atlas of the anterior optic tubercle and branching patterns of transmedulla neurons.** A: Based on an anti-synapsin staining an average shape atlas of the anterior optic tubercle was created, including a larger upper unit (purple structure) and a smaller lower unit complex, consisting of five sub-compartments (colored structures). B, C: Single confocal sections of a Dextran Texas Red injection (orange, Dex-TR) into transmedulla neurons in a brain labeled against synapsin (grey, syn-ir). The neurons show different projection areas in the lower unit complex of the anterior optic tubercle. D: Maximum intensity projection of 10 consecutive slices of the neurons shown in B & C. LUC: lower unit complex of the anterior optic tubercle, UU: upper unit of the anterior optic tubercle. Scale bars: A = 50  $\mu\text{m}$ , B-D = 30  $\mu\text{m}$ . A: Heinloth unpublished, 2013, B-D: adapted from Zeller et al., 2015.

To allow the bees to show walking behavior, a treadmill system based on the fruit fly system (Seelig et al., 2010) was developed and fabricated in multiple steps together with a camera system to record the walking trajectories. For visual stimulation,



an LED arena was used to present different patterns. The overall goal was to be able to align the behavioral recordings with the calcium responses to investigate state dependent influences. In the end, the delivery system for the dye, the preparation protocol, the calcium imaging and walking recording, and the analysis of the data was successfully established. This methodical advancement might open the door for future experiments to investigate the neurophysiological processes behind the astonishing behaviors of honeybees.

## MATERIAL AND METHODS

### **CALCIUM GREEN-1 DEXTRAN AND JF<sub>549</sub>-BAPTA-MPM ESTER**

The depolarization of a neuron, either due to spontaneous activity or caused by stimulation, causes voltage-gated  $\text{Ca}^{2+}$  channels in the membrane to open, which leads to a rapid increase of  $\text{Ca}^{2+}$  inside the cell. Therefore, calcium ion concentration can serve as an excellent readout of neural activity, and a large number of fluorescent calcium indicators that are able to reliably detect the calcium influx have been developed. Those can be separated into two groups: “synthetic” based on small-molecule fluorophores and “genetically encoded” based on fluorescent proteins (Bolbat and Schultz, 2017). Although genetically encoded reporters are routinely used in model organisms such as *Drosophila* or mice, they cannot be easily implemented in honeybees. I therefore focused on the use of synthetic calcium indicators for this project.

Many synthetic calcium indicators rely on the calcium chelator BAPTA (1,2-bis(o-aminophenoxy)ethane-*N,N,N',N'*-tetraacetic acid) that is attached to a fluorophore (Tsien, 1980). In the absence of calcium, the compound is only weakly fluorescent due to quenching by photo-induced electron transfer. This effect is suppressed upon binding of calcium, and fluorescence is recovered. For this project, we first examined the use of the commercially available Calcium Green-1 dextran (3,000MW, Molecular Probes, Invitrogen, ThermoFisher Scientific, Waltham, MA, USA). This dextran-conjugated calcium indicator is membrane-impermeant and needs to be physically introduced into neurons via bulk injections. After the dye is loaded into the cells, it is actively transported from the point of introduction anterogradely or retrogradely across the whole neuron (Russell, 2011). It exhibits a ~ 14 fold fluorescence increase with a slight wavelength shift upon  $\text{Ca}^{2+}$  binding. The excitation peak is at 506 nm and the emission maximum occurs at 531 nm (Fig. 4).

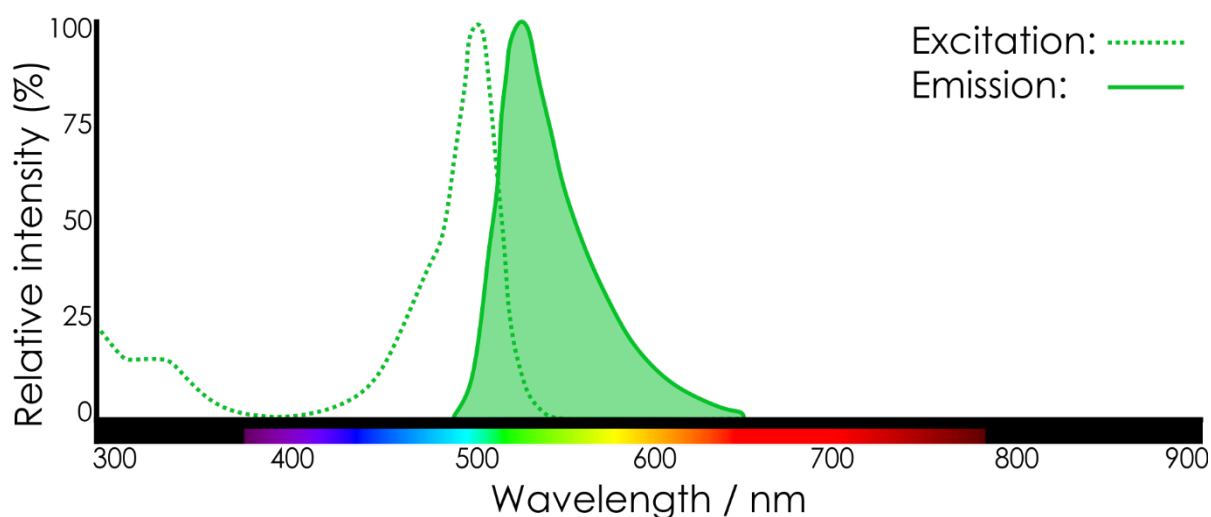


**Fig. 4: Excitation and emission spectra of Calcium Green-1 dextran.** The calcium sensitive fluorescence molecules of Calcium Green-1 dextran have the highest absorption level at 506 nm and show their emission peak with a slight wavelength shift at 531 nm. Adapted from SpectraViewer (ThermoFisher).

To circumvent the need for intracellular injection, we also evaluated the use of a cell-permeant calcium indicators in collaboration with the laboratory of Luke Lavis (HHMI Janelia Research Campus). Cell-permeant calcium indicators are usually designed by synthetically incorporating ester groups on the BAPTA moiety. The ester groups mask the highly polar carboxylic acids of the BAPTA, making it cell-permeant. Inside the cells, the ester groups are then cleaved by endogenous enzymes called esterases (Tian et al., 2012). The removal of the ester groups has two effects: the molecule is not cell-permeant anymore and therefore trapped inside the cell, and it reveals the  $\text{Ca}^{2+}$ -binding moieties. Esterases are however species-specific and cell-type dependent. In order to determine the most suitable ester group for esterases in the honeybee brain, a series of pre-experiments had to be conducted (see Preliminary ester tests).

## PREPARATION

All preliminary tests and calcium imaging experiments were performed on adult foraging worker bees that were caught from the hive entrance. Bees of three different locations were used: in summer 2016 and 2017 from the outdoor hive of the Janelia Research Campus (Ashburn, VA, USA), in winter 2017 and 2018 from an indoor hive of the Würzburg University bee station's greenhouse (Würzburg, Germany) and in summer 2018 and 2019 from outdoor hives of the Biocenter (Würzburg, Germany). Honeybees

were immobilized in plastic vials at 4°C in the refrigerator or on ice. They were then tethered with UV curable glue (Perfomic Pen midget, Conrad Electronic SE, Hirschau, Germany) to a custom-built holder (Fig. 5A). Caution had to be taken to keep the main part of the eye free from glue, as well as the abdomen, the legs, and the antennae tips (Fig. 5B & C). Preliminary tests showed that the animals would not walk in a proper fashion later in the experiments if the tips of the antennae, the abdomen and stinger or the legs had any glue on them but would rather try to clean themselves. Afterwards, the head capsule of the bees was opened with a scalpel by cutting a window frontally between the eyes, ocelli, and antennae base in the cuticle. To expose the brain and prevent artefacts later in the imaging process, all excess tissues surrounding the brain, like salivary glands, air sacks, and the neural sheath were removed (Fig. 5C).



**Fig. 5: Preparation of honeybees for preliminary testing and calcium imaging.** A: A custom-built holder was used for all experiments. The holder is composed of a flat part that can be attached to a micromanipulator and a reservoir that can be filled with Ringer's solution. At the bottom of the reservoir is a hole through which the preparation and the imaging is carried out. B: The bee was glued to the holder with the head capsule attached to the hole and the thorax glued to the holder. Abdomen, legs, the tips of the antennae, and the majority of the eyes were free of glue. C: View through the hole in the holder a window in the cuticle into the bee head through. The brain was exposed by removing air sacs, glands, and neural the sheath and the reservoir was filled with bee Ringer's solution.

At all stages of the preparation the brain was kept moist by regularly applying bee Ringer's solution (130 mM NaCl, 5 mM KCl, 4 mM MgCl<sub>2</sub>, 15 mM HEPES, 25 mM glucose, 160 mM saccharose, 5 mM CaCl<sub>2</sub>) into the head capsule. Up to this point, the preparation of all honeybees was following the same protocol, for the pre-tests,

Calcium Green-1 dextran, and JF<sub>549</sub>-BAPTA-MPM ester injection. Since two types of dyes were tested in the experiments, one as crystals the other one dissolved, the injection protocol varied from here on, depending on the used dye.

### **PRELIMINARY ESTER TESTS**

To find the most suitable ester group masking the indicator molecules for honeybee neurons, we systematically tested the loading and cleavage of twelve different ester groups *in vivo* (Table 1). These ester groups were linked to the basic fluorophore fluorescein (excitation/emission: 494/512 nm), resulting in twelve different molecules. These non-fluorescent compounds are not calcium sensitive, but become brightly fluorescent upon ester cleavage, which allows for a direct readout of cell loading and intracellular esterase activity. To achieve comparable results, the dyes were loaded into living honeybees following the same preparation protocol. To this end, the bee brains were exposed as described before. The dye molecules were all prepared the same way. First, the fluorescein crystals that were masked with different ester groups were dissolved in DMSO (dimethyl sulfoxide, Sigma-Aldrich, St. Louis, MO, USA). The final mixtures of 1000  $\mu$ l contained 1  $\mu$ M of the respective dye molecule, 0.25% DMSO, and 0.0025% Pluronic F127 (Sigma-Aldrich, St. Louis, MO, USA) in bee Ringer's solution. DMSO served here as an anti-freeze agent to avoid crystallization of the solution since it was stored after usage in the freezer. Pluronic F127 was used to solubilize the large dye molecules in a physiological medium. The dyes were always dissolved right before usage and mixed thoroughly on a shaker. 36  $\mu$ l of that solution were then transferred into a second vial and 4  $\mu$ l of dissolved rhodamine B (synthesized by the Lavis lab) dye was added. Rhodamine B has a different fluorescent spectrum (excitation/emission: 554/600 nm) and was used as an orientation aid during imaging. From the final mixture 2  $\mu$ l were pipetted into a glass microelectrode. The electrodes were fabricated by pulling borosilicate capillary tubes (outer diameter 1.5 mm, inner diameter 0.86 mm; Sutter Instrument, Novato, CA, USA) with a Flaming/Brown puller (P97, Sutter Instrument, Novato, CA, USA). After loading the dye solution, the microelectrode was inserted into a micromanipulator that was attached to a pressure injection setup (Pneumatic PicoPump PV820, WPI, Sarasota, FL, USA) and inserted into the region of interest of the exposed brain. In these tests, cell bodies of Kenyon cells in the mushroom body were chosen as target area since their structure allows for an easy

identification and their superficial position make them suitable to image in living tissue. Through short pressure pulses, the dye was injected into the brain over several minutes. Remaining superficial dye on the brain was removed by rinsing with bee Ringer's solution. Afterwards all bees were kept at room temperature for 30 minutes to ensure a comparable timeframe for distribution of the dye throughout the neurons and cleavage of the ester groups by esterases. Bees were then transferred into a two-photon microscope (Prairie Technologies, Bruker, Billerica, MA, USA) to image the cell bodies of the Kenyon cells. In all trials, the dyes were excited by an Insight two-photon laser at 20% power using a wavelength of 920 nm. The emitted fluorescence was detected with a photomultiplier tube (PMT) set at a gain of 700. Using the same settings across all dyes ensured that differences in the fluorescence intensity stem from efficiency differences of the uptake and cleavage of the varying ester groups and not excitation and detection disparities. The results were analyzed by comparing the mean intensity of 10 cell bodies across all dyes using the open source software ImageJ and Excel (Microsoft Corporation, Redmon, WA, USA). Following those tests, a JF<sub>549</sub>-BAPTA-MPM-ester dye was synthesized and tested (see Results and the next chapter).

#### **INJECTION JF<sub>549</sub>-BAPTA-MPM ESTER**

The preliminary testing of different ester groups (see Results) allowed us to identify the MPM ester (methoxypropiomethyl) as the most robustly loaded and cleaved ester in the honeybee brain. A bright, red-shifted, cell-permeant calcium indicator bearing MPM ester groups, called JF<sub>549</sub>-BAPTA-MPM ester dye, was custom-synthesized by the Lavis Lab (Fig. 6).

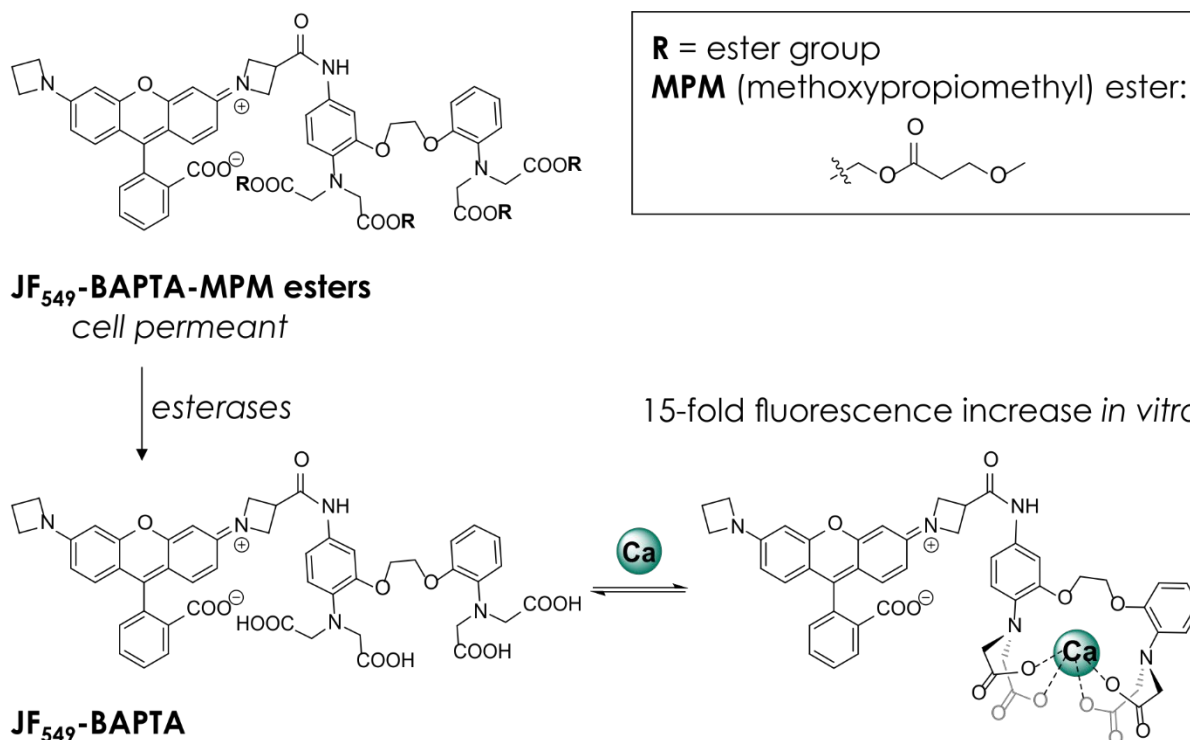


**Fig. 6: Chemical structure and processes upon cell entrance and calcium binding of JF<sub>549</sub>-BAPTA-MPM ester.** The molecule consists of two parts: the fluorophore JF<sub>549</sub> and the BAPTA moiety that is masked with four MPM esters. Those ester groups suspend the polarity of the molecule which makes it cell permeant. Inside the cell esterases cleave the ester groups off the BAPTA part which makes it calcium sensitive. Upon calcium inflow into the neuron the calcium binds to the BAPTA which in turn abolishes the quenching of the fluorophore part resulting into a 15-fold fluorescence increase (*in vitro*).

Following ester cleavage, this compound exhibits a 15-fold fluorescence increase upon binding calcium (Fig. 7; excitation/emission: 546/569 nm; Deo et al., 2019), and was used in the following experiments besides Calcium Green-1 dextran.



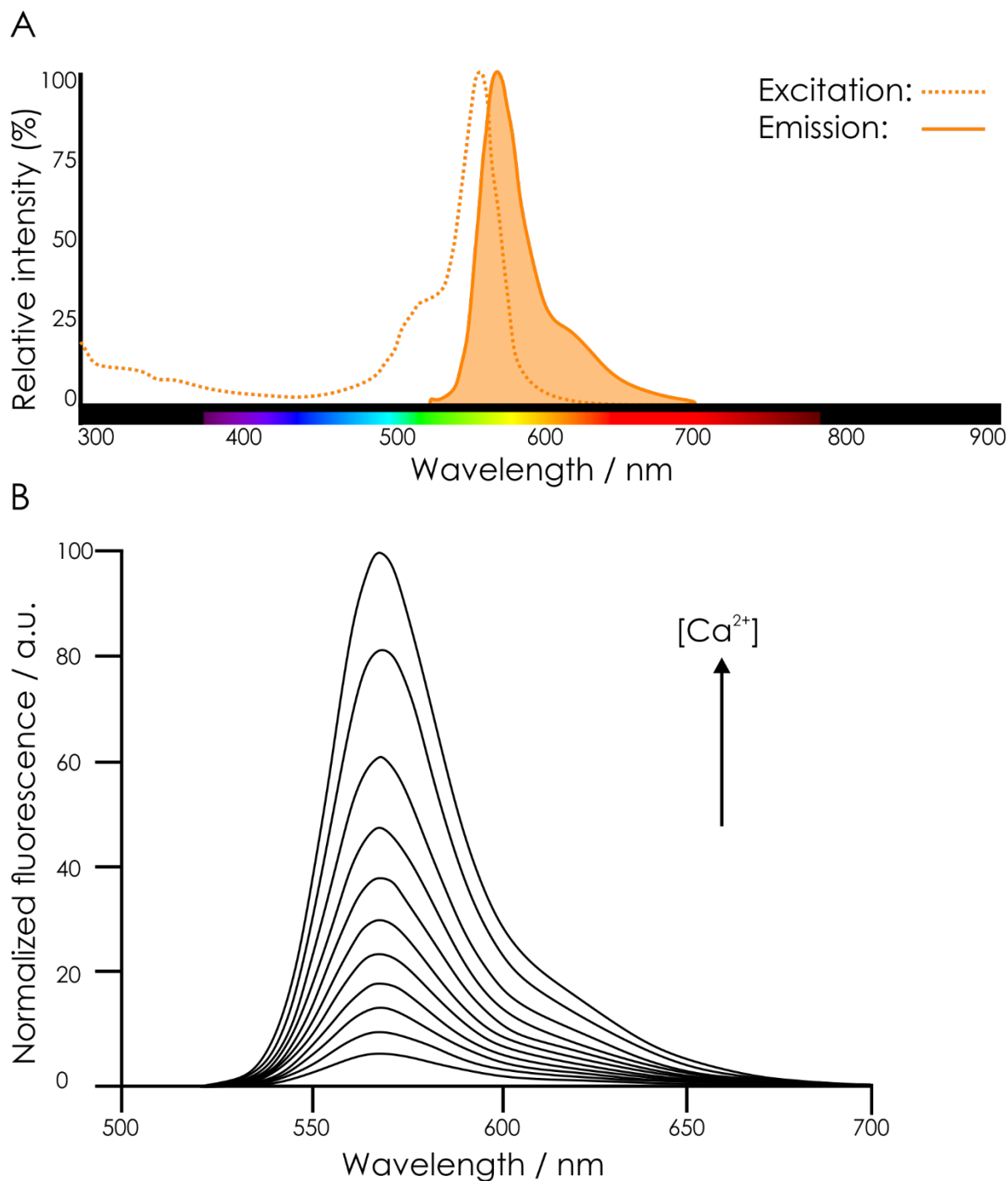


**Fig. 7: Excitation and emission spectra of JF<sub>549</sub> and fluorescence increase of JF<sub>549</sub>-BAPTA depending on Ca<sup>2+</sup> availability.** A: The fluorophore JF<sub>549</sub> exhibits the highest excitation at a wavelength of 546 nm and the emission peak at 569 nm. B: The fluorescence increase of JF<sub>549</sub>-BAPTA depends on the availability of Ca<sup>2+</sup>. Adapted from SpectraViewer (ThermoFisher) and Deo et al., 2019.

The injection of the JF<sub>549</sub>-BAPTA-MPM ester dye followed a similar protocol as the preliminary tests described before. First, 20% Pluronic F127 was mixed with DMSO by

heating the mixture to 40°C for 20 minutes. 4 µl of this mixture were added to the dye vial and then placed in an ultrasonic bath for 20 minutes to dissolve the dye crystals. Afterwards, 35 µl bee Ringer's solution was added and everything was further mixed on a shaker. For the final solution, 10 µl of this mixture was combined with 3.5 µl of fluid rhodamine B stock. The dye was then transferred to the microelectrode and injected in to the bee brain as described above. Here, transmedulla neurons were targeted by injecting the dye mixture in the MEDRA and AOT. To allow for a complete uptake of the molecules and cleavage of the ester groups bees were kept for 2 hours at room temperature.

To image a living brain without getting any movement artefacts the brain needs to be as still as possible. After testing a metal spoon to lift the brain up, two component glue, and UV glue, the final solution for the movement problem was agarose (LMP agarose, Carl Roth, Karlsruhe, Germany; low EEO agarose AppliChem GmbH, Darmstadt, Germany). The agarose was melted in a waterbath at 65°C (LMP agarose) or 85° (low EEO agarose) for 20 minutes until the mixture appeared clear. After testing different concentrations, 1.5% agarose was used for the following experiments since it gave enough stabilization for the brain but kept the agarose translucent enough so the light of the laser would not get scattered too much during the imaging process. The best stabilization results were achieved by removing all liquid around the brain with a tissue before applying the agarose. Any remaining fluids would allow the brain to move due to pumping movements of the bee's abdomen. In addition, the bees were immobilized at 4°C in the refrigerator before applying the agarose to prevent any movement that would cause and uneven agarose surface. After covering the brain with a drop of agarose, the bees were placed back into the refrigerator for 10 minutes until the agarose hardened. Afterwards bee Ringer's solution was added onto the agarose sheath for two purposes: it kept the agarose from drying out and the agarose let some nutrition of the solution through to nourish the brain. The bees were then transferred into the setup and imaged using either a custom-built two-photon microscope or a Leica Multiphoton Microscope TCS SP8 MP.

### **INJECTION CALCIUM GREEN-1 DEXTRAN**

For the injection of this calcium indicator, the bees were prepared as described above. Since Calcium Green-1 dextran is not masked by ester groups, the molecules need to be introduced into the cells physically. To this end, sharp microelectrodes were pulled like described before but this time the capillary tubes had an outer diameter of 1.5 mm and an inner one of 0.75 mm (Hilgenberg, Malsfeld, Germany). After pulling, the tips were broken to a diameter of 5 – 30  $\mu\text{m}$ . To attach a few dye crystals to the electrode, the tip was dipped in petroleum jelly and then into Calcium Green-1 dextran powder. After removing all fluids around the brain with a tissue, the microelectrode was inserted manually into the target area of the brain. The target was again to load the dye into transmedulla neurons. Afterwards, excess dye was rinsed off with bee Ringer's solution. For a complete uptake and distribution of the dye throughout the neuron, the bees were kept in a moist chamber at room temperature for 2-3 hours. The brains were afterwards covered with LMP agarose as described before and then transferred into the setup at the Leica Multiphoton Microscope TCS SP8 MP for imaging.

### **IMAGING AND BEHAVIORAL RECORDINGS WITH CUSTOM-BUILT TWO-PHOTON MICROSCOPE**

For the experiment during the time at the Janelia Research Campus in summer 2016 and 2017, a custom-built two-photon microscope was used as described in Seelig and Jayaraman (2015). The setup consisted of the imaging and the behavioral part (Fig. 8).

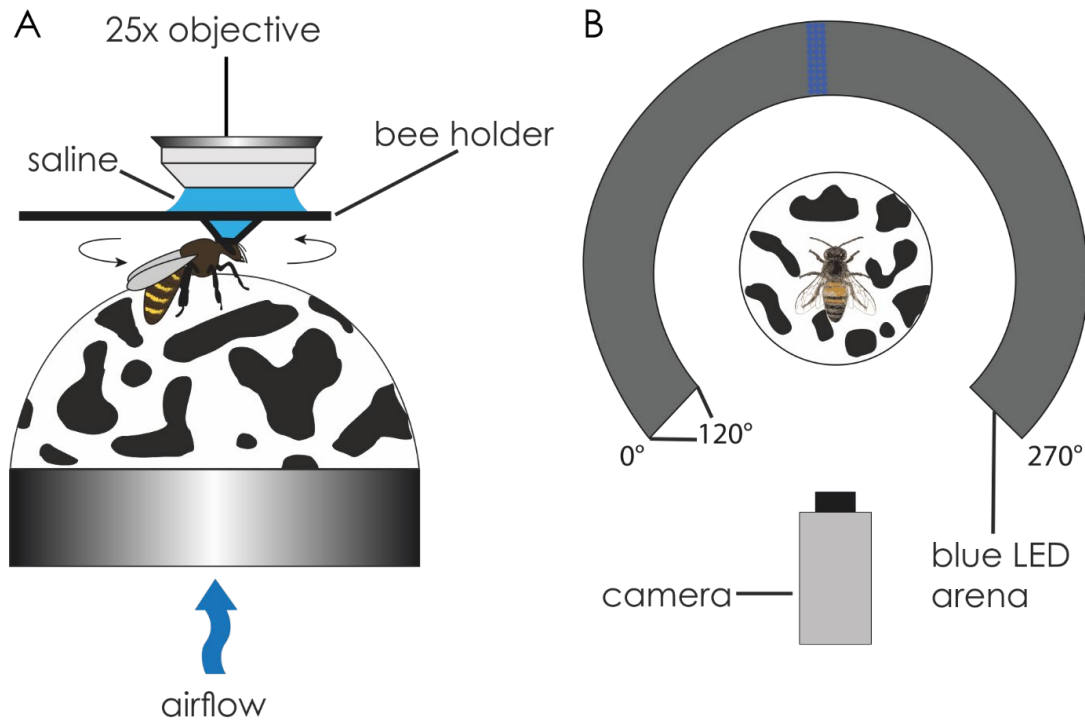


**Fig. 8: Schematic drawing of the setup.** The custom-built setup in Janelia and the Leica setup in Würzburg had a similar structure but parts of the microscope and ball tracking system differed. A: Side view. The Styrofoam ball is supported by an airflow from underneath. The bee is positioned on the ball with the head tethered to the bee holder. The objective is immersed in the saline in the reservoir of the holder. B: View from above. The stimulation is carried out by a blue LED arena, while the movements of the ball are recorded with a camera.

In the custom-built microscope, a Chameleon Ultra II laser (Coherent, Inc., Santa Clara, CA, USA), a GaAsP photomultiplier tube (H7 422PA-40, Hamamatsu) and an Olympus  $\times 40$  objective (LUMPlan /FI/IR, NA 0.8) was used for imaging. Those parts and the collecting of images was controlled via the program ScanImage 2015. To avoid missing any activity signals, a scanning frequency of over 8 Hz was chosen. For the experiment, the holder glued to the bee was attached to a three-axis micromanipulator and the bee was positioned on an air-supported Styrofoam ball with a diameter of 48 mm. The movement of the ball and therefore the walking behavior of the bee was recorded with a two-camera system with a 20 Hz frame rate as described by Seelig et al. (2010). The visual stimulation was carried out with a cylindrical blue LED arena, spanning  $270^\circ$  in azimuth and  $120^\circ$  in elevation with the animal on the ball in the center. Different patterns were used as stimuli: a single bright

stripe on a dark background, a dark stripe on a bright background, white noise, a single bright dot, and a grating pattern with several vertical stripes to mimic optic flow movements. The stimulation was either operated in open loop, meaning the experimenter controls the position of the pattern in the arena, or in closed-loop with the animal's movement controlling the pattern. The camera system was controlled and operated using MatLab (The Mathwork, Inc., Natick, MA, USA), and the imaging and behavioral recordings were synchronized using LabView (National Instruments, Austin, TX, USA).

### **IMAGING AND BEHAVIORAL RECORDINGS WITH THE LEICA MULTIPHOTON MICROSCOPE TCS SP8 MP**

The experiments done from 2017 until 2019 were carried out in a newly built rig with a Leica Multiphoton Microscope of the Zoology II department of the Biocenter at the University in Würzburg (Fig. 9).

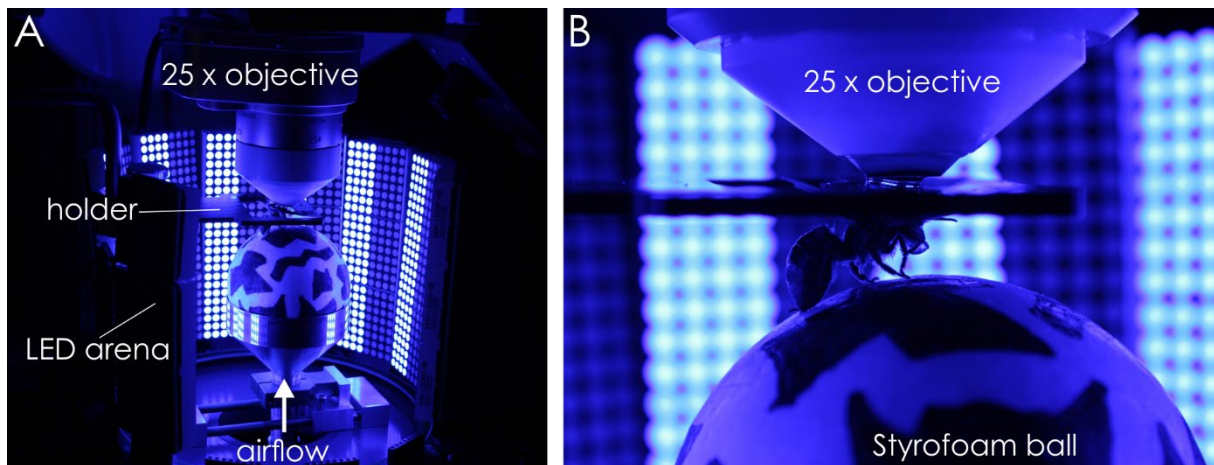


**Fig. 9: Setup for calcium imaging and behavioral recordings.** This setup was attached to a Leica Multiphoton Microscope TCS SP8 MP but the setup used at the Janelia Research Campus looked similar. A: The bee holder was attached to a micromanipulator and positioned between a Styrofoam ball and a  $\times 25$  objective. The ball floated on a constant airflow from underneath. The ball and the bee was positioned in the center of a  $330^\circ$  LED arena with an opening behind the animal. For the picture, LED panels lateral to the animal were removed. B: The bee was positioned on top of the ball with enough room for the animal to walk and turn. The reservoir of the holder was filled with bee Ringer's solution to keep the brain moist and to allow for a water column between the brain and the objective. Pictures ©Claudia Groh.

Overall, the setup was similar but key components differed between the Leica microscope and the custom-built one. In the microscope from Leica, three solid-state

lasers are available with excitation wavelengths of 488 nm, 552 nm, and 638 nm. In addition, for multiphoton microscopy and live imaging, a tunable Insight DeepSee Dual laser (SpectraPhysics, Santa Clara, CA, USA) ranging from 680 – 1300 nm was available as well as a second laser line set at 1040 nm. To detect the fluorescence signals different detectors were at hand: two internal tuneable photomultiplier tubes (PMT) and one tunable Hybrid Detector (HyD). In addition, two tuneable external PMTs and two tuneable HyDs were available with higher sensitivity settings. All experiments were conducted using a Leica × 25 water objective (HC IRAPO L motCORR, Leica Mikrosysteme GmbH, Wetzlar, Germany). In the experiments with Calcium Green-1 dextran, the specimens were looked at in the rhodamine B channel first to help with the orientation in the brain. If transmedulla neurons were labeled, an overview image was taken. For that, one internal PMTs tuned to detect light in the range from 560 – 650 nm was used at a gain of ~ 700 V while using the 552 nm laser for excitation. Afterwards the internal HyD was set to detect light with a wavelength of 520 – 580 nm with the tuneable multiphoton laser at 810 or 960 nm to perform the imaging experiments with Calcium Green-1 dextran, which has two excitation peaks. For experiments with the JF<sub>549</sub>-BAPTA-MPM ester dye, the internal HyD, tuned to 560 – 630 nm, was used right away. The excitation was carried out by the multiphoton laser tuned to 910 nm.

The microscope and image acquisition was controlled with the Leica software Leica Application Software X (LAS-X). For a quick overview and to identify the ROI the rhodamine B channel was used with the solid-state laser exciting the fluorophore with 552 nm and the corresponding PMT was used. After recording an overview z-stack of the location of the injection, the microscope was set to live imaging mode. The resolution, magnification, in some trials steps in z, and laser power were adjusted individually for every scan, depending on the signal strength and ROI. The scan speed was set to 600 Hz, or if the Galvo stage was used the speed was pre-set at 8000 Hz. The latter was just tested but not used regularly since the signal strength was not strong enough for such a high scanning frequency. The resolution and image size settings were adjusted to end up with a final frame rate of 8 Hz or higher with a trial length of 60 to 120 seconds, depending on the stimulus pattern. In addition, a trigger was set in the microscope software to send out a TTL signal at the beginning of every frame taken, to use those time stamps for later alignment with the behavioral and stimulus

data in the analysis. The first of those TTL signals did also trigger the LED arena to start the stimulus via an Arduino Uno board (Arduino LLC, Somerville, MA, USA) and the corresponding script in the open source Arduino software. The azimuth position of the visual stimulus was controlled via an analog signal that was generated by a digital-to-analog converter, which was driven by the Arduino board. The behavior was recorded using a full HD IR webcam (ELP, Ailipu Technology Co., Ltd., China) and the open source software FicTrac (Moore et al., 2014). The LED arena system (IO Rodeo Inc., Pasadena, CA, USA) consisted of a 12 ring board, 35 FlyPanels-G3 with 35 blue (470 nm peak emission) LED matrixes with  $8 \times 8$  LEDs each and a panel display controller unit. Due to the one-camera system, the arena was spanning in this setup  $330^\circ$  instead of  $270^\circ$  like in the custom-built setup. The tested patterns were displayed in open-loop control and included all LEDs on/off to determine a light reaction, and one bright stripe on dark background moving clockwise or counter-clockwise.

## ANALYSIS

The analysis of the imaging and behavioral data was a multiple step process. The imaging data were first examined with the open-source software LAS-X from Leica. These software packages allowed to look at individual images and whole series. With that, it was possible to create an overview image of the position in the brain. It was also determined, looking at the whole times series, if too many movement artefacts occurred or if the experiment was suitable for further analysis. Afterwards, the raw data of the imaging part and the behavioral part were imported into a Python script, aligned, and analyzed further. The first step was the correction of small movements in the x/y axis by aligning the pixels throughout the image series. To analyze the fluorescence changes over time and therefore the calcium activity  $\Delta F/F = (F - F_0)/(F_0 - F_b)$  had to be calculated. In this case,  $F$  is the fluorescence signal during stimulation of a region of interest (ROI) that was selected and manually defined in the image.  $F_0$  corresponds to the baseline fluorescence, meaning the fluorescence of that ROI before stimulation. To filter out background noise, one region where no obvious activity or dye was present was defined as background fluorescence  $F_b$ , which gets subtracted from the fluorescence signal. With the calculation of fluorescence changes over time, activity tracks for every ROI were visualized. To ensure that fluorescence changes did not stem from movement artefacts a correlation cluster



between movement in the x/y axis and the fluorescence values was created. For the behavioral part, the movement of the ball and therefore of the bee was derived from the raw data of the two tracking setups and visualized as walking traces. The pattern position in the arena was extracted for the single trials and connected to the behavioral data. In a last step, the fluorescence signals were compared to features of the walking behavior. This should allow for a readout of possible influences of the behavior on the calcium responses. For a step-by-step tutorial of the whole preparation, experimental procedure, and the analysis script see Appendix.

## RESULTS

### BEHAVIORAL DATA

To assess if neurons in the honeybee brain show state dependent responses due to walking behavior, the walking behavior itself was examined in preliminary tests first. The walking traces were recorded and analyzed in closed- and open-loop in dependence to the pattern position. In addition, the walking behavior was recorded after the head capsule was opened and dye was injected into the brain. Therefore, it is a suited readout to evaluate how much the preparation affected the bee's behavior. To explore which pattern is stimulating the most robust and constant walking behavior, different patterns were tested in a few bees in closed-loop and opened-loop control with a 270° arena in the custom-built setup. The closed-loop trials showed promising responses in single bees (example bee #170712 shown in Fig. 10-14) but in the end, a bright stripe on a dark background in open-loop control was the main stimulus for further experiments.

In closed-loop control, the animal stabilized the stripe lateral to one side but switched sides in between over a longer period of time (Fig. 10A). This behavior, stabilizing an object in one fixed position that is not in front of the animal is called *menotaxis* and has been observed for example in *Drosophila melanogaster* (Heisenberg and Wolf, 1979). During the experiments, the walking behavior showed in addition to the general *menotaxis* behavior an underlying constant motor pattern that was independent of the visual stimulation. In the walking trace, this motor pattern appeared as small regular yaw turns in both directions. Those turns did not influence the overall stripe position in closed-loop experiments, meaning the bees were not biased or inclined in one direction. The recorded walking behavior allowed for further analysis, with the position of the pattern in the arena being calculated first to confirm a stabilization of the pattern by the animal to predominantly one position (Fig. 10B). In addition, the walking trajectory was computed and visualized (Fig. 10C), to get a better overview over the tortuosity/straightness of the walked path. Additional information like the translational (Fig. 10C, blue shades) and rotational (Fig. 10D, red/blue shades) velocity were visualized as well, to gain a better assessment of the quality of the behavior. The walking trajectory could, for example, be straight and insinuate that the animal performed a stable straight walk. However, the translational

velocity, which indicates the walking speed, could be low at the same time, suggesting that the animal did actually not perform well. Very high or low turning velocities can be further indicators for experimental errors, like tilted tethering or unwanted behaviors like a retraction of all six legs. Therefore, those parameters were always checked for, even though they were not further analyzed.

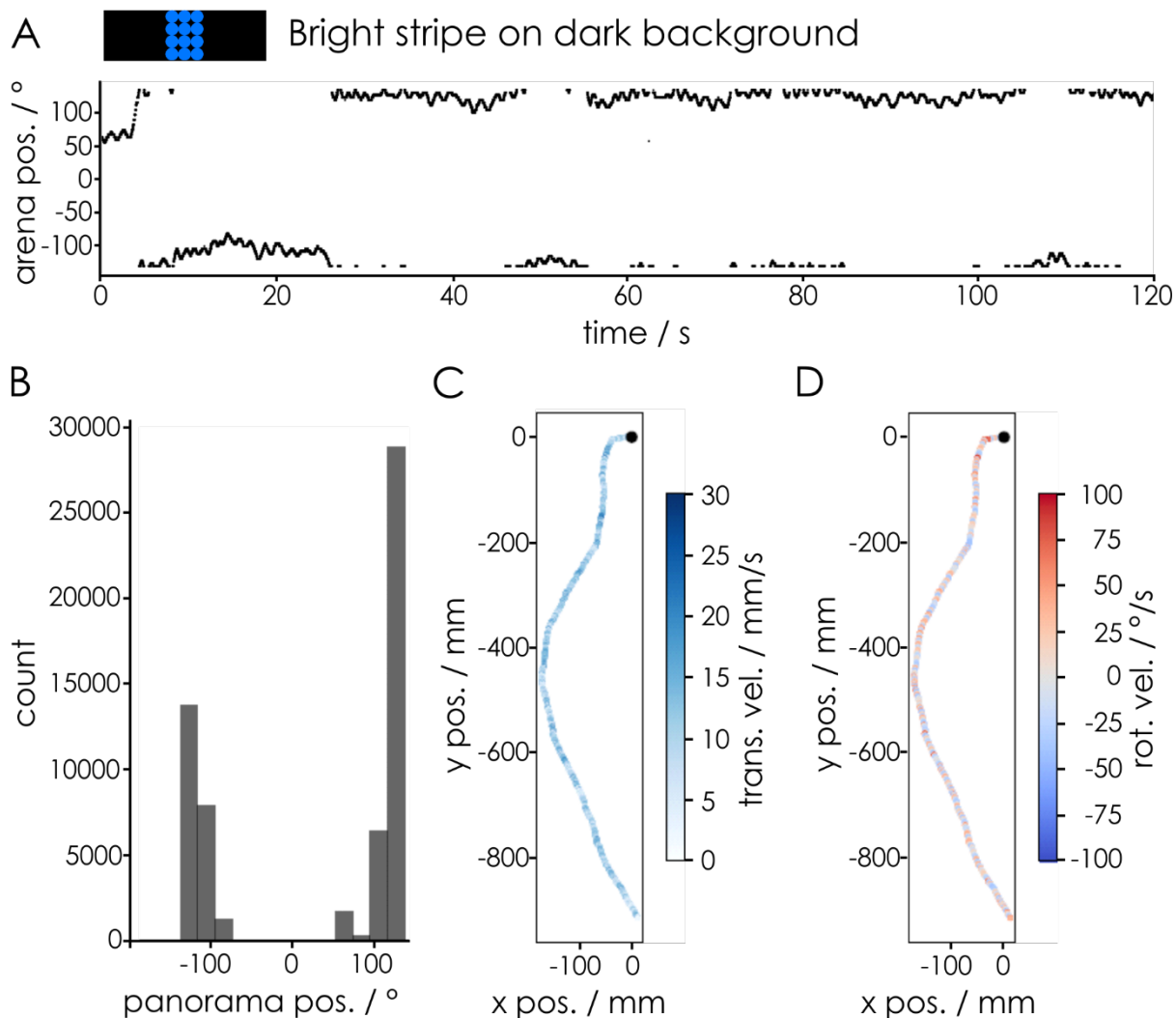


**Fig. 10: Behavioral analysis of the walking behavior of a honeybee (#170712) in closed-loop control of a visual pattern in the custom-built setup.** A: The black trace indicates the position of a bright blue stripe on dark background in a 270° LED arena around the animal over a 120 seconds long trial. B: The frequency of the stripe in one position was counted. C: The two-dimensional trajectory of the walking path was calculated and color-coded for the translational velocity. This shows the straightness or tortuosity of the walking path as well as the forward speed. D: The same trajectory as in C is shown but with the rotational velocity instead of the translational, to determine the yaw turning speed of the animal.

To test the strength of the behavior shown in closed-loop mode, in some trials pseudo-randomized jumps of the stripe by 90° or 180° were introduced (Fig. 11). Those trials revealed that the bee brings the stripe back to roughly the same position she kept it at before the jump. Here, it made no difference if the pattern was moved by 90° or 180°.

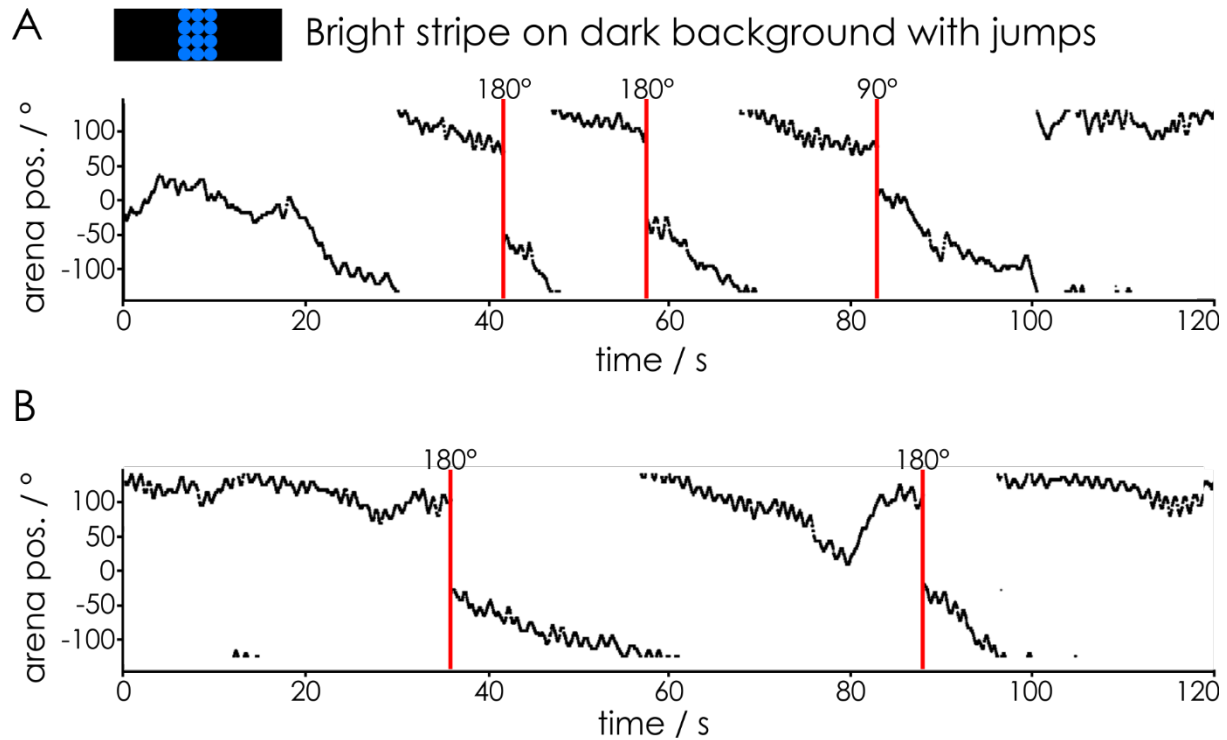


**Fig. 11: Pattern position in the arena in closed-loop control of a bee (#170712) with artificial jumps.** A: To test the robustness of the behavior, artificial jumps of 180° or 90° of the bright blue stripe on dark background are introduced pseudo-randomly during the trials. The position of the stripe in the 270° arena is illustrated by the black trace, while the displacements are indicated by the red lines. B: The behavioral response to the displacement of the stripe was tested several times.

In addition to this stimulus, a bright moving stripe on a stationary white noise background was tested. Even though this pattern was more complex, the bee exhibited a rather stable walking behavior with a menotactic tendency over longer periods of time (Fig. 12A). However, introducing a jump of 180° lead in this case to a fixation of the stripe at a new position, close to the center front of the animal, instead of returning it back to the former position as the bee did without the white noise (Fig. 12B). Changing the setting of the pattern to white noise and bright stripe moving together in closed-loop mode, lead to walking behavior without stabilizing the position

of the pattern in one place and therefore without a stable direction (Fig. 12C). Introducing a jump of  $180^\circ$  of the whole pattern did not show an effect on the undirected walking trajectory (Fig. 12D).

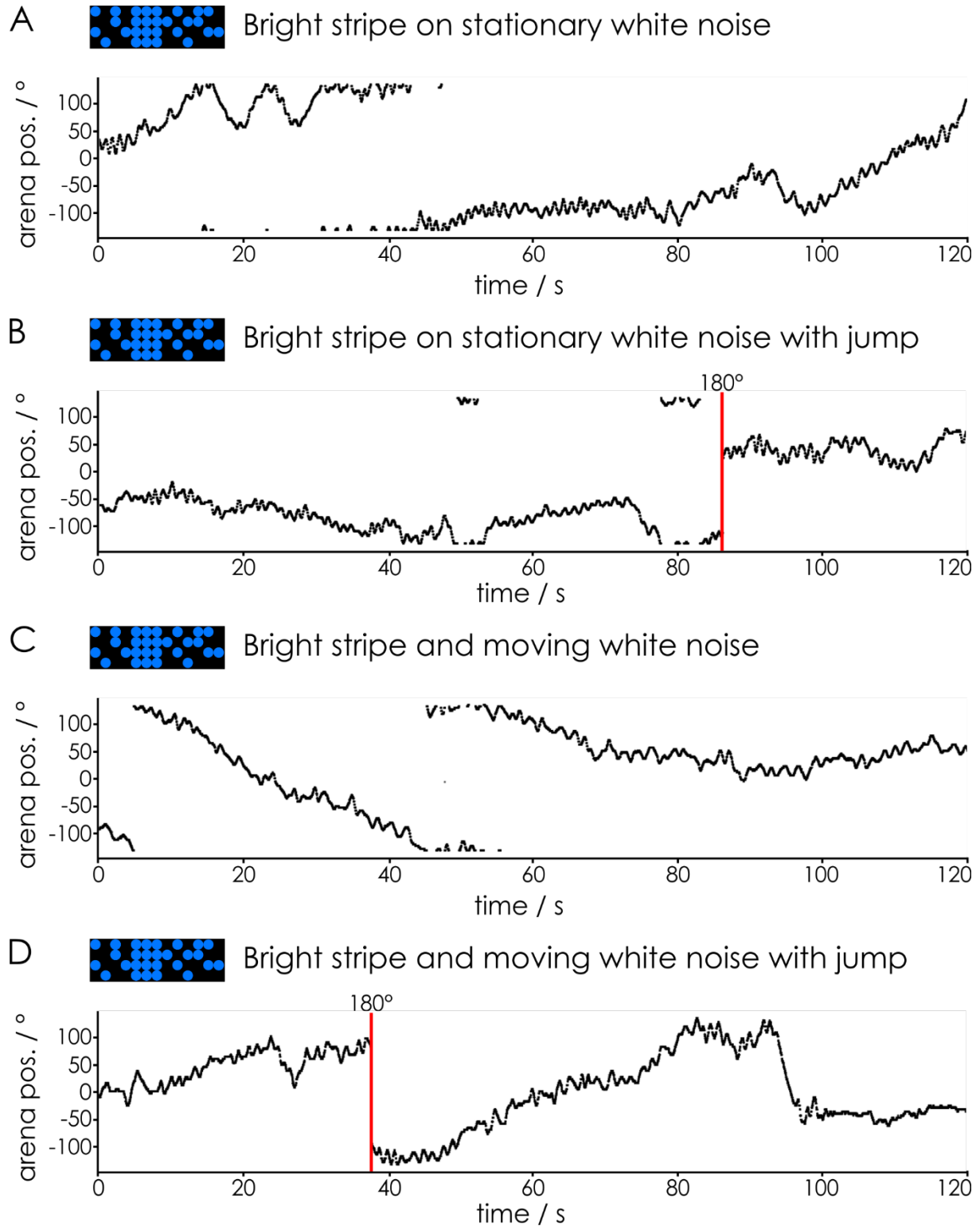


**Fig. 12: Positioning of different patterns in the LED arena in closed-loop control by a bee (#170712).** The response via walking behavior of a bee to different patterns was investigated by visualizing the pattern position (black traces) in the arena in 120 seconds long trials. A: A bright blue stripe was presented on a stationary white noise background pattern. B: The same pattern as in A was displayed but this time an artificial jump by 180° (red line) of the stripe was introduced. C: A bright blue stripe is presented on a white noise background pattern but stripe and background move together. D: Same pattern as in C but with an artificial 180° jump (red line).

Another important pattern is the inverse of the first pattern, a dark stripe on a bright background. In this visual stimulation setting, the bee showed a more tortuous walking trajectory than with a bright stripe on dark background (Fig. 13A). However, the bee was not completely disoriented but kept the stripe primarily to her left while walking forward. Following two 180° jumps, the bee exhibited a stripe-fixation behavior, meaning the bee kept the stripe in front of herself and was walking “towards” it for over 30 seconds (Fig. 13B). Bees did not showcase this stripe-fixation often though, most of the time they showed a menotactic behavior with the stripe to predominantly on one side.

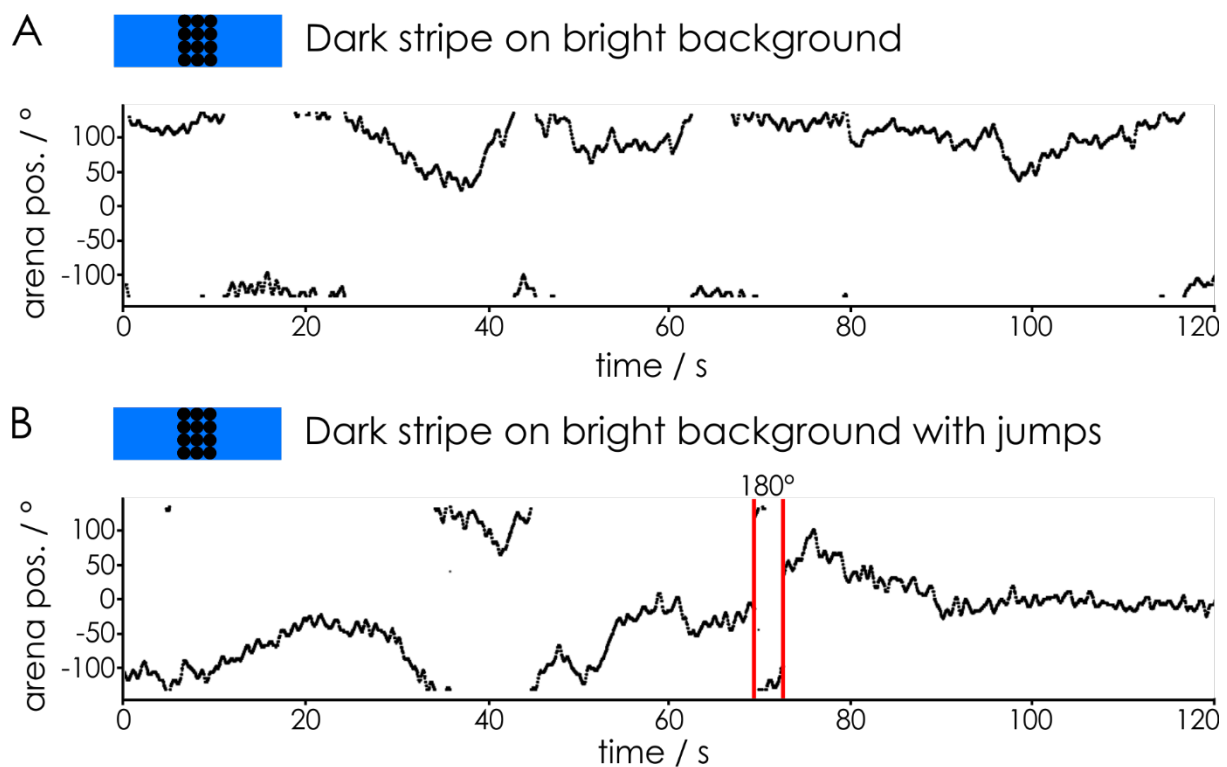


**Fig. 13: Positioning of a dark stripe on a bright blue background by a bee (#170712) in closed-loop control over an LED arena.** A: The inversed pattern of the previous trials was presented to the bee for 120 seconds in each trial. The position of the stripe is indicated by the black traces B: Introduction of two jumps by 180° is highlighted by red lines.

At the end of all the trials with different patterns, the first pattern of a bright stripe on dark background was displayed again to check, if the behavior shown in the beginning is still robust. Indeed, the bee showed again a constant menotaxis with the stripe to one side (Fig. 14A). Introducing two 180° jumps did also elicited the same behavior shown before with the bee bringing the stripe back into the position it has been before the jump (Fig. 14B).

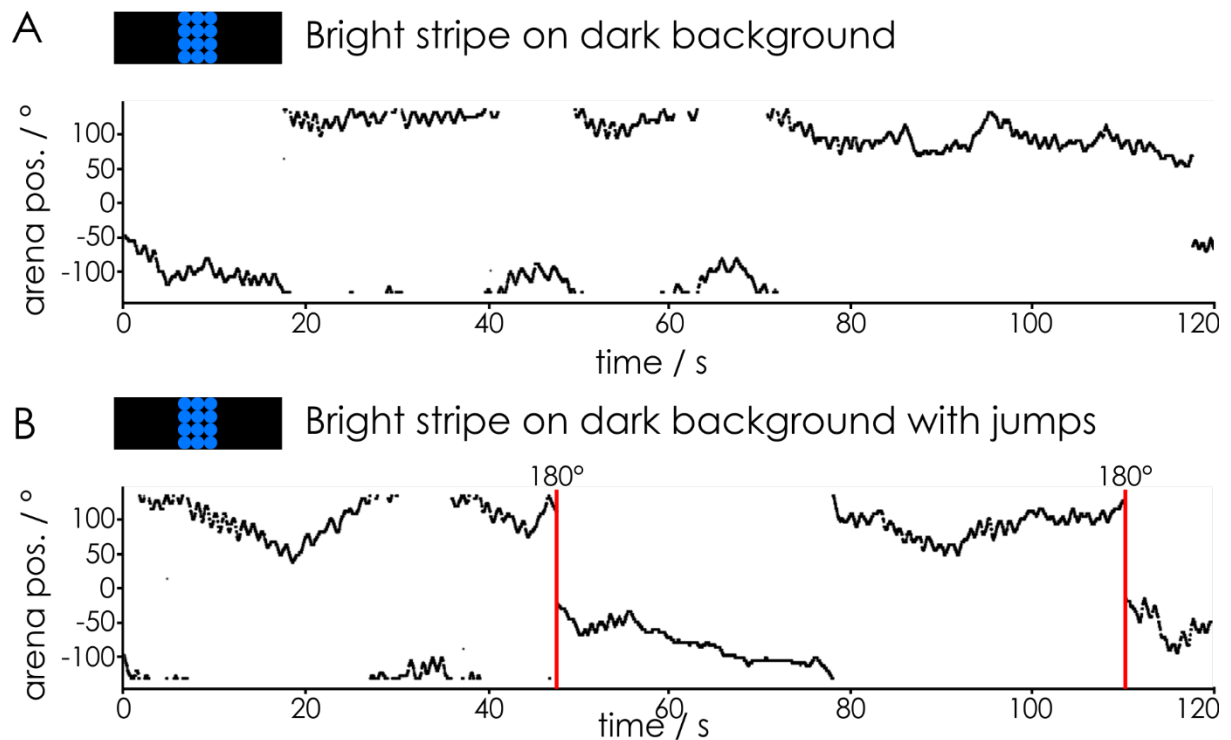


**Fig. 14: Re-testing of a bright stripe on dark background in a bee (#170712) in closed-loop control.** The robustness of the first tested pattern was investigated by showing the same pattern again after trialing the previous described patterns. The position of the stripe in the 270° arena is indicated by the black trace during 120 seconds long trials. A: Black trace indicates the position of the stripe in the arena. B: Artificial jumps of 180° (red lines) are introduced during the trial, the position of the stripe in the arena is indicated as black trace.

In addition to tests in closed-loop control, the behavior of a bee (#170920) was also tested during open-loop mode. In this setting, a bright stripe was rotated on a dark



background with  $60^\circ/\text{s}$  clockwise or counter-clockwise around the bee. This stimulus evoked an optomotor-response, with the bees following the stripe rotation when it was in their frontal field of view (Fig. 15). This optomotor-response occurred during several rotations within one trial and lasted several seconds each time. There was no noticeable difference in the response of the bees between clockwise and counter-clockwise rotation regarding translational velocity (Fig. 15).

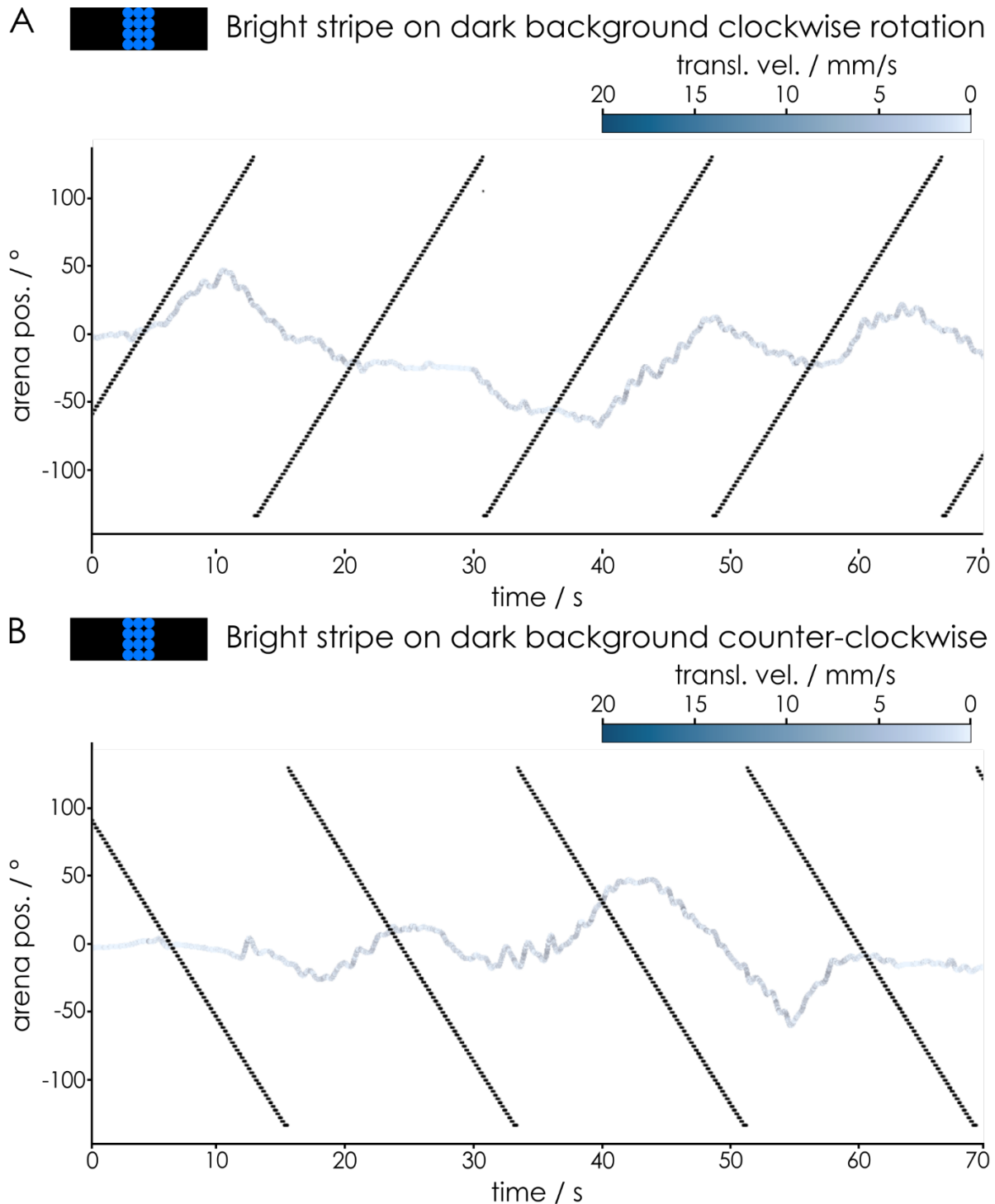
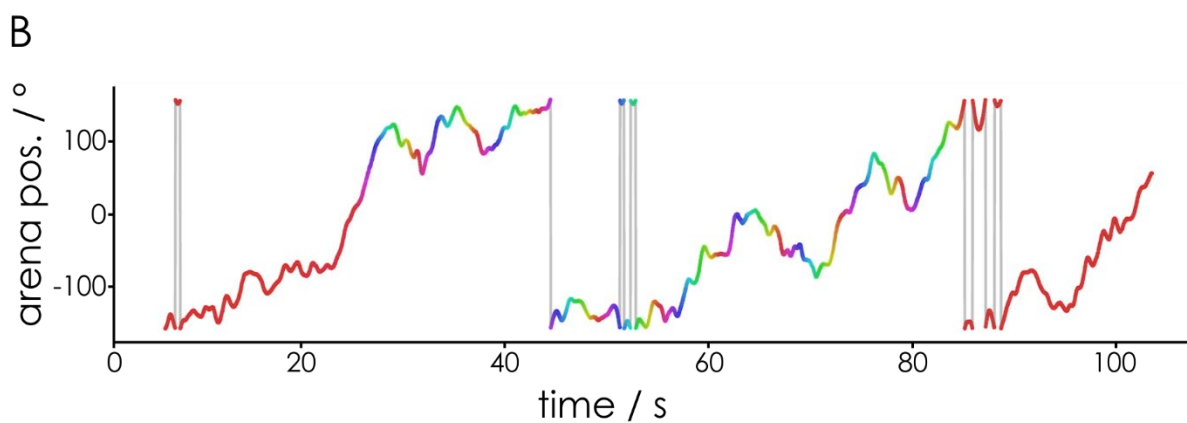
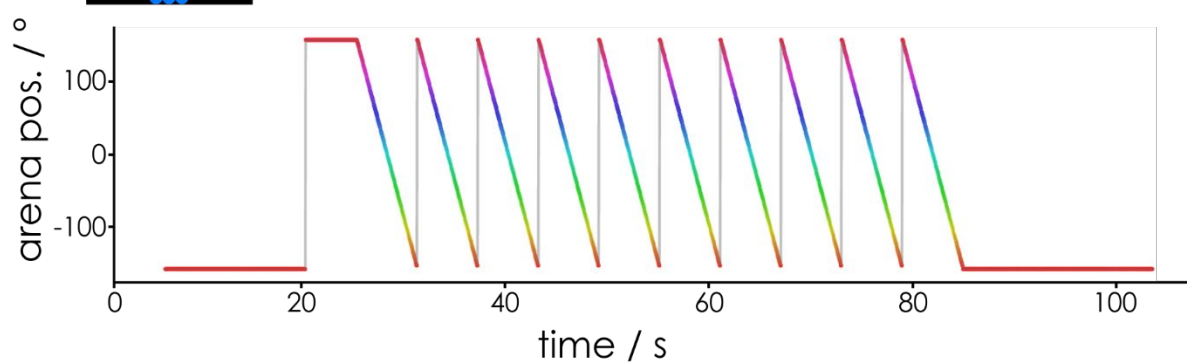


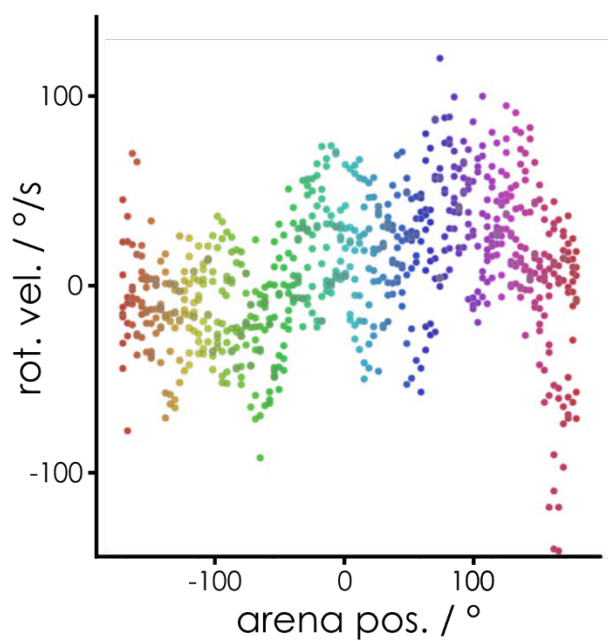
**Fig. 15: Walking behavior of a bee (#170920) in the custom-built setup during open-loop control of the stimulus.** A bright blue stripe on a dark background was displayed in the 270° arena and rotated around the animal with 60° per second. The position of the stripe is indicated by the black stripes, in blue the walking trajectory including the translational velocity is visualized. A: The stripe was rotated clockwise around the animal. B: Counter-clockwise rotation of the stripe around the bee.

In the setup with the Leica SP8 MP microscope in Würzburg only open-loop control was used and tested in the 330° arena. Here, only the behavioral response to a bright stripe on dark background stimulus was evaluated further. Since the output format of the data file acquired by the FicTrac software differed from the files obtained with the custom-built system, the analysis and visualization of the results differed slightly. In Fig. 16, one trial of one example bee (#20190717\_2) is shown. The position of the bright stripe in the arena was color coded (Fig. 16A) and the rotation with 60° per second clockwise or counter-clockwise was repeated in this example ten times. In the walking trajectory, the color code of the stripe position was included, to have one trace where both pieces of information were stored (Fig. 16B). During the first four rotations the bee showed an optomotor-response when the stripe was in front of the animal followed by a short period where the animal turned in the opposite direction. The optomotor-response was in this case contrary to the heading direction the animal had before the pattern started turning. However, not all ten rotations elicited that behavioral response. Therefore, the turning response of the first four rotations was visualized selectively, showing a higher rotation velocity when the stripe moved in the frontal view to the right of the animal (Fig. 16C), while rotation 5 – 10 elicited a more tortuous turning behavior (Fig. 16D).

A  Bright stripe on dark background clockwise rotation



C Rotation 1 - 4



D Rotation 5 - 10

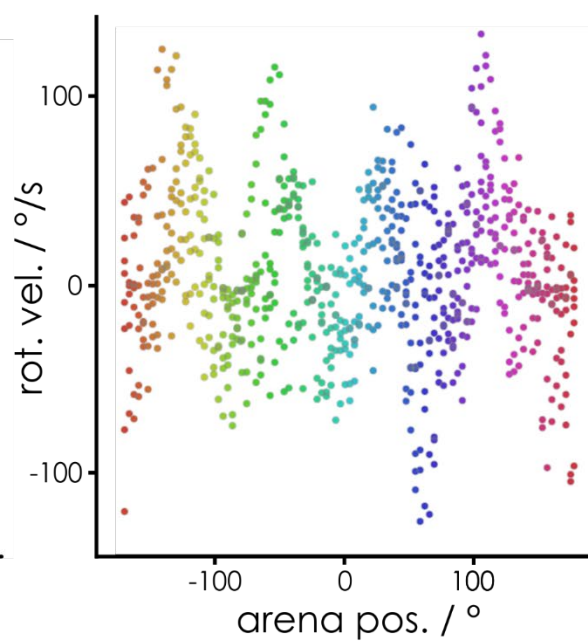
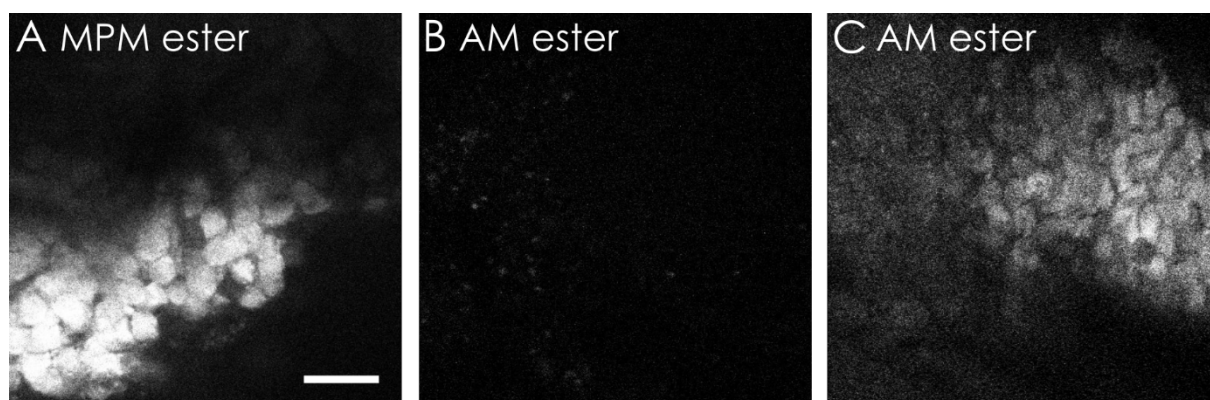


**Fig. 16: Pattern position and walking behavior of a bee (#20190717\_2) in an LED arena with open-loop control of the visual pattern in the Leica setup.** Combined data from the visual stimulus and the behavioral recordings with FicTrac. A: A bright stripe on dark background was rotated ten times clockwise around the bee. The position of the stripe in the 330° arena is annotated on the y axis but is also color-coded in the trace. B: Walking trajectory of the bee in the open-loop setup during the stimulation. The color of the trace displays the position of the stripe as introduced in A. C: Superimposition of the position of the stripe in the arena in ° and the rotation velocity in °/s for the first four rotations. D: Superimposition of the stripe position and the rotation velocity for rotation 5 – 10.

Other patterns, like all LEDs on and off, a grating pattern of many stripes that had a translational movement around the animal to mimic optic flow, and white noise was used as well. However, those pattern did not elicit robust walking behavior and therefore, those trajectories were not further analyzed.

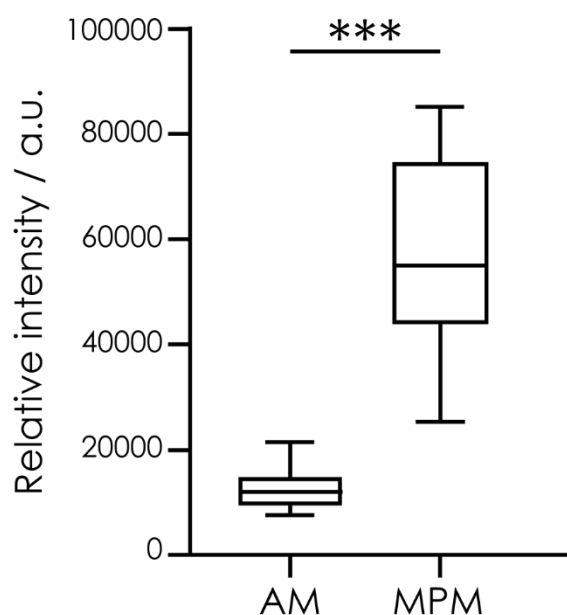
#### **PRELIMINARY TESTING OF ESTER COUPLED DYES**

In our preliminary tests, all fluorophores were measured with a microscope setting of 700 V PMT gain and 20% laser power (Fig. 17 and Fig. 18). Fluorophores coupled to methoxypropiomethyl (MPM) ester groups exhibited the brightest fluorescence labeling of all twelve tested molecules, with an even uptake and distribution throughout the cell bodies of Kenyon cells (Fig. 17A). In contrast, the dye coupled to acetoxymethyl (AM) ester, which is the most widely used ester for passive dye uptake (e.g. Hamad et al., 2015), did not exhibited similar labeling and emission results with the same setting (Fig. 17B). The laser power had to be increased to 30% and the PMT gain to 800 V to show labeling in cell bodies of Kenyon cells of the mushroom bodies (Fig. 17C).



**Fig. 17: Fluorescence signal compared between MPM ester and AM ester coupled dye.** The same dye molecules were masked with either methoxypropiomethyl (MPM) esters acetoxymethyl (AM) esters. A: Cell bodies of Kenyon cells that were labeled with dye molecules that were masked with MPM esters are imaged with 20% laser power and the PMT gain set to 700 V. B: Cell bodies of Kenyon cells filled with AM ester coupled dye imaged with the same microscope settings as in A. C: Cell bodies of Kenyon cells filled with dye that was coupled to AM esters were imaged with a laser power of 30% and the gain of the photomultiplier tube (PMT) at 800. Scale bar = 10  $\mu$ m (applies for A-C).

Statistical analysis revealed that the signal in cell bodies labeled with the AM ester coupled dye was indeed significantly weaker than in the ones labeled by the MPM ester coupled fluorophores (Fig. 18, Mann-Whitney U test:  $p = <0.0001$ ,  $U = 0$ ).

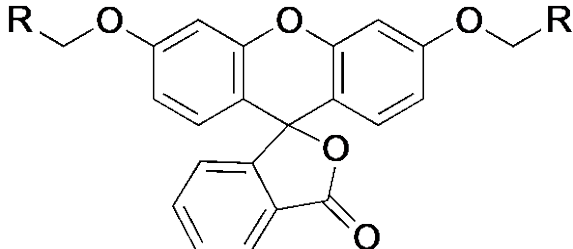
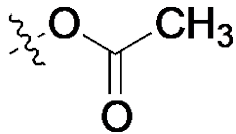
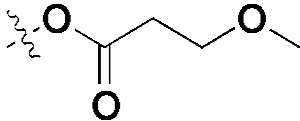
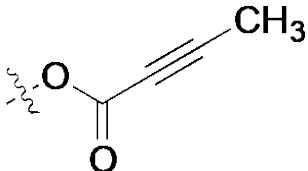
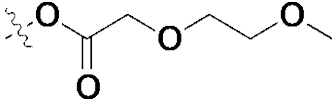
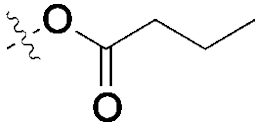
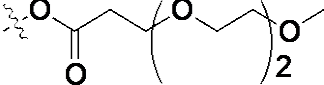


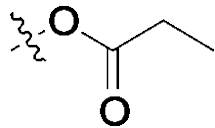
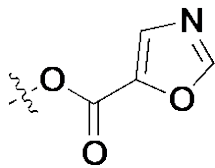
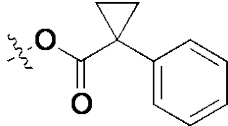
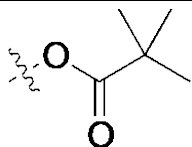
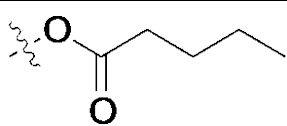
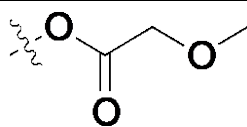
**Fig. 18: Statistical comparison of the emission brightness in cell bodies labeled with dyes coupled to AM and MPM esters.** The relative intensity of twenty labeled cell bodies of Fig. 17A & B was measured and statistically analyzed. The Mann-Whitney-U test resulted in  $p = <0.0001$  and  $U = 0$ , determining a significant difference and showing that cell bodies labeled with the MPM ester coupled fluorophores are brighter than the ones containing AM ester dye.

Some other ester groups showed a sufficient uptake into the cells but with a high background labeling. Other molecules revealed no labeling at all or strong artefacts like labeling of other structures than cell bodies like neural sheaths and trachea. In some brains the injection with an ester-masked dye lead to a staining of

cell bodies but with bright spots at the cell membranes and only a weak staining in the cytoplasm. For a more detailed summary of the results, see Table 1.

**Table 1: Observations about uptake, brightness, and distribution of Fluorescein molecules coupled to different ester groups.**

<b>Masked Fluorescein</b>		
<b>Ester group (=R) name</b>	<b>Chemical structure</b>	<b>Observation</b>
FD-ACE-DE (AM ester)		Cell bodies weakly stained but with background staining; strongest staining superficial at entrance point; sometimes bright spots at membrane of cell bodies → agglomerated dye?
FD-MPM-DE		Strong staining of cell bodies, single CBs clearly distinguishable; glomerular structures in lip and collar of MB visible as well; overall impression much better than with AM ester; worked in ants (Lavis, personal communication)
FD-BTY-DE		Weak staining; structures not clearly identifiable
FD-MEME-DE		Cell bodies weakly stained but with background; labeling just at the surface, no neurons traceable
FD-BUT-ME		Cell bodies visible but strong staining at the brain surface = neural sheaths?
FD-PEG-ME		Weak staining of cell bodies with bright spots at the membranes

FD-PRO-DE		Staining in cell bodies but accumulation of dye at the membranes
FD-OXZ-DE		Good labeling of cell bodies but very strong background staining; problem for calcium signal?
(HO-cPAM) <sub>2</sub> -FL		Cell bodies not distinguishable but string-like structures, tracheae?
FD-PIV-ME		No real structure visible but strong background; auto-fluorescence?
FD-VAL-ME		No structures visible
FD-MOA-DE		String-like structures visible but no cell bodies

Overall, the preliminary testing with twelve different ester groups revealed that MPM esters seemed to be preferable over the others.

### CALCIUM IMAGING DATA WITH JF<sub>549</sub>-BAPTA-MPM ESTER

Even though many experiments were conducted at the custom-built and the Leica setup with the custom-made calcium indicator JF<sub>549</sub>-BAPTA MPM ester, the analysis of the data revealed, that only a few data sets were considered valid. This had several reasons, for example artefacts during the acquisition process or chemical problems with the dye itself (see Discussion and Outlook). The visual stimulation protocol was changed multiple times in search for the most suitable setting. In the end, an experiment started with imaging the structure for 5 seconds without visual stimulation, then turning the pattern on but keeping it stationary for another 5 seconds. Then, the pattern was rotated for 12 seconds around the animal at a speed of 60° per second, followed by turning it off and imaging the brain further for 8-10 seconds



resulting in a total trial of 30-32 seconds. To evoke a broad response to visual stimulation, in the first trial of a new experiment all LEDS were turned for 17 seconds after 5 seconds of darkness and then turned off again. The 17 seconds of illumination made those trials more comparable to trials with a moving pattern.

In one data set (#20181113\_1), the targeted transmedulla neurons were labeled and structures in the lower unit complex (LUC) of the anterior optic tubercle (AOTU, Fig. 19A) were visible, while the upper unit (UU) showed no staining (Fig. 19B). In the LUC, four regions of interest (ROI) were chosen as an example to show regions that response and one in close proximity as comparison where no signal increase is visible. The calcium response to turning all LEDs on was analyzed (Fig. 19B). The  $(F-F_0)/(F_0-F_b)$  traces of those four ROIs revealed a response of varying strength to the onset of the stimulation in three of the ROIs and no response in the fourth ROI (Fig. 19C). The fluorescence signal of the three responding ROIs returned back to baseline after 5-6 seconds of stimulation. In two of those ROIs a small increase of fluorescence occurred when the LEDs were turned off. It is not possible though to tell from one animal if this indicates an on/off response to light in the neurons, as has been shown for example in ocellar neurons (Goodman, 1970), or if it is anomaly in the response of this bee. To ensure that the fluorescence increase in the ROIs is a result of a calcium response of the dye and not an artefact of brain movements, a correlation analysis of the  $(F-F_0)/(F_0-F_b)$  values were plotted against the estimated movement per pixel in x and y direction at those given points of time (Fig. 19D). A strong correlation, meaning an increase or decrease in fluorescence signals occurring with simultaneous increasing or decreasing movement values, would suggest that the effects seen in the fluorescence trace are movement artefacts rather than neuronal responses to visual stimulation. In the example in Fig. 19, this seems not to be the case.

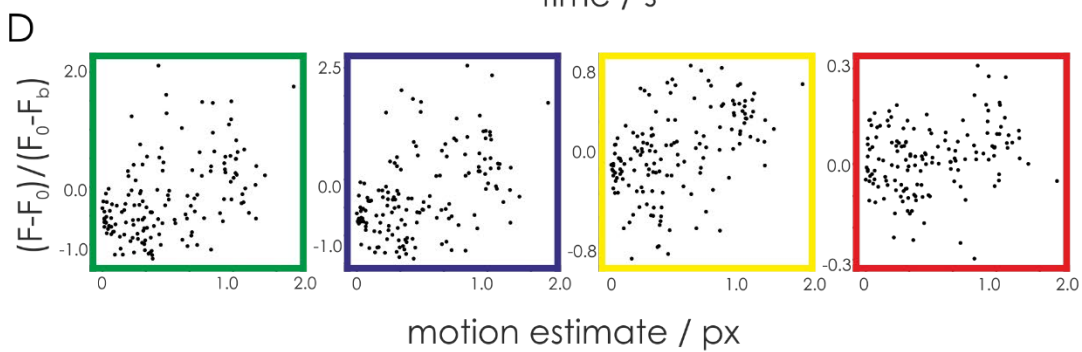
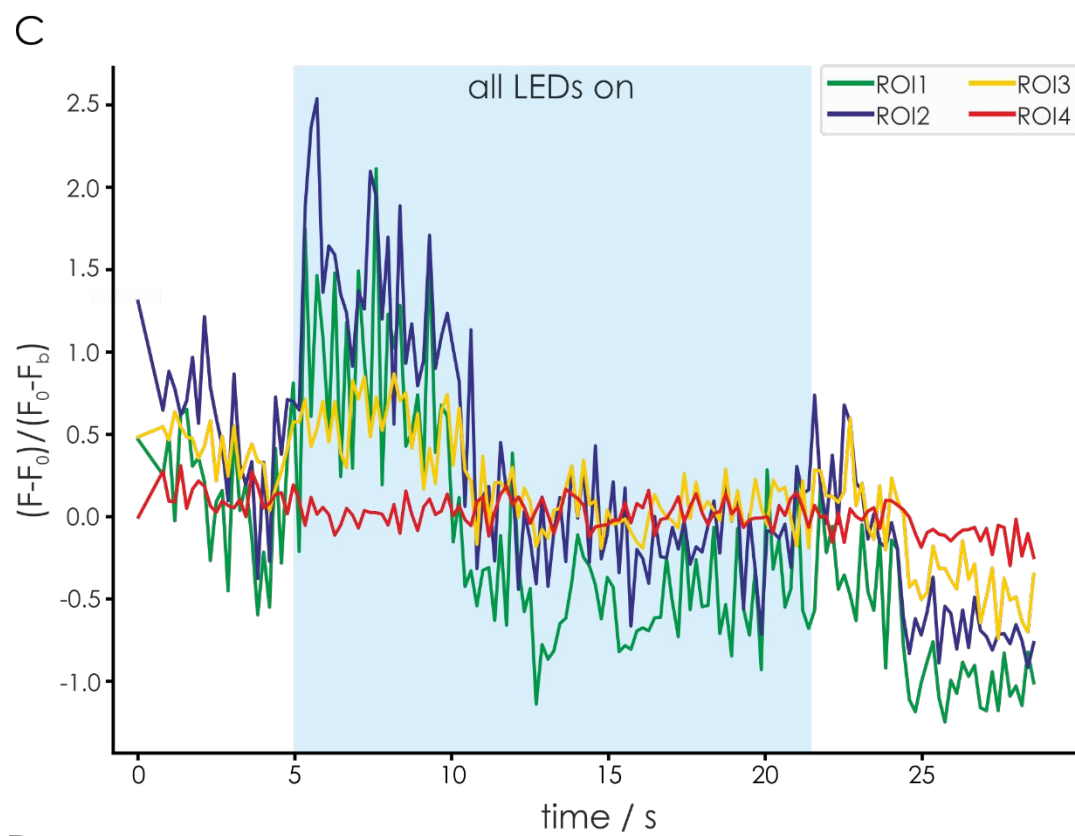
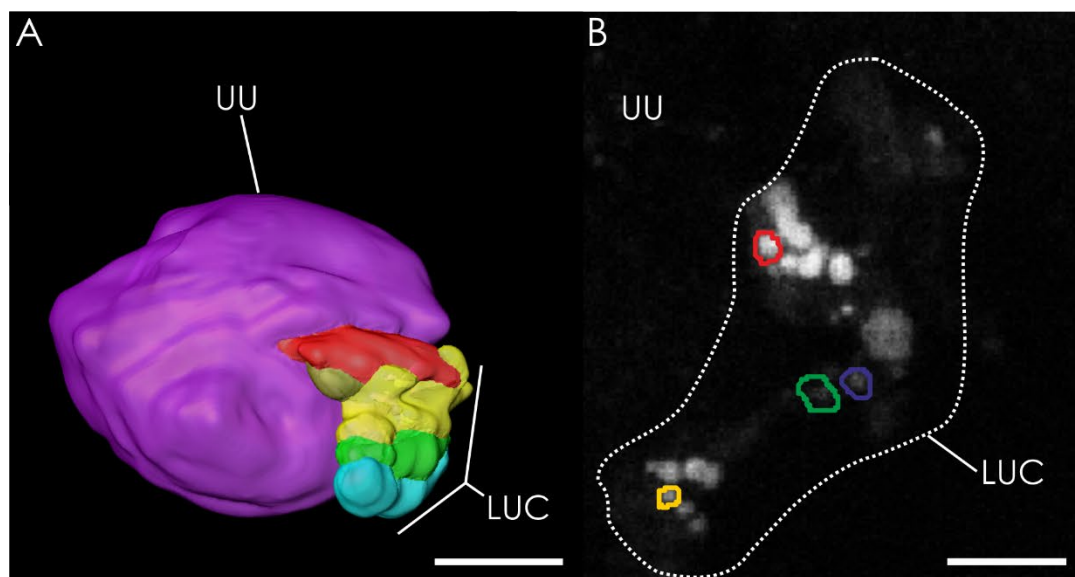


**Fig. 19: Calcium response of transmedulla neurons labeled with JF<sub>549</sub>-BAPTA-MPM ester dye to visual stimulation (bee #20181113\_1).** The calcium response to turning all blue LEDs of the arena on was imaged in the branchings of transmedulla neurons in the lower unit complex (LUC) of the anterior optic tubercle (AOTU). A: Three-dimensional average shape atlas of the AOTU, consisting of a large upper unit (UU) and the LUC, consisting of five subcompartments (Heinloth 2013, unpublished). B: Example frame from the calcium imaging time series. The imaged structures are located in the LUC while the UU shows not labeling. In the LUC four ROIs were selected and further analyzed. C: Calculation of the fluorescence changes as  $(F-F_0)/(F_0-F_b)$  over the 30 second long trial. After 5 seconds in darkness, all LEDs are turned on for 17 seconds, followed by 8 seconds in darkness. D:  $(F-F_0)/(F_0-F_b)$  values were connected to the concurrent estimated motion in x/y per pixel in the four ROIs. Color code for ROIs as in B and C. AOTU: anterior optic tubercle, LUC: lower unit complex of the anterior optic tubercle, ROI: region of interest, UU: upper unit of the anterior optic tubercle. Scale bars: A = 50  $\mu$ m, B = 20  $\mu$ m.

In another example bee (#20181012\_1), the LUC showed a strong labeling, while the UU remained again untinged (Fig. 20A). After analyzing the response in all labeled structures, three ROIs were chosen to visualize their fluorescence signals due to their strong responses (Fig. 20B). After turning all LEDs on, the fluorescence signal in two of the three ROIs changed with a time-delay of several seconds. ROI1 showed an increase in fluorescence, ROI2 showed no response, while in ROI3 a decrease of the fluorescent signal was detectable. The trace layout of ROI3 showed a strong resemblance to ROI1, but mirrored. After a few seconds after the onset of fluorescence changes, the curves of ROI1 and ROI3 returned back to roughly the level they had before the response. After turning all LEDs off after 17 seconds, ROI1 showed another but smaller fluorescence increase, again slightly time-delayed to the stimulus. The signal of ROI2 showed a similar course to ROI1 after the first 17 seconds but with smaller amplitudes. To test if the fluorescence changes seen in Fig. 20B are based on movement artefacts, an analysis was conducted, comparing the  $(F-F_0)/(F_0-F_b)$  values with the estimated movement in x and y (Fig. 20C). In this example, the fluorescence increase in ROI1 seemed to be correlated to more movement in x and y. ROI2 showed in some parts a correlation but a weaker one than ROI1. ROI3 showed a very similar picture to ROI1, just mirrored again. Taken together the similarities between ROI1 and ROI3, even though it was a mirrored, some similarities between ROI1 and ROI2, and the time-delay to the onset of the visual stimulation, it is likely that the effects seen in the

fluorescence traces are artefacts rather than responses to the stimulus.

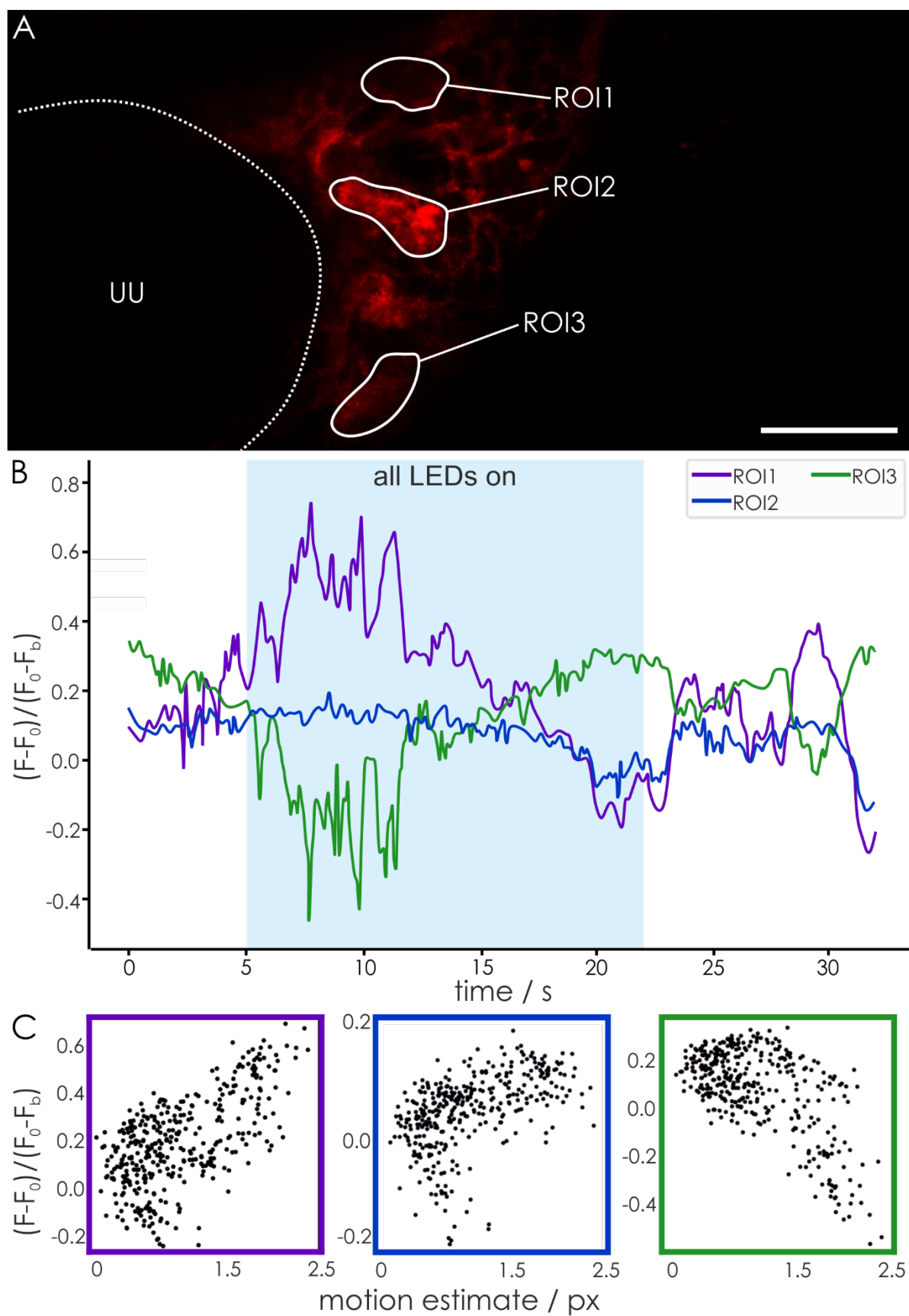


**Fig. 20: Example for possible movement artefact during imaging experiment with JF<sub>549</sub>-BAPTA-MPM ester labeled transmedulla neurons (bee #20181012\_1).** The branches of transmedulla neurons in the lower unit complex of the anterior optic tubercle were imaged during visual stimulation with all LEDs on. A: Example image of a time series during stimulation. Labeled structures are limited to the lower unit complex in which three ROIs were defined. B: Fluorescence traces of the three ROIs during a 32 second long trial. After 5 seconds in darkness all LEDs were turned on for 17 seconds. After turning them off the brain was imaged for 10 more seconds. C: Comparison between fluorescence values to the estimated motion per pixel in x/y during the same time. ROI: region of interest, UU: upper unit of the anterior optic tubercle. Scale bar = 50  $\mu$ m.

However, since the analysis was made after the experiment and since the signal in the LUC was strong more tests were made with this bee. After the trial with all LEDs on/off, the rotation of a bright stripe on dark background was tested in 10 trials with two rotations of 60° per second in each trial. To allow for a straightforward comparison of the responses across all 10 trials, the stripe was always rotated clockwise around the animal. The individual trials followed the same protocol as described before. First, the structure was imaged for 5 seconds without visual stimulation, then the pattern was turned on but kept stationary for another 5 seconds, and then rotated around the animal for a total of 12 seconds at 60°/s. Afterwards, the pattern was turned off and the structure was imaged in darkness, this time for 10 seconds, yielding a total time of 32 seconds for one trial. However, those tests did not deliver conclusive results with the traces of each of the three ROIs being different between trials. Only the traces of three out of ten trials showed a similar time course and were analyzed further. Averaging the fluorescence traces of the three ROIs of those three trials revealed strong similarities between the ROIs but no obvious correlation to the pattern position (Fig. 21). It has to be noted though, that only the mean fluorescence intensity was analyzed here, not the  $(F-F_0)/(F_0-F_b)$  values, meaning that the background fluorescence changes were not taken into account. Looking at the individual trials, the ROIs never showed response patterns based on the visual stimulation, like, for example, fluorescence peaks according to the stripe position. Taken together with the analysis of the stimulation with all LEDs on in Fig. 20, it is very likely that the fluorescence changes seen during those experiments were based on movement artefacts in x, y and probably also z and not on responses of the transmedulla neurons to visual stimulation.

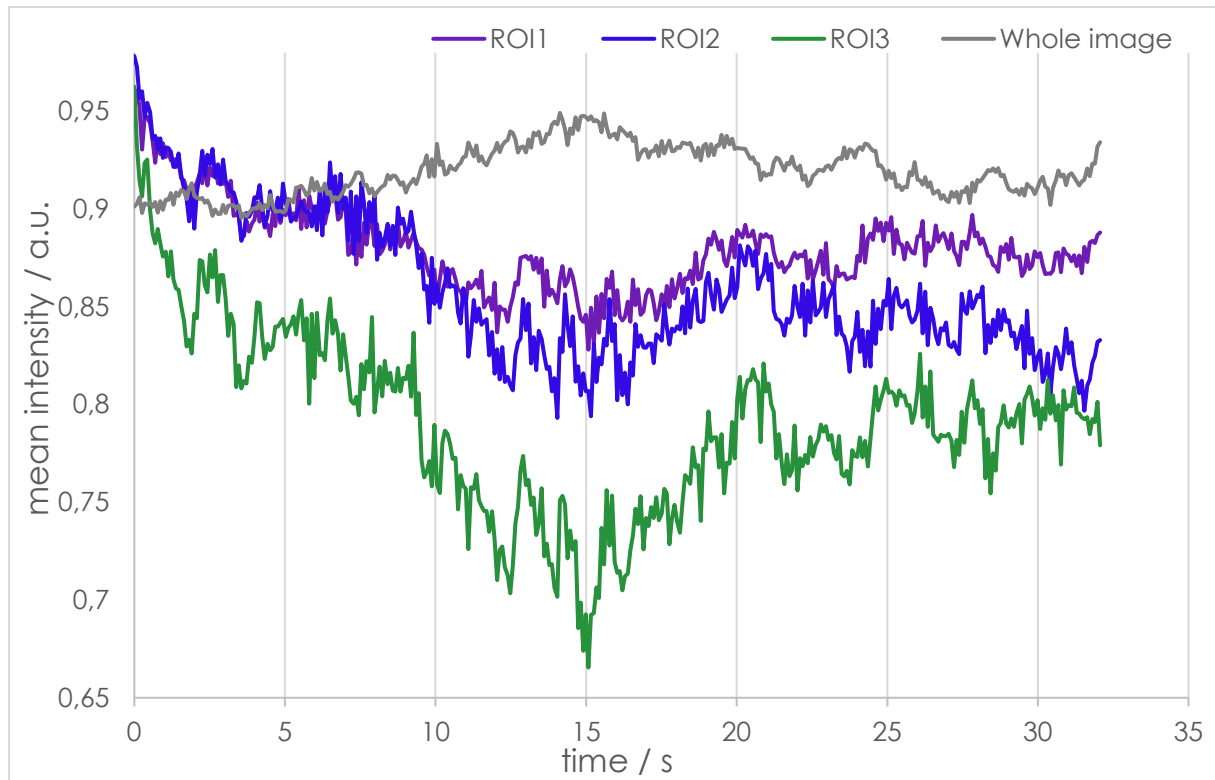


**Fig. 21: Mean fluorescence changes in three ROIs and the whole field of view over three trials with a rotating stripe.** One trial consisted of 5 seconds in darkness, 5 seconds bright stripe on but stationary and then two rotations with 60° per second clockwise around the animal, followed by 10 seconds in darkness. The mean fluorescence intensity of the three ROIs and the whole image was averaged over three out of ten trials to check for a pattern in the response to the two rotations in each trial. ROI: region of interest.

### CALCIUM IMAGING DATA WITH CALCIUM GREEN-1 DEXTRAN

Since the JF<sub>549</sub>-BAPTA-MPM ester dye showed issues concerning the chemical stability (see Discussion), Calcium Green-1 dextran was the predominantly used calcium sensor in the Leica setup. To check for the reliability of the calcium response of the dye, two test trials with potassium chloride (KCl) were conducted without any visual stimulation (bee #20180618\_1). Adding KCl in a high concentration, in our case 100 mM, via bath application onto the brain leads to a reliable depolarization of neurons, causing a Ca<sup>2+</sup> influx into functional neurons. Neurons filled with a calcium indicator will therefore show a fluorescence increase after the KCl application (Chen and Huang, 2017). Here, the test was conducted in cell bodies in the medulla (Fig. 22A). These cell bodies have the advantage that they are rather big, and lay superficially in the brain and are therefore easily accessible to imaging in living tissue.



They are also well defined structures and therefore choosing ROIs and analyzing the fluorescence responses is less demanding than in areas with fine branchings for example. The cell bodies were imaged for ten seconds in darkness. Then, a small amount of 100 mM KCl solution was added manually into the saline reservoir of the bee holder via a syringe system and the cell bodies were further imaged for 50 seconds. For the analysis, the mean fluorescence intensity traces of two cell bodies chosen at random as ROIs (Fig. 22A) were visualized during the 60 second long trial (Fig. 22B). The traces show a drop in fluorescence after around 12 seconds for about 7 seconds, which can be explained by the added volume onto the brain, which caused a drop in z until the fluid was distributed evenly in the reservoir. Immediately after the recovering at around 20 seconds into the trial, both traces displayed an increase in fluorescence. After additional 5 seconds, the fluorescence did go back to the baseline. The time-delay between application of KCl and  $\text{Ca}^{2+}$  response readout can be explained by different factors. First, the manual introduction of KCl caused probably a human error leading to an application that was not exactly at 10 seconds into the trial. Then, the movement in z due to the volume increase might have covered the detection of an earlier fluorescence increase. The distribution of the KCl in the fluid and into the brain takes some time as well. However, the  $\text{Ca}^{2+}$  response was so distinguishable that a reliable calcium detection of Calcium Green-1 dextran in this setup seems likely.

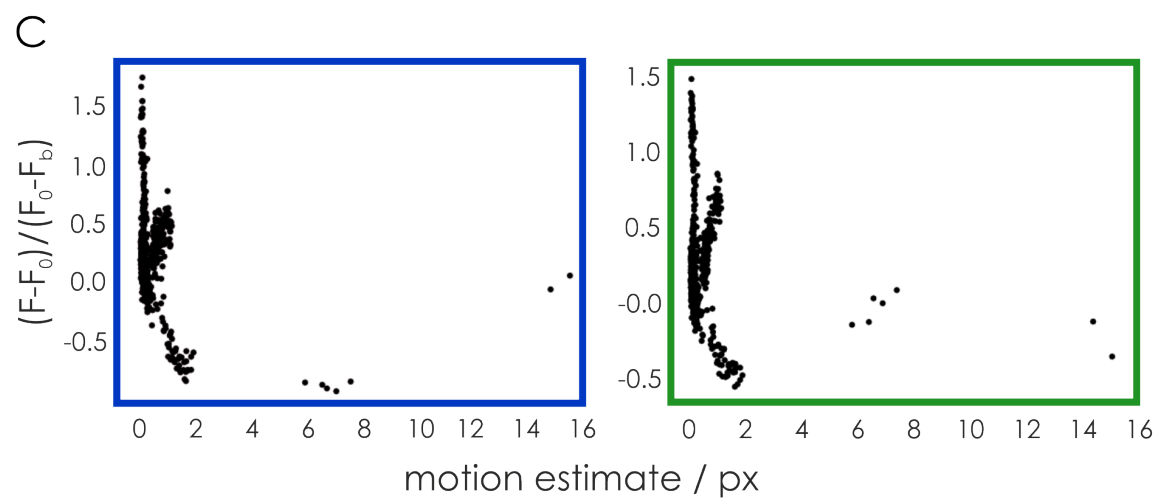
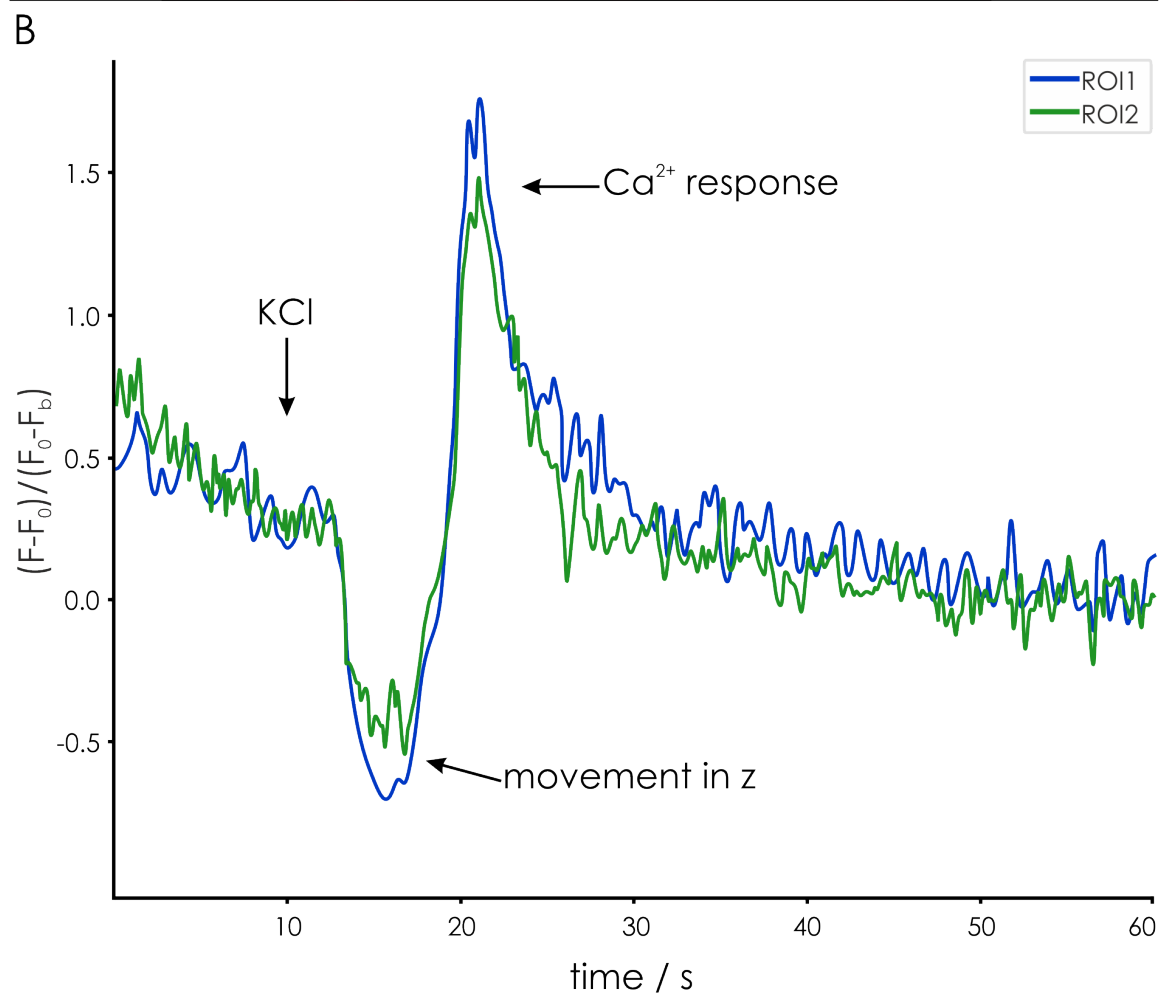
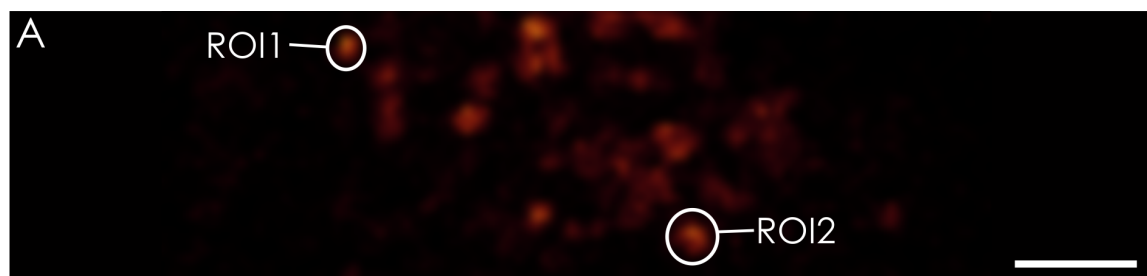


**Fig. 22: KCl induced  $\text{Ca}^{2+}$  response in cell bodies in the medulla (bee #20180618\_1).** A: Cell bodies in the medulla were filled with Calcium Green-1 dextran. Two cell bodies were marked as ROIs. B: KCl was added manually to the saline solution in the reservoir of the bee holder after 10 seconds of imaging. A drop of the mean fluorescence intensity right after the application is likely a movement in z due to the pressure of the added volume. Right after the drop a  $\text{Ca}^{2+}$  response via a fluorescence increase of various strength in both ROIs was detected.  $\text{Ca}^{2+}$ : calcium, KCL: potassium chloride, ROI: region of interest. Scale bar = 20  $\mu\text{m}$ .

After this pre-test of the dye, experiments with visual stimulation of animals were performed. In bees, the LUC is well distinguishable when many transmedulla neurons are labeled (Fig. 23A). In one example bee (#20180717\_1), the branching pattern of transmedulla neurons filled with rhodamine B and Calcium Green-1 dextran was clearly visible, even in uncleared living tissue (Fig. 23B & C). In the Calcium Green-1 dextran channel, two areas were selected as ROIs, ROI1 in the anterior optic tract, ROI2 in the LUC (Fig. 23C). The calcium response via the  $(F-F_0)/(F_0-F_b)$  traces over time was first investigated for an experiment where all LEDs were turned on after 5 seconds of darkness for 17 seconds (Fig. 23D). Shortly after the onset of the stimuli, the fluorescence increased in both ROIs, with a peak after around two seconds and the highest value around 10 seconds after switching the LEDs on. After the highest peak the fluorescence level decreased back to the level of before the stimulation and even lower. After turning the LEDs off, there was a small increase in fluorescence followed by a short dip and then a recovery to roughly the baseline. The analysis between the fluorescence values and the motion estimate in x/y showed no obvious connection between those two factors, a fluorescence increase caused by motion artefacts is therefore unlikely (Fig. 23E).

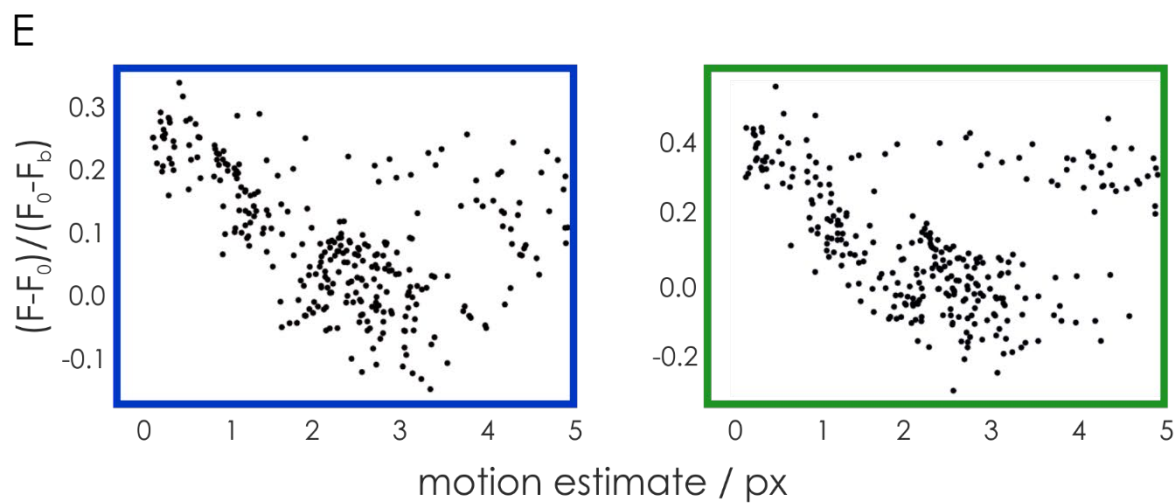
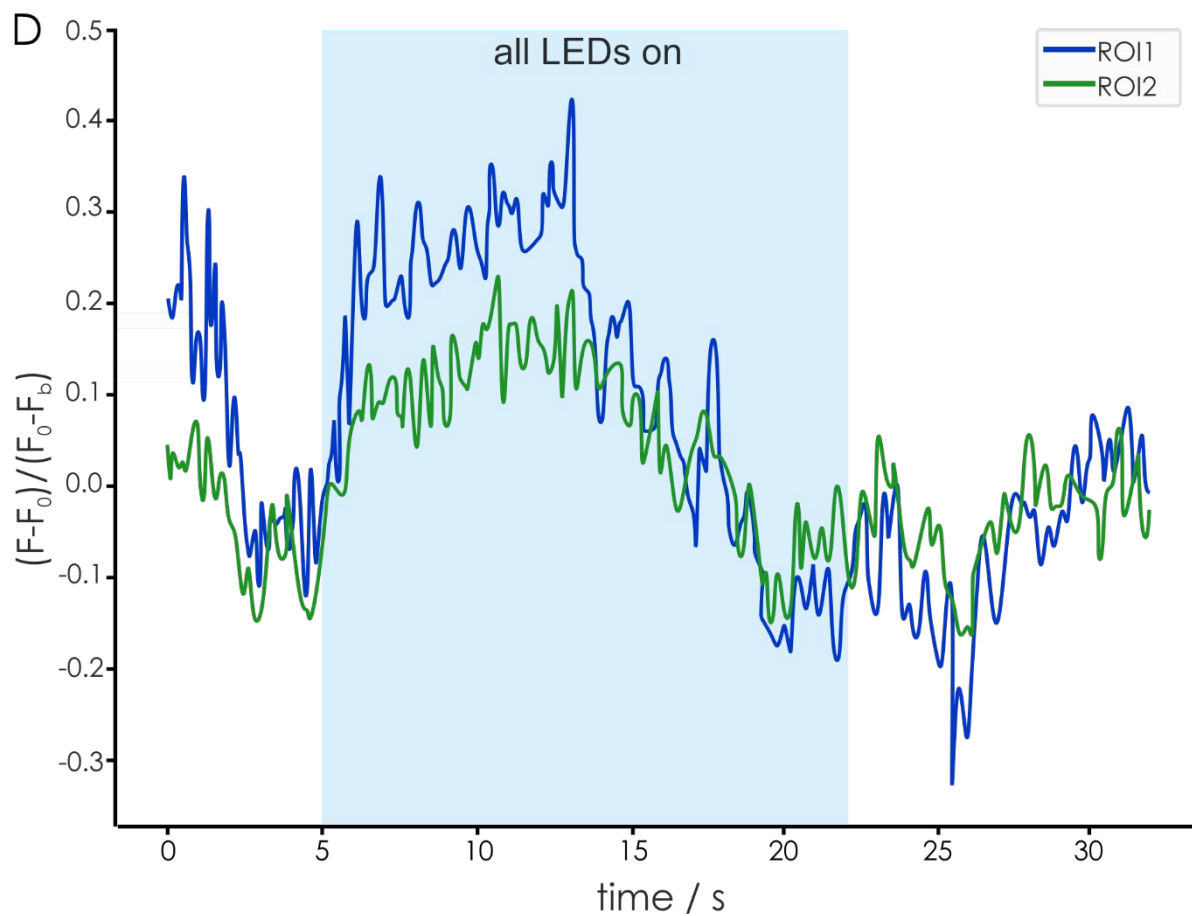
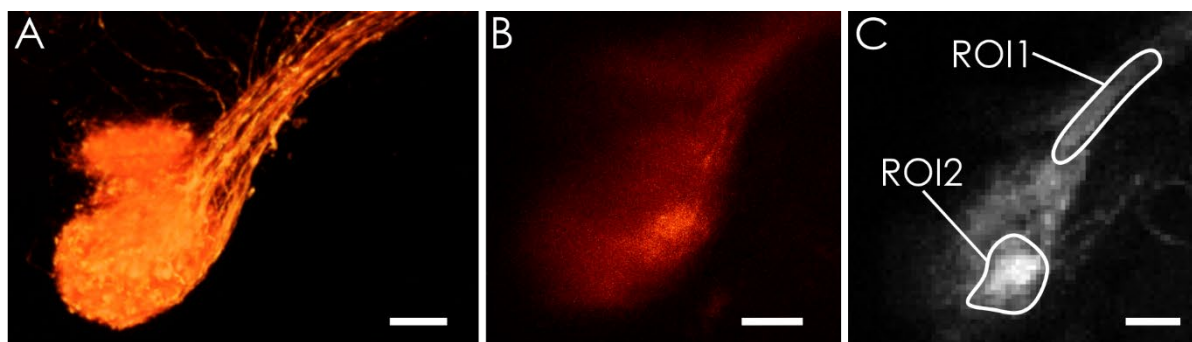
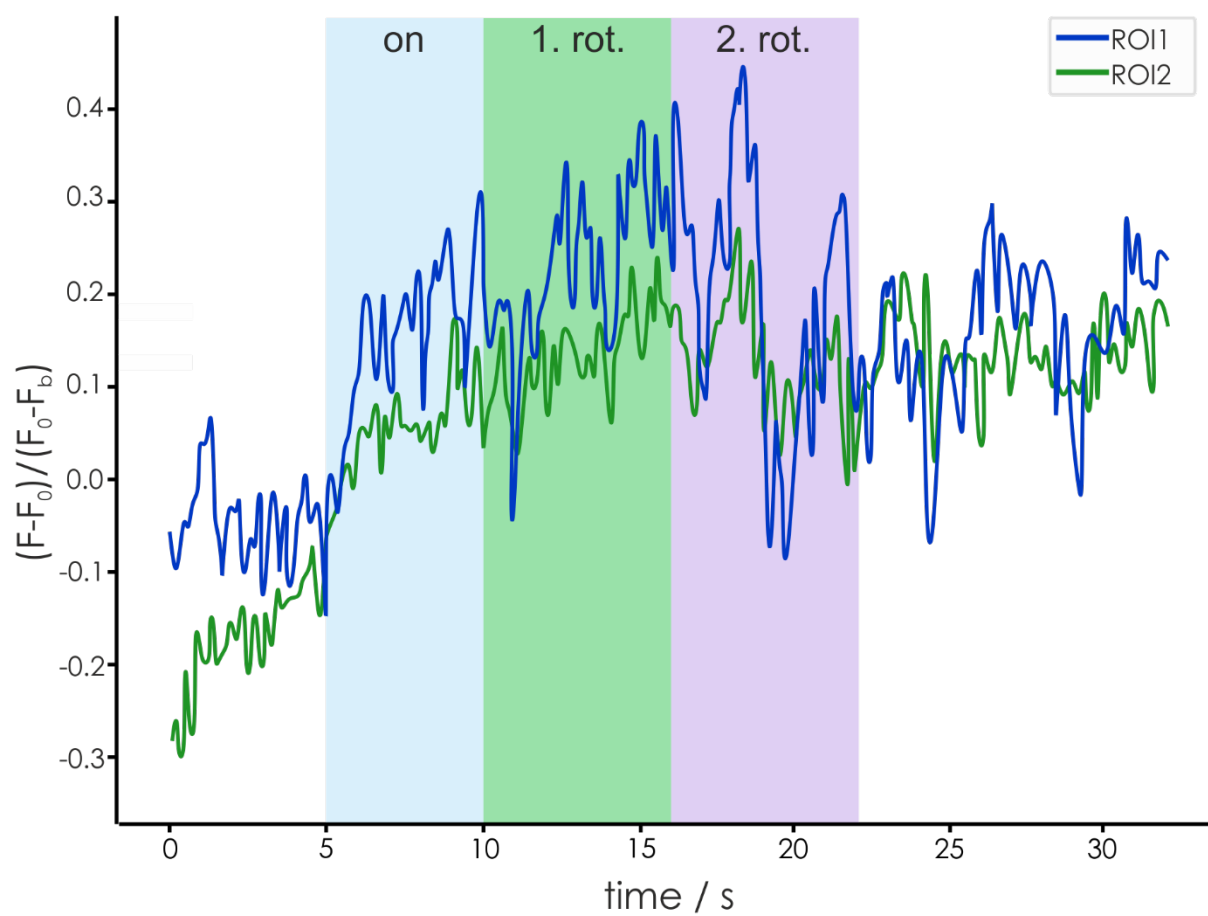


**Fig. 23: Morphology and calcium response of branchings of transmedulla neurons in the lower unit complex (bee #20180717\_1).** A: Branching pattern of Dextran Texas Red filled transmedulla neurons in the lower unit complex of the anterior optic tubercle in cleared tissue (from Zeller et al., 2015). B: Rhodamine B labeling of transmedulla neurons in the LUC in uncleared tissue of an alive bee. C: Calcium Green-1 dextran labeling of the same structure described in B. Two ROIs were selected for further analysis. D:  $(F-F_0)/(F_0-F_b)$  for both ROIs was calculated during a 32 second long trial. After 5 seconds in darkness, all LEDs were turned on for 17 seconds, followed by another 10 seconds in darkness. E:  $(F-F_0)/(F_0-F_b)$  was compared to the estimated motion per pixel in x/y. ROI: region of interest. Scale bars = 10  $\mu$ m.

Afterwards, the same structure in the same animal was tested for a response to a rotating bright stripe on a dark background (Fig. 24A). Here, the fluorescence increased in both ROIs shortly after the bright stripe was switched on but kept stationary 5 seconds into the trial. During the first rotation with 60° per second clockwise around the animal the fluorescence first showed a short decrease and then an increase. In the second rotation there was again a small decrease in the beginning, followed by an increase but unlike in the first rotation the fluorescence decreased then. After the stimulus was turned off, the fluorescence remained higher than before the stimulation but was overall, despite some fluctuations, slightly lower than during the stimulation. The comparison of the fluorescence to the concurrent motion in x/y showed again no obvious correlation (Fig. 24B).

A



B

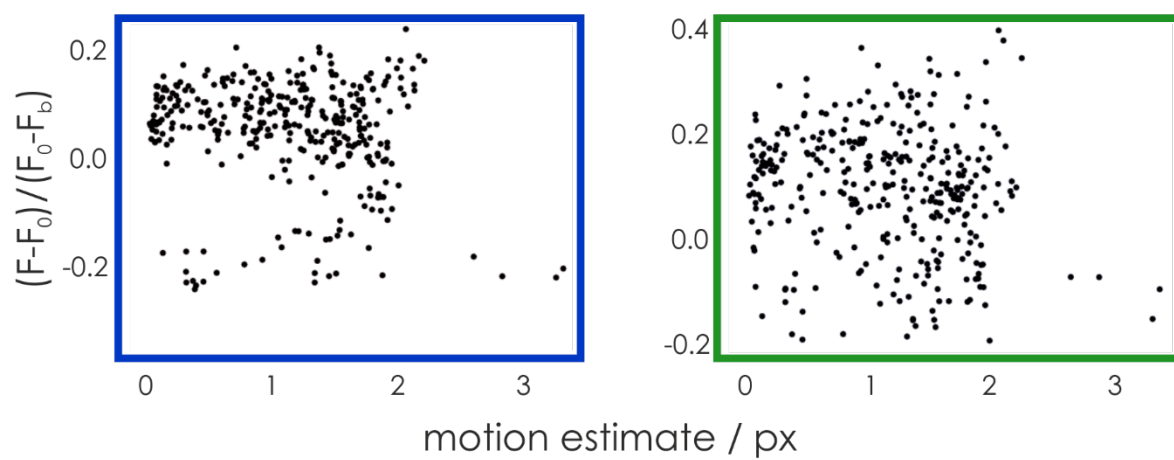


**Fig. 24: Calcium response to a rotating bright stripe on dark background.** The same structures in the lower unit complex of the anterior optic tubercle as in Fig. 20 were tested (bee #20180717\_1). A:  $(F-F_0)/(F_0-F_b)$  was calculated and visualized for the two ROIs from Fig. 20C. After 5 seconds in darkness, a bright stripe was turned on, but kept stationary for another 5 seconds. Afterwards it was rotated twice clockwise around the animal with a speed of 60° per second. After those 12 seconds of rotations the pattern was turned off but the brain was imaged for another 10 seconds. B: Fluorescence values were compared to the concurrent estimated motion per pixel in x/y. ROI: region of interest.

### **ALIGNMENT OF CALCIUM IMAGING DATA WITH THE BEHAVIOR**

One of the goals of establishing this method was, to create a readout if walking behavior influences physiological responses. If the investigated neurons showed some sort of state dependency it could either mean that during walking the response to visual stimulation is increased or decreased, or that the walking shows changes in the fluorescence traces even without stimulation. To this end, the data of the calcium imaging had to be analyzed together with the data from FicTrac. The data shown in Fig. 16 showed a robust walking behavior of the bee (#20190717\_2) and therefore this data set was used as an example. In that bee, cell bodies in the medulla were labeled with Calcium Green-1 dextran and two of them were selected as ROIs (Fig. 25A). As visual stimulus, one bright stripe was turned on after 5 seconds in darkness, kept stationary for another 5 seconds and then rotated clockwise around the animal 10 times, with 60° per second for 60 seconds in total. Afterwards the brain was imaged and the walking behavior was recorded for ~ 25 more seconds. Since it is difficult to see in continuous traces (Fig. 25B) if the stripe is stimulating the neurons during every rotation in a similar way and if there is a distinct response pattern towards to position of the stripe, the responses had to be visualized in a different way. To this end, single repeats of the stimulus were picked, in this case the first four, and the traces during those rotations were superimposed. The result was visualized for each ROI either with the single trial traces plus the average (Fig. 25C) or the just the average (Fig. 25D, bold lines) and the variability maxima of the four rotations (Fig. 25D, fine lighter lines). For both ROIs there is no distinct response pattern visible, the position of the stripe in the arena did not elicit a peak at one location for example.



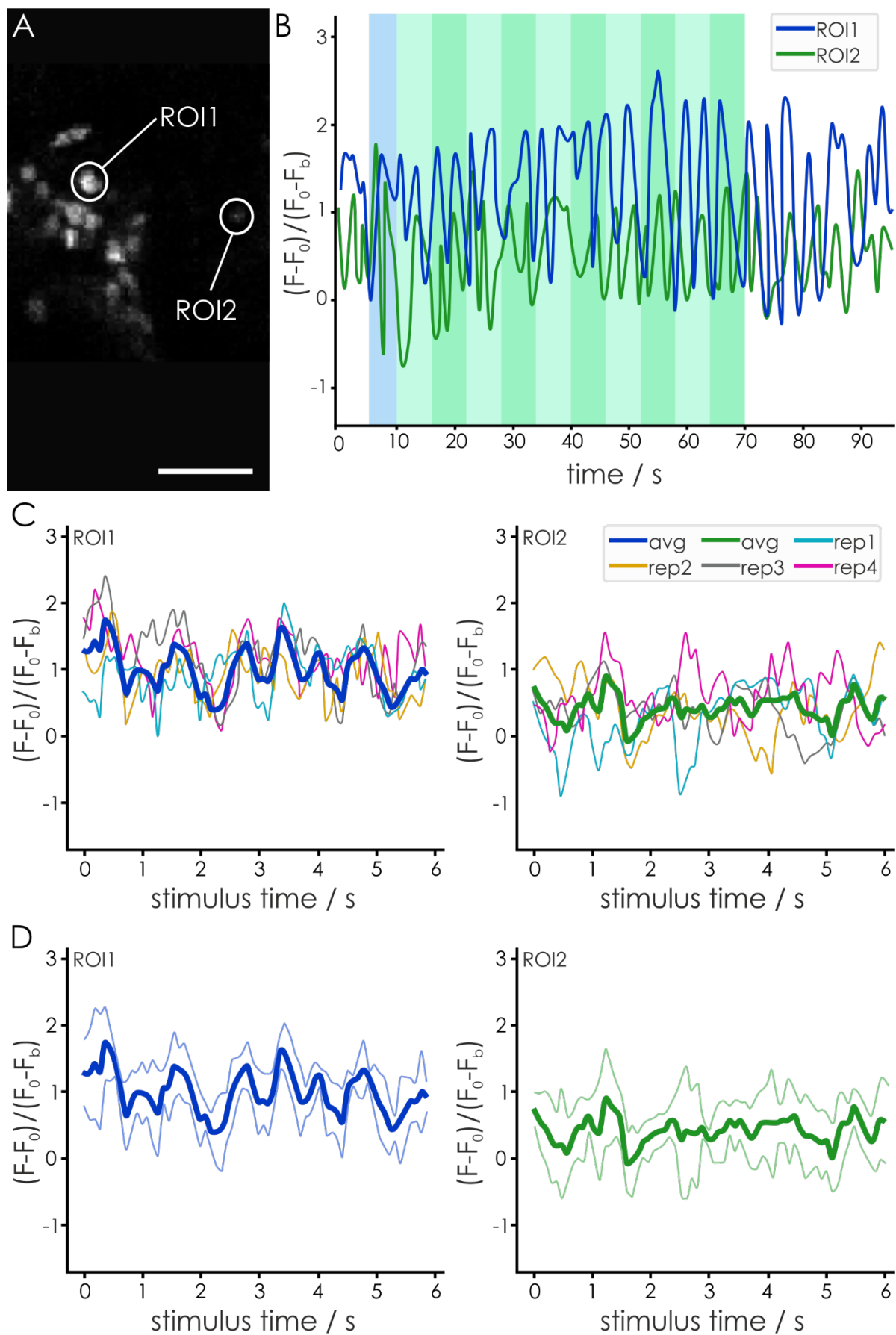


**Fig. 25: Example data set (#20190717\_2) used to align calcium response to the behavioral recordings.** A: Two cell bodies in the medulla labeled with Calcium Green-1 dextran were selected as ROIs. B: The fluorescence traces of those two ROIs were plotted as  $(F-F_0)/(F_0-F_b)$  for an experiment with a rotating bright stripe. After 5 seconds of darkness, the stripe was turned on but kept stationary for 5 seconds (blue box). Afterwards, the stripe rotated 10 times clockwise around the animal, with a speed of  $60^\circ$  per second (green boxes), resulting in 6 seconds per rotation and 60 seconds for the whole moving stimulus. After the 10<sup>th</sup> rotation, the stripe was turned off but the brain was imaged for another 25 seconds. C: For a better evaluation, the first four repeats of the stimulus were chosen and superimposed for both ROIs on the same time scale. In addition, the mean fluorescence traces for both ROIs over the course of those four repeats was displayed (bold lines). D: Overview of the mean response of the two ROIs (bold lines) of the four repeats from C and the variability (fine lighter lines). Scale bar = 20  $\mu$ m.

To connect the fluorescence response to the self-movement of the animal the data recorded by FicTrac (Fig. 16 and 26A) was plotted against the  $(F-F_0)/(F_0-F_b)$  values of Fig. 25. To this end, the fluorescence values in both ROIs were connected in one plot to the rotation velocity in  $^\circ$  per second and in a second plot to the translational velocity in mm/s (Fig. 26B).

Those plots visualize therefore if the animal performing yaw turns has an influence on the fluorescence. The same is true for the forward movement or translational velocity: the plots would show if there is an obvious correlation between walking forward and the fluorescence values. In this example this is not the case, there is no obvious state dependency. However, it shows that the data collection and analysis established in this project allows for such an investigation which opens many possibilities for future experiments.

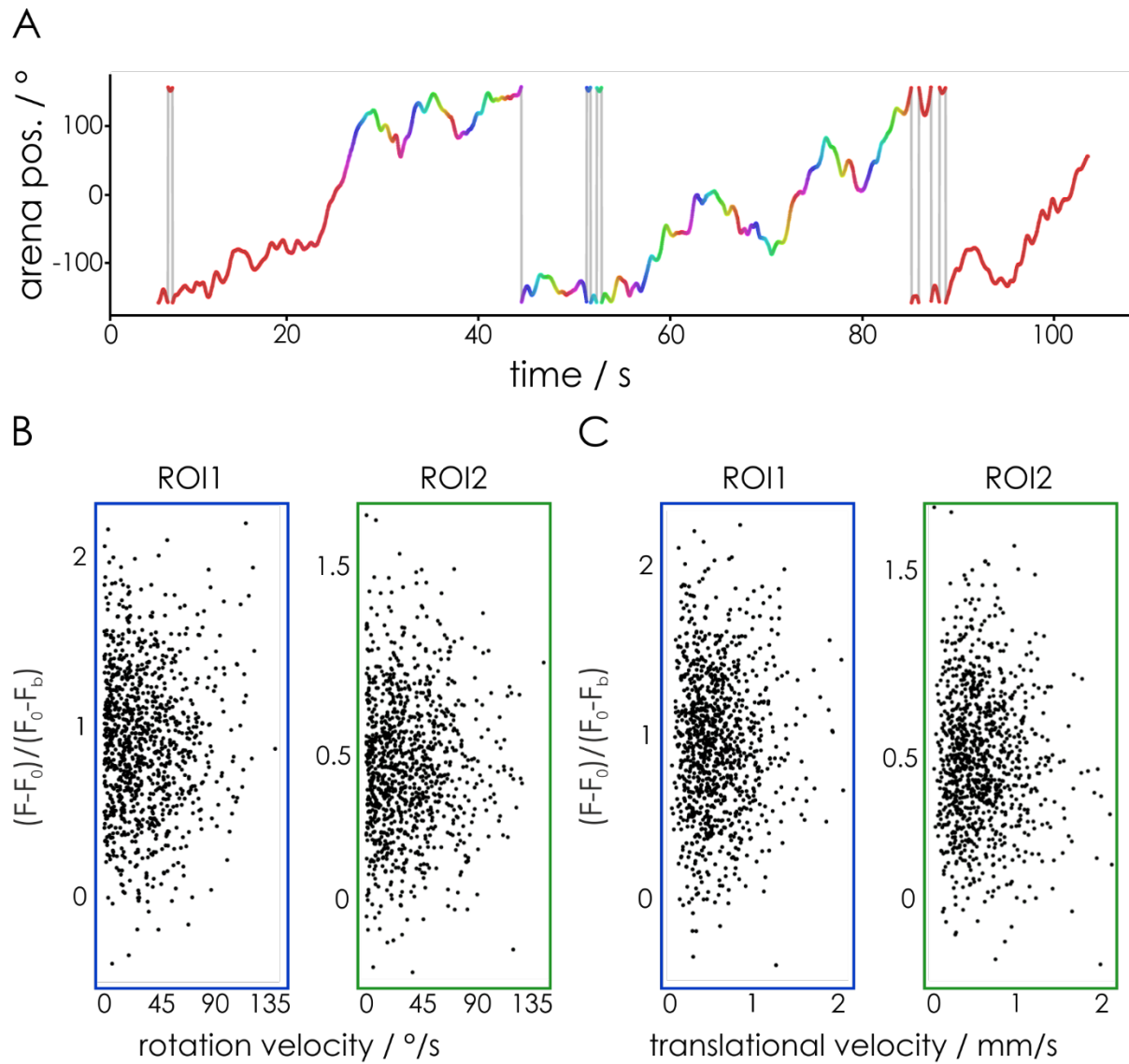


**Fig. 26: Example data set with aligned calcium response to a bright stripe stimulus and walking behavior.** A: The fluorescence traces belong to the experiment with the walking behavior shown in Fig. 16. The color code of the walking trace corresponds to the position of the stripe in the arena (see Fig. 16). B: The  $(F-F_0)/(F_0-F_b)$  values of the two ROIs were aligned and plotted with the walking behavior of the bee during the stimulation. As readout of the movement the rotation velocity in °/s was used (upper row) as well as the translational velocity in mm/s (lower row).

## DISCUSSION AND OUTLOOK

The aim of this project was to establish a new methodological protocol to combine calcium imaging in neurons of the sky-compass network while presenting visual stimuli to tethered animals walking on a treadmill. So far either calcium imaging (e.g. Mota et al., 2011; Mota et al., 2013; Rigosi et al., 2015) or behavioral experiments on a treadmill (e.g. Moore et al., 2014; Taylor et al., 2015; Buatois et al., 2017) were performed in honeybees, therefore an innovative preparation protocol as well as a novel setup in a multiphoton microscope had to be developed. The establishment of the method included many demanding steps and some challenging obstacles had to be overcome during the process. One important step was to find a suitable dye that had to meet several requirements. The calcium indicator had to have a high fluorescence increase upon calcium binding to ensure a detectable signal in living tissue. In addition, the excitation and emission of the fluorophore should ideally be in a longer wavelength range than the light from the LED arena to avoid noise in the emission detection. Using a red-shifted dye has the advantage that it is possible to image structures that are deeper in the brain because scattering and absorption effects of the tissue are reduced with light of a longer wavelength (Kobat et al., 2009). Another important factor is the size of the dye molecules, which had to be small enough for an even distribution throughout the cell. In this project, two calcium indicators were used: the commercially available and well-established Calcium Green-1 dextran and the custom-made innovative JF<sub>549</sub>-BAPTA-MPM ester dye. Calcium Green-1 dextran is with 3,000 MW a rather small indicator molecule allowing an even labeling of neurons. The fluorescence increases ~ 14 fold upon Ca<sup>2+</sup> binding and the compound has a high quantum yield at saturated Ca<sup>2+</sup> ( $\Phi_{\text{sat}} = 0.75$ ). The quantum yield describes the ratio between emitted photons to absorbed photons. The high fluorescence increase and high quantum yield mean that even small amounts of dye deliver strong signals and therefore phototoxicity can be reduced. The  $K_d$  value indicates the calcium amount needed to saturate half of the indicator and therefore the affinity. For Calcium Green-1 dextran the value is ~ 190 nM, meaning the indicator exhibits a high affinity (Paredes et al., 2008). However, one downside is the delivery system into the neurons. Since the potassium salt is cell-impermeant, it had to be introduced physically into the cells by scratching the

membranes with a sharp glass electrode with the attached dye. Depending on the amount of damage done to the cell, this method could have had an influence on the activity and therefore the calcium signal. Therefore, a second dye with a different delivery system was tested. JF<sub>549</sub>-BAPTA-MPM ester is a molecule consisting of a JF<sub>549</sub> fluorophore part, the calcium sensitive BAPTA moiety and MPM esters. These esters mask the molecule in a way that makes it cell-permeant when introduced into the brain and cell-impermeant after ester cleavage inside a neuron. Therefore, the dye only had to be injected into the area of interest and was then taken up by the neurons passively, allowing for the usage of blunt glass electrodes that cause less damage. Unfortunately, since this innovative dye molecule was custom-made for this project and has not been used *in vivo* before, the detailed characterization available for Calcium Green-1 dextran and other commercial indicators does not exist for JF<sub>549</sub>-BAPTA-MPM. However, single components have been tested to some extent, for example, the fluorophore is JF<sub>549</sub> known to be very bright and suitable for live-cell labeling (Grimm et al., 2015). In addition, the calcium sensitivity and brightness of the combination of JF<sub>549</sub> and BAPTA has been tested *in vitro*, revealing a high quantum yield at saturating Ca<sup>2+</sup> ( $\Phi_{\text{sat}} = 0.75$ ). The  $K_d$  value *in vitro* was ~ 310 nM, which is higher than the value of Calcium Green-1 dextran, meaning the Ca<sup>2+</sup> affinity of JF<sub>549</sub>-BAPTA is lower than of Calcium Green-1 dextran. It should be noted though that the  $K_d$  value is highly dependent on factors like pH level and temperature so the *in vivo* affinity could be different. With a ~15 fold fluorescence increase upon Ca<sup>2+</sup> binding the dye showed a high signal strength *in vitro* and together with the superior delivery system into the cells and the slightly longer excitation/emission wavelengths it was an attractive alternative for the project. During the experiments both indicators could be imaged in the areas of interest, thus both were suitable for imaging in the LUC of living honeybees. However, two main technical issues arose during the experiments and the analysis. The imaging data from the custom-built setup in Janelia turned out to contain artefacts from the microscope itself. A vibration of the scan head caused by a faulty ventilation system led to movement artefacts in the imaging data set, which became apparent after the project in Janelia ended and the analysis script was complete. Unfortunately, the movement artefacts led to missing data points, which did not allow for a correction during the analysis. Therefore, those data sets were not used further. In Würzburg a second technical issue arose when the JF<sub>549</sub>-BAPTA-MPM ester

turned out to have some chemical issues. The ester groups of the molecules tend to hydrolyze making them cell-impermeant before injecting them into tissue and thereby useless for calcium imaging in neurons. This probably happened with some vials of dye during shipping from the US to Germany, potentially resulting in poor labeling of the cells (personal communication with Dr. Claire Deo). As a result, JF<sub>549</sub>-BAPTA-MPM ester was only used in the beginning at the Leica setup in Würzburg, after this problem was detected only Calcium Green-1 dextran was used. However, in single trials both indicators showed fluorescence increases upon light stimulation but the yield of convincing imaging data was overall rather low, raising the question why the recordings were often not conclusive. One reason might have been the manual injection that could have resulted in a poor staining or a labeling of the unintended neurons. A considerable amount of honeybees died between injection and experiment or during the trials (see Appendix). The age of the bees could be one reason for the death rate. Only foraging honeybees were used which are the oldest worker bees in a hive and might therefore already exhibit a decreased fitness level. Another explanation could be that the bees were starving coming back from an exhausting foraging trip. By feeding them some sugar water before starting any preparation, it was attempted to avoid that the bees would starve during the long preparation and experiment time. Since the mouthparts were glued as soon as the preparation started, they could only be fed once though and if they would not take up enough, it was possible that they starved during the following hours. The preparation itself was very invasive too, so bees with a lower fitness level might have died due to the procedure. Another reason why many data sets were not analyzed further was the brain movement during imaging. Even though the application of agarose avoided this problem in many preparations, in some cases errors could have hindered a successful execution. For example remaining fluid in the head capsule could prevent the agarose from covering the entire surface of the brain. Pumping movements of the bee during the application could also have caused air pockets that facilitated passive displacement of the brain. Since movements in the  $\mu\text{m}$  range could already cause fluorescence artefacts, data sets from bees that showed obvious motion artifacts during the experiment were often not used further whereas for smaller movements a correction via x/y alignment was made. The last reason why the imaging data did not necessarily deliver the expected results could be the experiment design

itself. One assumption was, that rotating the stripe ten times around the animal would induce the same calcium response in the LUC for all ten rotations resulting in a distinct pattern in the fluorescence trace. The data did however never show such a pattern, not even in trials with only two rotations. The reasons for that could be manifold. For example could one explanation be that the region of interest, the transmedulla neuron projections in the LUC, do not respond to moving patterns as expected. Experiments in the locust sky-compass pathway showed that neurons, sensitive to polarized light, also code for the azimuth of unpolarized UV and green light (Kinoshita et al., 2007; Pfeiffer and Homberg, 2007). However, where exactly the information of the unpolarized light is integrated into the system is unknown. Anatomical investigations in locusts and honeybees suggested that transmedulla neurons are a potential candidate to receive unpolarized light information (el Jundi et al., 2011; Zeller et al., 2015). In addition, immunohistochemical stainings against pigment dispersing factor, serotonin and  $\gamma$ -aminobutyric acid in the bee also suggested that transmedulla neurons might receive neuromodulatory input, inter alia from the circadian clock (Zeller et al., 2015). However, beyond those hypotheses based on anatomical findings, the physiological properties of those transmedulla neurons have not been investigated yet and therefore it is not known if and how they code for moving stripes and other visual stimuli. In addition, phenomena like light adaptation, habituation and state dependency could also have had a considerable effect on the neuronal response. Habituation has been shown for example in neurons of the bumblebee lobula, that responded only to the first light flash of a flash series but not the following ones (Paulk et al., 2008). Since turning all LEDs on, or rotating a stripe multiple times around the animal might also lack the novelty factor, the transmedulla neurons could also habituate and therefore show no response beyond the initial one. Experiments in the fruit fly *Drosophila* showed, that neurons in their vision system showed state dependency, meaning the response frequency and the motion speed sensitivity was higher in walking animals than in stationary ones (Chiappe et al., 2010, Maimon et al., 2010). Even though the experimental setup and analysis of this project allowed to evaluate some aspects of state dependency, there were too few data sets to draw a conclusion on this matter.



Besides the challenging dye delivery into cells and the problems involving the imaging part of the project, several other steps of establishment had to be taken in the second important part, the behavior. First, the whole treadmill system had to be designed and custom-built in cooperation with the workshop of HHMI/Janelia Research Campus according to the size of a bee. In addition, the holder was developed in multiple steps over three prototypes, and fabricated trying out different materials. It had to fulfill three requirements: the bee had to be able to walk, meaning legs and abdomen needed to be moveable, the bee needed to be tethered in a way that allowed for as much coverage of the LED arena in the visual field as possible, and the brain needed to be accessible for the preparation. To track the ball movement and therefore the intended bee movement, a two-camera system was used in Janelia and a one-camera system based on FicTrac was established in Würzburg. Both tracking systems needed additional supporting systems to communicate with the microscopes, which made the data collection and the analysis more elaborate. In addition, the separation of the data acquisition of the imaging and walking part required another supporting system consisting of a trigger and time stamp encoder, to allow for a subsequent data alignment. Incorporating all those different systems in an existing two-photon microscope and run all systems simultaneous was a demanding task, which caused many bugs and added another reason to why the number of complete data sets that were suitable for further analysis is not as high as desired. Finally, the acquired data had to be analyzed in an appropriate fashion. To this end, a cooperation with Dr. Hannah Haberkern (Janelia Research Campus, Jayaraman lab) was established, to develop a new script that was constantly updated and tailored to incorporate the individual data files and execute all needed analysis steps (see Appendix).

All those challenges were overcome over time and in the end the preparation protocol, the handling of all the different parts of one experiment, and the analysis were established. As a result, it was possible to record the calcium response from walking animals while presenting visual stimulation for the first time in honeybees. The aim for the walking part was in the beginning to just measure if the bees are moving at all to be able to draw a conclusion about any type of state dependency. The first striking success was that the bees not only showed robust walking behavior after they

went through the whole injection procedure, some even showed directed behavior, either menotaxis in closed-loop control or an optomotor response in an open-loop setting. During the menotaxis, when they kept the pattern roughly at the same position lateral to them in the arena, they also exhibited small zigzag movements on the ball. One likely explanation for those small movements are the hexapod typical tripod gait where the front- and hind leg on one side are on the ground together with the middle leg of the other side, while the other legs swing forward. In freely walking honeybees, it has been shown that this tripod gait causes small and steady yaw turns of the whole body by just a few degrees (Zhao et al., 2018). Since the bees here were tethered the ball was doing those zigzag movements instead of the whole bee. It is also known that during walking and flying the trajectory of insects consist of straight stretches and fast body turns, called saccades that are preceded by even faster head saccades (Boeddeker et al., 2010; Boeddeker et al., 2015). The straight stretches contribute to the gaze stabilization of the animal during self-motion (Boeddeker et al., 2010). The insects also gain from the translational optic flow during the straight parts depth information of the surrounding scenery. That enables them to deduce the distance to objects from the visual motion parallax (Boeddeker et al., 2010; Geurten et al., 2014). The saccades in between the straight stretches are used to change the direction during flight or walking. Performing those directional changes in fast saccades maximizes the periods of gaze stabilization while minimizing the time the visual system is confronted with rotational optic flow (Boeddeker et al., 2010; Boeddeker et al., 2015). Since the tethered animals in this project were not able to perform head saccades that are independent from body saccades, it is possible that the small zigzag movements were actual head saccades preceding directional changes. However, it is not possible to determine from our recordings if the zigzag movements were performed intentionally or if they were just a product of the tripod gait. To answer this question, future experiments could record the legs of the bees in a higher resolution to allow for a more detailed analysis of the walking pattern.

Taken together, calcium imaging in walking and behaving honeybees while presenting them different visual patterns was successfully established. However, due to manifold problems during the development of the protocol and the setup, the initial questions could not be answered. They included the question how exactly calcium

responses in transmedulla neurons toward visual stimulation with different patterns would look like. Even though some conclusive  $\text{Ca}^{2+}$  responses were recorded, the amount of complete data sets with a stable fluorescence signal was too low to give a generally valid answer to that question (see Table in Appendix). It was furthermore of interest, if the anatomical subcompartmentalization of the LUC corresponds to a functional division, for example a retinotopic map. This question was difficult to investigate though since the span of the LUC made it hard to image the entire structure at once. The addition of walking behavior to the calcium imaging part was implemented to allow for the investigation of state dependency of the neurons based on self-motion of the animal. Even though it was possible in the end to connect the imaging data with the behavioral recording, it was not revealed if state dependency effects are present in transmedulla neurons. After establishing all the single steps, the limited time frame of this project impeded to record more data. Therefore, it would be desirable to continue the project in the future to gain enough data sets to follow up the successful establishment of the method with a complete study to answer the questions above. Especially the stabilization and characterization of the JF<sub>549</sub>-BATPA MPM ester dye should have a high priority here since this dye offers, as mentioned above, some very interesting advantages over the established indicators. In general, the development of calcium indicators and delivery systems is a continuous growing field in biochemistry and could therefore offer even better solutions in the future. Apart from that, the transmedulla neurons are just one possible investigation site that is accessible with this method. By adjusting the preparation slightly, the region of interest could be focused on other parts of the sky-compass pathway like the optic lobes or the protocerebral bridge. The only important factor is here the depth of the structure in the brain, which is currently limited by physical restrictions of the microscope to ~ 250  $\mu\text{m}$ . As described in the preliminary ester tests, cell bodies of Kenyon cells are also well visible and accessible for dye injections with the current protocol. This would allow for physiological characterizations in the mushroom bodies, which would open a whole new field, since these neuropils are known to be an integration site for olfactory and visual cues but also for memory and learning (e.g. Heisenberg, 1998; Plath et al., 2017). Even though physiological investigations via intra- and extracellular recordings (e.g. Homberg, 1984; Strube-Bloss and Rössler, 2018), patch-clamp (Kropf and Rössler, 2018), and calcium imaging (e.g. Szyszka et al., 2008; Haehnel et al., 2009) have been

performed in the mushroom bodies of honeybees before, they lack so far the state dependency aspect of moving animals. Overall, this innovative combination of different methods in the honeybee opens the door for many important and interesting questions, which have been asked so far for either behavioral aspects or for neuronal responses but not in a combined study. Similar experiments as performed here have been conducted in *Drosophila* for the last decade with astonishing and important results for the neuroethology field. The fly community has the advantage of genetic tools that abolish with genetically encoded calcium indicators one huge obstacle to combine calcium imaging with behavior. With this project, a powerful protocol has now been introduced that could help to close this methodical gap and allow to move forward to investigate the unique features that the honeybee offers as a model organism.

## REFERENCES

- Ache, J.M., Polsky, J., Alghailani, S., Parekh, R., Breads, P., Peek, M.Y., Bock, D.D., von Reyn, C.R., Card, G.M. Neural basis for looming size and velocity encoding in the *Drosophila* Giant Fiber escape pathway. *Curr. Biol.* 29, 1073-1081. DOI: 10.1016/j.cub.2019.01.079
- Boeddeker, N., Dittmar, L., Stürzl, W., Egelhaaf, M. 2010. The fine structure of honeybee head and body yaw movements in a homing task. *Proc. Biol. Sci. B.* 277:1899-1906. DOI: 10.1098/rspb.2009.2326
- Boeddeker, N., Mertes, M., Dittmar, L., Egelhaaf, M. 2015. Bumblebee homing: the fine structure of head turning movements. *PLoS One.* 10(9):e0135020. DOI: 10.1371/journal.pone.0135020
- Bolbat, A., Schulz, C. 2017. Recent developments of genetically encoded optical sensors for cell biology. *Biol. Cell.* 109:1-23. DOI: 10.1111/boc.201600040.
- Buatois, A., Pichot, C., Schultheiss, P., Sandoz, J.C., Lazzari, C.R., Chittka, L., Avarguès-Weber, A., Giurfa, M. 2017. Associative visual learning by tethered bees in a controlled visual environment. *Sci. Rep.* 7, 12903. DOI: 10.1038/s41598-017-12631-w
- Cabirol, A., Cope, A.J., Barron, A.B., Devaud, J.M. 2018. Relationship between brain plasticity, learning and foraging performance in honey bees. *PLoS One.* 13:e0196749. DOI: 10.1371/journal.pone.0196749
- Chen, Y., Huang, L.Y.M. 2017. A simple and fast method to image calcium activity of neurons from intact dorsal root ganglia using fluorescent chemical  $\text{Ca}^{2+}$  indicators. *Mol. Pain.* 13: 1744806917748051. DOI: 10.1177/1744806917748051
- Chiappe, M.E., Seelig, J.D., Reiser, M.B., Jayaraman, V. 2010. Walking modulates speed sensitivity in *Drosophila* motion vision. *Curr. Biol.* 20:1470-1475. DOI: 10.1016/j.cub.2010.06.072
- Deo, C., Sheu, S.H., Seo, J., Clapham, D.E., Lavis, L.D. 2019. Isomeric tuning yields bright and targetable red  $\text{Ca}^{2+}$  indicators. *J. Am. Chem. Soc.* 35, 13734-13738. DOI: 10.1021/jacs.9b06092
- el Jundi, B., Pfeiffer, K., Homberg, U. 2011. A distinct layer of the medulla integrates sky compass signals in the brain of an insect. *PLoS One.* 6:e27855. DOI: 10.1371/journal.pone.0027855
- Esch, H.E., Zhang, S., Srinivasan, M.V., Tautz, J. 2001. Honeybee dances communicate distances measured by optic flow. *Nature.* 411, 581-583. DOI: 10.1038/35079072
- Fahrbach, S.E., Moore, D., Capaldi, E.A., Farris, S.M., Robinson, G.E. 1998. Experience-expectant plasticity in the mushroom bodies of the honeybee. *Learn. Mem.* 5:115-123.
- Geurten, B.R.H., Jähde, P., Corthals, K., Göpfert, M.C. 2014. Saccadic body turns in walking *Drosophila*. *Front. Behav. Neurosci.* 8:365. DOI: 10.3389/fnbeh.2014.00365
- Goodman, L.J. 1970. The structure and function of insect dorsal ocellus. In: *Advances in insect physiology*, Volume 7. Academic Press.

Grimm, J.B., English, B.P., Chen, J., Slaughter, J.P., Zhang, Z., Revyakin, A., Patel, R., Macklin, J.J., Normanno, D., Singer, R.H., Lionnet, T., Lavis, L.D. 2015. A general method to improve fluorophores for live-cell and single-molecule microscopy. *Nat. Methods*. 12:244-50. DOI: 10.1038/nmeth.3256.

Groh, C., Lu, Z., Meinertzhagen, I.A., Rössler, W. 2012. Age-related plasticity in the synaptic ultrastructure of neurons in the mushroom body calyx of the adult honeybee *Apis mellifera*. 520:3509-3527. DOI: 10.1002/cne.23102

Haehnel, M., Froese, A., Menzel, R. 2009. *In vivo* Ca<sup>2+</sup>-imaging of mushroom body neurons during olfactory learning in the honey bee. *J. Vis. Exp.* 30:1353. DOI: 10.3791/1353

Heisenberg, M., Wolf, R. 1979. On the fine structure of yaw torque in visual flight orientation of *Drosophila melanogaster*. *J. Comp. Physiol.* 130, 113-130. DOI: 10.1007/BF00611046

Homberg, U. 1984. Processing of antennal information in extrinsic mushroom body neurons of the bee brain. *J. Comp. Physiol. A.* 154:825-836. DOI: 10.1007/BF00610683

Jernigan, C.M., Halby, R., Gerkin, R.C., Sinakevitch, I., Locatelli, F., Smith, B.H. 2020. Experience-dependent tuning of early olfactory processing in the adult honey bee, *Apis mellifera*. *J. Exp. Biol.* 223:jeb206748. DOI: 10.1242/jeb.206748

Kinoshita, M., Pfeiffer, K., Homberg, U. 2007. Spectral properties of identified polarized-light sensitive interneurons in the brain of the desert locust *Schistocerca gregaria*. *J. Exp. Biol.* 210, 1350-1361. DOI: 10.1242/jeb.02744

Kobat, D., Durst, M.E., Nishimura, N., Wong, A.W., Schaffer, C.B., Xu, C. 2009. Deep tissue multiphoton microscopy using longer wavelength excitation. *Opt. Express*. 17:13354-13364. DOI: 10.1364/OE.17.013354

Kraft, P., Evangelista, C., Dacke, M., Labhart, T., Srinivasan, M.V. 2011. Honeybee navigation: following routes using polarized-light cues. *Philos. Trans. R. Soc. B Biol. Sci.* 366:703-308. DOI: 10.1098/rstb.2010.0203

Kropf, J., Rössler, W. 2018. *In-situ* recording of ionic currents in projection neurons and Kenyon cells in the olfactory pathway of the honeybee. *PLoS One*. 13:e0191425. DOI: 10.1371/journal.pone.0191425

Menzel, R., Tison, L., Fischer-Nakai, J., Cheeseman, J., Balbuena, M.S., Chen, X., Landgraf, T., Petrasch, J., Polster, J., Greggers, U. 2019. Guidance of navigating honeybees by learned elongated ground structures. *Front. Behav. Neurosci.* DOI: 10.3389/fnbeh.2018.00322

Moore, R.J.D., Taylor, G., Paulk, A.C., Pearson, T.W.J., van Swinderen, B., Srinivasan, M.V. 2014. FicTrac: A visual method for tracking spherical motion and generating fictive animal paths. *J. Neurosci. Methods*. 225:106-119. DOI: 10.1016/j.jneumeth.2014.01.010

Mota, T., Yamagata, N., Giurfa, M., Gronenberg, W., Sandoz, J.C. 2011. Neural Organization and visual processing in the anterior optic tubercle of the honeybee brain. *J. Neurosci.* 31:11443-11456. DOI: 10.1523/JNEUROSCI.0995-11.2011

- Mota, T., Gronenberg, W., Giurfa, M., Sandoz, J.C. 2013. Chromatic processing in the anterior optic tubercle of the honey bee brain. *J. Neurosci.* 33:4-16. DOI: 10.1523/JNEUROSCI.1412-12.2013
- Paredes, R.M., Etzler, J.C., Watts, L.T., Zheng, W., Lechleiter, J.D. 2008. Chemical calcium indicators. *Methods.* 46:143-151. DOI: 10.1016/j.ymeth.2008.09.025
- Paulk, A.C., Phillips-Portillo, J., Dacks, A.M., Fellous, J.M., Gronenberg, W. 2008. The processing of color, motion, and stimulus timing are anatomically segregated in the bumblebee brain. *J. Neurosci.* 28:6319-6332. DOI: 10.1523/JNEUROSCI.1196-08.2008
- Pfeiffer, K., Homberg, U. 2007. Coding of azimuthal directions via time-compensated combination of celestial compass cues. *Curr. Biol.* 17, 960-965. DOI: 10.1016/j.cub.2007.04.059
- Rigosi, E., Haase, A., Rath, L., Anfora, G., Vallortigara, G., Szyszka, P. 2015. Asymmetric neural coding revealed by *in vivo* calcium imaging in the honey bee brain. *Proc. Soc. B* 282:20142571. DOI: 10.1098/rspb.2014.2571
- Rosner, R., Pegel, U., Homberg, U. 2019. Responses of compass neurons in the locust brain to visual motion and leg activity. *J. Exp. Biol.* 222:jeb196261. DOI: 10.1242/jeb.196261
- Rössler, W., Groh, C. 2012. Plasticity of Synaptic Microcircuits in the Mushroom-Body Calyx of the Honey Bee. In: Galizia C., Eisenhardt D., Giurfa M. (eds) *Honeybee Neurobiology and Behavior*. Springer. DOI: 10.1007/978-94-007-2099-2\_12
- Russell, T. 2011. Imaging calcium signals *in vivo*: a powerful tool in physiology and pharmacology. *Br. J. Pharmacol.* 163:1605-1625. DOI: 10.1111/j.1476-5381.2010.00988.x
- Seelig, J.D., Chiappe, M.E., Lott, G.K., Dutta, A., Osborne, J.E., Reiser, M.B., Jayaraman, V. 2010. Two-photon calcium imaging from head-fixed *Drosophila* during optomotor walking behavior. *Nat. Methods.* 7, 535-540. DOI: 10.1038/nmeth.1468
- Seelig, J.D., Jayaraman, V. 2013. Feature detection and orientation tuning in the *Drosophila* central complex. *Nature.* 503, 263-266. DOI: 10.1038/nature12601
- Seelig, J.D., Jayaraman, V. 2015. Neural dynamics for landmark orientation and angular path integration. *Nature.* 521:186-191. DOI: 10.1038/nature14446
- Strube-Bloss, M., Rössler, W. 2018. Multimodal integration and stimulus categorization in putative mushroom body output neurons of the honeybee. *R. Soc. Open Sci.* 5:171785. DOI: 10.1098/rsos.171785
- Srinivasan, M.V. 2014. Going with the flow: a brief history of the study of the honeybee's navigational "odometer". *J. Comp. Physiol. A.* 200:563-573. DOI: 10.1007/s00359-014-0902-6
- Srinivasan, M.V. 2015. Where paths meet and cross: navigation by path integration in the desert ant and the honeybee. *J. Comp. Physiol. A.* 201, 533-546. DOI: 10.1007/s00359-015-1000-0
- Szyszka, P., Galkin, A., Menzel, R. 2008. Associative and non-associative plasticity in Kenyon cells of the honeybee mushroom body. *Front. Syst. Neurosci.* 2:3. DOI: 10.3389/neuro.06.003.2008



- Taylor, G.J., Paulk, A.C., Pearson, T.W.J., Moore, R.J.D., Stacey, J.A., Ball, D., van Swinderen, B., Srinivasan, M.V. 2015. Insects modify their behaviour depending on the feedback sensor used when walking on a trackball in virtual reality. *J. Exp. Biol.* 218, 3118-3127. DOI: 10.1242/jeb.125617
- Tian, L., Yang, Y., Wysocki, L.M., Arnold, A.C., Hu, A., Ravichandran, B., Sternson, .SM., Looger, L.L., Lavis, L.D. 2012. Selective esterase-ester pair for targeting small molecules with cellular specificity. *Proc. Natl. Acad. Sci.* 109:4756-4761. DOI: 10.1073/pnas.1111943109
- Tsien, R.Y. 1980. New calcium indicators and buffers with high selectivity against magnesium and protons: design, synthesis, and properties of prototype structures. *Biochemistry.* 19:2396-2404. DOI: 10.1021/bi00552a018
- von Frisch, K. 1949. Die Polarisation des Himmelslichtes als orientierender Faktor bei den Tänzen der Bienen. *Experientia* 5, 142–148. DOI:10. 1007/bf02174424
- Wehner, R., Srinivasan, M.V. 2003. Path integration in insects. In: *The Neurobiology of Spatial Behavior*, Oxford University Press. Pp. 9-30. DOI: 10.1093/acprof:oso/9780198515241.003.0001
- Weir, P.T., Dickinson, M.H. 2015. Functional divisions for visual processing in the central brain of flying *Drosophila*. *Proc. Natl. Acad. Sci.* 112:E5523-5532. DOI: 10.1073/pnas.1514415112
- Zeil, J., Kelber, A., Voss, R. 1996. Structure and function of learning flights in ground-nesting bees and wasps. *J. Exp. Biol.* 199:345-252. DOI:
- Zeller, M., Held, M., Bender, J., Berz, A., Heinloth, T., Hellfritz, T., Pfeiffer, K. 2015. Transmedulla neurons in the sky compass network of the honeybee (*Apis mellifera*) are a possible site for circadian input. *PLoS One.* 10:e0143244. DOI: 10.1371/journal.pone.0143244
- Zhao, J.Z., Zhu, F., Yan, S. 2018. Honeybees prefer to steer on a smooth wall with tetrapod gaits. *J. Insect Sci.* 18, 45. DOI: 10.1093/jisesa/iey038

---

## **CHAPTER IV:**

### **ANATOMICAL AND ULTRASTRUCTURAL ANALYSIS OF THE POSTERIOR OPTIC TUBERCLE IN THE LOCUST *SCHISTOCERCA GREGARIA***

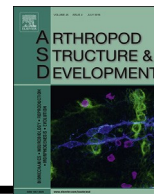
---





Contents lists available at ScienceDirect

## Arthropod Structure &amp; Development

Anatomical and ultrastructural analysis of the posterior optic tubercle in the locust *Schistocerca gregaria*Martina Held<sup>\*, 1</sup>, Kim Le<sup>2</sup>, Uta Pegel<sup>3</sup>, Florian Dersch, M. Jerome Beetz<sup>1</sup>, Keram Pfeiffer<sup>1, 4</sup>, Uwe Homberg<sup>4</sup>

Animal Physiology, Department of Biology &amp; Center for Mind, Brain and Behavior (CMBB), University of Marburg and Justus Liebig University Giessen, Germany

## ARTICLE INFO

## Article history:

Received 27 February  
2020 Received in revised  
form 22 June 2020  
Accepted 3 July  
2020 Available  
online xxx

## Keywords:

Posterior optic  
tubercle Ultrastructure  
Pigment-dispersing hormone  
Spatial orientation  
Time compensation  
*Schistocerca gregaria*

## ABSTRACT

Locusts, like other insects, partly rely on a sun compass mechanism for spatial orientation during seasonal migrations. To serve as a useful guiding cue throughout the day, however, the sun's apparent movement has to be accounted for. In locusts, a neural pathway from the accessory medulla, the circadian pacemaker, via the posterior optic tubercle, to the protocerebral bridge, part of the internal sky compass, has been proposed to mediate the required time compensation. Toward a better understanding of neural connectivities within the posterior optic tubercle, we investigated this neuropil using light and electron microscopy. Based on vesicle content, four types of synaptic profile were distinguished within the posterior optic tubercle. Immunogold labeling showed that pigment-dispersing hormone immuno-reactive neurons from the accessory medulla, containing large dense-core vesicles, have presynaptic terminals in the posterior optic tubercle. Ultrastructural examination of two Neurobiotin-injected tangential neurons of the protocerebral bridge revealed that these neurons are postsynaptic in the posterior optic tubercle. Our data, therefore, support a role of the posterior optic tubercles in mediating circadian input to the insect sky compass.

© 2020 Elsevier Ltd. All rights reserved.

## 1. INTRODUCTION

Insects use, among other sensory information, celestial cues for spatial orientation (Wehner, 1984). The most prominent celestial cue is the sun itself, which is used as reference point throughout the day (von Frisch, 1949; Lindauer, 1959). When the direct view of the sun is blocked, other skylight features like the chromatic gradient (Rossel and Wehner, 1984; el Jundi et al., 2014a) and the polarization pattern of the sky (von Frisch, 1949; von Frisch, 1965; Wehner,

1984; Wehner and Labhart, 2006) can be used to deduce the sun's position. The ability to use polarized light for orientation during walking or flight has been shown in behavioral assays in honeybees (von Frisch, 1949; Evangelista et al., 2014), locusts (Mappes and Homberg, 2004), dung beetles (el Jundi et al., 2014b), monarch butterflies (Merlin et al., 2012), desert ants (Wehner, 2008), houseflies (von Philippsborn and Labhart, 1990), and fruit flies (Weir and Dickinson, 2012; Mathejczyk and Wernet, 2019).

The anatomy and physiology of the underlying neuronal system have been studied most comprehensively in locusts. Two neuronal pathways that carry polarized light information from the compound eye to the central brain have been described: the anterior and posterior sky-compass pathways (Fig. 1A; el Jundi and Homberg, 2010). The angle of polarization is detected by a specialized region of the compound eye, the dorsal rim area (DRA). Photoreceptors of the DRA send axonal projections to dorsal rim areas of the lamina (LADRA) and medulla (MEDRA; Schmeling et al., 2015). From the MEDRA, the anterior sky-compass pathway extends via the lower unit of the anterior optic tubercle (AOTU; Homberg et al., 2003; Pfeiffer et al., 2005) and the bulbs into the central complex (CX; Fig. 1A, blue pathway; Träger et al., 2008).

\* Corresponding author. Department of Behavioral Physiology and Sociobiology (Zoology II), Julius-Maximilians University of Würzburg, Biocenter, Am Hubland, 97074, Würzburg, Germany.

E-mail address: [martina.held@uni-wuerzburg.de](mailto:martina.held@uni-wuerzburg.de) (M. Held).

<sup>1</sup> Present address: Behavioral Physiology and Sociobiology (Zoology II), Julius-Maximilians University of Würzburg, Biocenter, Am Hubland, 97074, Würzburg, Germany.

<sup>2</sup> Present address: Chemosensation, Institute for Biology II, RWTH Aachen University, Germany.

<sup>3</sup> Present address: Department of Biology, Case Western Reserve University, Cleveland, OH, USA.

<sup>4</sup> Shared senior authorship.

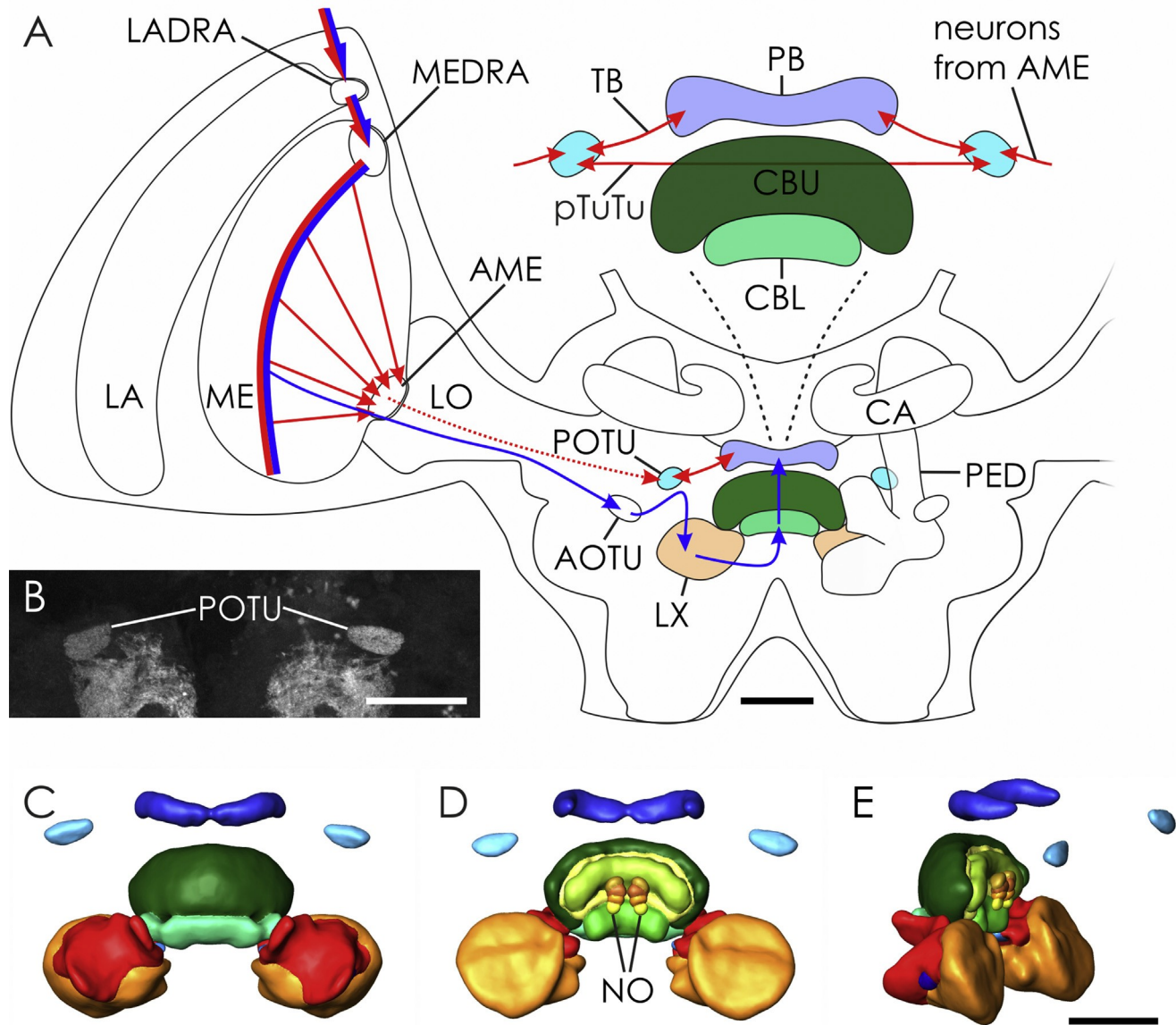


**Fig. 1.** Schematic overview of the locust brain and three-dimensional standardization of the posterior optic tubercle and central complex formation. A: Frontal schematic diagram of a locust brain, showing the anterior sky-compass pathway (blue) and the posterior sky-compass pathway (red) from the optic lobe to the central complex. The expanded diagram shows the connections of the posterior optic tubercles with each other, the protocerebral bridge, and other neuropils. Adapted from [el Jundi and Homberg \(2010\)](#). B: Anti-synapsin labeling in the posterior brain (specimen #9) illustrating the size and shape of the posterior optic tubercles (posterior view of maximum intensity projection). C: Anterior view, D: posterior view, E: posterior-lateral view. AME: accessory medulla, AOTU: anterior optic tubercle, CA: calyx, CBL: lower division of the central body, CBU: upper division of the central body, LA: lamina, LADRA: dorsal rim area of the lamina, LO: lobula, LX: lateral complex, ME: medulla, MEDRA: dorsal rim area of the medulla, NO: noduli, PB: protocerebral bridge, PED: peduncle, POTU: posterior optic tubercle, pTuTu: posterior intertubercle neuron, TB: tangential neuron of the protocerebral bridge. Scale bars = 200  $\mu$ m. (For interpretation of the references to color in this figure legend, the reader is referred to the Web version of this article.)

Evidence for similar pathways exist in dung beetles ([el Jundi et al., 2019](#)), monarch butterflies ([Merlin et al., 2012](#); [Heinze, 2014](#)), fruit flies ([Turner-Evans and Jayaraman, 2016](#); [Sun et al., 2017](#)), honeybees ([Mota et al., 2011](#); [Zeller et al., 2015](#); [Held et al., 2016](#)), and ants ([Grob et al., 2019](#)). The posterior sky-compass pathway has so far received less attention. In locusts, medulla tangential neurons connect the MEDRA with the accessory medulla (AME; [el Jundi and Homberg, 2010](#)). Neurons of the AME project to the posterior optic tubercle (POTU; [Fig. 1A](#), red pathway; [Homberg and Würden, 1997](#); [el Jundi and Homberg, 2010](#)), which is connected to the protocerebral bridge (PB) of the CX (TB neurons) and reciprocally with its contralateral counterpart (pTuTu neurons; [Fig. 1A](#), expanded

diagram; [el Jundi and Homberg, 2010](#); [Beetz et al., 2015](#)). Except for the neurons from the AME to the POTU, that have not been studied physiologically, all described connections are sensitive to the oscillation angle of polarized light ([Heinze and Homberg, 2007](#); [el Jundi and Homberg, 2010](#); [Beetz et al., 2015](#); [Bockhorst and Homberg, 2017](#); [Pegel et al., 2019](#)).

The CX, consisting of the PB, the central body and a pair of noduli, holds a topographic representation of heading directions in the fruit fly ([Seelig and Jayaraman, 2015](#); [Turner-Evans et al., 2017](#); [Kim et al., 2019](#)) and serves as an internal sky-compass for the locust ([Heinze and Homberg, 2007](#); [Pegel et al., 2019](#)). [Beetz et al. \(2015\)](#) proposed that feedback loops between both POTUs and

the PB serve to stabilize the sky compass representation in the locust PB.

Sky compass orientation usually requires a mechanism for time compensation, to constantly adjust the heading direction against the apparent movement of the sun across the sky. Based on evidence from flies and cockroaches that the AME houses the insect circadian clock (Helfrich-Förster et al., 1998), the POTU appears as a strong candidate neuropil for an integration of sky compass and timing information. The AME is connected with the POTU by two types of neuron, small field neurons that specifically connect the AME to the POTU (el Jundi et al., 2010) and wide-field neurons that are immunoreactive with an antiserum against the crustacean peptide pigment-dispersing hormone (PDH; Homberg et al., 1991). Those neurons, commonly termed pigment-dispersing factor (PDF)-neurons, connect the AME to wide areas in the brain including the POTUs and, as shown in flies and cockroaches (Renn et al., 1999; Stengl and Arendt, 2016), provide efferent signals from the internal clock to multiple brain areas. The polarity of TB neurons connecting the POTU and PB has been interpreted controversially. Whereas Heinze and Homberg (2007, 2009) who first described these neurons, reported their terminals as “strongly varicose”, a later study by Beetz et al. (2015) reported EPSPs in intracellular recordings from these neurons near the POTU and concluded that they receive synaptic input in the POTU. Finally, histochemical and immunocytochemical staining of TB neurons was intense (NAPH diaphorase) or weak (serotonin) in the POTU, suggesting that TB neurons may signal bidirectionally between the PB and POTU (Beetz et al., 2015). The present study was aimed at elucidating the synaptic organization and role of the POTU within the AME-PB pathway. Following 3D reconstruction and standardization of the POTU we provide an inventory of its synaptic profiles. Immunogold and preembedding immunoelectron microscopy showed that PDF neurons, assigned to specific synaptic profiles are, indeed, presynaptic whereas two Neurobiotin-labeled TB neurons were postsynaptic in the POTU.

## 2. MATERIALS AND METHODS

### 2.1 Animals

Experiments were performed on sexually mature female and male locusts (*Schistocerca gregaria*). Animals were reared under gregarious conditions at the University of Marburg, Department of Biology, under 12:12 h light:dark (LD) cycles, at 60–70% relative humidity with a temperature of 24 °C at night and 28 °C during the day.

### 2.2 Tissue preparation for standard average POTU and anti-PDH labeling

Brains were dissected from the head capsule and fixed overnight in 4% formaldehyde in 0.1 M phosphate-buffered saline (PBS) at 4 °C. The next day, brains were washed 4 × 15 min in 0.1 M PBS, embedded in gelatin/albumin, and fixed overnight in 4% formaldehyde in 0.1 M phosphate buffer. Brains were then sectioned in frontal plane into 130 µm sections using a vibrating blade microtome (Leica VT 1200S, Leica Microsystems, Wetzlar, Germany). Sections were rinsed 2 × 20 min in 0.1 M PBS with 0.3% Triton X-100 (PBT) and 3 × 20 min in 0.1 M PBS. To block unspecific binding of antibodies, sections were treated overnight at 4 °C with a solution containing 5% normal goat serum (NGS, Dianova, Hamburg, Germany), 0.02% sodium azide and 0.1 M PBS. Sections for the standard average POTU were then incubated for 5 days at 4 °C with a solution containing monoclonal mouse antibodies against the synaptic vesicle protein synapsin (dilution 1:50, SYNORF 1,

provided by Dr. E. Buchner), 1% NGS, and 0.2% Triton X-100 (TrX) in PBS. For immunolabeling of pigment dispersing hormone (PDH), brains were treated the same way but with the addition of a polyclonal rabbit antiserum against PDH (from the crab *Uca pugi-lator*, dilution 1:20 000, #TIM3B3, provided by Dr. H. Dirksen) to the solution. Next, sections were rinsed 2 × 20 min in 0.1 M PBT and 3 × 20 min in 0.1 M PBS. For visualization, sections were then incubated for 3 days at 4 °C with a solution containing goat-anti-mouse antiserum conjugated to Cy5 (dilution: 1:300, Dianova, Hamburg, Germany), 0.02% sodium azide, 1% NGS, and 0.1 M PBT. For anti-PDH staining goat-anti-rabbit antiserum conjugated to Cy2 (dilution 1:300, Dianova, Hamburg, Germany) was added to the solution. Following 5 rinses (2 × 20 min in 0.1 M PBT and 3 × 20 min in 0.1 M PBS), sections were dehydrated in an ascending ethanol series (15 min each, 30%, 50%, 70%, 90%, 95%, 100%), cleared (15 min 100% ethanol/methyl salicylate 1:1; 1 h methyl salicylate), and mounted with Permount (Fisher Scientific, NJ) on microslides. To avoid squeezing of the sections, spacers made from hole reinforcement rings were inserted between the slides and coverslips.

### 2.3 Tissue preparation for transmission electron microscopy

We dissected the brains from the head capsules and fixed them overnight at 4 °C in 2.5% glutaraldehyde and 2% paraformaldehyde in 0.1 M sodium cacodylate buffer (pH 7.2). The next day, the brains were rinsed in 0.1 M sodium cacodylate buffer (pH 7.2) and post-fixed with 1% osmium tetroxide in H<sub>2</sub>O<sub>millipore</sub> for 45–60 min. After dehydrating the brains in an ascending ethanol series, they were embedded in Epon 812 (Sigma-Aldrich Chemie GmbH, Steinheim, Germany). Reference sections (thickness 2 µm) were cut with a glass knife on an LKB Pyramitome (Reichert-Labtech, Wolf-ratshausen, Germany) and stained with methylene blue for light microscopy (Richardson et al., 1960). Ultrathin sections (~70 nm thickness) were cut with a diamond knife (Diatome, Biel, Switzerland) on an ultramicrotome (Ultracut, Reichert-Labtech, Wolf-ratshausen, Germany) and transferred to uncoated copper grids with a 200 × 75 mesh (Plano, Wetzlar, Germany). Sections were contrasted with 1% uranyl acetate and lead citrate (Reynolds, 1963).

### 2.4 Tissue preparation for immunogold labeling

Osmium tetroxide is known to mask antigens due to its high reactivity resulting in poor labeling (Deetz and Behrman, 1981). To compromise between tissue preservation, sufficient contrast, and antigenicity, the fixative was adjusted for brains used for immunogold labeling by reducing the concentration of glutaraldehyde and adding picric acid, leading to a solution containing 2% glutaraldehyde, 2% paraformaldehyde, and 0.1% picric acid in 0.1 M sodium cacodylate buffer. The post-fixation was carried out with only 0.05% osmium tetroxide in H<sub>2</sub>O<sub>millipore</sub> instead of 1% as described before to reduce antigen-masking effects. Embedding in epoxy resin and section preparation was conducted as described before. Instead of uncoated copper grids, coated nickel grids with a 200 × 75 mesh (Plano, Wetzlar, Germany) were used. To reduce unspecific antibody labeling, sections were first treated with 0.1% glycine in 0.01 M phosphate buffered saline (PBS; pH 7.4) and then with 1% bovine serum albumin (BSA) in 0.01 M PBS. Anti-PDH was used as primary antiserum at a concentration of 1:1000. After rinsing the sections with 0.1% BSA in 0.01 M PBS, the secondary antibody, goat anti rabbit IgG (BBI Solutions, Crumlin, United Kingdom) coupled with 10 nm colloidal gold particles, was applied. To fixate the linkage between antibody and epitope of the antigen, sections were treated with 2% glutaraldehyde in 0.01 M PBS.



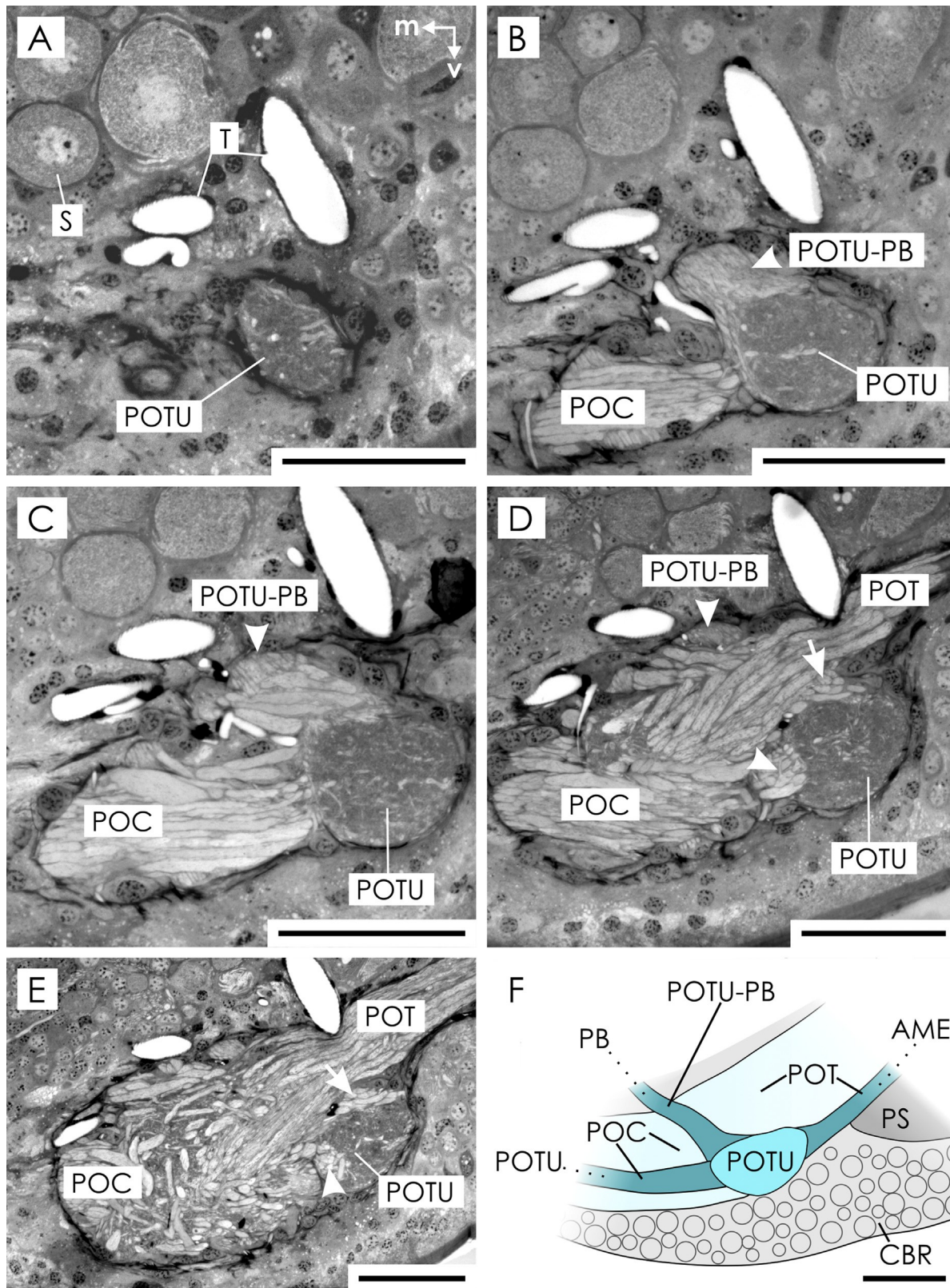


**Fig. 2.** Photomicrographs and reconstructed diagram of semi-thin sections through the posterior optic tubercle (POTU) stained with methylene blue. Semi-thin sectioning of the right hemisphere from posterior reveals the anatomy and position of the POTU as reference for ultra-thin sectioning. A: In the posteriormost section, the outer part of the POTU appears first, surrounded by cell bodies. B: Further anterior, the posterior optic commissure (POC) and the tubercle protocerebral bridge (POTU-PB) tract appear. The POC contains processes of intertubercle neurons (pTuTu neurons) connecting the right and left tubercle, while the POTU-PB tract contains processes of TB neurons that connect the POTU to the protocerebral bridge. C: At a more anterior level, the POC becomes larger. D: Deeper into the brain, the POTU-PB tract becomes smaller. A small bundle of fibers within the POC (white arrowhead) innervates the POTU. Lateral to the POTU fibers of the posterior optic tract (POT) become visible. Some fibers in the POT connect the accessory medulla to the POTU (white arrow). E: At an anterior level, numerous large fibers of the POT/POC bypass the POTU, while processes in distinct fascicles invade the tubercle. Arrow points to fibers of



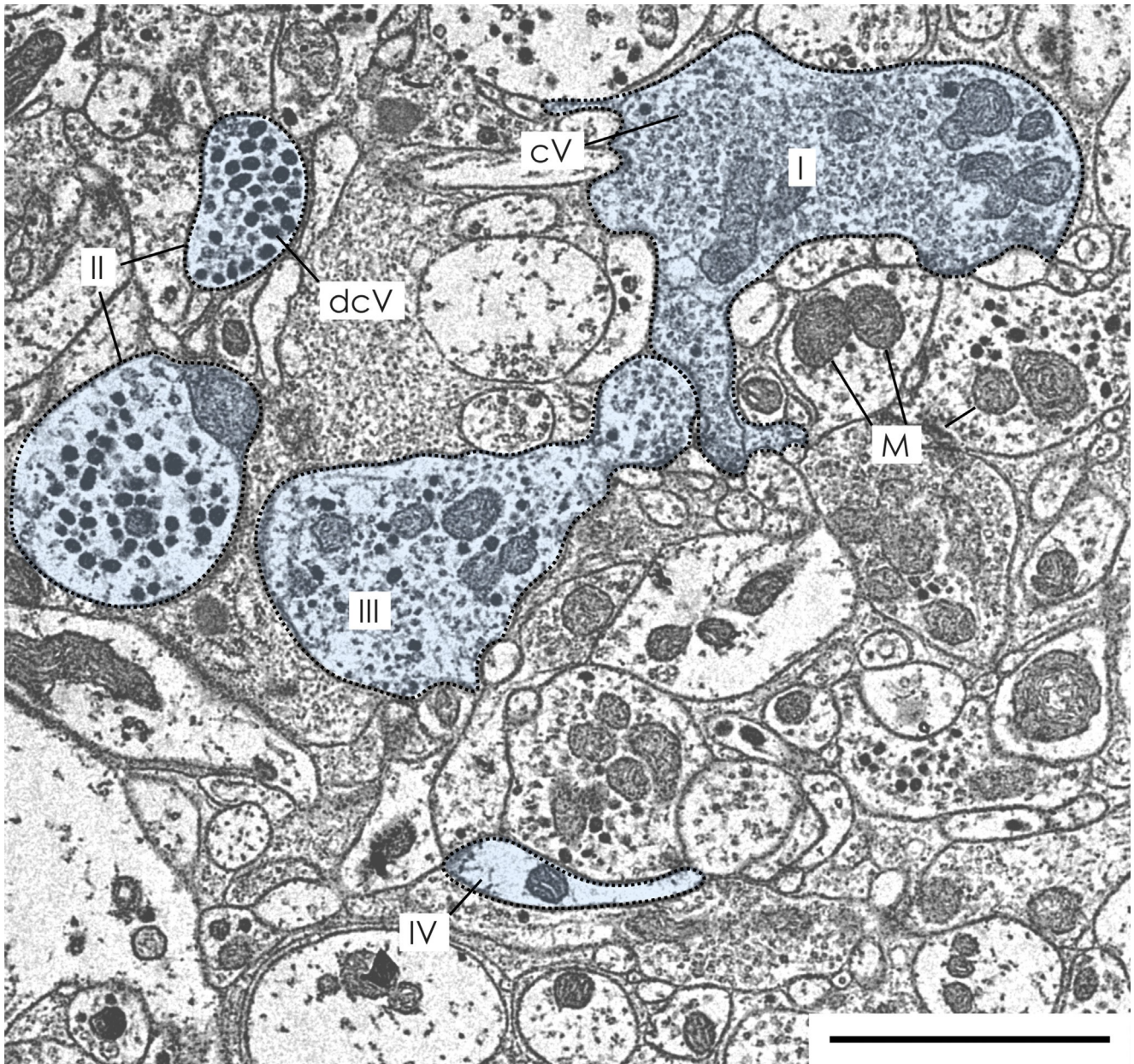


**Fig. 3.** Transmission electron micrograph of synaptic profiles in the posterior optic tubercle. Based on the synaptic vesicle content, four types of profile were identified: Profile type I: many small clear vesicles; profile type II: many large oval dense core vesicles; profile type III: a mixture of small clear vesicles and round dense core vesicles that are smaller than in type II profiles; profile type IV: only a few single clear vesicles and mitochondria, otherwise no organelles. cV: clear vesicle, dcV: dense core vesicle, M: mitochondrion. Scale bar = 2  $\mu$ m.

Contrast enhancement using uranyl acetate and lead citrate was performed as described above.

### 2.5 Tissue preparation for light microscopy combined with electron microscopy

As an additional approach to investigate profile types and the associated neuron types in the POTU, we combined light- and

electron microscopy. The protocol described by [Sun et al. \(1998\)](#) was used as a template and adjusted to our protocols for intracellular recordings in locusts (e.g., [Pegel et al., 2019](#)). Intracellular recordings were performed from two TB1 neurons, connecting the PB and POTU, with glass electrodes filled with 4% Neurobiotin (Vector Laboratories, Burlingame, USA) in 1 M KCl in the tip and 1 M KCl in the shaft. After recording the response of the TB1 neuron to light stimuli, the Neurobiotin mixture was iontophoretically injected

the POT invading the tubercle, white arrowhead indicates a bundle of neurons of the POC that innervate the POTU. F: Diagram reconstructed from semi-thin sections shows the POTU (light blue) and the tracts connecting it to other neuropils. A part of the POC (dark blue) runs towards the contralateral tubercle. The POTU-PB tract connects the POTU with the PB. Lateral to the POTU a fiber fascicle within the POT (dark blue) connects the tubercle to the AME. AME: accessory medulla, CBR: cell body rind, m: medial, PB: protocerebral bridge, POC: posterior optic commissure, POT: posterior optic tract, POTU-PB tract: posterior optic tubercle-protocerebral bridge tract, PS: posterior slope, S: cell soma in the ell body rind: T: trachea, v: ventral. Scale bars = 100  $\mu$ m. (For interpretation of the references to color in this figure legend, the reader is referred to the Web version of this article.)



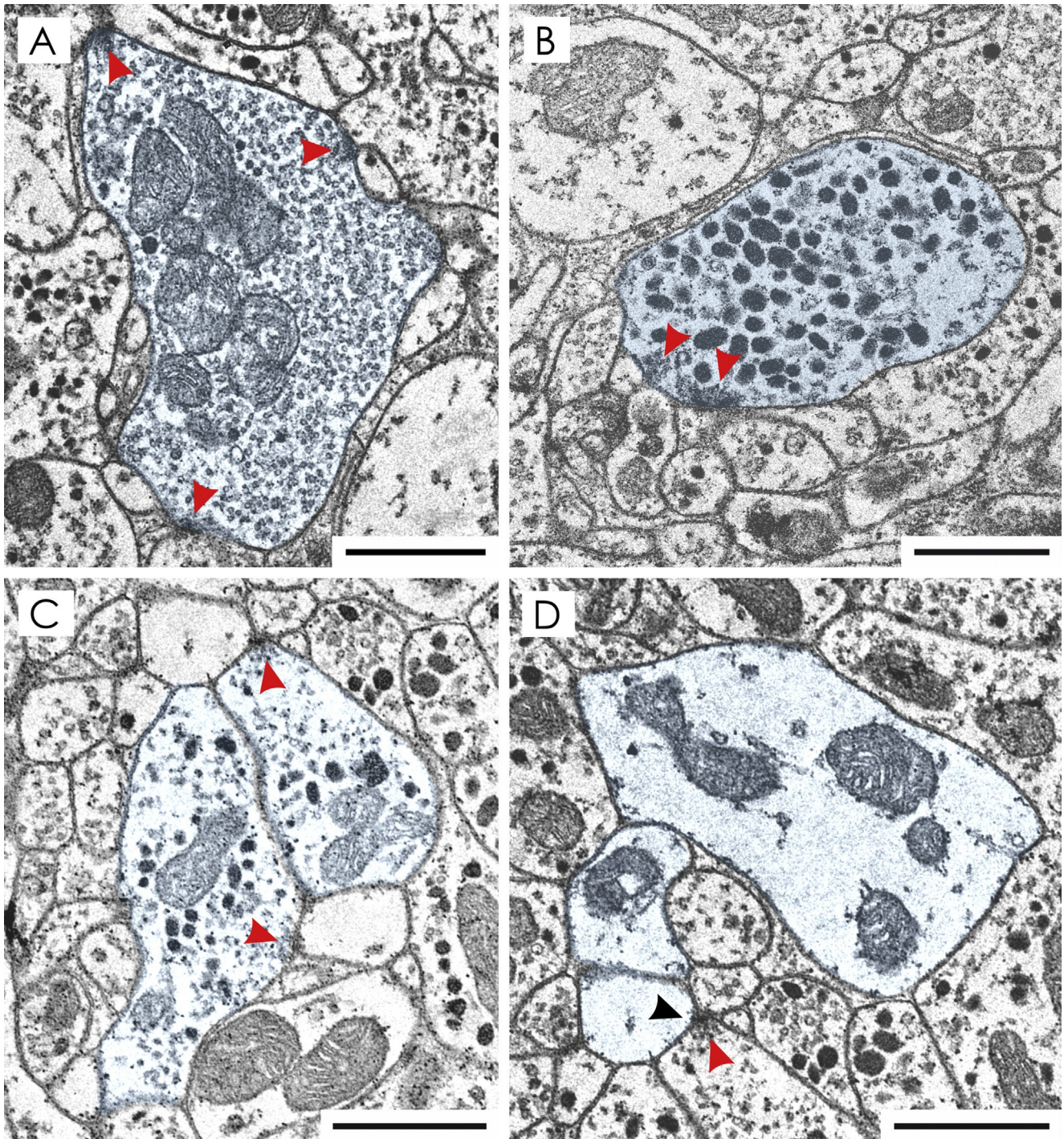


**Fig. 4.** Synaptic polarity of the four profile types in the posterior optic tubercle. A: Type I profile contains many small clear vesicles and some mitochondria. The displayed profile has three synaptic release sites (red arrowheads) showing typical accumulation of vesicles next to a presynaptic membrane thickening. B: Type II profile is defined by many large oval dense core vesicles. Only very few clear vesicles are present, adjacent to the active zones (red arrowheads). The postsynaptic partners in those synapses are profiles of type IV. C: Type III profiles contain small clear vesicles and dense core vesicles that are more round and smaller than the ones in profile type II. Red arrowheads point to two synapses in which profile type III has typical presynaptic vesicle accumulations next to an electron dense membrane thickening. Postsynaptic partners in these cases are type IV profiles. D: Type IV profiles contain a few clear vesicles and mitochondria. One synapse is visible in which profile type IV is postsynaptic (black arrowhead), showing the typical postsynaptic electron dense membrane due to receptors. Red arrowhead  $\frac{1}{4}$  presynaptic side. Scale bars = 1  $\mu$ m. (For interpretation of the references to color in this figure legend, the reader is referred to the Web version of this article.)

into the cell with a positive current of 1 nA. Afterwards the brain was dissected from the head capsule and immersed overnight in Neurobiotin-fixative (4% paraformaldehyde, 0.25% glutaraldehyde, and 0.2% saturated picric acid, in 0.1 M sodium phosphate buffer). After rinsing the brain in sodium phosphate buffer, it was

embedded in 7% low melting point agarose, and 100  $\mu$ m thick slices were made with a vibrating blade microtome (Leica VT1200 S, Leica Microsystems, Wetzlar, Germany). For light microscopy, the slices were incubated overnight with Cy3 conjugated streptavidin (Dianova, Hamburg, Germany) with a concentration of 1:1000 in 0.1 M



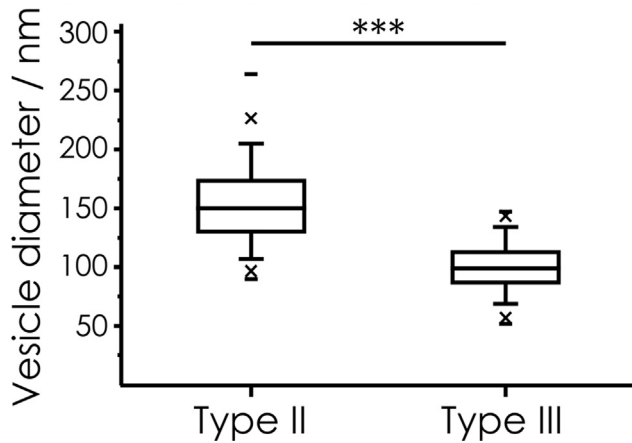


**Fig. 5.** Quantitative comparison of dense core vesicle size in profile type II and III. The maximum diameter of dense core vesicles differs significantly between type II and type III profiles, with type II containing significantly larger vesicles (Mann-Whitney-U-Test,  $p = 0$ ,  $U = 2620.5$ ). Median size for type II vesicles is 149.5 nm and for type III vesicles 99.0 nm. Boxes show 25th and 75th quantile, whiskers denote 5th/95th percentile, x denotes 1st/99th percentile, – denotes minimum and maximum values. Measurements are from  $N = 200$  vesicles in  $n = 10$  profiles (for each profile type).

PBS which binds to the injected Neurobiotin. After rinsing the slices with 0.1 M PBS, they were mounted in 80:20 glycerol/0.1 M PBS on a microscope slide and covered with a coverslip. To investigate the ultrastructure of the stained neuron via electron microscopy, the neuron had to be labeled with electron dense material. To this end, we transferred the slices out of the glycerol/PBS mixture into PBS to rinse them. Afterwards, they were incubated for 18 h in horseradish peroxidase (HRP) conjugated biotin (Life Technologies, Rockford, USA), dissolved 1:200 in 0.1 M PBS. After rinsing the slices in 0.1 M PBS, they were incubated in 0.25% 3,3'-diaminobenzidine tetrahydrochloride (DAB). The addition of 0.01% hydrogen peroxide ( $H_2O_2$ ) resulted in electron dense staining of the Neurobiotin-labeled TB1 neuron. After  $5 \times 10$  min the reaction was stopped by rinsing with 0.1 M PBS, and the slices were post-fixed with 0.5% osmium tetroxide in  $H_2O_{millipore}$ . Afterwards, they were prepared for ultrathin sectioning and electron microscopy as described above.

## 2.6 Microscopy and image processing

For the anti-synapsin and anti-PDH labeled brains, and the fluorescently labeled TB1 neurons, specimens were scanned with a confocal laser scanning microscope (Leica TCS-SP5, Leica Microsystems, Wetzlar, Germany). Fluorophores were excited with an argon laser at a wavelength of 488 nm (Cy2) and HeNe lasers operating at 543 nm (for Cy3) and 633 nm (for Cy5). Image stacks were acquired at 200 Hz with a resolution of  $1024 \times 1024$  pixels in 1 mm steps (neuron) or 2 mm steps (neuropils) in z axis, using a  $10\times$  oil objective (HC PL APO  $10\times / 0.4$  Imm Corr CS). Light microscopic images were obtained with a Zeiss Axioskop (Carl Zeiss, Jena, Germany). Fibers in tracts were counted from sagittal, horizontal, and frontal methylene blue stained 2 mm sections as close as possible to the POTU using a  $40\times$  or  $63\times$  oil immersion objective. For transmission electron microscopy a Jeol JEM-2100 200 kV TEM/FEG microscope (Jeol, Tokyo, Japan) with a  $2k \times 2k$  CCD-camera F214 was used. Electron micrographs were taken with the program EM-Menu 4 (TVIPS, Gauting, Germany). Contrast and brightness of images were adjusted with CorelDRAW2018 (Corel Corporation, Ottawa, Canada). For neuropils, we followed the terminology suggested by Ito et al. (2014) wherever possible. The nomenclature of all mentioned neurons follows earlier accounts (e.g., Pfeiffer and Homberg, 2014).

## 2.7 Analysis of transmission electron micrographs

Synaptic profiles were classified based on presence or absence of the following features: clear vesicles, dense core vesicles, and synaptic release sites. In two types of profile that both contained dense core vesicles but differed in the distribution of clear vesicles we analyzed the size of dense core vesicles. To this end, we randomly chose 10 profiles from randomly chosen micrographs and measured the diameter of 200 randomly chosen vesicles in each of the two profile types. The median for both profile types of all measured values was calculated. The size distributions were statistically tested against each other using the Mann-Whitney-U-Test.

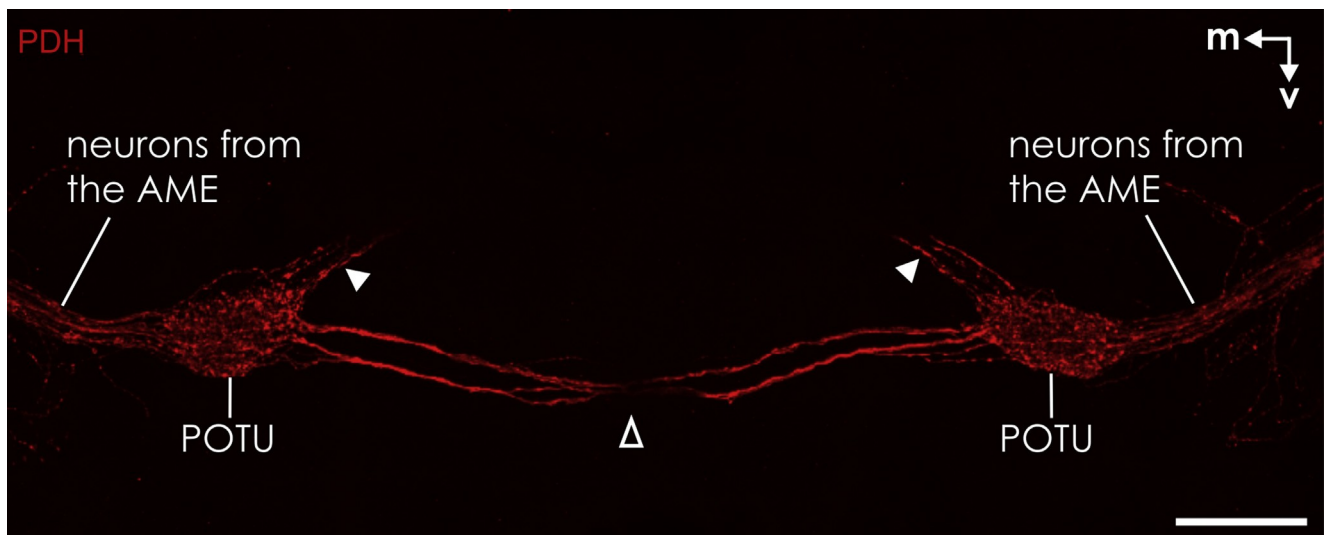


**Fig. 6.** Anti-pigment dispersing hormone (PDH) labeling of neurons innervating the posterior optic tubercles. Maximum intensity projection view of staining with an antiserum against PDH. Processes of neurons from the accessory medulla that invade the posterior optic tubercles, the intertubercle tract (contoured arrowhead), and the posterior optic tubercle-protocerebral bridge tract (filled arrowheads) are labeled. AME: accessory medulla, m: medial, POTU: posterior optic tubercle. Scale bar = 100  $\mu$ m.

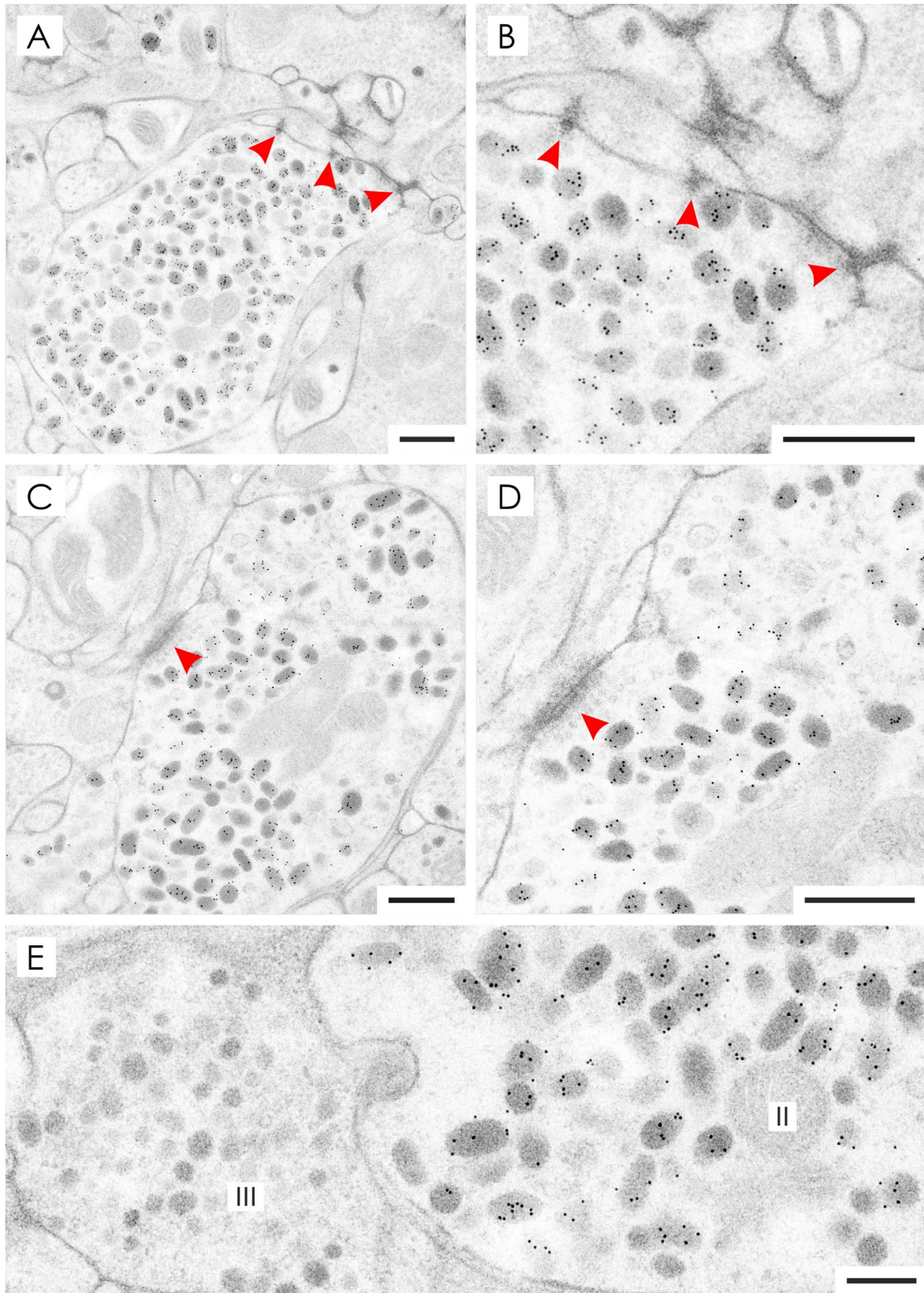


**Fig. 7.** Transmission electron micrographs of immunogold labeling of PDH in the posterior optic tubercle. Gold particles are concentrated on large dense core vesicles in type II profiles. A: A synaptic profile of type II shows many gold particles on the dense core vesicles. Three synapses are visible (red arrowheads). B: Magnified display of A. Profile type II shows presynaptic characteristics in the synaptic connections. C: Another type II profile shows labeling of the dense core vesicles as well. The red arrowhead points to a large active



## 2.8 Calculation of the standard average POTUs

A standard average POTU was calculated from 12 brains, 7 brains from female and 5 from male locusts. Because the volumes of the female and male POTUs were not significantly different (Mann Whitney U test,  $U = 56$ ,  $Z = 0.777918$ ,  $p = 0.436617$ ), all 12 specimens were integrated into the final standard average. All preprocessing of data before the actual standardization was carried out using Amira 5.3.3 (now Thermo Fisher Scientific, RRID:SCR\_007353). In order to be able to integrate the standardized POTUs into the standard CX (el Jundi et al., 2010), it was necessary to integrate both the POTUs and a part of the CX into the scans. We therefore first aligned and merged the scans from serial sections to obtain data stacks that contained both POTUs and the PB. Data stacks were then resampled to a voxel size of  $2 \times 2 \times 2$  mm. Neuropils were segmented using Amira's segmentation editor. In the confocal image stacks, data outside a 10-voxel margin around the neuropils were replaced by black pixels and the remaining data were normalized to cover the full 8-bit range of gray values. The standardization procedure was applied separately to the left and right POTU. Therefore, two data sets were generated, each with one POTU removed. One dataset out of 12 brains was chosen as template. The criteria for the template were: 1. Its volume had to be close to the median of the volumes of all specimens. The median volume of all 24 POTUs from the 12 brains was  $108\,516\,\mu\text{m}^3$  the volumes of the POTUs from the template brain were  $98\,176\,\mu\text{m}^3$  (left hemisphere) and  $121\,088\,\mu\text{m}^3$  (right hemisphere). 2: Its shape and position had to be a typical representation of the population. This was assessed through visual inspection of the 3D-reconstructions of all 12 specimens by two of the authors (KP and FD). It should be noted, that the template strongly influences the overall size of the resulting average, while it has only very minor effects on its shape. We then applied the iterative shape averaging method (ISA) using the computational morphometry toolkit (CMTK, version 3.2.3). For details on the ISA method, see Rohlfing et al. (2003) and Groothuis et al. (2019). Briefly, all datasets were registered onto the template using affine registrations. The average of all registered data stacks and the template served as the template for the subsequent elastic registration, where a 3D grid was applied to the data and grid points were individually moved to achieve the best possible fit between the current specimen and the template. After elastic registration of all data stacks, a new average was computed, which served as the template for the next round of elastic registrations. Each subsequent elastic registration had a finer 3D grid than the previous one. This process was carried out five times in total and the average of the fifth round was the final average. The transformation matrices of each stage (including the affine registration) were saved for each brain and applied to the segmentation data. Finally, a shape-based average was computed from the transformed segmentation data using Euclidean distance maps (Rohlfing and Maurer, 2007).

For the integration of the POTUs into the standard locust CX, the CBU that was segmented together with the POTUs was registered onto the CBU of the standard CX (el Jundi et al., 2010) using an affine registration with 9 degrees of freedom (rotation and translation along/around the x, y, and z axis, scaling of x, y, z axis). Transformation parameters of this registration were then applied to the POTUs.

## 3. RESULTS

We investigated the anatomy and ultrastructure of the POTU in the posterior sky compass pathway (Fig. 1A) of the desert locust *S. gregaria*. To aid future anatomical studies, a three-dimensional average standard of the POTU based on anti-synapsin immunostainings (Fig. 1B) was added to the locust standard brain. At the ultrastructural level, we describe four types of synaptic profile within the POTU based on differences in vesicle content, polarity, and synaptic connectivity patterns. One type of profile could be identified by PDH-immunogold labeling as terminals of neurons that originate in the accessory medulla (Homberg et al., 1991), the circadian pacemaker of insects. Likewise, single cell tracer injection into neurons connecting the POTU to the protocerebral bridge (TB1 neurons) allowed us to show their postsynaptic sites in the POTU ultrastructurally and assign them to one of the profile types.

### 3.1 Anatomy of the posterior optic tubercle

To reconstruct and compare the branching patterns of neurons in the POTU within a common frame of reference, we created a three-dimensional average shape atlas of the POTU based on anti-synapsin immunolabeling (Fig. 1B) of 12 specimens. The median volume of the POTU was  $108\,516\,\text{mm}^3$ . The average shape POTUs were registered into the coordinate frame of the locust standard CX (Fig. 1CeE; el Jundi et al., 2010).

The POTUs are small ovoid neuropils situated at the posterior face of the locust brain about 100 mm lateral, 150 mm posterior and slightly ventral of the protocerebral bridge (Fig. 1C-E). Their lateral extent was  $104\,\mu\text{m}$  (median of 24 POTUs from 12 brains, interquartile range:  $12.6\,\mu\text{m}$ ), and the axis of maximum lateral extent was tilted slightly upward at the medial, pointier side of the neuropil. Their thickness (anterior/posterior) was  $35.4\,\mu\text{m}$  (median of 24 POTUs from 12 brains, interquartile range:  $3.8\,\mu\text{m}$ ). The variability of the shape of individual POTUs can be viewed in Supplemental Fig. S1.

To investigate the internal organization of the POTU, we analyzed series of semi-thin sections stained with methylene blue (Fig. 2). In contrast to other neuropils, the POTU shows no internal compartmentalization in slices and layers. Three neuronal tracts connect the POTU with other brain regions. Except for these tracts, the POTU is largely separated from adjacent tissue by a glial sheath. Posteriorly, it is completely surrounded by cell bodies of the posterior soma rind (Fig. 2A). Neurites of the posterior optic tubercle-protocerebral bridge tract (POTU-PB tract) are the first to appear at a posterior level. The tract extends from the POTU in dorsomedial and anterior direction toward the PB (Fig. 2B) and largely contains fibers of TB1, TB2, and TB3 neurons (von Hadeln et al., 2020). More anteriorly, large fibers of the posterior optic tract which continue as the posterior optic commissure toward the brain midline bypass the tubercle dorsally and cover its anterior face (Fig. 2C-F). Within this large tract, a bundle of fibers in the commissure invades the POTU (Fig. 2D & E). It contains pTuTu neurons that specifically connect the POTUs of both hemispheres (el Jundi and Homberg, 2010). Likewise, a fiber bundle within the posterior optic tract invades the POTU (Fig. 2D-F). Neurons in this fascicle connect the AME with the POTU (el Jundi and Homberg, 2010).

zone. D: Magnified display of C illustrates that the type II profile is presynaptic. E: A type II profile is located adjacent to a profile of type III. Both types contain dense core vesicles. While those in profile type II are larger and oval-shaped, dense core vesicles in profile type III are smaller and rounder. Only the oval-shaped dense core vesicles of profile type II are labeled for PDH while the round ones in profile type III are not labeled. Scale bars =  $500\,\mu\text{m}$ . (For interpretation of the references to color in this figure legend, the reader is referred to the Web version of this article.)

Fiber counts in the three tracts connecting the POTU to other brain areas showed about 35 (32, 37,  $n = 2$ ) small fiber profiles in the POTU-PB tract (diameter  $1.5 - 3 \mu\text{m}$ ), about 16 (12, 20,  $n = 2$ ) large fiber profiles in the POC (diameter  $2 - 7 \mu\text{m}$ ), and about 43 (42, 38, 50) medium size fiber profiles in the POT (diameter  $3 - 4 \mu\text{m}$ ). Fiber profiles smaller than  $1 \mu\text{m}$  could not be resolved, therefore, the total number of fibers in these tracts may be larger.

### 3.2 Ultrastructure

Using transmission electron microscopy, the POTU was structurally well distinguishable from the surrounding tissue that consists mainly of cell bodies, neurites, and tracheae. Fig. 3 shows the general appearance of the POTU in ultrathin sections. It consists of many synaptic profiles, characterized by cell organelles like mitochondria and different types of synaptic vesicles. Based on the appearance of vesicles, we distinguished four different profile types (overview in Fig. 3, blue shaded (All colour indications refer to the web version), I-IV). Type I profiles were densely packed with small clear vesicles and often contained many mitochondria (Fig. 4A). In all sections examined ( $>1000$  images), we only found presynaptic features within synaptic connections of type I profiles, like a thickening of the membrane, in some cases an enlarged synaptic gap, and vesicles concentrated at the presynaptic side of an active zone (Fig. 4A, red arrowheads). Profile type II held many large, often ovoid, dense core vesicles, single clear vesicles adjacent to active zones, and some mitochondria (Fig. 4B). In sections showing synaptic contact sites type II profiles were always the presynaptic partners of type IV profiles (Fig. 4B, red arrowheads). Profile type III contained many clear vesicles and, in addition, dense core vesicles that appeared smaller and rounder than the ones in type II profiles. Because a size difference of dense core vesicles in different profile types could hint at differences in content of neuroactive substances, we quantified and compared the size of the dense core vesicles of profile II and III. We found a median of  $149.5 \text{ nm}$  (maximum vesicle diameter) for vesicles in type II profiles and  $99.0 \text{ nm}$  for vesicles in type III profiles. The vesicle size was significantly different between the two profile types (Mann-Whitney-U-Test,  $p = 0$ ,  $U = 2620.5$ ; Fig. 5). In synaptic connections, profile type III was the presynaptic partner of profile type IV, with mainly clear vesicles accumulated at the active zones (Fig. 4C, red arrowheads). Profile type IV contained only a few mitochondria and some scattered vesicles but appeared “empty” compared to all other profile types. In synaptic connections, this type of profile was always identified as the postsynaptic partner of profile type I, II and III, with electron dense membrane foldings adjacent to a presynaptic active zone but no synaptic vesicles present (Fig. 4D, black arrowhead postsynaptic side, red arrowhead presynaptic side).

### 3.3 Immunogold labeling

To identify the neuronal cell types corresponding to the different types of profile, we used an antiserum against pigment dispersing hormone (PDH), which in insects labels the peptide pigment dispersing factor (Homberg et al., 1991; Rao and Riehm, 1993). In locusts, this antiserum labels neurons from the AME that have processes in the POTU (Fig. 6; Homberg et al., 1991). Labeling was highly specific, with virtually no background and was highly concentrated in the dense core vesicles of type II profiles (Fig. 7). In all sections examined, all profiles of type II were labeled but within those profiles not all vesicles were marked. Numerous immunogold-labeled profiles of type II had synaptic release sites, identifying profile type II as presynaptic in the POTU (Fig. 7AeD, red arrowheads). Like profile type II, type III profiles also contained dense-core vesicles. However, these slightly smaller dense core

vesicles were never labeled by the anti-PDH antiserum, which provides further evidence that type II and type III profiles originate from different neuronal cell types. This is illustrated in Fig. 7E, showing a labeled profile of type II adjacent to a profile of type III.

### 3.4 Combined fluorescence staining with electron microscopy

To further investigate the neuronal identity of profiles in the POTU, we used a combination of fluorescence microscopy and electron microscopy. TB1 neurons connect the POTU with the PB (Fig. 8A, B) and were previously described as part of the CX compass network (Heinze and Homberg, 2007). Electrophysiological data suggest that TB1 neurons are postsynaptic in the POTU (Beetz et al., 2015). We used Neurobiotin filled preparations of two TB1 neurons (Fig. S2). In a first step, Neurobiotin was visualized using streptavidin conjugated to Cy3, to confirm the neuronal cell type. In the second step the Neurobiotin tracer was transformed into an electron dense signal that allowed identification of labeled profiles of the TB1 neurons ultrastructurally (Fig. 8CeE). The stained neurites of the TB1 neurons were located in a neurite bundle close to the POTU (Fig. 8C). Within the POTU, multiple labeled profiles were found. While strong staining of the TB1 neuron profiles precluded the attribution of a profile type to them, most TB1 profiles appeared adjacent to profiles of type III. In some slices, we found characteristics indicating that the stained profile is postsynaptic to profiles of type III (Fig. 8D, E). Those characteristics include a postsynaptic membrane folding in the labeled profile at the active zone as well as vesicle accumulation on the presynaptic side (Fig. 8D, red arrowhead). In one of those labeled profiles, we found a divergent dyad, meaning that a labeled profile is again postsynaptic but together with a second unlabeled profile in the same synaptic connection (Fig. 8E, red arrowhead). We did not find any instances of TB1 neuron appearing as a presynaptic profile. Because profile types I, II and III are presynaptic output profiles, we conclude that the TB1 neuron profiles are of type IV.

## 4. DISCUSSION

At present, it is not known where and how time compensation is integrated into the navigation system of insects. Because the POTU in the brain of the desert locust is connected with the AME, the PB, and the contralateral POTU, it has been hypothesized that this neuropil is the link between the circadian clock and the orientation system (el Jundi and Homberg, 2010). However, it has been an open question how these neurons are connected with each other and how the information flow is directed in the POTU. Our ultrastructural analysis revealed four different types of synaptic profiles that were distinguishable based on synaptic vesicle content. We also investigated the polarity of those profiles in synaptic connections and found that profiles of type I, II, and III were always presynaptic with profiles of type IV as postsynaptic partners. Two neuron types could be assigned to those profiles. Some type IV profiles belonged to TB1 neurons, while all profiles of type II arose from PDH-immunoreactive neurons (Table 1), which, in locusts, have ramifications in the AME (Homberg et al., 1991). The synaptic polarity of these neurons supports earlier hypotheses that the POTU is involved in connecting the circadian clock with the spatial orientation system in locusts.

We investigated the POTU at the light microscopic and ultrastructural level to gain more insights into its neuron types, their vesicle content, synaptic connections, and polarity within this neuropil. The addition of a three-dimensional average shape POTU to the locust standard brain extends the possible use of the locust standard CX platform and allows for further neural network analyses and registration of neuronal cell types that have ramifications



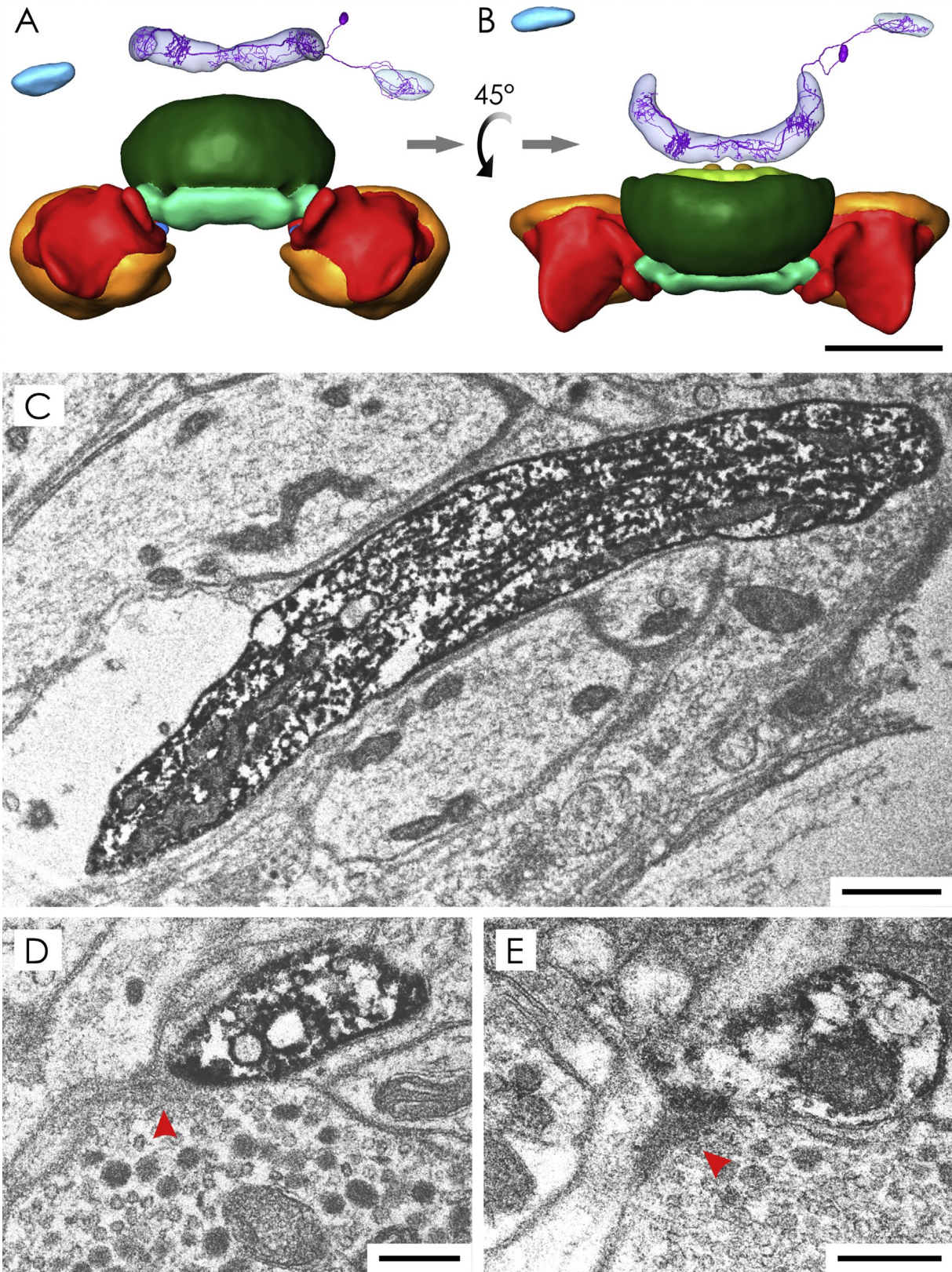


Fig. 8. Three-dimensional reconstruction and transmission electron micrographs of a dye-filled TB1 neuron. A: Frontal view of the central complex showing a three-dimensionally reconstructed TB1 neuron registered into the protocerebral bridge and posterior optic tubercle of the locust standard central complex. The neuron connects the posterior optic tubercle with the protocerebral bridge. In the protocerebral bridge, the neuron has alternating smooth and varicose ramifications, with the varicose ramifications being eight slices apart. B: Same as A tilted horizontally by 45°. C: In an electron micrograph one neurite of a TB1 neuron in a bundle is labeled with electron dense material. D: Labeled profile of the TB1 neuron in the posterior optic tubercle. The profile is postsynaptic to a type III profile. At the active zone (red arrowhead) vesicles are visible at the presynaptic membrane. E: Labeled profile from the second TB1 neuron is postsynaptic to a type III profile. In this synaptic connection the presynaptic side (red arrowhead), indicated by small vesicles and membrane thickening, is connected to two postsynaptic profiles, one labeled and one unlabeled. Scale bar A – B = 200 nm, C = 1 μm, D – E = 300 nm (three-dimensional reconstruction of the TB1 neuron from Beetz et al., 2015). (For interpretation of the references to color in this figure legend, the reader is referred to the Web version of this article.)



**Table 1**

Summary of the ultrastructural findings. dcV: dense core vesicle, PDH-ir: pigment dispersing hormone-immunoreactive.

	Type I	Type II	Type III	Type IV
Polarity	Presynaptic	Presynaptic	Presynaptic	Postsynaptic
Vesicle types	Many clear vesicles	Many large dcV, very few clear vesicles	Clear vesicles & small dcV	Few clear vesicles
Neuron types	TB, pTuTu?	PDH-ir neurons from AME	pTuTu?	TB1, pTuTu?

in the POTU like TB1, TB2 and TB3 neurons (von Hadeln et al., 2020). The series of semi-thin slices confirmed the highly restricted connections of the POTU to the PB, the posterior POTU and the optic lobe but no additional connections to the surrounding posterior slope. Fiber counts provided numbers of larger fibers in the three tracts but could not resolve fibers below diameters of about 1 mm. Nevertheless, the number of about 35 fibers in the POTU-PB tract fits well with the collective number of about 30 serotonin-, Dipallatostatin-, and Mas-allatotropin-immunoreactive neurons in this tract (Beetz et al., 2015). Ultrastructural analysis revealed four different types of synaptic profiles based on vesicle stock. Different neuroactive substances are stored in different types of vesicle. Classical transmitters like acetylcholine or g-aminobutyric acid are present in clear vesicles while neuropeptides like PDH are stocked in dense core vesicles (reviewed by Watson and Schürmann, 2002). In cockroaches, synaptic profiles in the AME contain four different types of dense core vesicles: small, medium, large, and granular ones. Of these, only medium and large vesicles contained PDH (Reischig and Stengl, 1996). We found two types of dense core vesicles in the profiles of the POTU in locusts: larger ones in type II profiles and smaller ones in type III profiles. Immunogold labeling revealed that only the large dense core vesicles in type II profiles were PDH-immunoreactive but not all of them were labeled in one profile. This finding shows that PDH-immunoreactive neurons from the AME provide input to the POTU but beyond that suggests that in type II profiles PDH is co-localized with other transmitters. Candidate neuropeptides are members of the RFamide peptide family that are co-localized with PDH in the locust AME (Würden and Homberg, 1995). RFamide-labeled neurons, like PDH-labeled AME neurons target the POTU.

Light microscopic immunohistochemical studies revealed the presence of allatostatins, allatotropin, and serotonin in TB neurons connecting the POTU and PB (Beetz et al., 2015) and dopamine in the intertubercle pTuTu neurons (Wendt and Homberg, 1992). Unfortunately, immunogold labeling using antisera against these peptides and amines were unsuccessful in our hands. We, therefore, investigated TB1 neurons by transforming Neurobiotin- fluorescence in two TB1 neurons into electron dense material. Both TB1 neurons were postsynaptic in the POTU indicating that they formed type IV profiles. Based on spiking behavior in intra- cellular recordings, Beetz et al. (2015) suggested that some TB1 subtypes receive input in the POTU, which is supported by our data. A third type of neurons of the POTU are pTuTu neurons. At the light- microscopic level, their neuroanatomy suggests that they receive input in the POTU ipsilateral to their soma and provide synaptic output in the contralateral POTU. Therefore, some type IV profiles might correspond to dendritic inputs of pTuTu neurons. Because dopamine, the likely neurotransmitter of pTuTu neurons (Wendt and Homberg, 1992), is usually stored in dense core vesicles (Watson and Schürmann, 2002), their axonal projections might be the type III profiles. Because type III profiles contained dense core vesicles and clear vesicles, it is likely that there is a co-localization with a classical transmitter. These hypotheses suggest that type IV profiles are a heterogeneous group, corresponding to input regions of TB1 and pTuTu neurons.

We could not identify direct connections between PDH-immunoreactive neurons from the AME and TB1 neurons because we did not perform immunogold labeling in a specimen with a labeled TB1 neuron. This could be an interesting step for future experiments aimed at identifying direct cell-to-cell connections. Further studies might reveal the cellular identity of type I and III profiles. Possible candidates are other subtypes of TB neurons that form reciprocal connections between the POTU and the PB (Beetz et al., 2015) or pTuTu neurons connecting both POTUs.

It is likely that integration of time information into the orientation system differs between insect species. While in monarch butterflies the core compass network is very similar to that in the locust (Heinze and Reppert, 2012), the picture is different in the fruit fly *Drosophila melanogaster* and in dung beetles, where POTUs are apparently missing. Nevertheless, *Drosophila* is capable of long- range flights and thus might require a mechanism for time compensation in sun-compass orientation (Jones et al., 1981; Coyne et al., 1982, 1987). The question arises where fruit flies integrate time information into their orientation system (Franconville et al., 2018). A newly discovered set of PDF-expressing clock neurons target the anterior optic tubercle, a neuropil that is two steps up- stream from the CX in the sky compass pathway (Schubert et al., 2018). Time information might be fed via this connection into the sky compass. Another possibility is that *Drosophila* does not use a time-compensated sun compass. Experiments in tethered flight showed that *Drosophila* adjusts flight directions relative to a simulated sun but does not change its heading over time, even after a time gap of several hours (Giraldo et al., 2018). The authors concluded that their data corresponded better to a fixed memory model than a time-compensated model of sun compass orientation. The same could be true for dung beetles that are known for straight-line orientation using a snapshot-based celestial compass (el Jundi et al., 2018) for which time compensation might not be necessary. Future studies might further test those hypotheses and the role of connections by the circadian system.

So far, the most detailed knowledge of the POTU has been acquired in locusts including insights into its ultrastructure and synaptic network provided here. Being a small neuropil with confined connections to only few other brain areas and small number of innervating cell types, the POTU might be ideal for a connectomics analysis that can help to better understand how time compensation in a celestial navigation system works.

## Author statement

**M. Held:** methodology, validation, formal analysis, visualization, writing – original draft, review & editing. **K. Le:** investigation, methodology, validation, writing – review & editing. **U. Pegel, F. Dersch:** investigation, formal analysis, writing – review & editing. **J. Beetz:** validation, formal analysis, writing – review & editing. **K. Pfeiffer:** formal analysis, visualization, writing – review & editing, supervision, validation, resources, funding acquisition. **U. Homberg:** conceptualization, validation, resources, writing – review & editing, supervision, funding acquisition.

## Funding

This work was supported by grant HO 950/24-1 from Deutsche Forschungsgemeinschaft to UH.

## Acknowledgments

We thank Jana Schäfer for initial experiments, Dr. Basil el Jundi for the registration of the TB neuron into the standard brain, Prof. Dr. Andreas Klingl for the introduction into electron microscopy, and Prof. Dr. Uwe Maier for access to his facility. We are grateful to Prof. Dr. Heinrich Dirksen for providing the anti-PDH antiserum, Prof. Dr. Erich Buchner for providing the anti-synapsin antiserum, to Helga Kisselbach-Heckman for assistance with ultrathin sectioning and Martina Kern for maintaining the locust stock.

## Appendix A. Supplementary data

Supplementary data to this article can be found online at <https://doi.org/10.1016/j.asd.2020.100971>.

## REFERENCES

- Beetz, M.J., el Jundi, B., Heinze, S., Homberg, U., 2015. Topographic organization and possible function of the posterior optic tubercles in the brain of the desert locust *Schistocerca gregaria*. *J. Comp. Neurol.* 523, 1589–1607. <https://doi.org/10.1002/cne.23736>.
- Bockhorst, T., Homberg, U., 2017. Interaction of compass sensing and object-motion detection in the locust central complex. *J. Neurophysiol.* 118, 496–506. <https://doi.org/10.1152/jn.00927.2016>.
- Coyne, J.A., Boussy, I.A., Prout, T., Bryant, S.H., Jones, J.S., Moore, J.A., 1982. Long-distance migration of *Drosophila*. *Am. Nat.* 119, 589–595.
- Coyne, J.A., Bryant, S.H., Turelli, M., 1987. Long-distance migration of *Drosophila*. 2. Presence in desolate sites and dispersal near a desert oasis. *Am. Nat.* 129, 847–861.
- Deetz, J.S., Behrman, E.J., 1981. Reaction of osmium reagents with amino acids and proteins. Reactivity of amino acids residues and peptide bond cleavage. *Int. J. Pept. Protein Res.* 4, 495–500. <https://doi.org/10.1111/j.1399-3011.1981.tb02019.x>.
- el Jundi, B., Heinze, S., Lenschow, C., Kurylas, A., Rohlfing, T., Homberg, U., 2010. The locust standard brain: a 3D standard of the central complex as a platform for neural network analysis. *Front. Syst. Neurosci.* 3, 21. <https://doi.org/10.3389/fnro.06.021.2009>.
- el Jundi, B., Homberg, U., 2010. Evidence for the possible existence of a second polarization-vision pathway in the locust brain. *J. Insect Physiol.* 56, 971–979. <https://doi.org/10.1016/j.jinsphys.2010.05.011>.
- el Jundi, B., Pfeiffer, K., Heinze, S., Homberg, U., 2014a. Integration of polarization and chromatic cues in the insect sky compass. *J. Comp. Physiol. A* 200, 575–589. <https://doi.org/10.1007/s00359-014-0890-6>.
- el Jundi, B., Smolka, J., Baird, E., Byrne, M.J., Dacke, M., 2014b. Diurnal dung beetles use the intensity gradient and the polarization pattern of the sky for orientation. *J. Exp. Biol.* 217, 2422–2429. <https://doi.org/10.1242/jeb.101154>.
- el Jundi, B., Warrant, E.J., Pfeiffer, K., Dacke, M., 2018. Neuroarchitecture of the dung beetle central complex. *J. Comp. Neurol.* 526, 2612–2630. <https://doi.org/10.1002/cne.24520>.
- el Jundi, B., Baird, E., Byrne, M., Dacke, M., 2019. The brain behind straight-line orientation in dung beetles. *J. Exp. Biol.* 222, jeb192450. <https://doi.org/10.1242/jeb.192450>.
- Evangelista, C., Kraft, P., Dacke, M., Labhart, T., Srinivasan, M.V., 2014. Honeybee navigation: critically examining the role of the polarization compass. *Philos. Trans. R. Soc. B* 369, 20130037. <https://doi.org/10.1098/rstb.2013.0037>.
- Franconville, R., Beron, C., Jayaraman, V., 2018. Building a functional connectome of the *Drosophila* central complex. *eLife* 7, e37017. <https://doi.org/10.7554/eLife.37017>.
- Giraldo, Y.M., Leitch, K.J., Ros, I.G., Warren, T.L., Weir, P.T., Dickinson, M.H., 2018. Sun navigation requires compass neurons in *Drosophila*. *Curr. Biol.* 28, 2845–2852. <https://doi.org/10.1016/j.cub.2018.07.002>.
- Grob, R., Fleischmann, P., Rössler, W., 2019. Learning to navigate e how desert ants calibrate their compass systems. *Neuroforum* 25, 109–120. <https://doi.org/10.1515/nf-2018-0011>.
- Groothuis, J., Pfeiffer, K., el Jundi, B., Smid, H.M., 2019. The jewel wasp standard brain. Average shape atlas and morphology of the female *Nasonia vitripennis* brain. *Arthropod Struct. Dev.* 51, 41–51. <https://doi.org/10.1016/j.asd.2019.100878>.
- Heinze, S., Homberg, U., 2007. Maplike representation of celestial E-vector orientations in the brain of an insect. *Science* 315, 995–997. <https://doi.org/10.1126/science.1135531>.
- Heinze, S., Homberg, U., 2009. Linking the input to the output: new sets of neurons complement the polarization vision network in the locust central complex. *J. Neurosci.* 29, 4911–4921. <https://doi.org/10.1523/JNEUROSCI.0332-09.2009>.
- Heinze, S., Reppert, S.M., 2012. Anatomical basis of sun compass navigation I: the general layout of the monarch butterfly brain. *J. Comp. Neurol.* 520, 1599–1628. <https://doi.org/10.1002/cne.23054>.
- Heinze, S., 2014. Polarization vision. In: Jaeger, D., Jung, R. (Eds.), *Encyclopedia of Computational Neuroscience*. Springer, New York, pp. 1e30. [https://doi.org/10.1007/978-1-4614-7320-6\\_334-4](https://doi.org/10.1007/978-1-4614-7320-6_334-4).
- Held, M., Berz, A., Hensgen, R., Muenz, T.S., Scholl, C., Rössler, W., Homberg, U., Pfeiffer, K., 2016. Microglomerular synaptic complexes in the sky-compass network of the honeybee connect parallel pathways from the anterior optic tubercle to the central complex. *Front. Behav. Neurosci.* 10, 186. <https://doi.org/10.3389/fnbeh.2016.00186>.
- Helfrich-Förster, C., Stengl, M., Homberg, U., 1998. Organization of the circadian system in insects. *Chronobiol. Int.* 15, 567–594. <https://doi.org/10.3109/07420529808993195>.
- Homberg, U., Würden, S., Dirksen, H., Rao, K.R., 1991. Comparative anatomy of pigment-dispersing hormone-immunoreactive neurons in the brain of orthoptoid insects. *Cell Tissue Res.* 266, 343–357. <https://doi.org/10.1007/BF00318190>.
- Homberg, U., Würden, S., 1997. Movement-sensitive, polarization-sensitive, and light-sensitive neurons of the medulla and accessory medulla of the locust, *Schistocerca gregaria*. *J. Comp. Neurol.* 386, 329–346. [https://doi.org/10.1002/\(SICI\)1096-9861\(19970929\)386:3<329::AID-CNE1>3.0.CO;2-3](https://doi.org/10.1002/(SICI)1096-9861(19970929)386:3<329::AID-CNE1>3.0.CO;2-3).
- Homberg, U., Hofer, S., Pfeiffer, K., Gebhardt, S., 2003. Organization and neural connections of the anterior optic tubercle in the brain of the locust, *Schistocerca gregaria*. *J. Comp. Neurol.* 462, 415–430. <https://doi.org/10.1002/cne.10771>.
- Ito, K., Shinomiya, K., Ito, M., Armstrong, J.D., Boyan, G., Hartenstein, V., Harzsch, S., Heisenberg, M., Homberg, U., Jenett, A., Keshishian, H., Restifo, L.L., Rössler, W., Simpson, J.H., Strausfeld, N.J., Strauss, R., Vossahl, L.B., 2014. A systematic nomenclature for the insect brain. *Neuron* 81, 755–765. <https://doi.org/10.1016/j.neuron.2013.12.017>.
- Jones, J.S., Bryant, S.H., Lewontin, R.C., Moore, J.A., Prout, T., 1981. Gene flow and the geographical distribution of a molecular polymorphism in *Drosophila melanogaster*. *Genetics* 98, 157–178.
- Kim, S.S., Hermundstad, A.M., Romani, S., Abbott, L.F., Jayaraman, V., 2019. Generation of stable heading representations in diverse visual scenes. *Nature* 76, 126–131. <https://doi.org/10.1038/s41586-019-1767-1>.
- Lindauer, M., 1959. Angeborene und erlernte Komponenten in der Sonnenorientierung der Bienen. *Z. Vgl. Physiol.* 42, 43–62.
- Mappes, M., Homberg, U., 2004. Behavioral analysis of polarization vision in tethered flying locusts. *J. Comp. Physiol. A* 190, 61–68. <https://doi.org/10.1007/s00359-003-0473-4>.
- Mathejczyk, T.F., Wernet, M.F., 2019. Heading choices of flying *Drosophila* under changing angles of polarized light. *Sci. Rep.* 9, 16773. <https://doi.org/10.1038/s41598-019-53330-y>.
- Merlin, C., Heinze, S., Reppert, S.M., 2012. Unraveling navigational strategies in migratory insects. *Curr. Opin. Neurobiol.* 22, 353–361. <https://doi.org/10.1016/j.conb.2011.11.009>.
- Mota, T., Yamagata, N., Giurfa, M., Gronenberg, W., Sandoz, J.C., 2011. Neural organization and visual processing in the anterior optic tubercle of the honeybee brain. *J. Neurosci.* 31, 11443–11456. <https://doi.org/10.1523/jneurosci.0995-11.2011>.
- Pegel, U., Pfeiffer, K., Zittrell, F., Scholtyssek, C., Homberg, U., 2019. Two compasses in the central complex of the locust brain. *J. Neurosci.* 39, 3070–3080. <https://doi.org/10.1523/JNEUROSCI.0940-18.2019>.
- Pfeiffer, K., Kinoshita, M., Homberg, U., 2005. Polarization-sensitive and light-sensitive neurons in two parallel pathways passing through the anterior optic tubercle in the locust brain. *J. Neurophysiol.* 94, 3903–3915. <https://doi.org/10.1152/jn.00276.2005>.
- Pfeiffer, K., Homberg, U., 2014. Organization and functional roles of the central complex in the insect brain. *Annu. Rev. Entomol.* 59, 165–184. <https://doi.org/10.1146/annurev-ento-011613-162031>.
- Rao, K.R., Riehm, J.P., 1993. Pigment-dispersing hormones. *Ann. N. Y. Acad. Sci.* 680, 78–88. <https://doi.org/10.1111/j.1749-6632.1993.tb19676.x>.
- Reischig, T., Stengl, M., 1996. Morphology and pigment-dispersing hormone immunocytochemistry of the accessory medulla, the presumptive circadian pacemaker of the cockroach *Leucophaea maderae*: a light- and electron-microscopic study. *Cell Tissue Res.* 285, 305–319. <https://doi.org/10.1007/s004410050648>.
- Renn, S.C., Park, J.H., Rosbash, M., Hall, J.C., Taghert, P.H., 1999. A pdf neuropeptide gene mutation and ablation of PDF neurons each cause severe abnormalities of behavioral circadian rhythms in *Drosophila*. *Cell* 99, 791–802. [https://doi.org/10.1016/s0092-8674\(00\)81676-1](https://doi.org/10.1016/s0092-8674(00)81676-1).
- Reynolds, E.S., 1963. The use of lead citrate at high pH as an electron-opaque stain in electron microscopy. *J. Cell Biol.* 17, 208–213. <https://doi.org/10.1083/jcb.17.1.208>.
- Richardson, K., Jarett, I., Finke, E., 1960. Embedding in epoxy resins for ultrathin sectioning in electron microscopy. *Stain Technol.* 31, 313–323. <https://doi.org/10.3109/10520296009114754>.
- Rohlfing, T., Maurer Jr., C.R., 2003. Nonrigid image registration in shared-memory multiprocessor environments with application to brains, breasts, and bees. *IEEE Trans. Inf. Technol. Biomed.* 7, 16–25. <https://doi.org/10.1109/TITB.2003.808506>.

- Rohlfing, T., Maurer Jr., C.R., 2007. Shape-based averaging. *IEEE T. Image Process.* 16, 153–161. <https://doi.org/10.1109/TIP.2006.884936>.
- Rossel, S., Wehner, R., 1984. Celestial orientation in bees: the use of spectral cues. *J. Comp. Physiol. A* 155, 605–613. <https://doi.org/10.1007/BF00610846>.
- Schmeling, F., Tegtmeier, J., Kinoshita, M., Homberg, U., 2015. Photoreceptor projections and receptive fields in the dorsal rim area and main retina of the locust eye. *J. Comp. Physiol. A* 201, 427–440. <https://doi.org/10.1007/s00359-015-0990-y>.
- Schubert, F.K., Hagedorn, N., Yoshii, T., Helfrich-Förster, C., Rieger, D., 2018. Neuroanatomical details of the lateral neurons of *Drosophila melanogaster* support their functional role in the circadian system. *J. Comp. Neurol.* 526, 1209–1231. <https://doi.org/10.1002/cne.24406>.
- Seelig, J., Jayaraman, V., 2015. Neural dynamics for landmark orientation and angular path integration. *Nature* 521, 186–191. <https://doi.org/10.1038/nature14446>.
- Stengl, M., Arendt, A., 2016. Peptidergic circadian clock circuits in the Madeira cockroach. *Curr. Opin. Neurobiol.* 41, 44–52. <https://doi.org/10.1016/j.conb.2016.07.010>.
- Sun, X.J., Tolbert, L.P., Hildebrand, J.G., Meinertzhagen, I.A., 1998. A rapid method for combined laser scanning confocal microscopic and electron microscopic visualization of biocytin or neurobiotin-labeled neurons. *J. Histochem. Cytochem.* 46, 263–273. <https://doi.org/10.1177/002215549804600216>.
- Sun, Y., Nern, A., Franconville, R., Dana, H., Schreier, E.R., Looger, L.L., Svoboda, K., Kim, D.S., Hermundstad, A.M., Jayaraman, V., 2017. Neural signatures of dynamic stimulus selection in *Drosophila*. *Nat. Neurosci.* 20, 1104–1113. <https://doi.org/10.1038/nn.4581>.
- Träger, U., Wagner, R., Bausenwein, B., Homberg, U., 2008. A novel type of microglomerular synaptic complex in the polarization vision pathway of the locust brain. *J. Comp. Neurol.* 506, 288–300. <https://doi.org/10.1002/cne.21512>.
- Turner-Evans, D., Jayaraman, V., 2016. The insect central complex. *Curr. Biol.* 26, R453–R457. <https://doi.org/10.1016/j.cub.2016.04.006>.
- Turner-Evans, D., Wegener, S., Rouault, H., Franconville, R., Wolff, T., Seelig, J.D., Druckmann, S., Jayaraman, V., 2017. Angular velocity integration in a fly heading circuit. *eLife* 6, e23496. <https://doi.org/10.7554/eLife.23496>.
- von Frisch, K., 1949. Die Polarisation des Himmelslichtes als orientierender Faktor bei den Tänzen der Bienen. *Experientia* 5, 142–148.
- von Frisch, K., 1965. *Tanzsprache und Orientierung der Bienen*. Springer, Berlin.
- von Hadeln, J., Hensgen, R., Bockhorst, T., Rosner, R., Heidach, R., Pegel, U., Quintero-Pérez, M., Homberg, U., 2020. Neuroarchitecture of the central complex of the desert locust: tangential neurons. *J. Comp. Neurol.* 528, 906–934. <https://doi.org/10.1002/cne.24796>.
- von Philippsborn, A., Labhart, T., 1990. A behavioral study of polarization vision in the fly, *Musca domestica*. *J. Comp. Physiol. A* 167, 737–743. <https://doi.org/10.1007/BF00189764>.
- Watson, A.H., Schürmann, F.W., 2002. Synaptic structure, distribution, and circuitry in the central nervous system of the locust and related insects. *Microsc. Res. Tech.* 56, 210–226. <https://doi.org/10.1002/jemt.10031>.
- Wehner, R., 1984. Astronavigation in insects. *Annu. Rev. Entomol.* 29, 277e298.
- Wehner, R., Labhart, T., 2006. Polarization vision. In: Warrant, E.J., Nilsson, D.E. (Eds.), *Invertebrate Vision*. Cambridge University Press, Cambridge, pp. 291–348.
- Wehner, R., 2008. The desert ant's navigational toolkit: procedural rather than positional knowledge. *Navigation* 55, 101–114. <https://doi.org/10.1002/j.2161-4296.2008.tb00421.x>.
- Weir, P.T., Dickinson, M.H., 2012. Flying *Drosophila* orient to sky polarization. *Curr. Biol.* 22, 21–27. <https://doi.org/10.1016/j.cub.2011.11.026>.
- Wendt, B., Homberg, U., 1992. Immunocytochemistry of dopamine in the brain of the locust *Schistocerca gregaria*. *J. Comp. Neurol.* 321, 387–403. <https://doi.org/10.1002/cne.903210307>.
- Würden, S., Homberg, U., 1995. Immunocytochemical mapping of serotonin and neuropeptides in the accessory medulla of the locust, *Schistocerca gregaria*. *J. Comp. Neurol.* 362, 305–319. <https://doi.org/10.1002/cne.903620302>.
- Zeller, M., Held, M., Bender, J., Berz, A., Heinloth, T., Hellfritz, T., Pfeiffer, K., 2015. Transmedulla neurons in the sky compass network of the honeybee (*Apis mellifera*) are a possible site of circadian input. *PLoS One* 10, e0143244. <https://doi.org/10.1371/journal.pone.0143244>.

## APPENDIX

### PROTOCOL CALCIUM IMAGING

1. Catch bee:
  - Catch a worker bee at the hive entrance with a “*Drosophila*” vial
2. Cooling:
  - Cool the animal in the fridge or on ice until immobilization
3. Tethering:
  - Tether the bee with UV curable glue (Perfomic Pen midget, Conrad Electronic SE, Hirschau, Germany) to the holder with the head sticking slightly through the hole; glue the head with a small amount of glue to the edge of the hole
  - Leave the tips of antennae free of the otherwise the bees will show less walking behavior
  - Glue the wings and the thorax to the bridge next to the hole
  - Apply some glue on the mouthparts but keep eyes, abdomen and legs as free from glue as possible

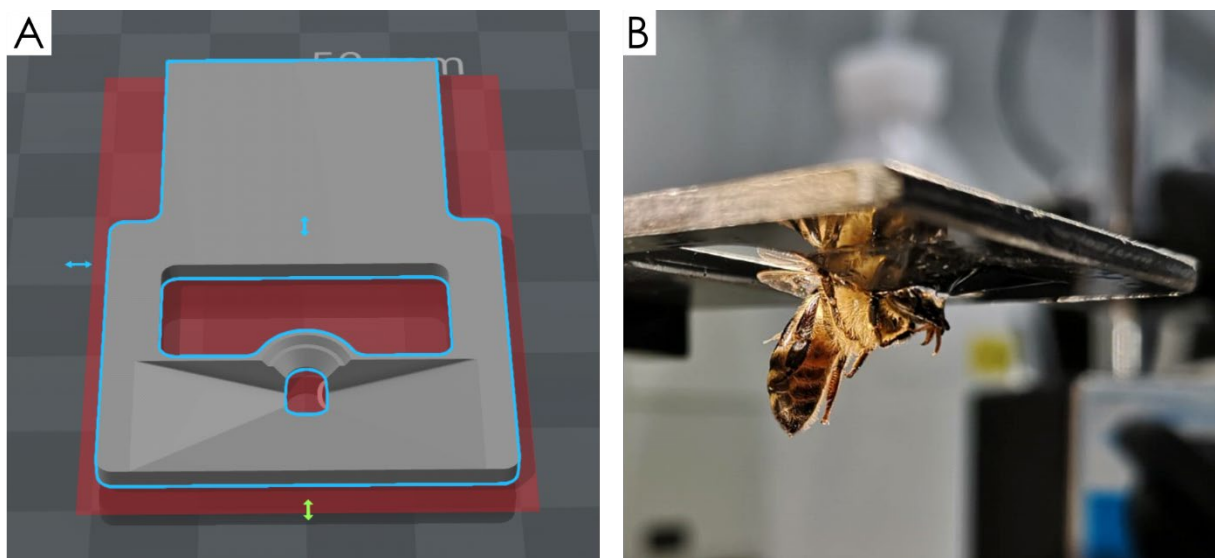


**Fig. S1:** Bee holder and tethering position of the bee to the holder.

4. Preparation:
  - Cut a window through the hole in the cuticle of the head. Remove air sacs, fat bodies, salivary glands and neural sheaths
  - Add bee Ringer's saline if necessary to keep the brain moist
5. Calciumindicator injection:
  - For the injections, pull with a Flaming/Brown puller (P97, Sutter instrument, Novato, CA, USA) glass microelectrodes from borosilicate capillary tubes (outer diameter 1.5 mm, inner diameter 0.86 mm; Sutter Instrument, Novato, CA, USA).
  - a. Calcium Green-1 dextran: If Calcium Green-1 dextran is used break the tip of the electrode off and insert it into petroleum jelly which allows you to pick up small dye crystals. Pick up a few crystals with the electrode tip. Remove all

fluids from the head capsule and pierce the handheld electrode shortly into the target region. Remove excess dye by rinsing with bee's saline. Keep the bees in a dark moist chamber for 2 – 3 hours to allow for complete dye uptake into the cells.

- b. JF<sub>549</sub>-BAPTA MPM ester dye: To use the JF<sub>549</sub>-BAPTA MPM ester dye, mix 20% Pluronic F127 with DMSO by heating the mixture to 40°C for 20 minutes. This mixture can be stored at room temperature and re-used until crystals are visible in the vial. Add 4 µl of this mixture to the vial with the dye and place it in an ultrasonic bath for 20 minutes to dissolve the dye crystals. Afterwards, add 35 µl bee Ringer's solution and mix further on a shaker. For the final solution, combine 10 µl of this solution with 3.5 µl of fluid rhodamine B stock. Transfer 2.5 µl of the final solution into the microelectrode. Place the electrode with a micromanipulator into the target area of the brain and inject the dye using short pulses over several minutes with a pressure injection system (Pneumatic PicoPump PV820, WPI, Sarasota, FL, USA). Rinse the brain with bee Ringer's saline and place the bee for 2 hours in a dark moist chamber.

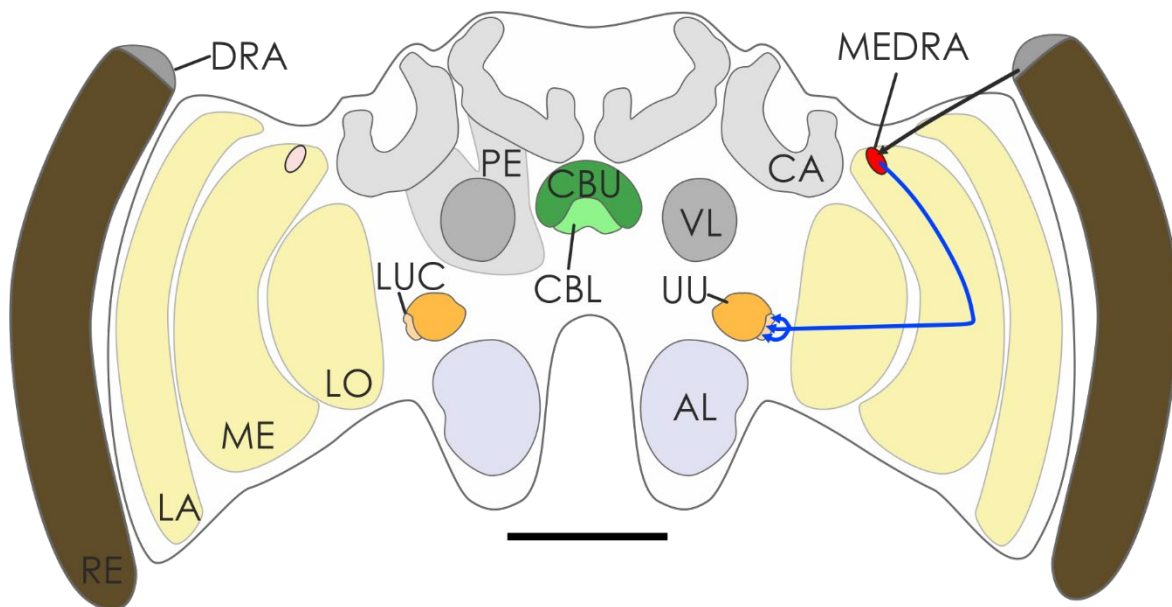


**Fig. S2:** Schematic drawing of the bee brain with the red neuropil (MEDRA) indicating the target area and the blue path outlining the targeted Transmedulla neurons.

#### 6. Preparation of the Setup:

- If necessary exchange objective revolver with the × 25 objective
- Install LED arena in the setup
- Install camera in the setup.

#### 7. Positioning in Setup:

- Attach the holder with the tethered bee to the micromanipulator in the setup and then position the bee on top of the ball; make sure the distance between ball and bee body is high enough for her to move her legs freely but not too high since this could cause movement artefacts



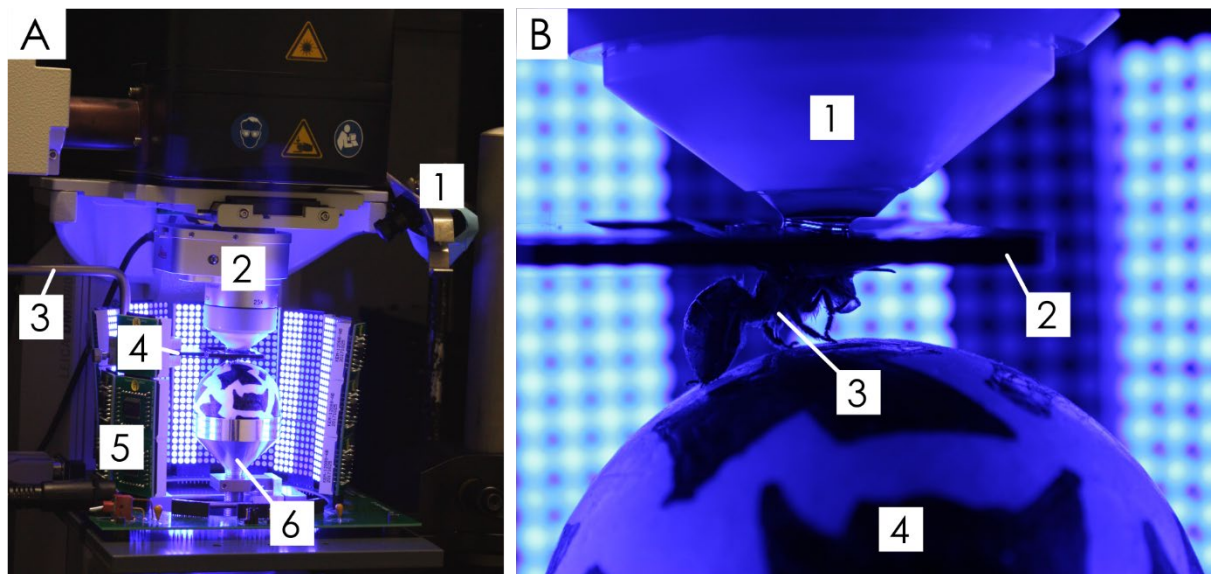


**Fig. S3:** Setup and positioning of bee on the ball. A: 1: camera to record ball movements, 2: objective, 3: micromanipulator arm to position holder/bee, 4: bee holder that is attached to the micromanipulator arm, 5: LED arena (panels removed for picture), 6: Styrofoam ball holder that guides the air flow to support the ball. B: 1: objective, 2: bee holder with saline reservoir, 4: honeybee, 4: Styrofoam ball.

#### 8. Preparation FicTrac System:

- Start Linux laptop and log in
- Open terminal (F12)
- Position IR LEDs underneath the arena to get in the camera an even illumination of the ball
- Type "qv4l2 -device=X" with X being the port of the camera (0 or 1) to open camera program to check for position and illumination of the ball
- Calibrate the FicTrac software to the ball position by entering "../bin/configGui" into the terminal and follow the instructions
- Set path in terminal by entering "cd fictrac" and then "cd FicTrac/Martina"

#### 9. Preparation Leica System:

Switch on the setup in the following order:

- Workstation and wait until the PC has booted
- HyD supply unit (if needed)
- Microscope electronics box
- Fluorescence Lamp (if needed)
- CSU box: scanner button, laser power button, turn laser key
- STP box 8000
- Start Leica Application Suite X (LAS X) program
- Select desired settings (e.g. resonant scanner)



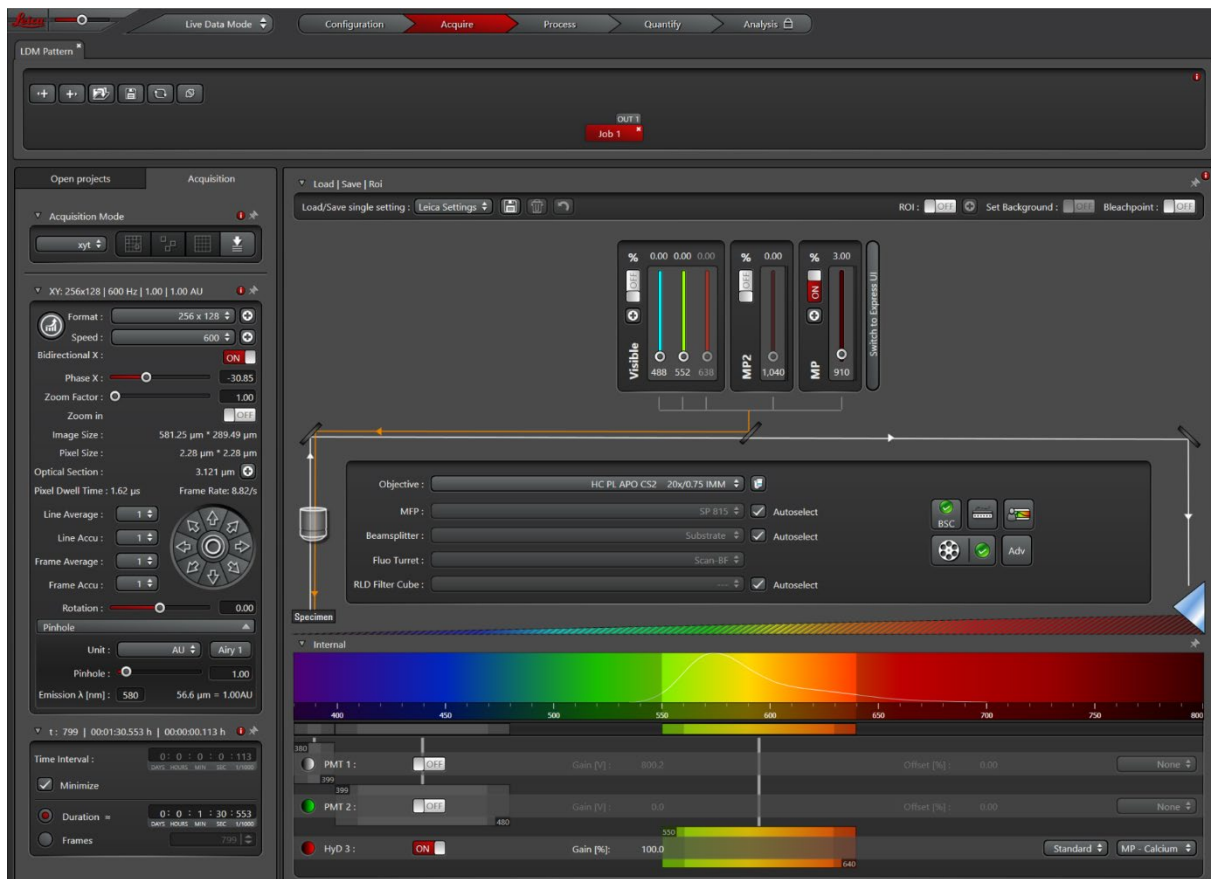


**Fig. S4:** Overview Leica Application Suite X (LAS X) program.

- Change mode to "Live Data Mode"
- Select xyt or xyzt as acquisition mode

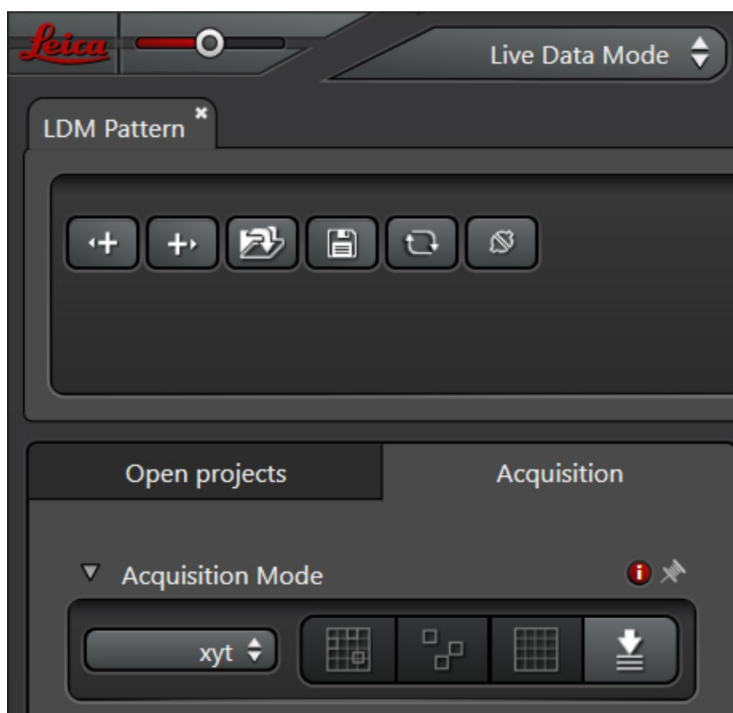


**Fig. S5:** Acquisition mode set to "Live Data Mode" and "xyt" scan.

- Select needed lasers in "Configuration"
- Tune MP laser to desired wavelength

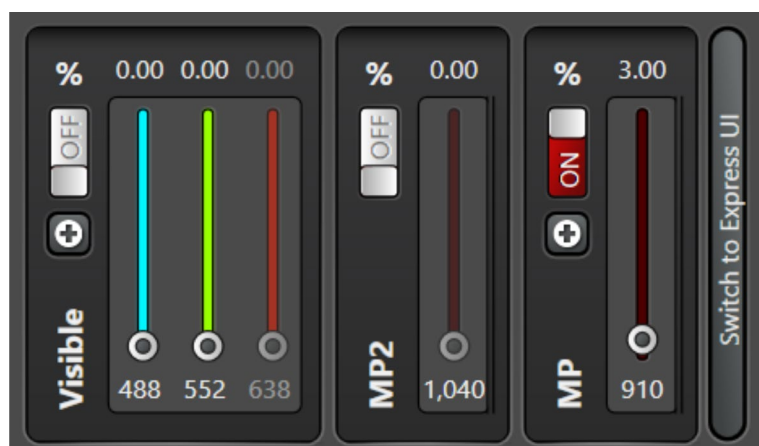


**Fig. S6:** Example setting for the JF<sub>549</sub>-BAPTA-MPM indicator with the multiphoton laser tuned to 910 nm at 3% power.

- Tune detectors (PMT or HyD) to desired detection wavelength window

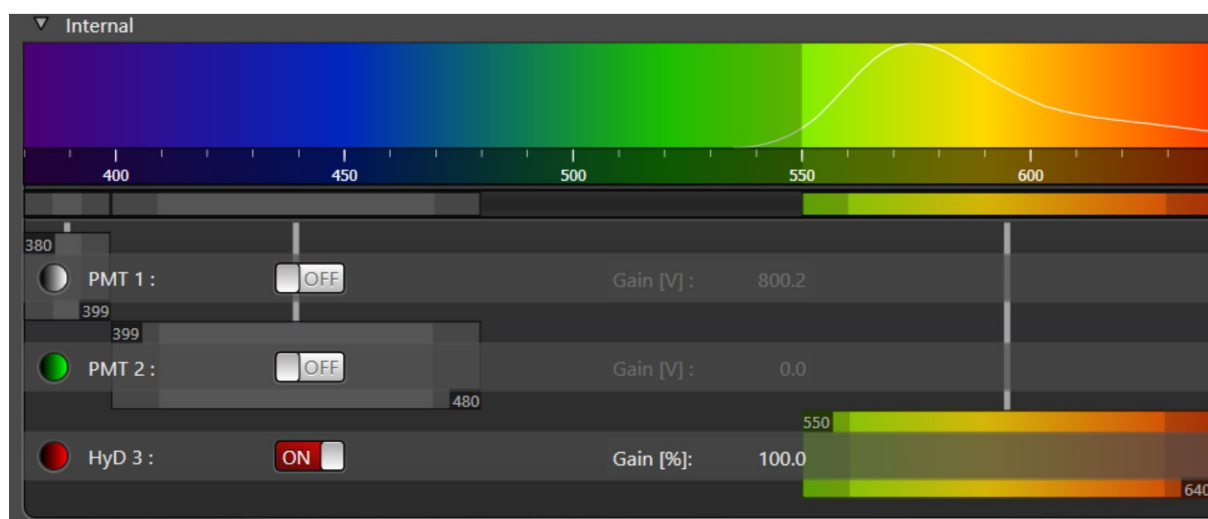


**Fig. S7:** Example setting of the internal HyD detector for the JF<sub>549</sub>-BAPTA-MPM indicator (emission peak at 571 nm) with a detection range of 550 – 640 nm.

- Set trigger to "Output 1" and "every frame"

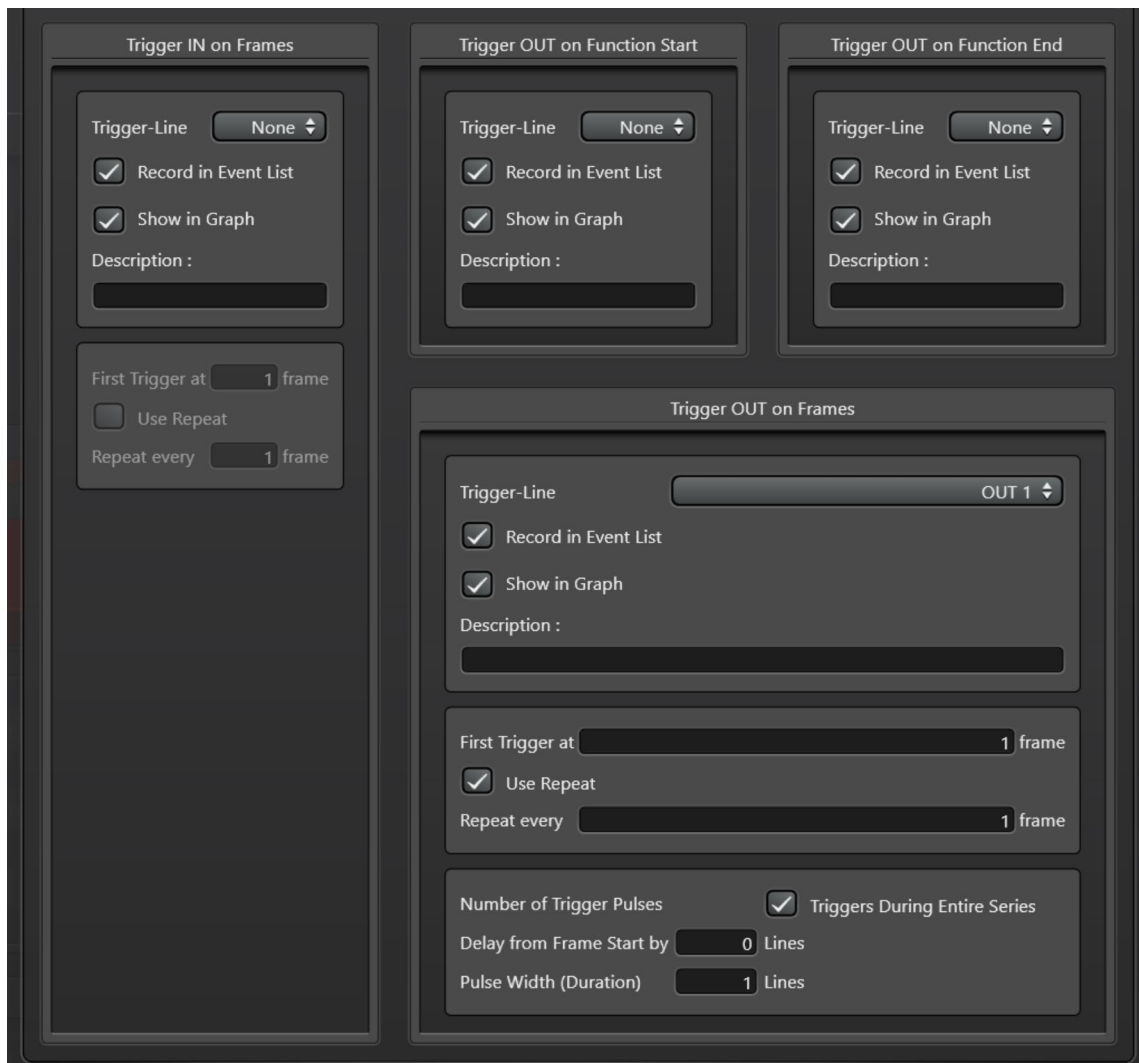


**Fig. S8:** Trigger setting window with trigger out set to output slot 1, with a trigger pulse for every frame, beginning with the first one.

#### 10. Preparation LED arena and arena controller

- Turn on laptop (Thinkpad)
- Start Arduino program
- Start Matlab
- Turn on power supply for LED arena and LED arena itself
- Turn on controller

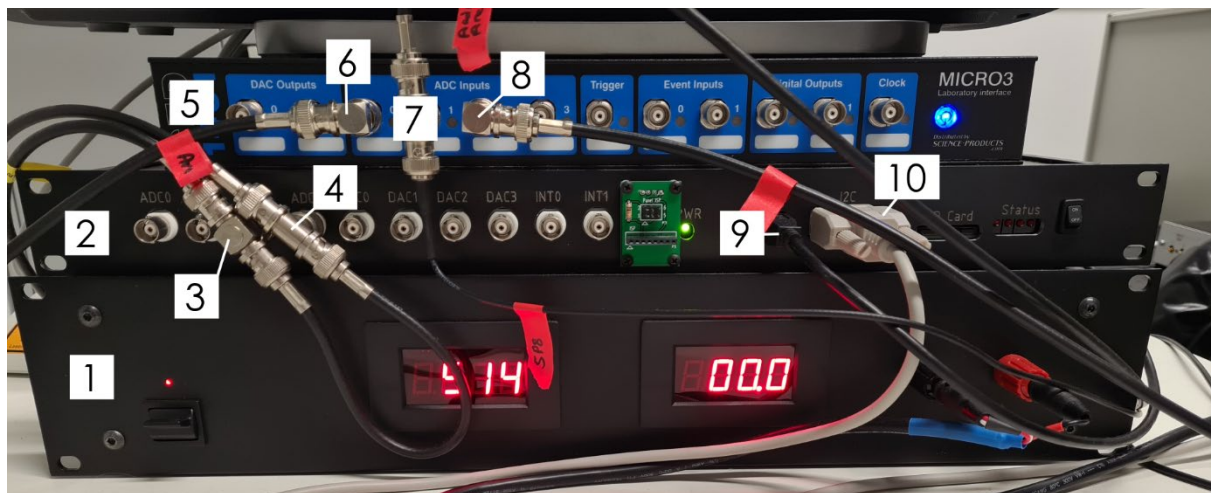


**Fig. S9:** 1: Arena panels power supply unit, 2: Panels display controller unit, 3: Arena controller signal to Arena Arduino, 4: Arena Controller signal output, 5: CED 1401 Micro 3 data acquisition board (previously Axon CNS DigiData), 6: Arena signal input, 7: Input Arduino from Arena and Arduino from FicTrac software, 8: Input SP8, 9: USB connection to Laptop, 10: Connection to arena board

- Turn on CED bard (previously Axon CNS DigiData)
- Start AxoScope software
- Run in Matlab "PControl" script
- Select pattern
- Open in Arduino the latest "Reiser\_arena" script
- The first part defines the input and output pins

Reiser\_arena\_10\_MH | Arduino 1.8.9

Datei Bearbeiten Sketch Werkzeuge Hilfe

```

Reiser_arena_10_MH

int clockPin = 4;           //yellow
int dataPin = 5;            //red
int latchPin = 6;           //green

int command;                //command read from serial input
int numrot = 3;              //number of times a stimulus motion is carried out.
int FromMicroscopePin = 2;   //TTL in pin

void setup() {

    //define digital pins
    pinMode(latchPin, OUTPUT);
    pinMode(dataPin, OUTPUT);
    pinMode(clockPin, OUTPUT);
    pinMode(FromMicroscopePin, INPUT);

    dacout(0);                //set DAC output to 0 V

    Serial.begin(115200);      //Create Serial Object
    Serial.println("Ready \n");
}

```

- In the next part, the commands in the serial monitor window are set; the user has the option to show the pattern in clockwise, counterclockwise, downward, and upward motion, or as on/off

```

void loop() {
  Serial.println("Please input 1000 for clockwise,
  2000 for counterclockwise, 3000 for upward, or
  4000 for downward motion of pattern, 5000 for on/of of stimuli\n");
  while (getCommand() == 0);          //do nothing until data is being received from serial object

  if (command == 1000)                //command 1000 = clockwise
  {
    Serial.println("Rotation direction: clockwise");
    Serial.println("Please enter rotation velocity (°/s)");
    while (getCommand() == 0);
    Serial.println("Waiting for trigger from microscope");
    while (digitalRead(FromMicroscopePin) == 0);    //wait for trigger
    rotatecw(command, numrot);
  }

  if (command == 2000)                //command 2000 = counterclockwise
  {
    Serial.println("Rotation direction: counterclockwise");
    Serial.println("Please enter rotation velocity (°/s)");
    while (getCommand() == 0);
    Serial.println("Waiting for trigger from microscope");
    while (digitalRead(FromMicroscopePin) == 0);    //wait for trigger
    rotateccw(command, numrot);
  }

  if (command == 3000)                //command 3000 = downward motion
  {
    Serial.println("Motion direction: downwards");
    Serial.println("Please enter rotation velocity (°/s)");
    while (getCommand() == 0);
    Serial.println("Waiting for trigger from microscope");
    while (digitalRead(FromMicroscopePin) == 0);    //wait for trigger
    movedown(command, numrot);
  }

  if (command == 4000)                //command 4000 = upward motion
  {
    Serial.println("Motion direction: upwards");
    Serial.println("Please enter rotation velocity (°/s)");
    while (getCommand() == 0);
    Serial.println("Waiting for trigger from microscope");
    while (digitalRead(FromMicroscopePin) == 0);    //wait for trigger
    moveup(command, numrot);
  }

  if (command == 5000)                //command 5000 = on/off of stimuli
  {
    Serial.println("on/off of stimuli");
    Serial.println("Waiting for trigger from microscope");
    while (digitalRead(FromMicroscopePin) == 0);    //wait for trigger
    onoff();
  }
}

```

- Then those options are coded as commands for the Arduino

```

////////////////////////////////////
//rotatecw()
//rotate stimulus clockwise (generate increasing sawtooth)
////////////////////////////////////
void rotatecw(int rotvel, int n) {
    float wait; int jaja = 0;
    //wait = 1000 * (360.0 / rotvel) / 96;
    wait = 1000 * (360.0 / rotvel) / 97;

    dacout(0);      //Output 0 mV to display first (dark frame)
    delay(10000);   //wait 10 s
    dacout(63);      //Output 1.5* 10 V /97 to display second frame
    delay(5000);     //wait 5 s
    for (int j = 0; j < n; j++) {
        for (int i = 63; i <= 4095; i += 42) {
            // jaja++;
            // Serial.print("Step ");Serial.println(jaja);
            //Serial.print("i= ");Serial.println(i);
            dacout(i);
            delay(wait);
        }
    }
    dacout(0);
}

////////////////////////////////////
//rotateccw()
//rotate stimulus counterclockwise (generate decreasing sawtooth)
////////////////////////////////////
void rotateccw(int rotvel, int n) {
    float wait;
    wait = 1000 * (360.0 / rotvel) / 97;

    dacout(0);      //Output 0 mV to display first (dark frame)
    delay(10000);   //wait 10 s
    dacout(4095);    //Output 10 V to display last frame
    delay(5000);     //wait 5 s
    for (int j = 0; j < n; j++) {
        for (int i = 4095; i >= 63; i -= 42) {
            dacout(i);
            delay(wait);
        }
    }
    dacout(0);      //Output 0 mV to display first (dark frame)
}

```



```

////////////////////////////////////
//moveup()
//move stimulus upwards (generate increasing sawtooth)
////////////////////////////////////
void moveup(int rotvel, int n) {
    float wait; int jaja = 0;
    wait = 1000 * (90.0 / rotvel) / 25;

    dacout(0);      //Output 0 mV to display first (dark frame)
    delay(10000);   //wait 10 s
    dacout(300);     //Output 1* (10 V /33) to display second frame
    delay(5000);     //wait 5 s
    for (int j = 0; j < n; j++) {
        for (int i = 300; i <= 4095; i += 156) {
            dacout(i);
            delay(wait);
        }
    }
    dacout(0);
}

////////////////////////////////////
//movedown()
//move stimulus downwards (generate decreasing sawtooth)
////////////////////////////////////
void movedown(int rotvel, int n) {
    float wait;
    wait = 1000 * (90.0 / rotvel) / 25;

    dacout(0);      //Output 0 mV to display first (dark frame)
    delay(10000);   //wait 10 s
    dacout(4095);    //Output 10 V to display last frame
    delay(5000);     //wait 5 s
    for (int j = 0; j < n; j++) {
        for (int i = 4095; i >= 186; i -= 156) {
            dacout(i);
            delay(wait);
        }
    }
    dacout(0);      //Output 0 mV to display first (dark frame)
}

```

```

////////////////////////////////////
//on/off of stimuli()
//turns stimuli on and off
////////////////////////////////////
void onoff(){
  dacout(0);      //Output 0 mV to display first (dark frame)
  delay(10000);   //wait 10 s
  dacout(4095);   //Output 10 V to display last frame
  delay(5000);    //wait 5 s
  dacout(0);      //Output 0 mV to display first (dark frame)
  delay(5000);    //wait 5 s
  dacout(4095);   //Output 10 V to display last frame
  delay(5000);    //wait 5 s
  dacout(0);      //Output 0 mV to display first (dark frame)
  delay(5000);    //wait 5 s
  dacout(4095);   //Output 10 V to display last frame
  delay(5000);    //wait 5 s
  dacout(0);      //Output 0 mV to display first (dark frame)
}

```

- The last part of the script defines to get the information from the serial monitor and send the options chosen by the user to the digital-to-analog converter (DAC)

```

////////////////////////////////////
//dacout()
//send data to DAC
////////////////////////////////////
void dacout(int outval) {
  digitalWrite(latchPin, HIGH);
  digitalWrite(clockPin, LOW);
  shiftOut(dataPin, clockPin, MSBFIRST, (outval >> 8));
  shiftOut(dataPin, clockPin, MSBFIRST, outval);
  digitalWrite(latchPin, LOW);
  digitalWrite(latchPin, HIGH);
}

```

```

////////////////////////////////////.
//getcommand()
//read integer value from serial object
////////////////////////////////////.
int getCommand() {
    //Read from serial monitor if data available
    if (Serial.available()) {
        //command = Serial.read() - '0';
        command = Serial.parseInt();
        Serial.print("Received: "); Serial.println(command);
        return 1;
    }
    else
        return 0;          //keep waiting for input
} // end of getCommand()

```

---

- Select in the Arduino software "Tools/Serial monitor"
- Select movement direction of pattern
- Select speed of pattern movement (°/s)
- Now the LED arena is waiting for the trigger of the first frame of the microscope

#### 11. Imaging settings

- Turn on needed laser and detector
- Click on "live", set gain of detector and search for region of interest
- Adjust zoom, laser power, gain and offset of detector
- Turn "live" off, set biderctional scan, and adjust scanning speed to 600 (if resonant scanner is off)
- Adjust resolution and image section to see enough details with the highest temporal resolution possible, in the end the desired temporal resolution should be above eight frames per second

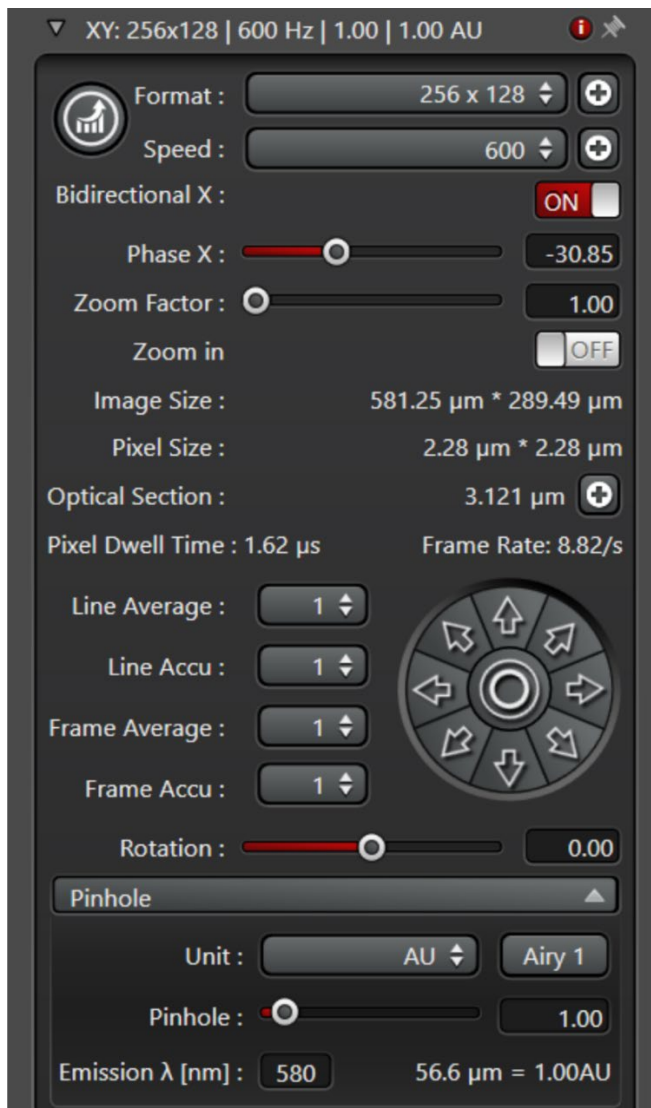


**Fig. S10:** Example setting for a live calcium imaging experiments with the resolution and speed set to values that allow for a scanning speed of 8.82 frames per second.

- Set desired scanning time for one experiment
- 

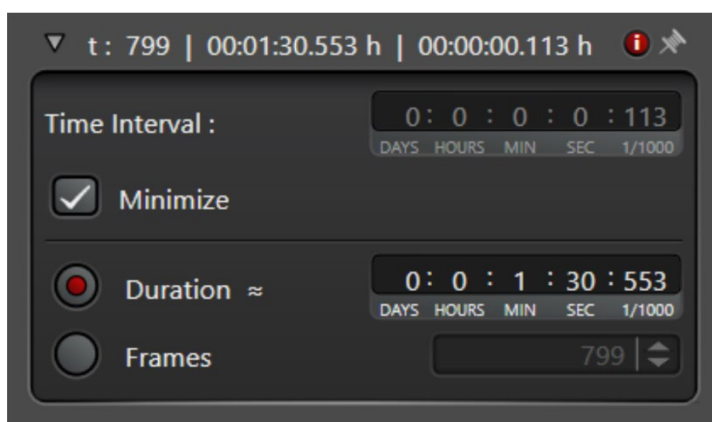


**Fig. S11:** Example setting for imaging experiment duration at ~ 90 seconds. The time interval between frames is set to minimize, resulting with a scanning speed of 8.82 frames per second in 799 frames for the whole trial.

## 12. Run imaging, Fictrac, and AxoScope

- Hit "record" in AxoScope software, three rows should start recording: one for the pattern position in the arena, one for the microscope signals per frame, and one for the FicTrac frames

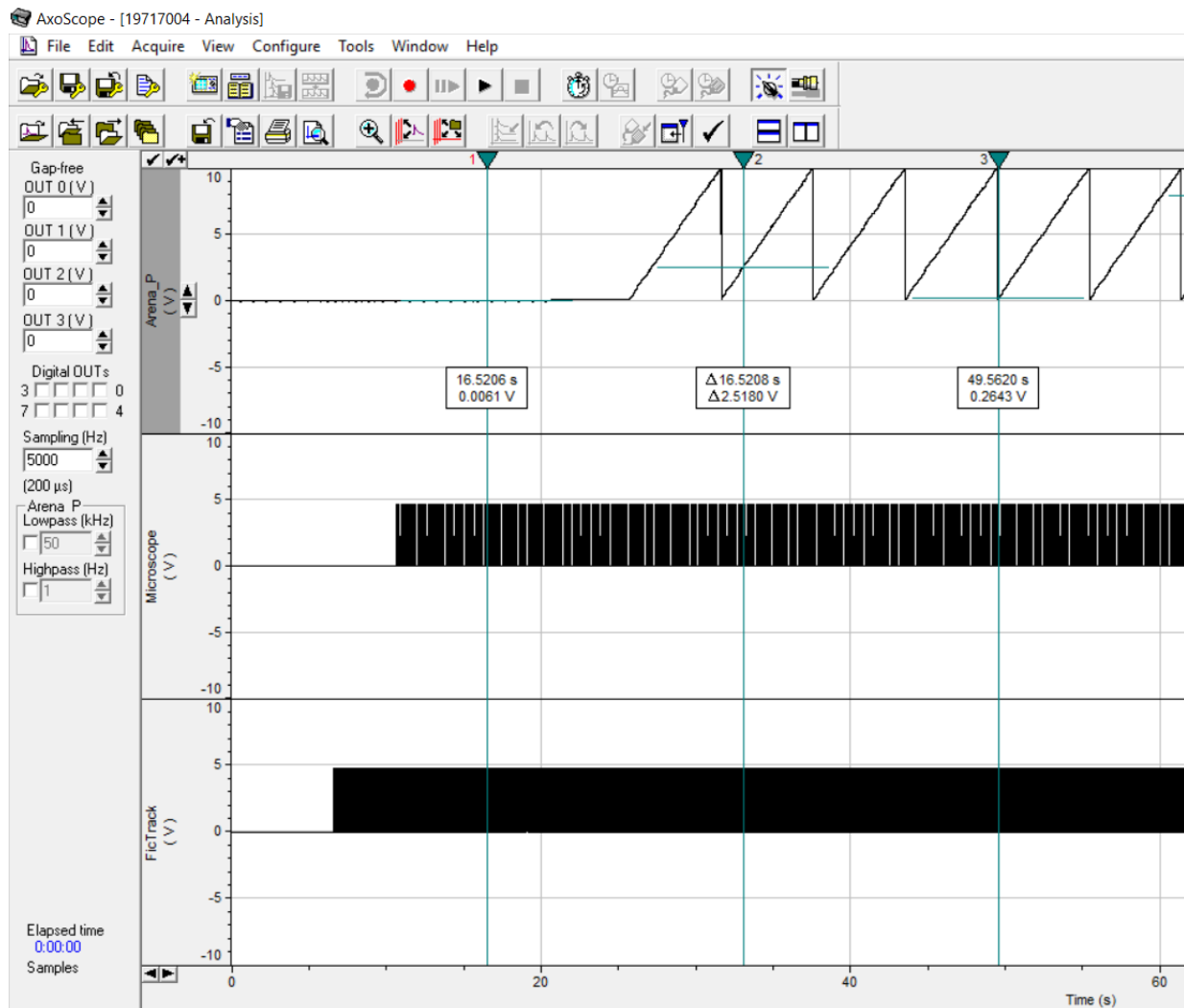


**Fig. S12:** AxoScope window with three recording traces as volt over time. The top row shows the recording of the position of the pattern in the arena, the second the output signal for every frame of the microscope, and in the row below every frame of the FicTrac software is shown.

- Start Fictrac script by entering "`../bin/FicTrac/Martina/Martina_config.txt`"; FicTrac will start when hitting enter

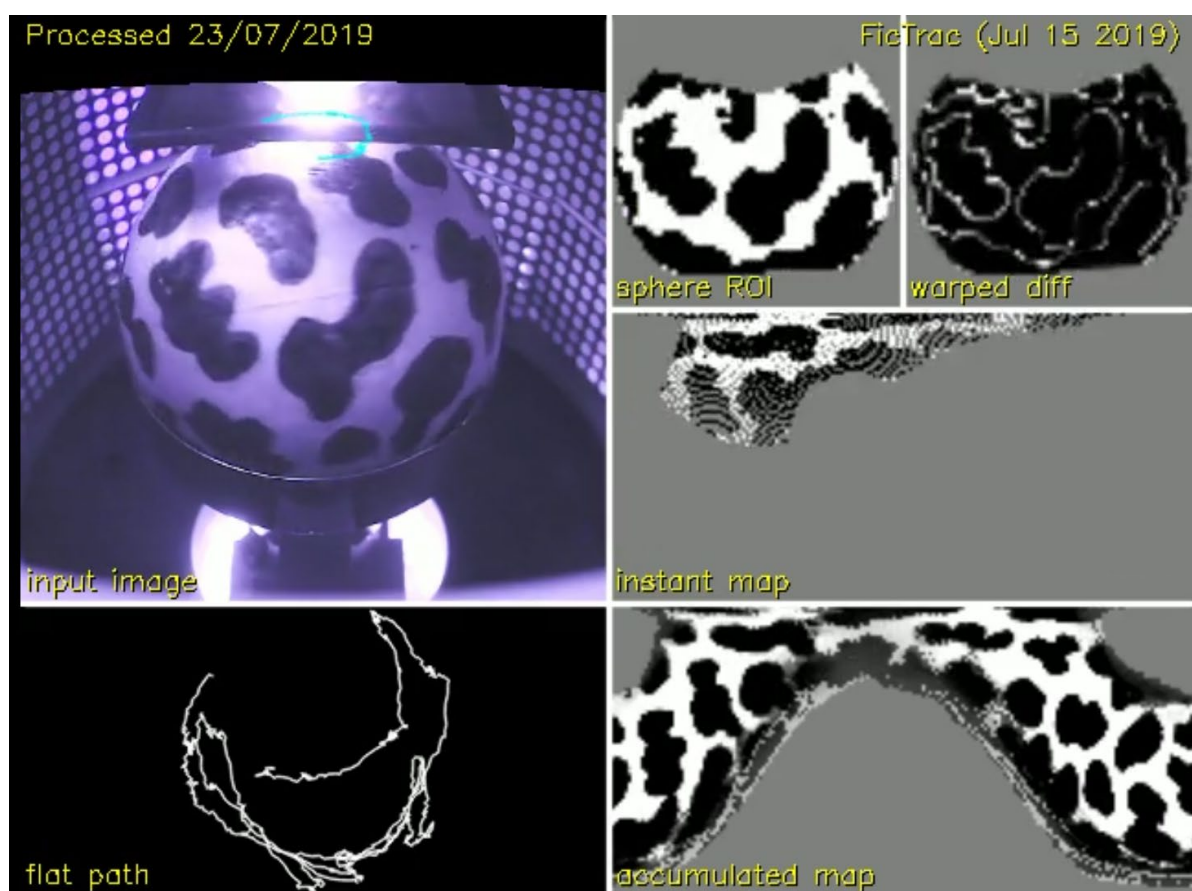


**Fig. S13:** FicTrac recording window with the live video, the fictive walking path of the bee, the defined sphere ROI, the difference of the sphere ROI to the previous frame, the instand map of the ball tracking and the accumulated map. For more information see Moore et al., 2014.

- Hit "Start" in Leica software to start imaging and to send first trigger impuls to the Arduino that controls the arena to start the pattern display
- After the Leica software is done with the imaging part, stop FicTrac by pressing "strg +c" and AxoScope by pressing "stop"
- Save all files and rename if necessary

### 13. Analysis imaging data

- First, look at the imaging stacks with the free Leica LAS X software
- You can also extract the properties and settings of each stack in the software
- Afterwards analyze the data in more detail with the Python script in Jupyter Notebook (written by Dr. Hannah Haberkern):
- Check if all needed libraries are installed



## Overview of steps

1. Import tiff stack
2. Open using pyqtgraph (interactive browsing of data)
3. Simple movement correction
4. Draw ROIs
5. Extraction of time series from ROIs
6. Some visualizations of ROI time series

```
In [1]: from skimage.io import imread, imshow
import h5py
from matplotlib import pyplot as plt
import matplotlib.colors as colors
import numpy as np
from sys import path
from os.path import sep, exists
from os import mkdir, makedirs, getcwd

import flika as flk
from flika.window import Window as flw

from scipy.signal import savgol_filter

%matplotlib inline
```

- Import tiff file by changing directory/name of "rawtiff"; check if printed directories are correct

### 1. Import tiff stack

Choose and import tiff file (imaging data) and generate directory for storing analysis plots

```
In [2]: parentDir = sep.join(getcwd().split(sep)[-1])

rawtiff = '180618_1.tif'
expt = rawtiff[:-5] #adjust manually, if experiment name should be different from imaging stack name

explenght = 60 #need to adjust this manually (experiment duration in s used to compute fps)
# @ Tina: I got this value from the Leica pdf file and interpreted the "," in the German sense, i.e. that
# the experiment took about 103 s not 103000 s.

#stack parameter
stackOrganization = {
    'singlePlane': ['t', 'y', 'x'],
    'zStack': ['t', 'z', 'y', 'x']
}

dataDir = sep.join([parentDir, 'Data', 'LeicaData'])
plotDir = sep.join([parentDir, 'Plots', 'LeicaData'])
roiDir = sep.join([parentDir, 'ROIs', 'LeicaData'])

print(parentDir)
print(dataDir)
print(plotDir)

print(expt)
```

```
C:\Users\Mah33Ex\Dropbox\BeeImagingCoop (1)
C:\Users\Mah33Ex\Dropbox\BeeImagingCoop (1)\Data\LeicaData
C:\Users\Mah33Ex\Dropbox\BeeImagingCoop (1)\Plots\LeicaData
180618_
```

- Check in the next step if the script reads out the dimensions of the stack correctly

```
In [4]: rawstack = imread(dataDir + sep + rawtiff)

if len(rawstack.shape) == 3:
    imgType = 'singlePlane'
    singlePlaneStack = rawstack
elif len(rawstack.shape) == 4:
    imgType = 'zStack'
    singlePlaneStack = np.max(rawstack, axis=1)
else:
    print('Imaging stack has unexpected dimensions.')
stackDims = dict(zip(stackOrganization[imgType],rawstack.shape))

print('raw stack dimensions:\n\t{}'.format(stackDims))
print('single stack (max proj.) dimensions [t, y, x]:\n\t{}'.format(singlePlaneStack.shape))

raw stack dimensions:
    {'t': 692, 'y': 96, 'x': 96}
single stack (max proj.) dimensions [t, y, x]:
    (692, 96, 96)
```

- Check if printed frames/second and information about z-stack/volume matches the original data set

```
In [5]: fps = stackDims['t']/explenght #volume rate
print(fps)

11.533333333333333
```

```
In [6]: numTimePts = stackDims['t']

if imgType == 'singlePlane':
    fpv = 1
elif imgType == 'zStack':
    fpv = stackDims['z']
else:
    print('something went wrong')
print("# frames: {}\n# frames per vol: {}".format(numTimePts,fpv))

# frames: 692
# frames per vol: 1
```

- The stack gets opened with the Plug-in "flika" which will open in an additional pop-up window

## 2. Open stack

```
In [7]: flk.start_flika()
```

```
Starting flika  
Starting flika inside IPython
```

```
Out[7]: <flika.app.application.FlikaApplication at 0x236229b2dc8>
```

```
In [8]: if imgType == 'singlePlane':  
        rawVidWin = flw(rawstack)  
        else: #stack images of z-stack in x-dimension  
        rawVidWin = flw(rawstack.reshape(stackDims['t'], stackDims['y'] * stackDims['z'], stackDims['x']))  
        maxVidWin = flw(singlePlaneStack)
```

Optional: Collapse volume using max projection

```
In [9]: # Use max projection?  
useMaxProj = True  
  
if useMaxProj:  
    tiffstack = singlePlaneStack  
else:  
    tiffstack = rawstack  
  
nVols = tiffstack.shape[0]  
print('number of frames: {}'.format(nVols))
```

```
number of frames: 692
```

```
In [10]: time = np.linspace(0, nVols/fps, nVols)  
print('Duration of experiment: {}'.format(nVols/fps))
```

```
frameIDs = np.arange(nVols)
```

```
Duration of experiment: 60.0s
```

- The movement in the x/y axes of the opened stack gets analyzed; for that a reference frame gets picked manually, normally at the beginning of the experiment (in this case it is the tenth frame)

```
In [11]: from skimage.feature import register_translation  
        from skimage.feature.register_translation import _upsampled_dft  
        from scipy.ndimage import fourier_shift
```

Settings

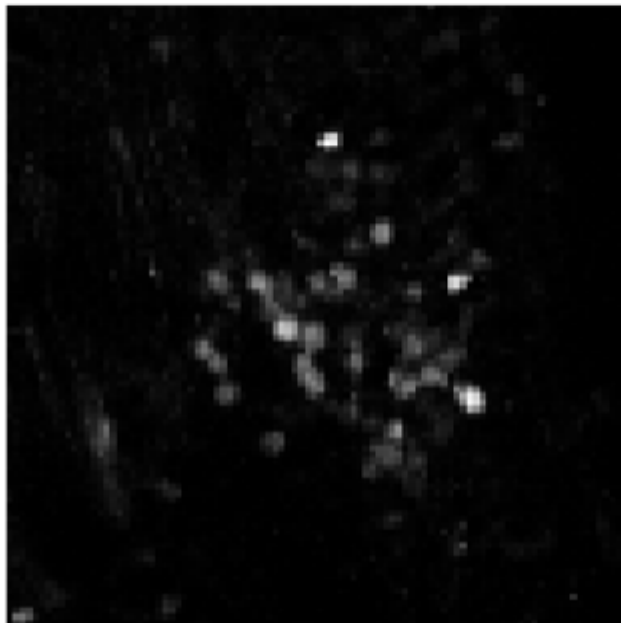
```
In [12]: ## reference image
numRefImg = 10
locRefImg = round(numTimePts/3.)

## registration
upsampleFactor = 100

# Generate reference image
refImg = np.mean(tiffstack[locRefImg:locRefImg+numRefImg,:,:],axis=0)

fig, ax = plt.subplots(1,1,figsize=(6,6))
ax.imshow(refImg.T,cmap='Greys_r', vmin=0, origin='upper')
ax.set_title('Reference frame')
ax.axis('off');
fig.savefig(saveDir+sep+expt+'_roiReferenceframe.pdf', format = 'pdf')
```

Reference frame

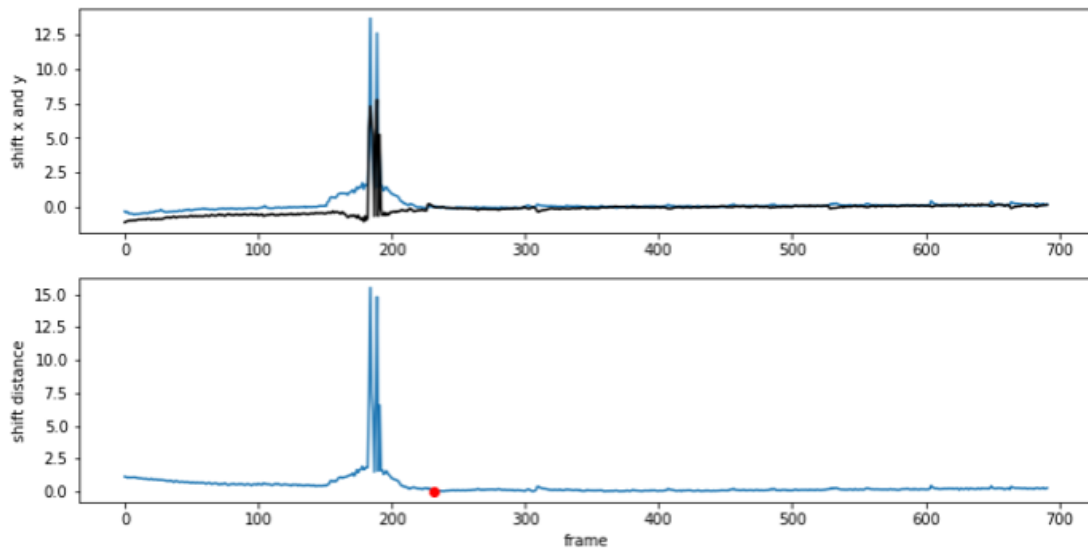


- The shift of the other frames compared to the reference frame gets computed and visualized in a figure

```
In [15]: fig, axs = plt.subplots(2,1,figsize=(12,6))
axs[0].plot(shift[0,:])
axs[0].plot(shift[1,:],'k')
axs[0].set_ylabel('shift x and y')

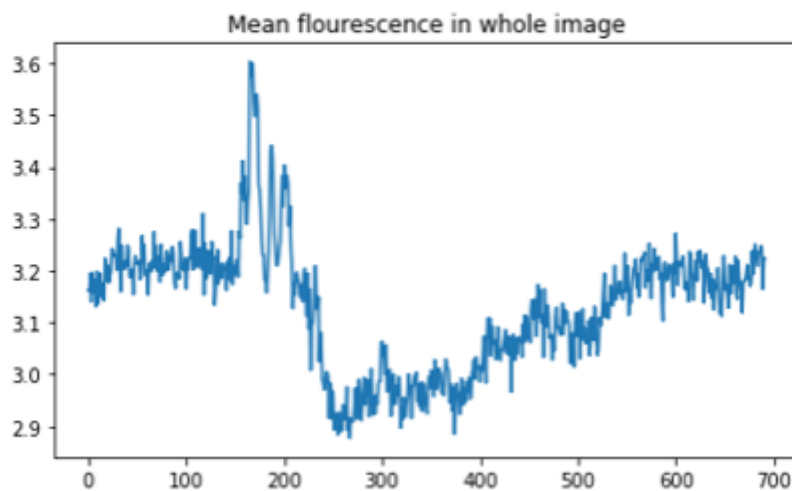
axs[1].plot(np.hypot(shift[0,:],shift[1,:]))
axs[1].plot(locRefImg,0,'ro')
axs[1].set_xlabel('frame')
axs[1].set_ylabel('shift distance')
```

Out[15]: Text(0,0.5,'shift distance')



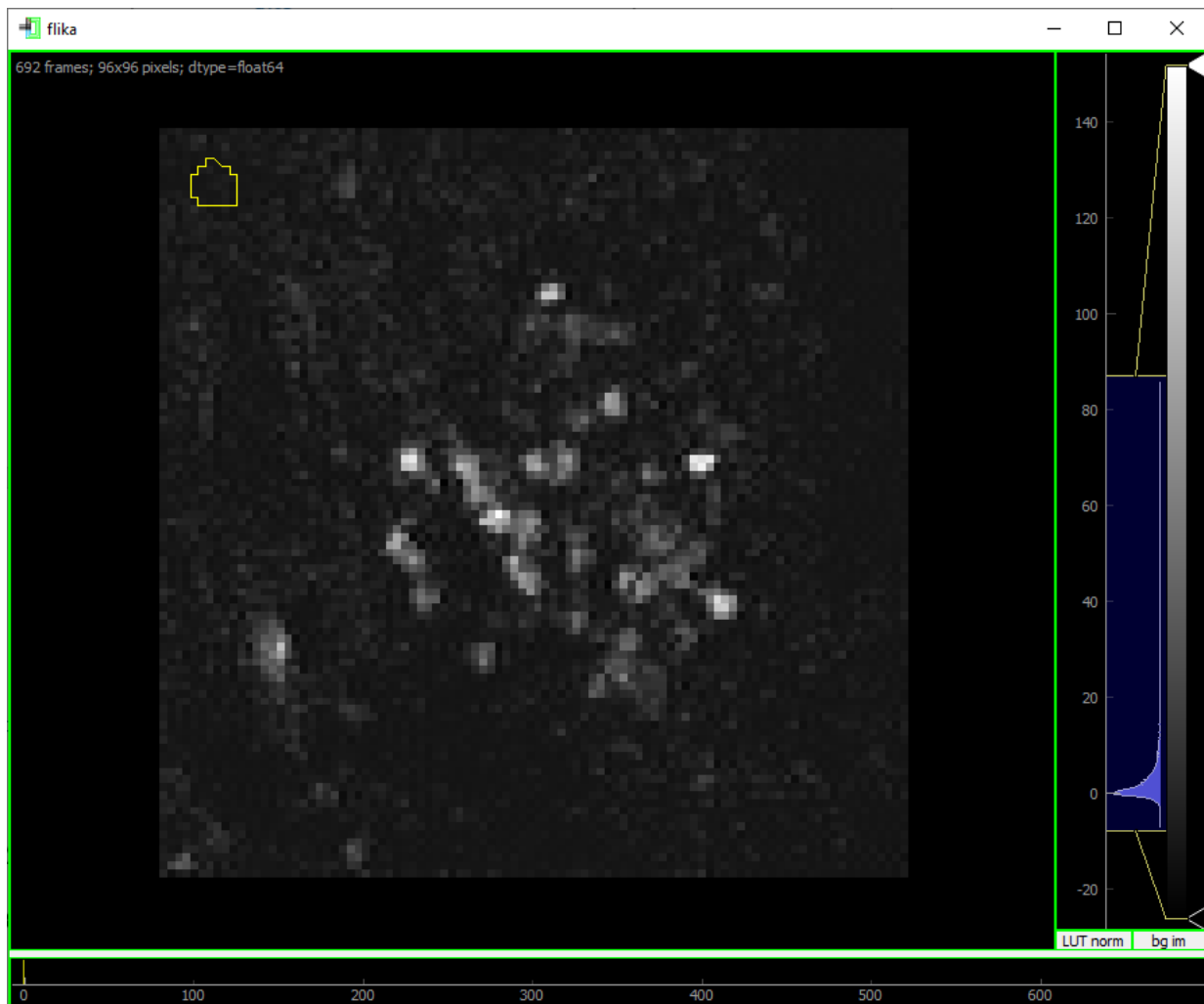
- In the next step the mean fluorescence of the whole image across all frames gets visualized

```
In [16]: fig, axs = plt.subplots(1,1,figsize=(7,4))
axs.plot(np.mean(np.mean(stackMC,axis=1), axis=1))
axs.set_title('Mean flourescence in whole image');
```



- Flika opens in the next step a new window with whole stack where one region of interest gets manually defined to extract the background signal. This region should lay outside any stained structures

```
In [18]: backgrdExtr = flw(stackMC)
```



- The fluorescence in that region gets extracted and is in further steps used as background fluorescence



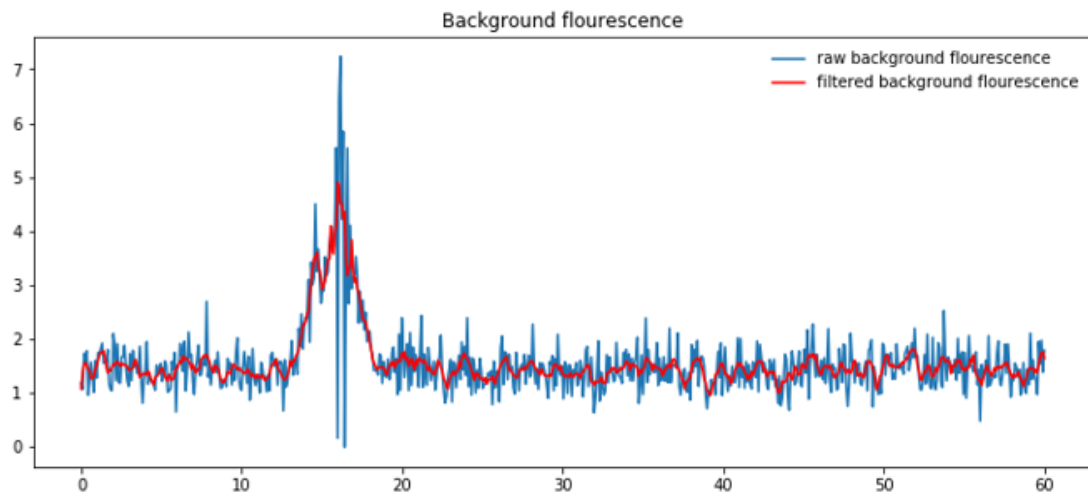
### Draw ROI for background extraction

```
In [18]: backgrdExtr = flw(stackMC)
```

```
In [19]: # extract background signal from flika
backgrdROI = backgrdExtr.rois
backgrdFraw = backgrdROI[0].getTrace()

# filter background signal
sgwindow = 11
sgorder = 3
backgrdF = savgol_filter(backgrdFraw, sgwindow, sgorder)

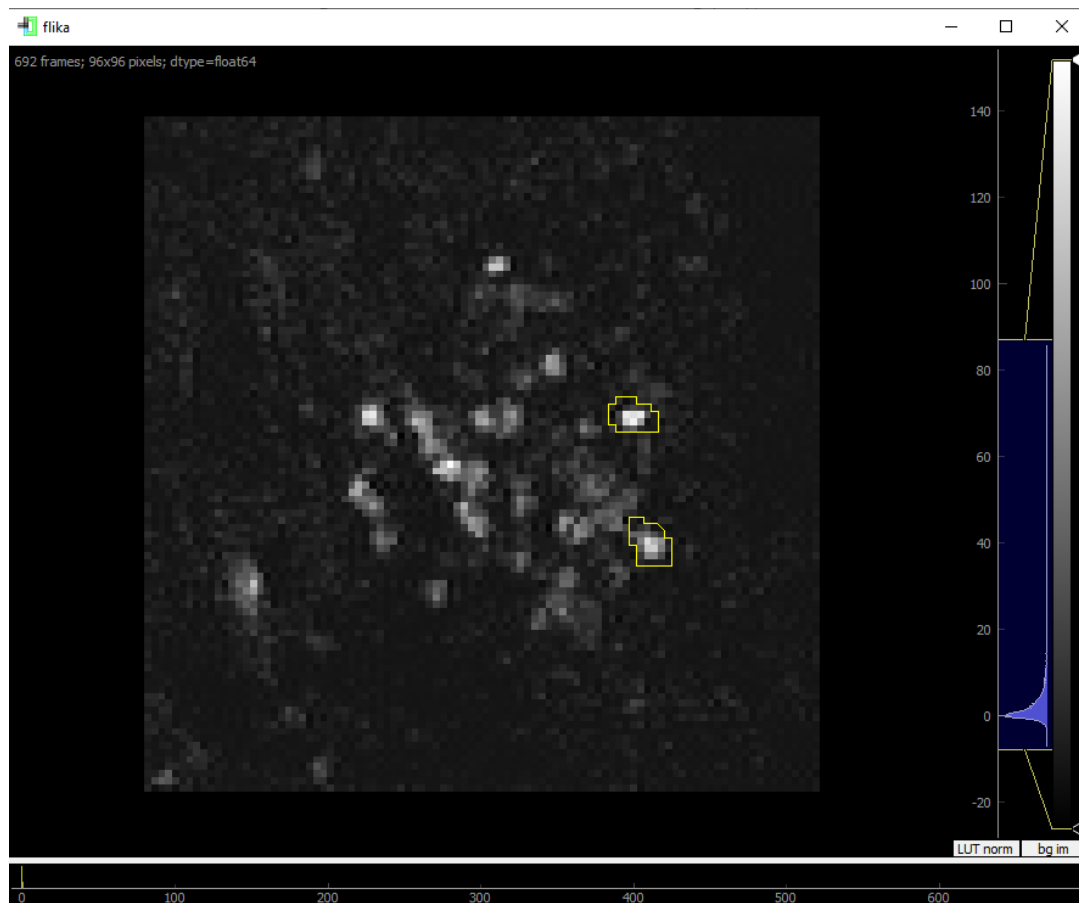
# plot background signal
fig, axs = plt.subplots(1,1,figsize=(12,5))
axs.plot(time,backgrdFraw,label='raw background flourescence')
axs.plot(time,backgrdF, 'r',label='filtered background flourescence')
axs.set_title('Background flourescence')
axs.legend(frameon=False);
fig.savefig(saveDir+sep+expt+'_roiBackground.pdf', format = 'pdf')
```



- Now the actual regions of interest are defined in an additional window in flika and the fluorescence in those ROIs get extracted over the whole time series; with the background fluorescence and the fluorescence in the ROIs  $dF/F$  is calculated

### 5. Draw ROI's using flika's menu

```
In [50]: # Open with flika, select e.g. freehand form, right click on image and draw ROI
slctStackWin = flw(stackMC)
```



## 6. Extraction of time series from ROIs

```
In [51]: rois = slctStackWin.rois
```

Compute dF/F

```
In [52]: # Currently F_0 is estimated for the whole time series (ok, if time series is short)
baseLinePercent = 20
offset = 0.0001
```

```
In [53]: F_raw = np.nan*np.ones((nVols,len(rois)))
dFF = np.nan*np.ones((nVols,len(rois)))
roiPts = []
for i, r in enumerate(rois):
    # get pixel coordinates defining the ROI
    roiPts.append(r.getPoints())

    # Compute the average of the pixels within this ROI in its window
    F_raw[:,i] = r.getTrace()

    # Estimate baseline
    F_0 = np.percentile(r.getTrace(), baseLinePercent)
    if F_0 == 0: F_0 += offset

    # Compute dF/F_0 = (F_raw - F_0)/F_0
    #dFF[:,i] = (r.getTrace() - F_0) / F_0

    # Compute dF/F_0 = (F_raw - F_0)/(F_0 - F_b)
    # F_b is measured in ROI far away from where we expect signal.
    dFF[:,i] = (r.getTrace() - F_0 - backgrdF) / (F_0 - backgrdF)
```

- The data extracted from the ROIs are getting saved

#### Save ROI data to file

```
In [54]: # Generate dictionary with all ROI information -- assumes max projection, i.e.
roiData = {
    'imgData': rawtiff,
    'img': refImg,
    'numframes': nVols,
    'slctframes': frameIDs,
    'fpv': fpv,
    'fps': fps,
    'time': time,
    'numRoi': len(rois),
    'Fraw': F_raw,
    'DFF': dFF,
    'Pts': roiPts,
    'Fb': backgrdF
}

np.save(roiDir+sep+expt+'_roiData',roiData) # save as npy file (easy to load into python)
np.savetxt(roiDir+sep+expt+'_roiFraw'+'.csv',F_raw, delimiter=',') # save as csv (easy to open e.g. in excel)
```

- The borders of the ROIs get extracted from Flika and visualized

#### Visualize chosen ROIs and plot time series

```
In [55]: from roiVisualization import myAxisTheme, illustrateRoiOutline, illustrateRoiArea,\
illustrateRoiTrace, illustrateRoiTraceOffset
```

```
In [56]: # Select time window and sampling rate for plot
frameRange = np.arange(0,len(roiData['time'])) # in seconds
slct_fps = 1

# Select ROIs
slctROIs = np.arange(roiData['numRoi'])
```

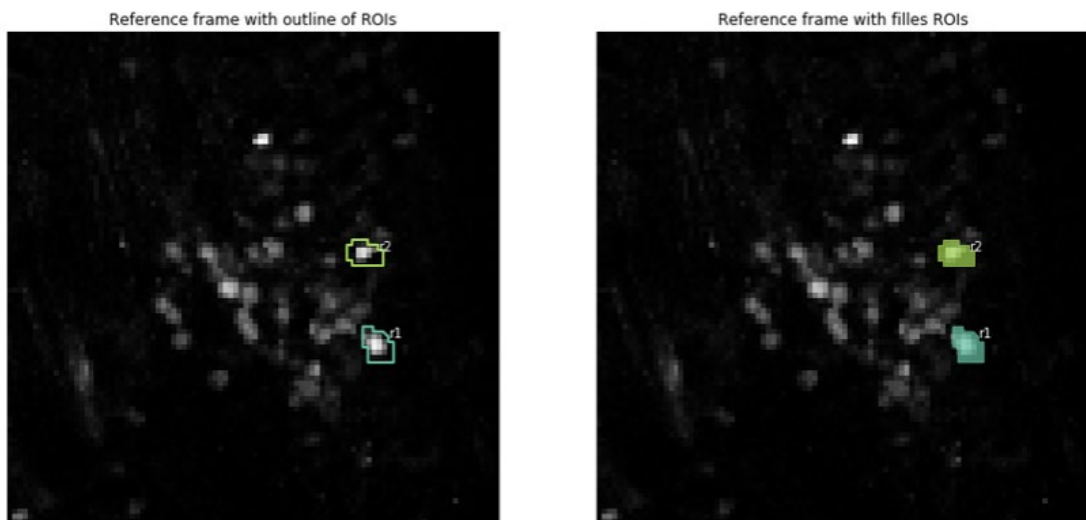
```
In [57]: # generate roi color map
nrois = len(rois)
cNorm = colors.Normalize(vmin=0, vmax=roiData['numRoi'])
roiCMap = plt.cm.ScalarMappable(norm=cNorm,cmap='Set2')
```

- The visualized ROIs are saved as figure as further reference

```
In [58]: fig, axs = plt.subplots(1,2, figsize=(15,8))
axs[0] = illustrateRoiOutline(roiData, axs[0], roiCMap, 'r', 'Reference frame with outline of ROIs')
axs[1] = illustrateRoiArea(roiData, axs[1], roiCMap, 'r', 'Reference frame with filled ROIs')

for ax in axs:
    ax.axis('off')

fig.savefig(saveDir+sep+expt+'_roiViz.pdf', format = 'pdf')
```



- $dF/F ((F-F_0)/(F_0-F_b))$  gets plotted as graph with the fluorescence trace over time and saved as a figure for future reference

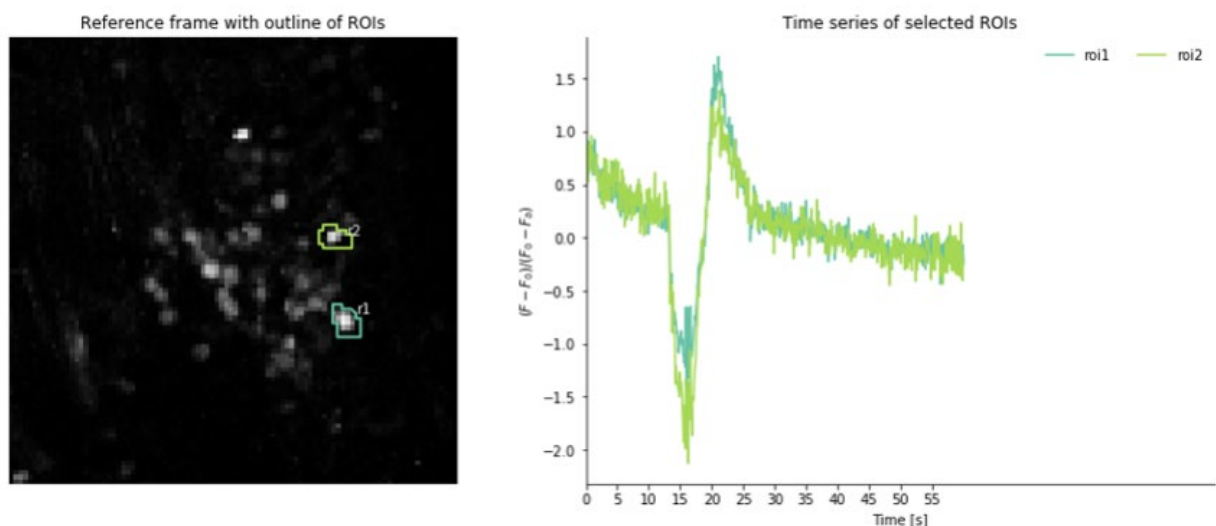
```
In [59]: fig, axs = plt.subplots(1,2, figsize=(16,6), gridspec_kw={'width_ratios':[1,1.3]})

axs[0] = illustrateRoiOutline(roiData, axs[0], roiCMap, 'r', 'Reference frame with outline of ROIs')
axs[1] = illustrateRoiTrace(roiData,roiData['time'], axs[1], roiCMap, frameRange, slctROIs,
                            'Time [s]', '$(F - F_0) / (F_0 - F_b)$', 'Time series of selected ROIs')

axs[1].set_xticks(np.arange(roiData['time'][0],roiData['time'][-1],5));
axs[1].set_xlim(0,100)
axs[1].legend(['roi'+str(i+1) for i in range(len(rois))], ncol=2, frameon=False)

myAxisTheme(axs[1])
axs[0].axis('off')

fig.savefig(saveDir+sep+expt+'_roiTraces2.pdf', format = 'pdf')
```



- For a better visualization the traces of the individual ROIs gets plotted with an offset and saved as a figure for future reference

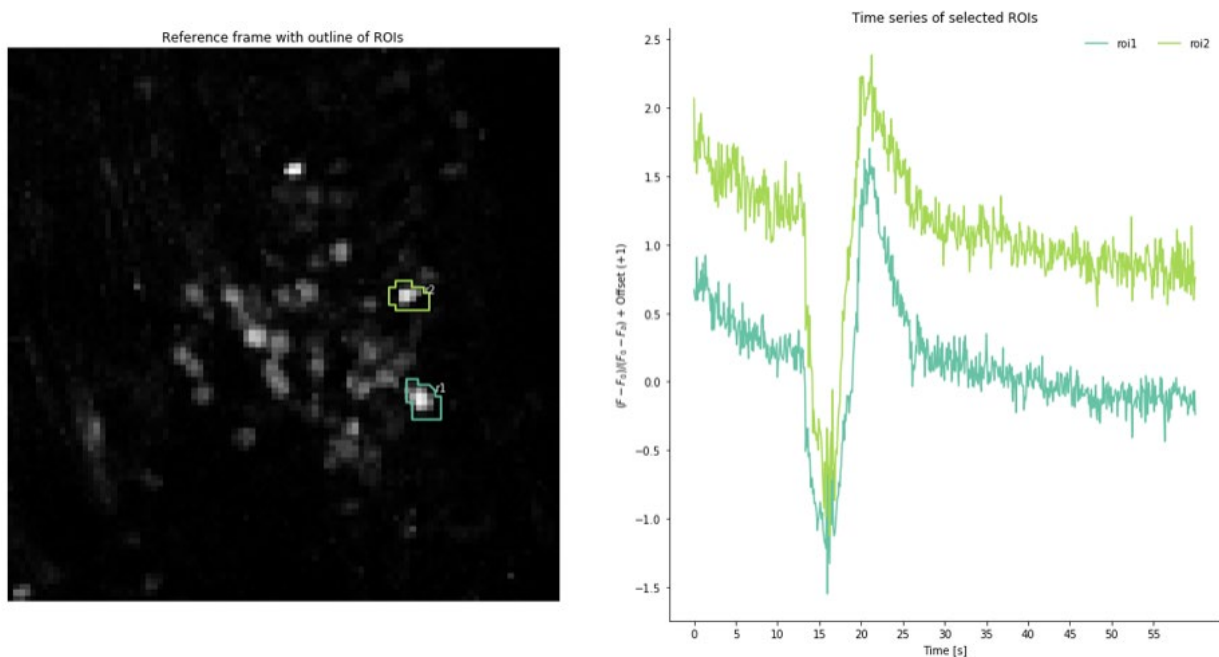
Plot ROI traces with offset to visually separate them

```
In [60]: fig, axs = plt.subplots(1,2, figsize=(20,10), gridspec_kw={'width_ratios':[1,1]})

axs[0] = illustrateRoiOutline(roiData, axs[0], roiCMap, 'r','Reference frame with outline of ROIs')
axs[1] = illustrateRoiTraceOffset(roiData, roiData['time'], axs[1], roiCMap, frameRange, slctROIs,
                                'Time [s]', '$(F - F_0) / (F_0 - F_b)$ + Offset (+1)', 'Time series of selected ROIs')
axs[1].legend(['roi'+str(i+1) for i in slctROIs], ncol=2, frameon=False)
axs[1].set_xticks(np.arange(roiData['time'][0],roiData['time'][-1],5))

myAxisTheme(axs[1])
axs[0].axis('off')

# Save after making adjustments through figure window GUI
fig.savefig(saveDir+sep+expt+'_roiTraces-offset.pdf', format = 'pdf')
```



- In the end of the imaging evaluation a correlation analysis is conducted between the fluorescence signal and the estimated motion in x/y for each ROI. If there would be a strong connection between fluorescence increase and stronger movements this could hint towards artefacts in the calcium signal. The correlation plots get saved as a figure for future reference.

### Correlation between ROI signal and estimated motion signal

```
In [61]: fig, axs = plt.subplots(1, len(slctROIs), figsize=(15,4))

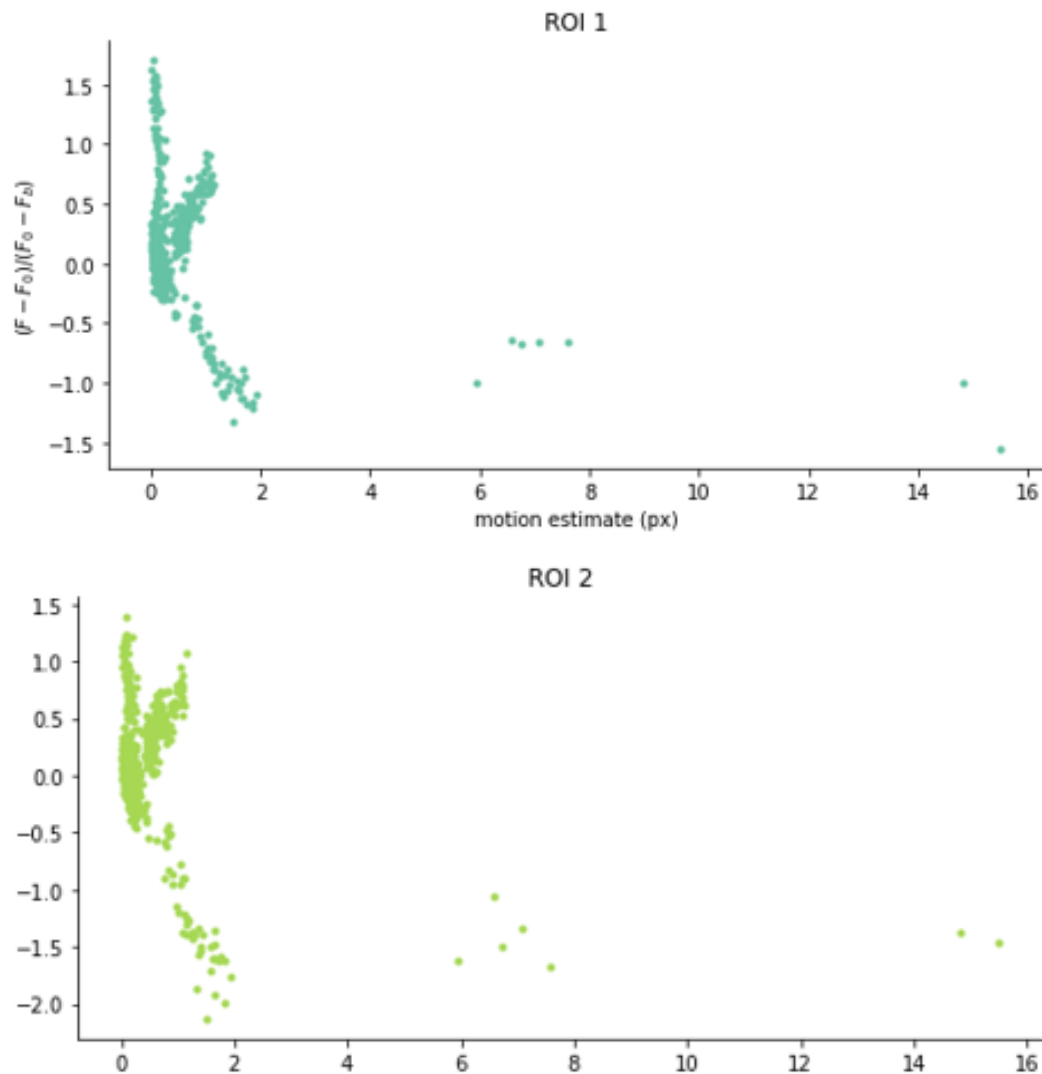
movEst = np.hypot(shift[0,:], shift[1,:])

for i, val in enumerate(slctROIs):
    axs[i].plot(movEst, roiData['DFF'][:,val], '.', color=roiCMap.to_rgba(val))
    axs[i].set_title('ROI {}'.format(val+1))
    myAxisTheme(axs[i])

axs[0].set_xlabel('motion estimate (px)')
axs[0].set_ylabel('$(F - F_0) / (F_0 - F_b)$')

fig.tight_layout()

# Save after making adjustments through figure window GUI
fig.savefig(saveDir+sep+expt+'_roiCorrWithMotion.pdf', format = 'pdf')
```





#### 14. Analysis FicTrac

- Open the Python analysis script (written by Dr. Hannah Haberkern) for FicTrac data in Jupyter Notebook
- First, the necessary libraries are located and the directions for the raw data and plots are defined

```
In [1]: import numpy as np
import matplotlib.pyplot as plt
import pandas as pd
import cmocean
from os.path import sep, exists
from os import mkdir, makedirs, getcwd
import csv

from roiVisualization import myAxisTheme
```

```
In [2]: parentDir = sep.join(getcwd().split(sep)[: -1])
dataDir = sep.join([parentDir, 'Data', 'FicTracData'])
plotDir = sep.join([parentDir, 'Plots', 'FicTracData'])

print(parentDir)
print(dataDir)
print(plotDir)

C:\Users\Mah33Ex\Dropbox\BeeImagingCoop (1)
C:\Users\Mah33Ex\Dropbox\BeeImagingCoop (1)\Data\FicTracData
C:\Users\Mah33Ex\Dropbox\BeeImagingCoop (1)\Plots\FicTracData
```

```
In [3]: # Generate directory where to save plots
saveDir = plotDir#sep.join([plotDir, dye, date, expt[: -4]])
if not exists(saveDir):
    makedirs(saveDir)
print(saveDir)

C:\Users\Mah33Ex\Dropbox\BeeImagingCoop (1)\Plots\FicTracData
```

- Then, the data from the .dat file generated by FicTrac gets loaded into the script. Change filename to the desired data set and change "expt" which is going to be the name of the plots the script is going to generate

```
In [4]: filename = '20190717_2_stripe_ccw.dat'
        expt = '20190717_2_stripe_ccw'

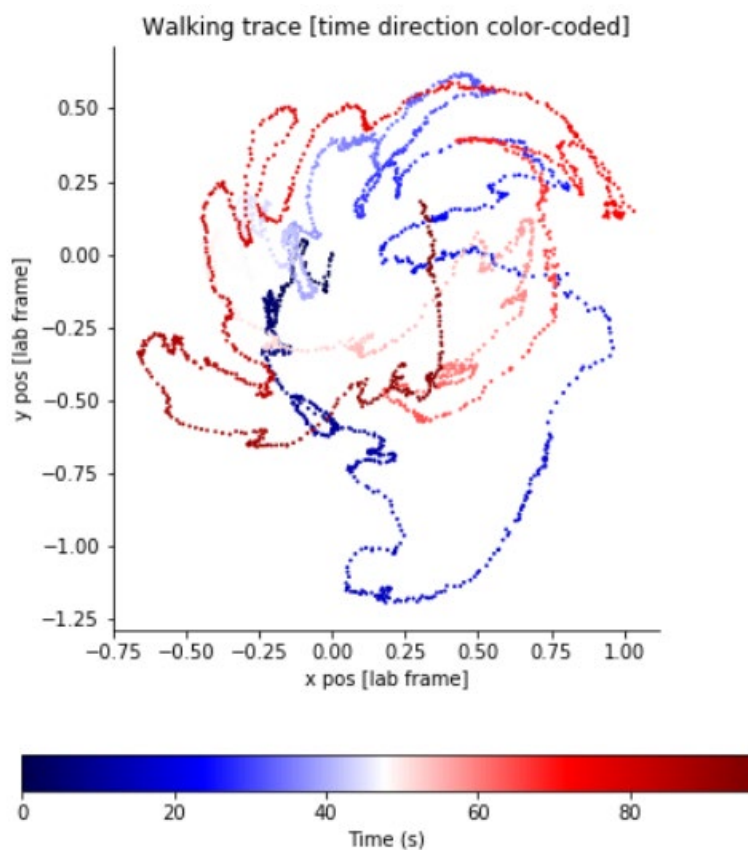
        keylist = ['frame',
                    'dRight_cam', 'dDown_cam', 'dFwd_cam',
                    'rotError',
                    'dRight_lab', 'dDown_lab', 'dFwd_lab',
                    'Right_cam', 'Down_cam', 'Fwd_cam',
                    'Right_lab', 'Down_lab', 'Fwd_lab',
                    'x', 'y', 'alpha',
                    'transDir', 'transV_rad',
                    'xpos', 'ypos',
                    'time', 'seqcount']
```

- The script is then retrieving the data saved in the .dat file

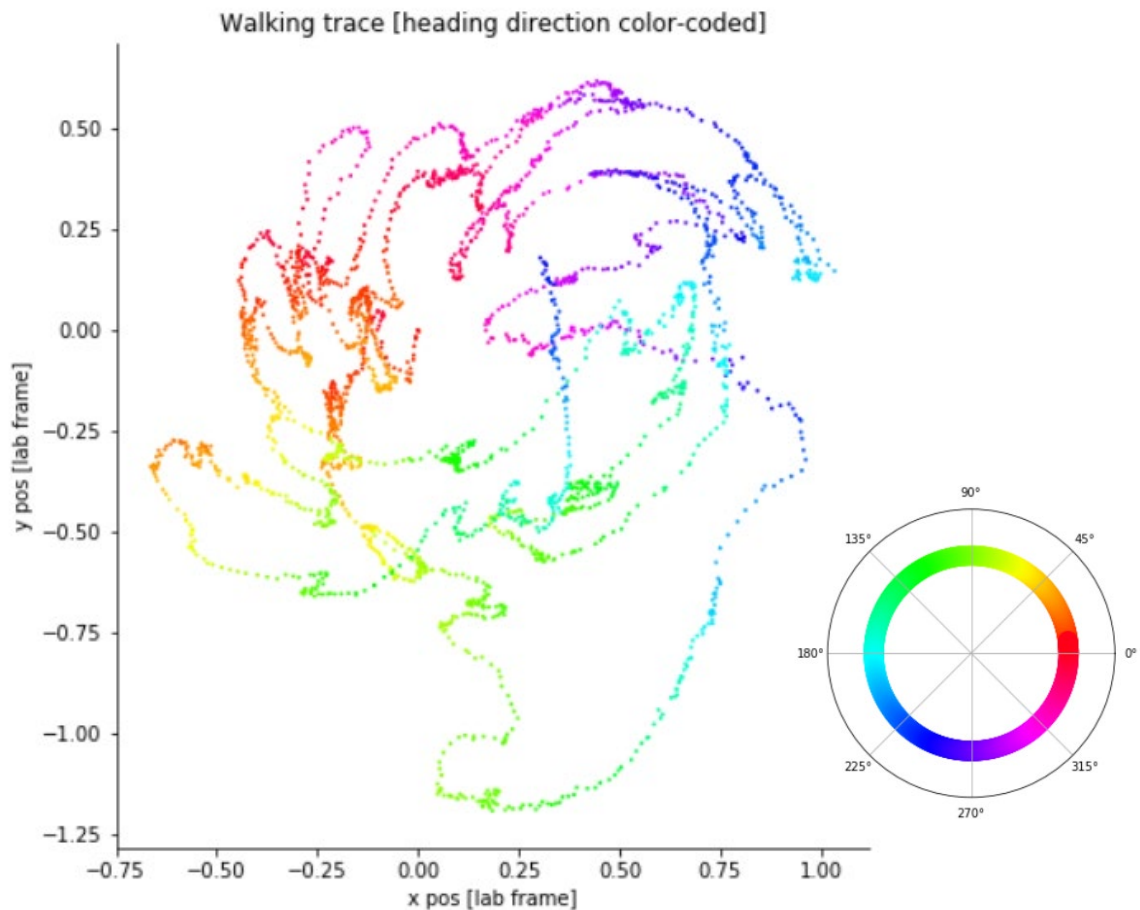
```
In [5]: fictrackDf = pd.read_csv(sep.join([parentDir, 'Data', 'FicTracData', filename]),
                                index_col=False,
                                names=keylist)
```

```
In [6]: fictrackDf.head()
```

- Out of the data the virtual walking path gets plotted with different color codes, one for the time of the whole trace, the other plot has a color-code for the heading direction. The plots get saved as figures for future reference.



- In addition, the walking path gets also plotted as graphs with heading, ball movement direction, and movement speed traces over all frames. Those graphs get saved for further reference.



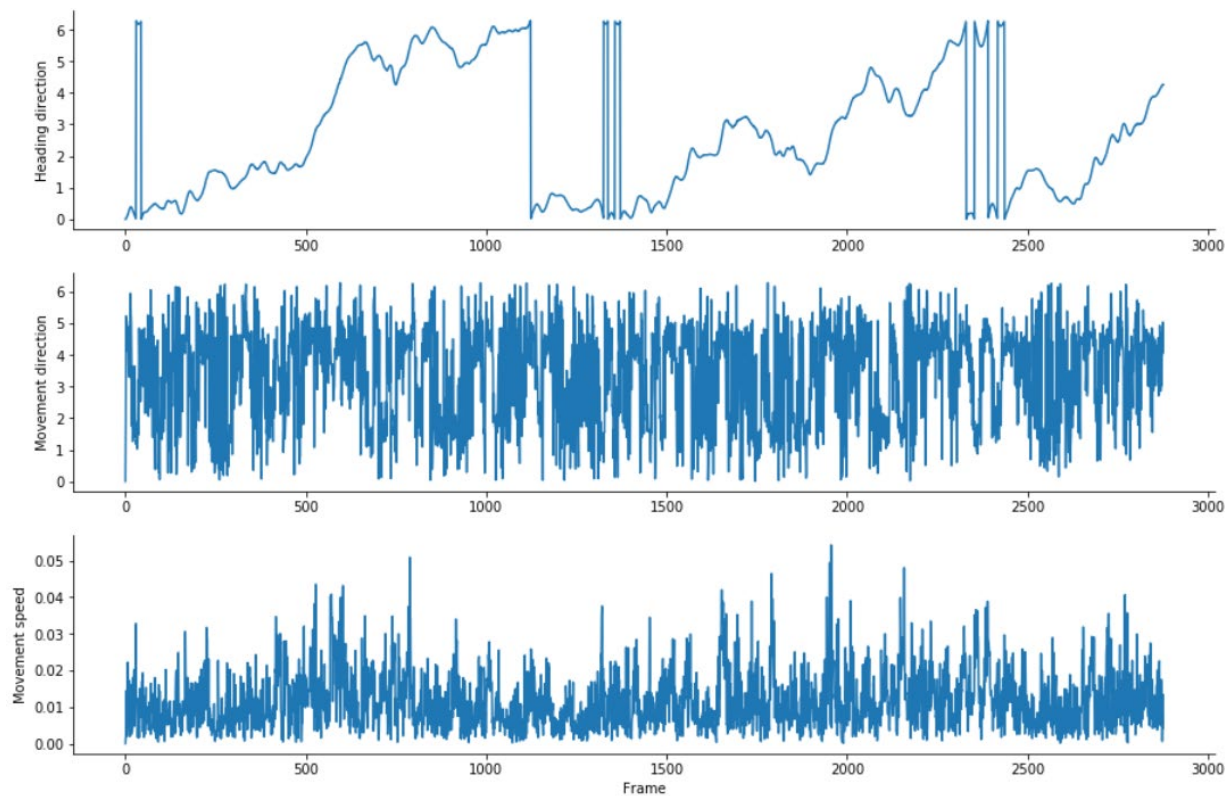
```
In [10]: fig, axs = plt.subplots(3,1,figsize=(15,10))
axs[0].plot(fictrackDf['frame'].values,fictrackDf['alpha'].values)
axs[0].set_ylabel('Heading direction')

axs[1].plot(fictrackDf['frame'].values,fictrackDf['transDir'].values)
axs[1].set_ylabel('Movement direction')

axs[2].plot(fictrackDf['frame'].values,fictrackDf['transV_rad'].values)
#axs[2].plot(fictrackDf['frame'].values,vTrans)
axs[2].set_xlabel('Frame')
axs[2].set_ylabel('Movement speed')

for ax in axs:
    myAxisTheme(ax)

fig.savefig(saveDir+sep+expt+'_HeadingMovementSpeed.pdf', format = 'pdf')
```



## 15. Alignment of behavior and imaging data

- First, the script needs to load the needed libraries

### Align behavior and imaging data

#### Three data files are necessary for each experiment:

- Behavior data collected with Fictrac (.dat file)
- Imaging data collected with Leica microscope (.tiff file)
- Data on the relative timing of imaging frames and behavior data is saved by DigiData in an .abf file

```
In [1]: import numpy as np
import matplotlib.pyplot as plt
import matplotlib.gridspec as gs
import pandas as pd
import cmocean
from os.path import sep, exists
from os import mkdir, makedirs, getcwd
import csv
import pyabf as pad # need to pip install this: pip install pyadf
```

```
In [2]: from roiVisualization import myAxisTheme
```

- The folder paths of the different data files is set as well as the directory of where to save the plots

```
In [3]: parentDir = sep.join(getcwd().split(sep)[: -1])
dataDir = sep.join([parentDir, 'Data'])
plotDir = sep.join([parentDir, 'Plots', 'AlignedData'])

FTDir = sep.join([dataDir, 'FicTracData'])
ImgDir = sep.join([dataDir, 'LeicaData'])
DDDir = sep.join([dataDir, 'DigiData'])

ROIDir = sep.join([parentDir, 'ROIs', 'LeicaData'])

print(parentDir)
print(dataDir)
print(plotDir)

C:\Users\Mah33Ex\Dropbox\BeeImagingCoop (1)
C:\Users\Mah33Ex\Dropbox\BeeImagingCoop (1)\Data
C:\Users\Mah33Ex\Dropbox\BeeImagingCoop (1)\Plots\AlignedData
```

```
In [4]: # Generate directory where to save plots
saveDir = plotDir
if not exists(saveDir):
    makedirs(saveDir)
print(saveDir)

C:\Users\Mah33Ex\Dropbox\BeeImagingCoop (1)\Plots\AlignedData
```

- The names of the individual files (FicTrac .dat file, imaging .tiff file, and Digidata .abf file) in the folder path set before needs to be inserted manually for every new analysis

```
In [5]: expt = '20190717_2_stripe_ccw'

FTfile = '20190717_2_stripe_ccw.dat'
Imgfile = '20190717_2_vertical_stripe_ccw.tiff'
DDfile = '20190717_2_stripe_ccw.abf'

FTfps = 30 #fictrac

ballrad = 48 #mm
```

- In the next steps the .abf file is used to synchronize the imaging and the behavior part

```
In [6]: syndat = pad.ABF(sep.join([DDDir, DDfile]))

DDtime = syndat.sweepX
arenaPos = syndat.data[0]
imgFrame = syndat.data[1]
FTFrame = syndat.data[2]
```

```
In [7]: ## resize arena position; 0 in front of animal (initially 5 on scale from 0 to 10)
arenaPos = (arenaPos - min(arenaPos)) / (max(arenaPos) - min(arenaPos)) * np.pi * 2 - np.pi
```

```
In [8]: imgTH = 3
dImgFrame = np.hstack((0,np.diff(imgFrame)))
imgFrameSt = np.where(dImgFrame > imgTH)[0]

print('{} imaging frames detected'.format(len(imgFrameSt)))

plt.plot(DDtime,dImgFrame)
plt.plot(DDtime[imgFrameSt], dImgFrame[imgFrameSt], 'r.')
plt.xlim(10,15)

1000 imaging frames detected
```

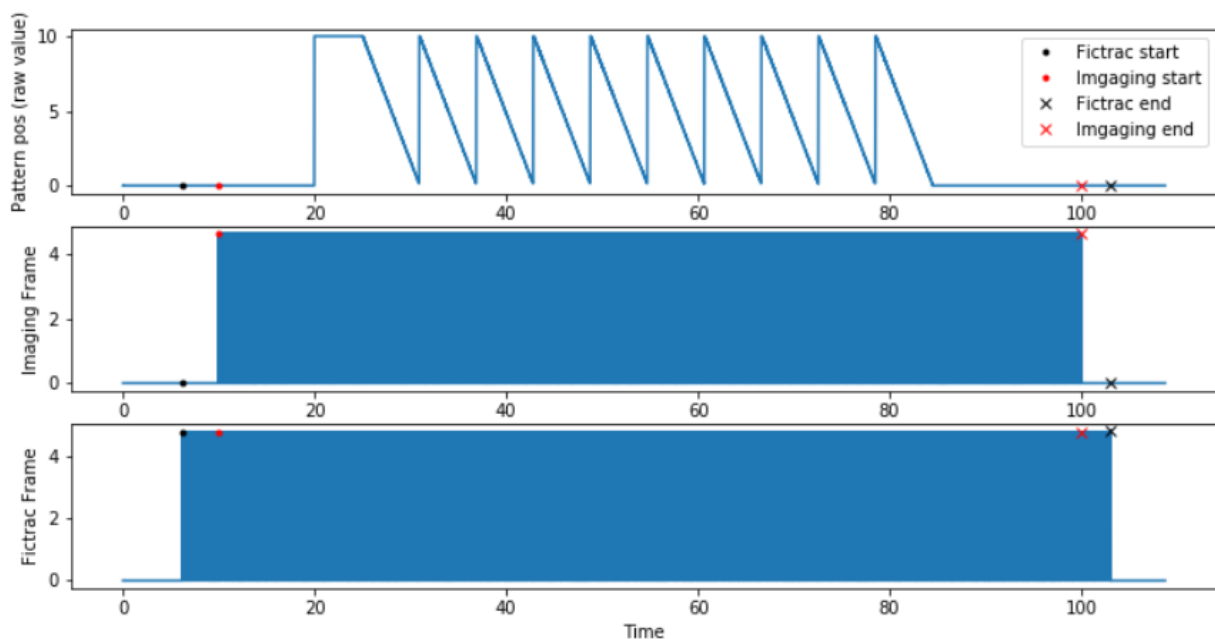
### Fictrac

```
In [9]: FTTH = 4
dFTFrame = np.hstack((0,np.diff(FTFrame)))
FTFrameSt = np.where(dFTFrame > FTTH)[0][0]
plt.plot(DDtime,FTFrame)
plt.plot(DDtime[FTFrameSt], FTFrame[FTFrameSt], 'r.')
plt.xlim(DDtime[FTFrameSt]-.01,DDtime[FTFrameSt]+.01)

FTFrameEd = np.where(dFTFrame > FTTH)[0][-1]
```

```
In [10]: st = 0#30000
ed = -1#140000

ylabs = ['Pattern pos (raw value)', 'Imaging Frame', 'Fictrac Frame']
fig, axs = plt.subplots(3,1,figsize=(12,6))
for i in range(3):
    axs[i].plot(DDtime[st:ed], syndat.data[i][st:ed], '-')
    axs[i].set_ylabel(ylabs[i])
    axs[i].plot(DDtime[FTFrameSt], syndat.data[i][FTFrameSt], 'k.', label='Fictrac start')
    axs[i].plot(DDtime[imgFrameSt[0]], syndat.data[i][imgFrameSt[0]], 'r.', label='Imaging start')
    axs[i].plot(DDtime[FTFrameEd], syndat.data[i][FTFrameEd], 'kx', label='Fictrac end')
    axs[i].plot(DDtime[imgFrameSt[-1]], syndat.data[i][imgFrameSt[-1]], 'rx', label='Imaging end')
axs[i].set_xlabel('Time')
axs[0].legend()
```





- In the next steps the Fictrac data get aligned with the pattern position in the arena

```
In [12]: FTkeylist = ['frame',
                    'dRight_cam', 'dDown_cam', 'dFwd_cam',
                    'rotError',
                    'dRight_lab', 'dDown_lab', 'dFwd_lab',
                    'Right_cam', 'Down_cam', 'Fwd_cam',
                    'Right_lab', 'Down_lab', 'Fwd_lab',
                    'x', 'y', 'alpha',
                    'transDir', 'transV_rad',
                    'xpos', 'ypos',
                    'time', 'seqcount']

fictrackDf = pd.read_csv(sep.join([FTDir, FTfile]), index_col=False, names=FTkeylist)

In [13]: fictrackDf['time'] = fictrackDf['time'].values / 1000. #convert to sec
fictrackDf['transV_mm'] = fictrackDf['transV_rad'].values * ballrad
fictrackDf['rotV_rad'] = np.hstack((0, (np.diff(np.unwrap(fictrackDf['alpha'].values)) /
                                         np.diff(fictrackDf['time'].values))))

In [14]: fictrackDf.head()

In [15]: DDtime_at_FTfr = np.linspace(DDtime[FTFrameSt], DDtime[FTFrameEd], len(fictrackDf))
FTframes = np.arange(len(fictrackDf))

In [16]: DDArena_at_FTfr = np.interp(DDtime_at_FTfr, DDtime[FTFrameSt:FTFrameEd], arenaPos[FTFrameSt:FTFrameEd])
plt.plot(DDtime_at_FTfr, DDArena_at_FTfr)
```

- Then the Fictrac data get interpolated with the imaging frames

```
In [17]: FTframe_at_imgfr = np.interp(imgTime, DDtime_at_FTfr, FTframes)
FTframe_at_imgfr = FTframe_at_imgfr.round().astype('int')
#plt.plot(DDtime_at_FTfr[FTframe_at_imgfr], imgTime)

Downsample other FT data to imaging sampling points

In [18]: x = fictrackDf['x'].values
y = fictrackDf['y'].values
alpha = fictrackDf['alpha'].values
vTransRad = fictrackDf['transV_rad'].values

In [19]: x_at_imgfr = np.interp(imgTime, DDtime_at_FTfr, x)
y_at_imgfr = np.interp(imgTime, DDtime_at_FTfr, y)
alpha_at_imgfr = np.interp(imgTime, DDtime_at_FTfr, alpha)
vTransMM_at_imgfr = np.interp(imgTime, DDtime_at_FTfr, fictrackDf['transV_mm'].values)
vTransRad_at_imgfr = np.interp(imgTime, DDtime_at_FTfr, vTransRad)
vRotRad_at_imgfr = np.interp(imgTime, DDtime_at_FTfr, fictrackDf['rotV_rad'].values)
```

- The alignment of the Fictrac data and the arena position of the stimulus gets visualized and saved for future reference

```

In [21]: arenaPosFT = DDArena_at_FTfr
arenaVelo = np.hstack((0, np.diff(DDArena_at_FTfr)))
arenaVelo[arenaVelo>2] = np.nan

fig = plt.figure(figsize=(15,8))
ax0 = plt.subplot2grid((3, 3), (0, 0), rowspan=3)
cb = ax0.scatter(fictrackDf['x'].values,fictrackDf['y'].values,s=1, c=arenaPosFT,cmap='hsv', vmin=-np.pi, vmax=np.pi)
ax0.set_title('Walking trace [arena pos color-coded]')
plt.colorbar(cb, ax=ax0,label='Arena position',orientation='horizontal')
ax0.set_aspect('equal')
ax0.set_xlabel('x pos [lab frame]')
ax0.set_ylabel('y pos [lab frame]')
myAxisTheme(ax0)

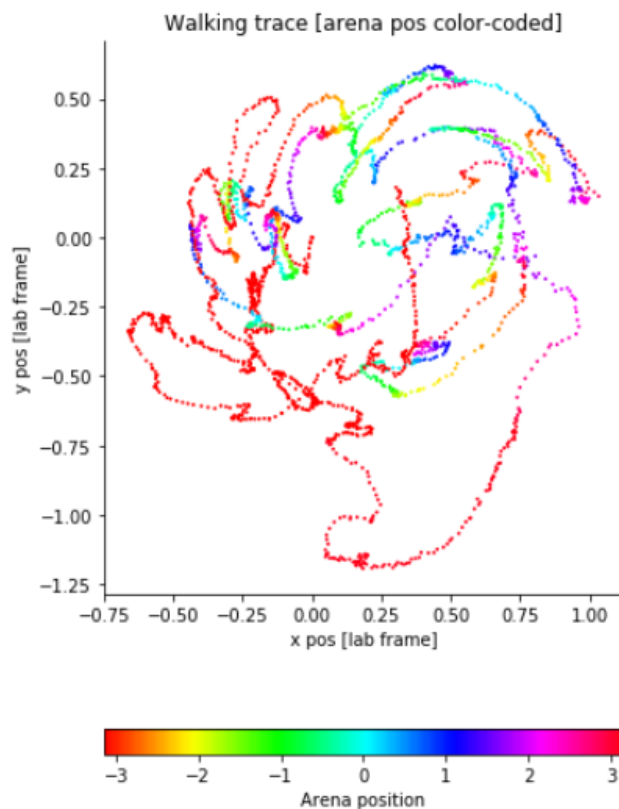
ax1 = plt.subplot2grid((3, 3), (0, 1), colspan=2)
ax1.plot(DDtime_at_FTfr,arenaPosFT,color = 'grey', alpha=0.5)
ax1.scatter(DDtime_at_FTfr,arenaPosFT, s=2,c=arenaPosFT,cmap='hsv', vmin=-np.pi, vmax=np.pi)
ax1.set_ylabel('Movement direction')
myAxisTheme(ax1)

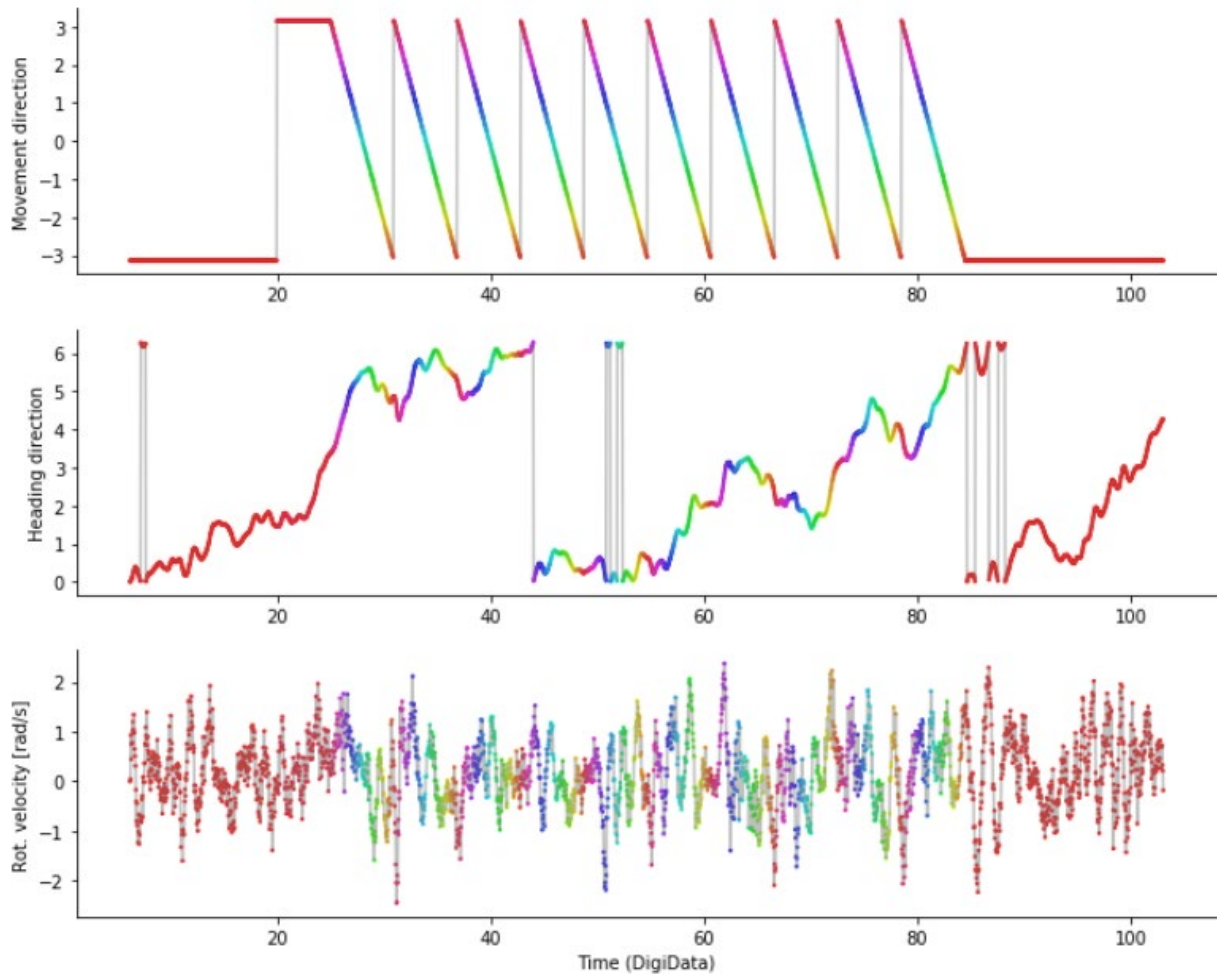
ax2 = plt.subplot2grid((3, 3), (1, 1), colspan=2)
ax2.plot(DDtime_at_FTfr,fictrackDf['alpha'].values,color = 'grey', alpha=0.5)
ax2.scatter(DDtime_at_FTfr,fictrackDf['alpha'].values, s=2,c=arenaPosFT,cmap='hsv',vmin=-np.pi, vmax=np.pi)
ax2.set_ylabel('Heading direction')
myAxisTheme(ax2)

ax3 = plt.subplot2grid((3, 3), (2, 1), colspan=2)
ax3.plot(DDtime_at_FTfr,fictrackDf['rotV_rad'].values,color = 'grey',alpha=0.5)
ax3.scatter(DDtime_at_FTfr,fictrackDf['rotV_rad'].values, s=2,c=arenaPosFT,cmap='hsv', vmin=-np.pi, vmax=np.pi)
ax3.set_xlabel('Time (DigiData)')
ax3.set_ylabel('Rot. velocity [rad/s]')
myAxisTheme(ax3)

fig.tight_layout()
fig.savefig(saveDir+sep+expt+'_WalkingTrace2.pdf', format = 'pdf')

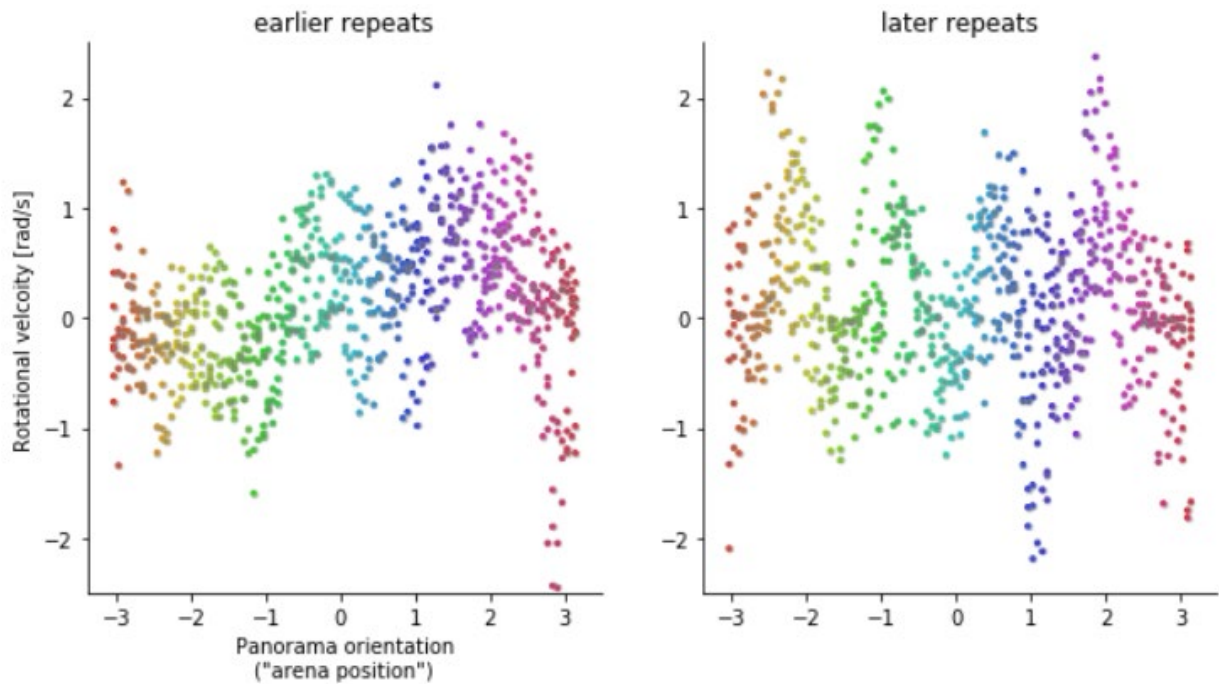
```





- To allow for a better evaluation if the bee showed a behavioral response to the stimulus, the whole trial can get divided into early repeats that correspond to the first five rotations of the stimulus and later repeats including rotation six to ten. The data is plotted as a graph of the bee's movement as rotational velocity matched to the panorama position of the pattern in the arena.

```
In [50]: fig, axs = plt.subplots(1,2,figsize=(10,5))
mask = np.where(np.logical_and(DDtime_at_FTfr>25,DDtime_at_FTfr<=50))
axs[0].plot(arenaPosFT[mask], fictrackDf['rotV_rad'].values[mask], '.', color='grey', alpha=0.4)
axs[0].scatter(arenaPosFT[mask], fictrackDf['rotV_rad'].values[mask], s=5, c=arenaPosFT[mask],
               cmap='hsv', vmin=-np.pi, vmax=np.pi)
axs[0].set_title('earlier repeats')
mask = np.where(np.logical_and(DDtime_at_FTfr>50,DDtime_at_FTfr<=75))
axs[1].plot(arenaPosFT[mask], fictrackDf['rotV_rad'].values[mask], '.', color='grey', alpha=0.4)
axs[1].scatter(arenaPosFT[mask], fictrackDf['rotV_rad'].values[mask], s=5, c=arenaPosFT[mask],
               cmap='hsv', vmin=-np.pi, vmax=np.pi)
axs[1].set_title('later repeats')
for ax in axs:
    myAxisTheme(ax)
    ax.set_ylim(-2.5, 2.5)
axs[0].set_xlabel('Panorama orientation\n("arena position")')
axs[0].set_ylabel('Rotational velocity [rad/s]')
fig.savefig(saveDir+sep+expt+'_stimrot.pdf', format = 'pdf')
```



- In the next steps the imaging data file name needs to be inserted manually to allow the script to load the data

```
In [26]: #test by Tina
parentDir = sep.join(getcwd().split(sep)[-1])

rawtiff = '20190717_2_vertical_stripe_cw.tif'
expt = rawtiff[:-5] #adjust manually, if experiment name should be different from imaging stack name

explenght = 100.727 #need to adjust this manually (experiment duration in s used to compute fps)

#stack parameter
stackOrganization = {
    'singlePlane': ['t','y','x'],
    'zStack': ['t','z','y','x']
}

dataDir = sep.join([parentDir, 'Data', 'LeicaData'])
plotDir = sep.join([parentDir, 'Plots', 'LeicaData'])
roiDir = sep.join([parentDir, 'ROIs', 'LeicaData'])

print(parentDir)
print(dataDir)
print(plotDir)

print(expt)

C:\Users\Mah33Ex\Dropbox\BeeImagingCoop (1)
C:\Users\Mah33Ex\Dropbox\BeeImagingCoop (1)\Data\LeicaData
C:\Users\Mah33Ex\Dropbox\BeeImagingCoop (1)\Plots\LeicaData
20190717_2_vertical_stripe_c
```

- The dimensions and other information are extracted from the file

```
In [27]: #test by Tina
rawstack = imread(dataDir + sep + rawtiff)

if len(rawstack.shape) == 3:
    imgType = 'singlePlane'
    singlePlaneStack = rawstack
elif len(rawstack.shape) == 4:
    imgType = 'zStack'
    singlePlaneStack = np.max(rawstack, axis=1)
else:
    print('Imaging stack has unexpected dimensions.')
stackDims = dict(zip(stackOrganization[imgType], rawstack.shape))

print('raw stack dimensions:\n\t{}'.format(stackDims))
print('single stack (max proj.) dimensions [t, y, x]:\n\t{}'.format(singlePlaneStack.shape))

raw stack dimensions:
      {'t': 1001, 'y': 100, 'x': 256}
single stack (max proj.) dimensions [t, y, x]:
      (1001, 100, 256)
```

```
In [28]: #test by Tina
numTimePts = stackDims['t']

if imgType == 'singlePlane':
    fpv = 1
elif imgType == 'zStack':
    fpv = stackDims['z']
else:
    print('something went wrong')
print("# frames: {}\n# frames per vol: {}".format(numTimePts, fpv))

# frames: 1001
# frames per vol: 1
```

- In the next steps the ROIs set in step 13 and all attached information get extracted for this experiment

```
In [29]: from roiVisualization import illustrateRoiOutline, illustrateRoiArea, illustrateRoiTrace
from matplotlib import colors
```

```
In [31]: roiData = np.load(ROIDir+sep+Imgfile[:-5]+'_roiData.npy')

roiData = roiData.item()
print(roiData.keys())

dict_keys(['imgData', 'img', 'numframes', 'slctframes', 'fpv', 'fps', 'time', 'numRoi', 'Fraw', 'DFF', 'Pts', 'Fb'])
```

```
In [32]: # smooth DFF values
dffsmooth = np.zeros((roiData['DFF'].shape))

from scipy.signal import savgol_filter
order = 3
window = 7

for roi in range(roiData['DFF'].shape[1]):
    dffsmooth[:,roi] = savgol_filter(roiData['DFF'][:,roi], window, order)
```

```

In [33]: # generate roi color map
nrois = roiData['numRoi']
cNorm = colors.Normalize(vmin=0, vmax=roiData['numRoi'])
roiCMap = plt.cm.ScalarMappable(norm=cNorm, cmap='Set2')
slctROIs = np.arange(roiData['numRoi'])

In [34]: #frameRange = np.arange(0,roiData['numframes'])
frameRange = np.arange(0,len(roiData['time'])) # in seconds
slct_fps = 1

# Select ROIs
slctROIs = np.arange(roiData['numRoi'])

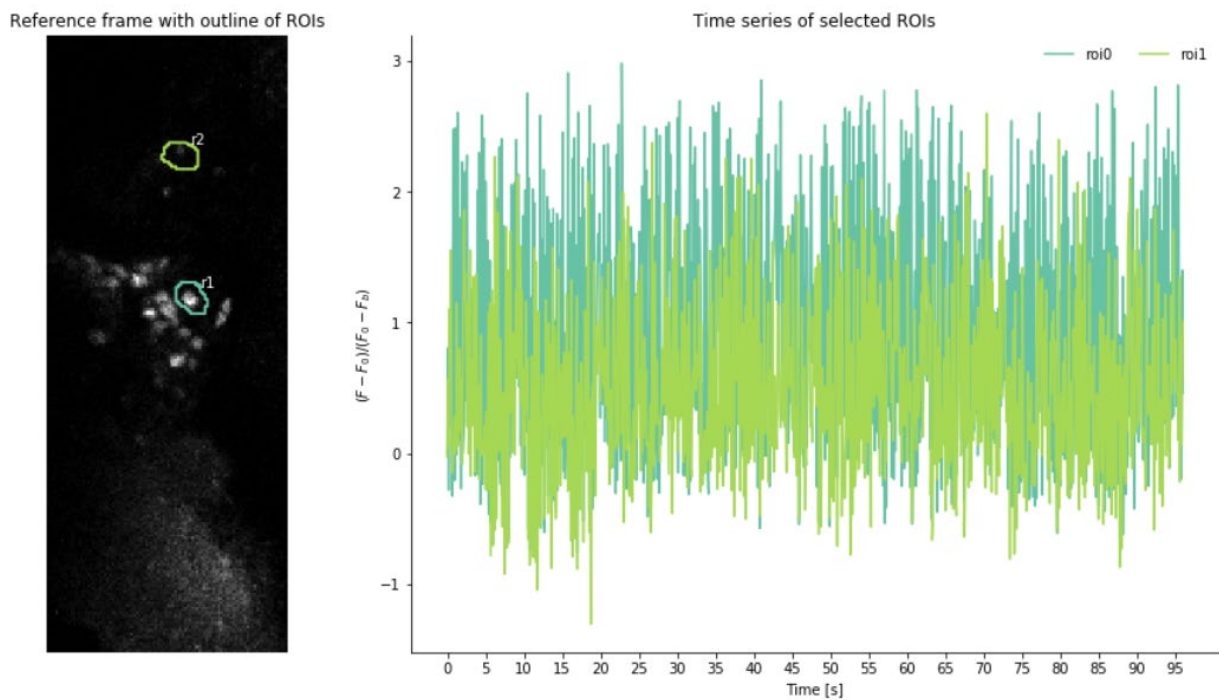
fig, axs = plt.subplots(1,2, figsize=(15,8), gridspec_kw={'width_ratios':[1,3]})
axs[0] = illustrateRoiOutline(roiData, axs[0], roiCMap, 'r', 'Reference frame with outline of ROIs')

#axs[1] = illustrateRoiTrace(roiData, np.hstack((0,imgTime-imgTime[0])), axs[1], roiCMap, frameRange, slctROIs,
# #
# 'Time [s]', '$(F - F_0) / (F_0 - F_b)$', 'Time series of selected ROIs')

axs[1] = illustrateRoiTrace(roiData,roiData['time'], axs[1], roiCMap, frameRange, slctROIs,
'Time [s]', '$(F - F_0) / (F_0 - F_b)$', 'Time series of selected ROIs')

axs[1].legend(['roi'+str(i) for i in range(nrois)], ncol=2, frameon=False)
axs[1].set_xticks(np.arange(roiData['time'][0],roiData['time'][-1],5));
myAxisTheme(axs[1])
axs[0].axis('off')

```



- The ROI fluorescence data get now aligned with information from Fictrac like the rotation and translational velocity to evaluate self-movement influences on the neuronal activity to check for state dependency. The resulting plots are getting saved for further reference.



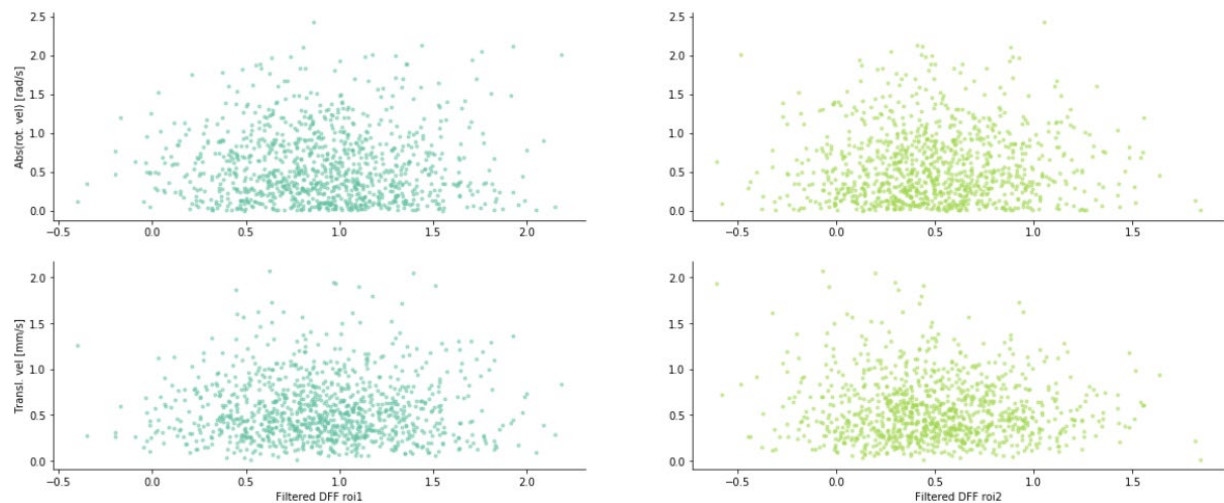
```
In [35]: arenaPos_at_imgfr = np.interp(imgTime,DDtime,arenaPos)
arenaVel_at_imgfr = np.hstack((0,np.diff(arenaPos_at_imgfr)))
imframes = np.arange(len(imgTime))
```

```
In [36]: fig, axes = plt.subplots(2,roiData['numRoi'],figsize=(20,8))

for i, val in enumerate(slctROIs):
    axes[0,i].plot(dffsmooth[imframes,val],abs(vRotRad_at_imgfr),'.', color=roiCMap.to_rgba(val),alpha=0.5)
    axes[1,i].plot(dffsmooth[imframes,val],vTransMM_at_imgfr,'.', color=roiCMap.to_rgba(val),alpha=0.5)
    axes[1,i].set_xlabel('Filtered DFF roi{}'.format(val+1))
    #axes[0,i].set_ylim([-0.3,0.3])
    #axes[1,i].set_ylim([0,0.04])
    for ax in axes[:,i]: myAxisTheme(ax)

axes[0,0].set_ylabel('Abs(rot. vel) [rad/s]')
axes[1,0].set_ylabel('Transl. vel [mm/s]')

fig.savefig(saveDir+sep+expt+'_ROIalignedWithFictrac.pdf', format = 'pdf')
```



- In the next steps, all data are getting combined. For a better visualization single rotation repeats of the stimulus are getting picked, in this example the first four rotations.

```
In [40]: stimSlct = [0,1,2,3]
```

```
In [41]: # filter walking velocity

from scipy.signal import savgol_filter
order = 3
window = 7

filtvTransMM_at_imgfr = savgol_filter(vTransMM_at_imgfr, window, order)
filtvRotRad_at_imgfr = savgol_filter(vRotRad_at_imgfr, window, order)

#plt.plot(imgTime,vTransMM_at_imgfr,color = 'grey',alpha=0.5)
#plt.plot(imgTime,filtFwdV,color = 'black',alpha=0.5)
```

- The filtered rotational and translational velocity of the chosen repeats, in this case the first four stimulus rotations, gets overlayed and plotted for the stimulus time of six seconds (colored lines). The mean of those four rotations is plotted as well into the graph (black bold line). The graphs are getting saved for future reference.

```

In [42]: dffRepeat = np.zeros((len(stimSlct), stimLen))

stimtime = imgTime[arenaRepeat[0]:arenaRepeat[0]+stimLen]-imgTime[arenaRepeat[0]]

fig, axs = plt.subplots(1,3, figsize=(10,4))

arenaStimRep = np.zeros((len(stimSlct),stimLen))
vRStimRep = np.zeros((len(stimSlct),stimLen))
filtvRStimRep = np.zeros((len(stimSlct),stimLen))
vTStimRep = np.zeros((len(stimSlct),stimLen))
filtvTStimRep = np.zeros((len(stimSlct),stimLen))

for i, s in enumerate(stimSlct):
    st = arenaRepeat[s]
    se = st + stimLen
    arenaStimRep[i,:] = arenaPos_at_imgfr[st:se]
    vRStimRep[i,:] = vRotRad_at_imgfr[st:se]
    filtvRStimRep[i,:] = filtvRotRad_at_imgfr[st:se]
    vTStimRep[i,:] = vTransMM_at_imgfr[st:se]
    filtvTStimRep[i,:] = filtvTransMM_at_imgfr[st:se]

    axs[0].plot(stimtime, arenaPos_at_imgfr[st:se], '-', alpha=0.8, linewidth=.5, label='rep {}'.format(s+1))
    axs[1].plot(stimtime, filtvRotRad_at_imgfr[st:se], '-', alpha=0.8, linewidth=.5)
    axs[2].plot(stimtime, filtvTransMM_at_imgfr[st:se], '-', alpha=0.8, linewidth=.5)

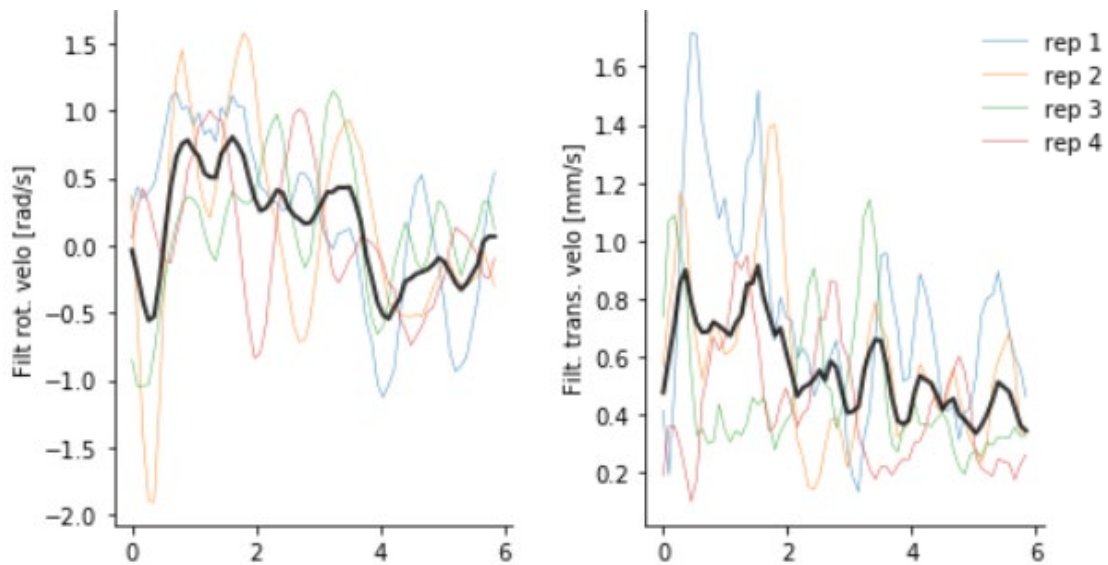
axs[0].plot(stimtime, arenaStimRep.mean(axis=0), 'k-', alpha=0.8, linewidth=2)
axs[1].plot(stimtime, filtvRStimRep.mean(axis=0), 'k-', alpha=0.8, linewidth=2)
axs[2].plot(stimtime, filtvTStimRep.mean(axis=0), 'k-', alpha=0.8, linewidth=2)

axs[0].legend(frameon=False)
axs[0].set_xlabel('Stimulus time [s]')
axs[0].set_ylabel('Arena position [rad]')
axs[1].set_ylabel('Filt rot. velo [rad/s]')
axs[2].set_ylabel('Filt. trans. velo [mm/s]')

for ax in axs:
    myAxisTheme(ax)

fig.tight_layout()

```



- As last step of the analysis,  $dF/F$  of each ROI is plotted in the same chosen repeats as before over the stimulus time (colored lines) together with the mean (green bold line). The graph is getting saved for future reference.

```

In [43]: dffRepeat = np.zeros((len(stimSlct), len(slctROIs), stimLen))
stimtime = imgTime[arenaRepeat[0]:arenaRepeat[0]+stimLen]-imgTime[arenaRepeat[0]]

for k, s in enumerate(stimSlct):
    st = arenaRepeat[s]
    se = st + stimLen
    for i, val in enumerate(slctROIs):
        #smooth trace
        dfftrace = dffsmooth[st:se,val]
        dffRepeat[k,i] = dfftrace

In [44]: fig = plt.figure(figsize=(10,12))
gsax = gs.GridSpec(len(slctROIs),2, figure=fig)
axs0 = fig.add_subplot(gsax[:, 0])
axs0 = illustrateRoiOutline(roiData, axs0, roiCMap, 'r','Reference frame with outline of ROIs')
for k, s in enumerate(stimSlct):
    for i, val in enumerate(slctROIs):
        axRoi = fig.add_subplot(gsax[i,1])
        axRoi.plot(stimtime, dffRepeat[k,i],'-', linewidth=.5, alpha=0.8)
        axRoi.plot(stimtime, dffRepeat[:,i].mean(axis=0),'-', linewidth=2, color=roiCMap.to_rgba(val))
        axRoi.set_ylim(-1,5)
        axRoi.set_ylabel('roi{}'.format(val+1))
        myAxisTheme(axRoi)
axRoi.set_xlabel('Stimulus time [s]')
fig.tight_layout()

```

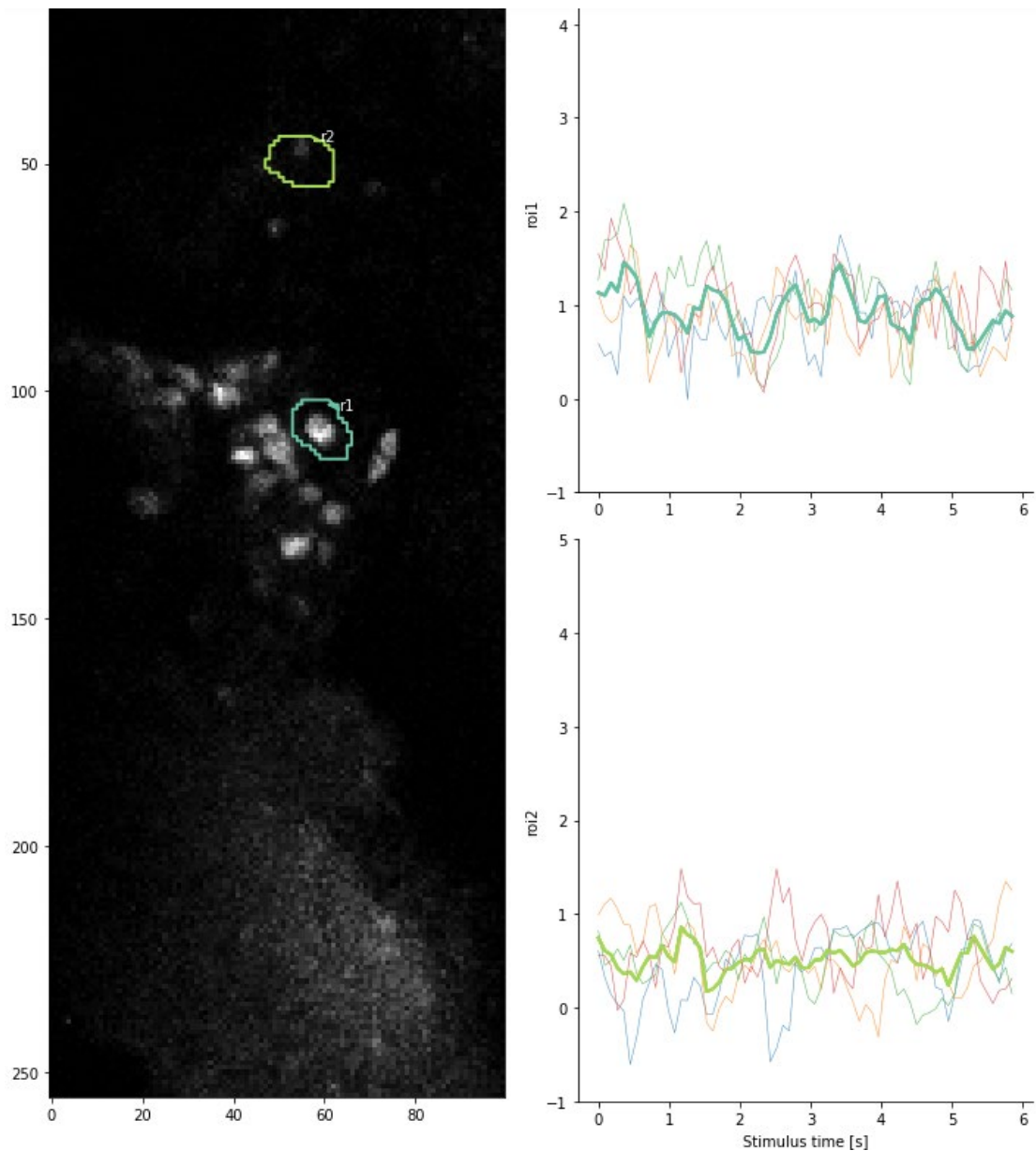


## TABLE NOTES FOR CALCIUM IMAGING IN LEICA SETUP

Abbreviations: AOT: anterior optic tract, AOTU: anterior optic tubercle, CaG: Calcium Green-1 dextran, JF<sub>549</sub>MPM: JF549-BAPTA-MPM ester, MB: mushroom body, ME: medulla, MEDRA: dorsal rim area of the medulla, LO: lobula, LUC: lower unit complex of the AOTU, TR: Dextran Texas Red, UU: upper unit of the AOTU, VL: vertical lobe

Specimen	Dyes	Injection site	Comments
180221_1	TR	ME, LO right; VL left	overnight 4°C, too much movement
180222_1	CaG	ME left; VL right	Agarose too fluid, too much movement for in vivo
180405_1	TR	OL right, VL left	cell bodies visible but no other structures -> wholemount preparation -> AOTU staining and collar
180405_2	TR	OL right, VL left	cell bodies visible -> wholemount preparation -> AOTU staining
180511_1	TR & CaG	MEDRA	no imaging possible, objective can't reach ROI
180514_1	TR & CaG	MEDRA both sides	usage of Marburg holder -> wholemount preparation -> AOTU staining
180520_1	TR & CaG	MEDRA both sides	SP8 broke, control with fluoBino; -> wholemount preparation -> AOTU UU and LUC stained on both sides
180523_1	TR & CaG	MEDRA both sides	z stacks of TR shows staining in AOTU UU, LUC hard to see; 2 channel stack: CaG very dim
180525_1	TR & CaG	MEDRA both sides	Scan of AOTU but no staining visible
180613_1	TR & CaG	MEDRA/ME both sides	staining in both channels, CaG at least cell bodies in ME, UU and LUC (bright spots?), KCl application during scan but signal not stable
180613_2	TR & CaG	MEDRA/ME both sides	weak staining, dark material (Retina?) on the brain, no scan
180618_1	TR & CaG	MEDRA both sides	syringe system for KCl application, KCl after 10s -> brain has a short drop in z but afterwards Ca response in ME cell bodies
180618_2	TR & CaG	MEDRA both sides	bee dead
180620_1	TR & CaG	MEDRA/ME both sides	Overnight at 4°C, tested all patterns, staining in UU and LUC? Imaged in LUC; problems with arena (pattern from the beginning shown)
180620_2	TR & CaG	MEDRA/ME both sides	bee dead
180626_1	TR & CaG	MEDRA/ME both sides	no visible structures

180626_2	TR & CaG	MEDRA/ME both sides	all patterns tested, F increases also in the background -> artefact from the arena; HyD must be more narrow
180628_1	TR & CaG	MEDRA/ME both sides	no clear staining in central brain visible, only cell bodies; objective can't go deep enough
180628_2	TR & CaG	MEDRA/ME both sides	no clear staining in AOTU, runtime of dye too short?
180710_1	TR & CaG	MEDRA/ME both sides	Overnight 4°C, bee dead the next day
180711_1	TR & CaG	MEDRA	no clear staining in AOTU, HyD at 510nm still shows leakage, excitation at 820nm seems suitable
180716_1	TR & CaG	MEDRA both sides	no clear staining in AOTU; Imaging of ME cell bodies, all LEDs on; bee in the end dead?
180716_2	TR & CaG	MEDRA both sides	bee dead
180717_1	TR & CaG	MEDRA/ME both sides	strong staining in AOTU, LUC lowest unit in both channels, different patterns tested, response?
180717_2	TR & CaG	MEDRA/ME both sides	staining in AOTU but too much movement (pumping) to image
180724_1	TR & CaG	MEDRA/ME both sides	maybe staining in AOTU but not clear; imaging in MB calyx, response? -> wholemount preparation
180724_2	TR & CaG	MEDRA/ME both sides	too much movement; no clear staining
180730_1	TR & CaG	AOTU left side	bee dead
180730_2	TR & CaG	AOTU right side	clear staining of TUTU neurons on contralateral side in TR channel; CaG very dim; still leaking arena signal
180808_1	TR & CaG	ME left; MEDRA and ME right	bee dead
180821_1	JF <sub>549</sub> MPM&TR	AOTU right side	objective not deep enough
180821_2	JF <sub>549</sub> AM&TR	AOTU right side	no staining visible
181001_1	JF <sub>549</sub> MPM&TR	MEDRA and ME both sides	no clear staining, too much movement
181010_1	JF <sub>549</sub> MPM&A488	AOTU right side	bee dead
181010_2	JF <sub>549</sub> MPM&A488	AOTU left side	some patterns tested, bee walking, following pattern?
181010_3	JF <sub>549</sub> MPM&A488	MB medial left	Bee dead
181012_1	JF <sub>549</sub> MPM&A488	AOTU left side	staining in UU and LUC?, patterns tested and bee was walking but not very smoothly
181012_2	JF <sub>549</sub> MPM&A488	AOTU left side	bee dead
20181112_1	JF <sub>549</sub> MPM&A488	MEDRA both sides	TR staining in LUC; CaG very dim; bar tested, bee did not walk a lot
20181112_2	JF <sub>549</sub> MPM&A488	MEDRA both sides	bee dead
20181113_1	JF <sub>549</sub> MPM&A488	MEDRA both sides	imaged with horizontal bar and all LEDs on; bee not walking

20181113_2	JF <sub>549</sub> MPM&A488	MEDRA both sides	?
20181113_3	JF <sub>549</sub> MPM&A488	MEDRA both sides	bee dead
20181128_1	JF <sub>549</sub> MPM&A488	MEDRA both sides	resonant scanner, AOTU LUC left?, ME cell bodies right, imaged with all on/off, response?
20181128_2	JF <sub>549</sub> MPM&A488	MEDRA both sides	microscope crashed during imaging
190123_1	JF <sub>549</sub> MPM&A488	MEDRA both sides	bee dead
190123_2	JF <sub>549</sub> MPM&A488	MB both sides	too much movement; no clear staining
20190204_1	TR & CaG	ME/AOT both sides	good staining in AOTU UU, maybe LUC; bee walked only in the beginning
20190213_1	CaGreen	ME/AOT both sides	AOTU hard to find, imaging of cell bodies in ME; bee alive but not really walking
20190218_1	TR & CaG	MEDRA both sides	ME cell bodies imaged but too much movement, z-stack
20190227_1	TR & CaG	MEDRA both sides	bee alive but barely walking, staining very weak
20190227_2	TR & CaG	MEDRA both sides	<i>Bombus terrestris</i> ; AOT visible but AOTU not; imaging of LO cell bodies, bumblebee followed stripe for a short period of time
20190228_1	TR & CaG	MEDRA both sides	imaged in AOT, LUC? With different patterns, no walking
20190228_2	TR & CaG	MEDRA both sides	<i>Bombus terrestris</i> ; no clear staining
20190326_1	TR & CaG	MB both sides	<i>Bombus terrestris</i> ; microscope crashed 3 times
20190327_1	TR & CaG	MEDRA both sides	UV glue instead of Agarose; too blurry to image
20190328_1	TR & CaG	MEDRA both sides	QuickSeal instead of Agarose; not curing; no imaging
20190328_2	TR & CaG	MEDRA both sides	QuickSeal instead of Agarose; not curing; no imaging
20190402_1	?	?	no notes, cell bodies?
20190410_1	JF <sub>549</sub> MPM&A488	AOT both sides	bee positioned badly; objective can't go deep enough
20190410_2	JF <sub>549</sub> MPM&A488	AOT right side	bee dead
20190525_1	TR & CaG	ME/AOT both sides	too much eye covered, AOTU not visible but cell bodies in central brain and OL (also in CaG channel)
20190625_2	TR & CaG	ME/AOT both sides	TR staining in AOTUr but no staining visible in CaG channel; bee dead
20190626_1	TR & CaG	ME/AOT both sides	TR staining in UU but not clear staining in CaG channel, no visible structures; no signal during test
20190704_1	TR & CaG	ME/AOT both sides	bee dead
20190704_2	TR & CaG	ME/AOT both sides	very dim signal in AOT and UU; no signal in CaG channel
20190705_1	JF <sub>549</sub> MPM	MEDRA both sides	dim staining in AOT and maybe LUC; all on/off tested and horizontal optic flow up; reaction to all on? No walking



20190716_1	TR & CaG	AOT both sides	bee dead
20190716_2	TR & CaG	AOT/MEDRA both sides	bee dead
20190717_1	TR & CaG	AOT both sides	staining in AOT and UU; all on/off tested, vertical stripe; no reaction
20190717_2	TR & CaG	MB both sides	very bright staining in TR and CaG channel, KC cell bodies; all on/off, vertical stripe cw/ccw/, all on/off 2 channels, z-stack/t-stack 2 channels in darkness; no signal, lot of noise
20190718_1	TR & CaG	AOT/ME both sides	staining in TR channel, CaG very dim, z-stack of left AOTU but too much movement for further testing
20190718_2	TR & CaG	AOT/ME both sides	Strong staining in AOTU UU in TR channel, very dim in CaG; a lot of movement in z, no testing; new Agarose batch; wholemount preparation
20190723_1	TR & CaG	AOT both sides	New CaG batch, good staining in r AOTU, less movement then before, all on/off, stripe cw/ccw, optic flow tested, z-stack both channels, maybe reaction
20190723_2	TR & CaG	AOT both sides	bright staining in AOT and UU in TR channel but not in CaG
20190730_1	TR & CaG	ME/AOT both sides	Legs and abdomen fixed with dental wax; bee dead
20190730_2	TR & CaG	AOT both sides	Legs and abdomen fixed with dental wax; bee dead; wax too hot?
20190731_1	TR & CaG	AOT both sides	Fixated animal with UV glue; leaking of saline; no imaging possible
20190809_1	TR & CaG	ME both sides	Fixated with UV glue; staining in AOTU but very dim?; imaging of cell bodies in ME; stripe cw/ccw; no reaction
20190813_1	TR & CaG	MEDRA/AOT both sides	staining in right AOT and UU right side in both channels; z-stack TR and CaG; cw/ccw/cw2 tested; no reaction, signal very weak/noisy
20190813_2	TR & CaG	MEDRA/ME both sides	staining in TR channel in left AOT and UU; no structures visible in CaG; cw/ccw tested, no reaction?
20190913_1	TR & CaG	MEDRA/AOT both sides	dim staining in right AOT in TR channel but not in AOTU; z-stack + t-series in CaG channel with all on/off, cw, cww; no reaction
20190913_2	TR & CaG	MEDRA/AOT both sides	staining in right AOT, UU, and LUC in TR channel, CaG channel very dim; z-stack + t-series with CaG stripe cw; cw without z; signal too dim

## WHOLEMOUNT PREPARATION

### 1. Preparation:

- After the experiment, remove bee from holder and cut off the head with a scalpel
- Arrange and fixate the head in a wax bowl
- Widen with the scalpel the window of the cuticula and remove with forceps rests of the cuticula, muscles and neural sheaths
- Remove brain from head capsule
- Transfer brain in Neurobiotin fixative and store it overnight at 4°C in the fridge
- Next day: wash 4 × 15 minutes with phosphate-buffered saline (PBS)
- Dehydrate brain in an ascending ethanol series for 15 minutes in each concentration: 30%, 50%, 70%, 90%, 95%, two times 100%
- Transfer to 50:50 absolute ethanol:methyl salicylate for 20 minutes
- Exchange for pure methyl salicylate for 1 hour or more
- Embed in permount on a cover slip with 9 spacers, seal with cover slip and put weights overnight on it



## DANKSAGUNG

An dieser Stelle möchte ich mich bei allen bedanken, die mich auf meinem Weg zur Promotion begleitet haben:

Prof. Dr. Keram Pfeiffer: Dir gebührt der größte Dank, da Du mir durch die Vergabe dieses anspruchsvollen Projektes die Promotion ermöglicht hast. Zudem hast Du mir auch mit viel Vertrauen den Raum zur Entwicklung gegeben. Darüber hinaus hat Deine akurate Denkweise, verbunden mit viel Humor, meine Arbeitsweise maßgeblich beeinflusst.

Prof. Dr. Uwe Homberg: Zunächst möchte ich mich bei Dir für die Zweitkorrektur meiner Dissertation bedanken. Ich bin jedoch auch für die jahrelange, gute Zusammenarbeit an verschiedenen Projekten und der angenehmen Zeit in Deinem Labor in Marburg dankbar. Durch hilfreiche Diskussionen und Korrekturen hast Du außerdem mein kritisches Denken weiterentwickelt.

Prof. Dr. Monika Hassel & Prof. Dr. Frank Bremmer: Ihnen danke ich herzlich für die Bereitschaft meine Arbeit als Kommissionsmitglieder zu bewerten.

Dr. Vivek Jayaraman: Dir gilt ebenfalls ein großer Dank, da Deine Unterstützung und mein Aufenthalt in Deinem Labor mich und meinen professionellen Weg nachhaltig beeinflusst haben.

Dr. Luke Lavis, Dr. Claire Deo & Dr. Hannah Haberkern: Euch danke ich für Eure Unterstützung jeglicher Art und den vielen hilfreichen Diskussionen.

Myriam & Lisa: Euch danke ich von Herzen für Eure Freundschaft, Aufmunterung und die tolle Atmosphäre im Büro. Darüber hinaus schätze ich Euch sehr für die vielen wissenschaftlichen Diskussionen und hilfreichen Korrekturen dieser Arbeit. Vor allem in den letzten Monaten habt Ihr mich oft vor dem Aufgeben bewahrt.

Dr. Anna Stöckl & Dr. Basil el Jundi: Anna, Dir danke ich für Deine Bereitschaft, mir in kürzester Zeit eine neue Methode beizubringen. Außerdem gilt Dir und Basil ein besonderer Dank, da Ihr mir mit unermüdlicher Hilfsbereitschaft wertvolle Werkzeuge für meine berufliche Zukunft in die Hand gegeben habt.

Alle Labormitglieder in Marburg, Würzburg und Janelia: Ich danke allen Kollegen, mit denen ich zusammenarbeiten durfte, vor allem für die familiäre Atmosphäre. Besonders die entstandenen Freundschaften zu Ronja, Annuska, Sarah, Tanja, Fred, Joss und Martina bedeuten mir viel.

Meine Familie: Mama & Papa, ohne Euer Vertrauen in mich und Eure Unterstützung, wäre all das nicht möglich gewesen. Ich bin Euch für immer dankbar, dass Ihr mich stets begleitet habt. Dreli, danke für Deine Aufmunterung und die „Auszeiten“, die ich mir mit Dir in den letzten Monaten von der Arbeit nehmen konnte. Suse, Kristof, Noah und Helena: danke, dass Ihr mir nicht nur das beste Patenkind anvertraut, sondern auch für all Eure Unterstützung auf verschiedenen Wegen. Ich sehe es als großes Geschenk an, dass wir nach Marburg nun auch gemeinsam in Würzburg leben. Zu guter Letzt möchte ich mich bei Dir, Brendan, für Deinen Mut Deine Heimat zu verlassen und mit mir nach Würzburg zu gehen bedanken. Durch all Deine Unterstützung und Fürsorge daheim, hast Du mir bei dieser Arbeit sehr geholfen und mir mit unserem Hund Boba zudem einen langjährigen Traum erfüllt.



## ERKLÄRUNG

Ich versichere hiermit, dass meine Dissertation

**Investigation of visual pathways in honeybees (*Apis mellifera*) and desert locusts (*Schistocerca gregaria*): anatomical, ultrastructural, and physiological approaches**

(Untersuchung visueller Signalwege in Honigbienen (*Apis mellifera*) und Wüstenheuschrecken (*Schistocerca gregaria*): anatomische, ultrastrukturelle und physiologische Betrachtungen)

selbstständig, ohne unerlaubte Hilfe angefertigt und mich dabei keiner anderen als der von mir ausdrücklich bezeichneten Quellen und Hilfen bedient habe.

Die Dissertation wurde in der jetzigen oder einer ähnlichen Form noch bei keiner anderen Hochschule eingereicht und hat noch keinen sonstigen Prüfungszwecken gedient.

Würzburg, den

Martina Held